

**Characterisation and optimisation of nitroreductase-
prodrug combinations for bacterial-directed enzyme-
prodrug therapy**

By

Jasmine Violet Esna Chan-Hyams

A thesis submitted to the Victoria University of Wellington in fulfilment of the
requirements for the degree of Doctor of Philosophy

Victoria University of Wellington

2020

Abstract

Gene-directed enzyme-prodrug therapy (GDEPT) employs tumour-tropic vectors including viruses (VDEPT) and bacteria (BDEPT) to deliver a genetically-encoded prodrug-converting enzyme to the tumour environment, thereby sensitising the tumour to a prodrug. Bacterial nitroreductases, which are able to activate a range of anti-cancer nitroaromatic prodrugs to genotoxic metabolites, are of particular interest for GDEPT.

The bystander effect is crucial to the success of GDEPT. The bystander effect is a measure of how efficiently activated prodrug metabolites are transferred from gene-expressing cells to neighbouring tissues. This promotes more extensive tumour cell killing. The bystander effect has been quantified for multiple nitroaromatic prodrugs in mixed multilayer human cell cultures. Although this is a good model for VDEPT it cannot simulate the ability of these prodrug metabolites to exit the bacterial vectors relevant to BDEPT. Prior to this work there was an unmet need for an *in vitro* method of quantifying the bystander effect as it occurs in BDEPT, i.e. a bacterial model of cell-to-cell transfer of activated prodrug metabolites.

This thesis presents a method for measuring the bacterial bystander effect *in vitro* in a microplate based assay that was validated by flow cytometry. In this assay two *Escherichia coli* strains are grown in co-culture; an activator strain expressing the nitroreductase *E. coli nfsA* and a recipient strain containing an SOS-GFP DNA damage responsive gene construct. In this system, induction of GFP by reduced prodrug metabolites can only occur following their transfer from the activators to the recipients.

Using this method, the bacterial bystander effect of the clinically relevant prodrugs, metronidazole, CB1954, nitro-CBI-DEI, PR-104A and SN27686, was assessed. Consistent with the bystander efficiencies in human cell multilayers, reduced metronidazole exhibited little bacterial cell-to-cell transfer, whereas nitro-CBI-DEI was passed very efficiently from activator to recipient cells post-reduction. In contrast with observations in human cell multilayers, the PR-104A and SN27686 metabolites were not effectively passed between the two bacterial strains, whereas reduced CB1954 was transferred efficiently. Using nitroreductase enzymes that exhibit different biases for the 2- versus 4-nitro substituents of CB1954, I further showed that the 2-nitro reduction products exhibit

substantially higher levels of bacterial cell-to-cell transfer than the 4-nitro reduction products. The outcomes of this investigation highlighted the importance of evaluating enzyme-prodrug combinations in models relevant to the intended GDEPT vector, as there can evidently be profound differences in efficacy in different settings.

These findings motivated an investigation into the influence of the bystander effect on certain screening strategies used for directed evolution of nitroreductases. It was observed that the bacterial bystander effect can occur during fluorescence activated cell sorting (FACS) of a nitroreductase variant library and negatively impact the recovery of more active variants. Significantly fewer *nfsA*-expressing cells were recovered from FACS when using CB1954 and nitro-CBI-DEI, when the bystander effect was given time to occur, as compared to controls in which the bystander effect was given no time to occur. In contrast, at the preferred challenge concentrations the mustard prodrugs PR-104A and SN27686 did not yield significantly lower proportions of *nfsA*-expressing cells under bystander condition.

A subsequent investigation compared the evolutionary outcomes arising from screening a nitroreductase variant library using FACS, in which the bystander effect can occur, in parallel to a manual pre-selection method of individual clones for detoxification of structurally divergent nitroaromatic antibiotics. Overall the results of this investigation were inconclusive after just a single round of selection, but there is some evidence that the FACS strategy was more effective than niclosamide/chloramphenicol pre-selection in enriching for superior CB1954-reducing variants.

Finally, a panel of nitroreductase candidates was evaluated with the next generation prodrugs PR-104A and SN36506 for possible *Clostridia*-DEPT development. It was found that the *Vibrio vulnificus* NfsB F70A/F108Y variant displayed the highest catalytic efficiency with PR-104A reported thus far compared to any other nitroreductase, and was the only NfsB family nitroreductase to exhibit any activity with SN36506 at the purified protein level. At the time this research was performed only NfsB family nitroreductases had been successfully expressed in *C. sporogenes* by our collaborators, hence the *V. vulnificus* NfsB F70A/F108Y variant was selected as a promising lead enzyme for further development.

Acknowledgements

Firstly, I would like to thank Victoria University of Wellington for their funding, without which this PhD could not have been completed.

I would like thank Professor David Ackerley. He generously supported and me with both his intellectual guidance and time. Thank you for the many, many hours of consideration and thought you put into making my thesis more a robust scientific document that I can be proud of. Thank you for the opportunity to work under you supervision and with the rest of the Ackerley lab team.

I would also like to thank my secondary supervisor Paul Teesdale-Spittle. Thank you Paul for helping understand some of the biochemistry of the prodrugs I worked with and for wrangling with my kinetics data. I admire the way you for always explain difficult concepts with kindness and patience.

Sometimes I needed to remind myself why I started this journey in the first place. I always return to the where my love of science was first ignited – reading *Dune* by Frank Herbert and *Red Mars* by Kim Stanley Robinson. The concepts of controlling planetary wide evolution and terraforming still fill me with wonder. For me a true miracle is when technology, thought to be a pipe-dream, is brought to life by scientists and innovators.

However science research in reality is filled with hurdles, heartaches and triumphs (and if you are extremely lucky they will occur in equal measure). I have reflected on my mantra *“I will face my fear. I will permit it to pass over me and through me. And when it has gone past I will turn the inner eye to see its path. Where the fear has gone there will be nothing. Only I will remain”* - Frank Herbert, *Dune*.

I have come realize that after facing my fears, during six years of PhD life that I am not standing alone. In fact I am surrounded by people who support me and whom I support in return. I have drawn so much strength from so many people throughout my research. Without you I would not have made it to this sandy shore of sanity. So without further ado let me name a few...

The Ackerley lab group past and present you were all a blast to work with. I'd especially like to thank Rory L., Luke, Abbey, Kelsi and Sarah. Thank you for noticing when I was

having a hard time and cheering me on. Your support and friendship helped me more than you know. Mitch and Manu thanks for always taking my hare-brained schemes seriously! You all helped me over the hardest hurdles at the end of my long PhD journey. I can't wait to see where your science and entrepreneurship takes you!

To my wonderful KK702 office crew; Jacob (Master of Ships) you are such a sweetheart and your kind words often lift my spirits. Vaughan (Master of Coin) your cheeky humour brought the whole office together and I can always count on you to have my back. James (Master of Ceremonies) your mischievousness and sage wisdom are always welcome. Kyle (Master of Whispers) your dry wit and networking prowess are awe-inspiring. Sonja you are so strong and creative. Thank you for lending me some of your confidence! Kate and Melz I so admire your initiative and curiosity and I can't wait to see what you do in the future. Jack and Mitch thank you for helping me through those dark days of enormous FACS experiments. It was super fun jamming tunes with you in the office. Jen! I miss having coffee with you. You are so driven and talented, you inspired me to get off my butt and do something to better myself. Izzy we had so many laughs together but I can't remember what was so funny! Thank you for letting borrow some of your feistiness and teaching me to say "duck" with a Northern accent. Rory B! It was a pleasure to watch you grow as a scientist and leader! Thank you for your stalwart friendship and the many cups of tea. And last but not least fabulous Fabian – let's kill more trolls with great swords and glaives again soon!

To my new workmates at IPONZ Ryan, Kimberley and especially my manager Gaby – thank for taking care of me and helping me to finish my thesis even while working fulltime.

To my parents, Mum and Dad I hope you are both happy. I know you always say you were already proud of me but now I have finally finished school! Your constant encouragement and love bolstered me throughout my research.

Lastly, to my partner Ruan, there is no way I could have made it without you by my side! I can't count the times you had to scrape my spirit up off the proverbial floor and reassemble me with hot food and anime after a long hard day in the lab. I can't wait to go on more adventures with you!

Contents

Abstract	i
Acknowledgements	iii
Figures	xvii
Tables	xxi
1 Introduction	1
1.1 Obstacles for current cancer therapies	1
1.2 Targeted cancer therapies	2
1.2.1 Viral cancer therapy	2
1.2.1.1 Clinical advance in virotherapy	3
1.2.2 Bacterial cancer therapy	3
1.2.2.1 Mechanisms of target bacterial cancer therapy	5
1.2.2.2 Advance of oncolytic bacterial cancer therapy	6
1.3 Gene Directed Enzyme Prodrug Therapy	7
1.3.1 The bystander effect	8
1.3.2 GDEPT enzyme/prodrug partnerships	9
1.3.2.1 Thymidine kinase/ganciclovir	9
1.3.2.2 Cytosine deaminase/ 5-fluorocytosine	10
1.3.2.3 Cytochrome P450/ oxazaphosphorines	11
1.3.2.4 Nitroreductase/nitroaromatic prodrug	11
1.4 Nitroreductases	11
1.4.1 Nitroreductase reduction mechanism	11
1.4.2 Historic partnership: <i>E. coli</i> NfsB/CB1954	14
1.4.2.1 Genotoxic mechanisms of CB1954	14
1.4.2.2 Bystander effect of CB1954	15

1.4.2.3	Barriers to clinical <i>E. coli</i> NfsB/CB1954-----	16
1.4.3	Discovery of nitroreductases for GDEPT-----	16
1.4.3.1	<i>Neisseria meningitidis</i> NfsB -----	17
1.4.3.2	<i>E. coli</i> NfsA -----	17
1.4.3.3	Library of 47 wild-type oxidoreductases -----	18
1.4.4	Engineering of nitroreductases for GDEPT-----	18
1.4.4.1	Directed evolution of nitroreductases-----	18
1.4.4.1.1	Directed evolution of nitroreductases for improved CB1954 reduction 20	
1.4.4.1.2	Novel screens for directed evolution of nitroreductases-----	22
1.4.4.1.2.1	SOS-R2 screening strain -----	23
1.4.4.1.2.2	SOS-R4 screening strain -----	24
1.4.4.1.2.3	High-throughput screening with SOS-R4 -----	25
1.5	Next generation nitroaromatic prodrugs-----	27
1.5.1	Hypoxia activated prodrugs -----	27
1.5.1.1	PR-104A -----	27
1.5.1.1.1	Clinical trials of hypoxia activated PR-104 -----	28
1.5.1.1.2	Oxic activation of PR-104 -----	29
1.5.1.1.3	Nitroreductase activated PR-104A-----	29
1.5.2	Alternative next generation prodrugs-----	30
1.6	Measuring the bystander effect -----	32
1.6.1	A multilayer human carcinoma bystander effect assay -----	32
1.6.1.1	Bystander effect of PR-104A-----	33
1.6.1.2	Bystander effect of CB1954 and analogues -----	34
1.6.1.3	Bystander effect of nitro-CB-DEI-----	34
1.6.2	Importance of bacterial bystander effect -----	36

1.7	Thesis aims	37
2	Methods	39
2.1	Chemicals and growth media	39
2.2	Software	39
2.3	Wild-type Nitroreductases used in this study	40
2.4	Oligonucleotide primers	40
2.5	Bacterial strains and plasmids	42
2.5.1	Bacterial strains	42
2.5.2	2.4.2 Bacterial sources of genomic DNA	43
2.5.3	Plasmids	43
2.6	Growth media	46
2.6.1	Liquid media	46
2.6.2	Solid Media	46
2.6.3	Bacterial antibiotics and indication agents	47
2.7	Growth and storage of bacterial strains and variants	47
2.8	Cloning methods & routine molecular biology	47
2.8.1	Isolation of plasmid DNA	47
2.8.2	Polymerase chain reaction (PCR) protocol	48
2.8.2.1	Protocol for PCR with Biomix™ Red	48
2.8.2.2	Protocol for PCR with Phusion™	49
2.8.3	DNA product purification	50
2.8.4	DNA quantification	50
2.8.5	DNA Sequencing	50
2.8.6	Agarose gel electrophoresis	51
2.8.7	Restriction digests	51
2.8.8	Ligation	52

2.8.9	Transformation of <i>E. coli</i> -----	53
2.8.9.1	Preparation of electrocompetent cells used between 2014-2017 (Chapters 3-4)-----	53
2.8.9.2	Preparation of electrocompetent cells used between 2018-2019 (Chapter 5)-----	54
2.8.9.3	Transformation of electrocompetent cells -----	54
2.8.9.4	Preparation of chemically competent cells 2014-2017 (Chapters 3-4)	55
2.8.9.5	Preparation of chemically competent cells 2018-2019 (Chapter 5) ---	55
2.8.9.6	Transformation into chemically competent cells -----	56
2.8.10	SDS-PAGE -----	57
2.9	Protein expression culture and cell lysis -----	59
2.9.1	Long over-expression protein culture -----	59
2.9.1.1	Pressure based cell lysis: French Press method -----	60
2.9.2	Short expression protein culture -----	60
2.9.2.1	Chemical cell lysis: BugBuster®-----	61
2.9.3	Protein purification by Immobilised metal affinity chromatography (IMAC)	61
2.9.3.1	IMAC protein purification with a peristaltic pump -----	61
2.9.3.2	FMN incubation and de-salting -----	63
2.9.4	Purified protein quantification-----	64
2.9.5	Protein storage-----	64
2.10	Purified Enzyme Kinetics -----	64
2.11	Bacterial fluorescence and growth assays-----	65
2.11.1	SOS-GFP screening assay -----	65
2.11.2	Bacterial growth inhibition screening assay-----	66
2.11.3	Bacterial IC ₅₀ inhibition screening assay -----	66
2.12	Bacterial bystander effect assays and preparations -----	67

2.12.1	Bacterial bystander assay	67
2.12.2	Bacterial bystander effect flow cytometry procedures	70
2.12.3	Prodrug pre-activation assay	70
2.13	Bacterial bystander effect FACS assays and preparations	72
2.13.1	Setting the collection gates and sample preparation for FACS	72
2.13.2	Recovery of cells post-FACS	73
2.13.3	Diagnosing expression of <i>nfsA</i> in samples recovered from FACS	73
2.14	FACS nitroreductase library selection	74
2.14.1	Preparation of 7SM library for FACS with CB1954 selection pressure	74
2.14.2	FACS of 7SM library under CB1954 selection pressure	74
2.14.3	FACS of 7SM library under CB1954 selection pressure collected in 384 microtitre plates	74
2.14.4	FACS of 7SM library under CB1954 selection pressure collected into microcentrifuge tubes	75
2.14.5	Screening cells collected from FACS for activity with CB1954	75
2.14.5.1	Making and storing primary screening plates from cells collected in 384 well plates	75
2.14.5.2	Making and storing primary screening plates from cells collected into microcentrifuge tubes	75
2.14.5.3	Creating hit plates from primary screening plates	76
2.15	Pre-selection of nitroreductase libraries using positive selection compounds	76
2.16	HPLC identification of CB1954 nitroreduction products	77
3	Evaluating the abilities of diverse nitroaromatic prodrug metabolites to exit a model Gram negative vector for bacterial-directed enzyme-prodrug therapy	79
3.1	Overview	79
3.1.1	Aims:	80
3.2	Introduction	80

3.2.1	Key terminology for the bacterial bystander effect assay	80
3.3	Results	81
3.3.1	Bacterial bystander effect assay design, optimization and execution	81
3.3.1.1	Design: Prodrugs, bacterial strains, genes and plasmids	81
3.3.1.2	Optimizing the bacterial bystander effect assay	82
3.3.1.2.1	Selecting prodrug concentrations for bacterial bystander microtitre plate assay	82
3.3.1.2.2	Selecting appropriate prodrug concentrations for the bacterial bystander assays in 384 well microtitre plates	83
3.3.2	SOS and bacterial bystander assays in 384 well microtitre plates	87
3.3.2.1	Results of the bacterial bystander microtitre assay	87
3.3.3	Bacterial bystander assays in flow cytometry	89
3.3.3.1	Results of the bacterial bystander flow cytometry assay	89
3.3.4	The bystander effect of CB1954 is dependent on the reduction product(s)	93
3.3.5	Prodrug pre-activation assay	97
3.4	Discussion	100
4	Assessing the impact of the bystander effect on directed evolution of nitroreductases via SOS-GFP selection	104
4.1	Overview	104
4.1.1	Aims:	105
4.2	Introduction	105
4.2.1	Key Terminology	106
4.3	Results	109
4.3.1	Designing an assay to measure the impact of the bystander effect on FACS enrichment	109
4.3.1.1	Setting the collection gates and sample preparation for FACS	111
4.3.1.2	Recovery of cells post-FACS	111

4.3.1.3	Diagnosing expression of <i>nfsA</i> in samples recovered from FACS ----	112
4.3.2	Yield of <i>nfsA</i> -expressing clones recovered from FACS using prodrugs of a high bacterial bystander effect potential -----	114
4.3.3	4.3.6 GFP profiles of bacterial populations in the collection gate under different conditions-----	118
4.3.4	Yield of <i>nfsA</i> -expressing clones recovered from FACS using alternative concentrations of prodrugs -----	119
4.3.4.1	Evidence for artefactual inflation of the influence of the bystander effect on FACS under the 50 μ M SN27686 treatment-----	122
4.3.4.2	Exogenous protein expression inhibits growth of <i>nfsA</i> -expressing activators	126
4.3.5	Results of diagnosing expression of <i>YfkO</i> in samples recovered from FACS	128
4.4	Discussion-----	130
5	Chapter 5: Comparison of a manual positive pre-selection method to an automated FACS screening method for recovery of <i>E. coli</i> NfsA variants improved in CB1954 activation	134
5.1	Overview-----	134
5.1.1	Aims:-----	135
5.2	Introduction-----	136
5.2.1	Choosing the prodrug CB1954 for this investigation -----	138
5.2.2	NfsA <i>E. coli</i> site saturation mutagenesis library -----	138
5.2.3	Key terminology-----	139
5.3	Results-----	140
5.3.1	Results of FACS screening the 7SM library to recover superior CB1954-activating variants-----	140
5.3.1.1	Preparation of 7SM library for FACS with CB1954 selection pressure	140

5.3.1.2	FACS of 7SM library under CB1954 selection pressure collected in 384 microtitre plates-----	140
5.3.1.3	FACS of 7SM library under CB1954 selection pressure collected into microcentrifuge tubes-----	141
5.3.1.4	Screening cells collected from FACS for activity with CB1954 -----	141
5.3.2	Selection pressure: evaluating the effects of CB1954 challenge on variants during FACS -----	143
5.3.3	Identifying the top twenty nitroreductase variants from the FACS strategy	145
5.3.3.1	Characterisation of the top twenty nitroreductase variants from the FACS strategy-----	145
5.3.3.1.1	IC ₅₀ analysis of the top twenty variants isolated by the FACS strategy	146
5.3.3.1.2	Sequence analysis of the top twenty variants isolated by the FACS strategy	147
5.3.4	Results of the niclosamide and chloramphenicol pre-selection of the 7SM library for variants exhibiting superior activation of CB1954-----	148
5.3.4.1	Analysing the top twenty nitroreductase variants from the niclosamide/chloramphenicol pre-selection strategy -----	152
5.3.4.1.1	IC ₅₀ analysis of top twenty variants from pre-selection strategy -	154
5.3.4.1.2	Sequence analysis of top twenty variants from pre-selection strategy	155
5.3.5	CB1954 enzyme kinetics with purified protein of the top five variants from each screening approach -----	158
5.3.6	HPLC analysis of the reduced metabolites from the top five variants -----	161
5.4	Discussion-----	166
5.4.1	Outcomes of directed evolution of 7SM library for activity with CB1954 -	166

5.4.2	Considerations in comparing FACS to pre-selection strategies for directed evolution of nitroreductases-----	167
6	Evaluating a panel of nitroreductases for potential applications in <i>Clostridia</i> -directed enzyme prodrug therapy-----	169
6.1	Overview-----	169
6.1.1	Aims:-----	170
6.2	Introduction-----	170
6.2.1	Expressing nitroreductases in <i>Clostridium</i> -----	171
6.2.2	Selecting panel of nitroreductase enzymes-----	172
6.2.3	Prodrug candidates for CDEPT-----	174
6.3	PR-104A Analysis-----	176
6.3.1	Protein purification and steady state enzyme kinetics-----	176
6.3.2	PR-104A steady-state kinetic parameters-----	177
6.3.3	PR-104A IC ₅₀ assay-----	179
6.4	SN36506 Analysis-----	181
6.4.1	SN36506 steady-state kinetic parameters-----	181
6.4.2	SN36506 IC ₅₀ assay-----	183
6.5	Alternative mustard prodrugs tested in bacterial bystander assays-----	185
6.5.1	Testing next generation prodrugs in the bacterial bystander effect assay	186
6.5.2	Activator strain with functional TolC efflux pump-----	188
6.5.2.1	Retesting PR-104A and analogues with a tolC expressing activator strain	188
6.5.2.2	Retesting CB1954 and nitro-CBI-DEI with a tolC functional activator strain	189
6.6	Discussion-----	191
6.6.1	Evaluation of PR-104A and SN36506 activity across a panel of nitroreductases	191

6.6.2	Bacterial bystander effect assays with next generation prodrugs using activator strains that express a functional TolC efflux pump-----	193
7	Key findings, conclusions and future directions -----	195
7.1	Research motivation -----	195
7.2	Summary of key findings -----	197
7.2.1	Evaluating the abilities of diverse nitroaromatic prodrug metabolites to exit a model Gram-negative vector for bacterial-directed enzyme-prodrug therapy ----	197
7.2.2	Assessing the impact of the bystander effect on directed evolution of nitroreductases using a SOS-GFP screening strain -----	198
7.2.3	Comparing a manual pre-selection method to FACS for recovery of <i>E. coli</i> NfsA variants improved in CB1954 activation-----	199
7.2.4	Evaluating a panel of nitroreductases for potential applications in <i>Clostridia-directed</i> Enzyme Prodrug Therapy-----	201
7.3	Critical evaluations of methods used in this research -----	203
7.3.1	Development of the bacterial bystander model-----	203
7.3.2	Investigating the effect of the bacterial bystander effect on FACS selection efficiency -----	205
7.3.3	Comparing directed evolution outcomes using two different screening strategies: FACS and pre-selection-----	207
7.4	Future directions -----	208
7.4.1	BDEPT with CB1954 -----	208
7.4.2	Bacterial bystander effect model with other BDEPT vectors -----	208
7.4.3	Developing a bystander effect model of CDEPT with carcinoma cells -----	209
7.4.4	Further optimizing FACS for future nitroreductase directed evolution ----	211
7.4.5	Optimizing bacterial vectors for BDEPT-----	212
7.5	Concluding remarks and recommendations for immediate future work -----	213
	References cited -----	214

Appendices -----	230
Appendix A: Supplementary material Chapter 4 - Number of recovered activator and recipient cells for bystander and null bystander conditions from as model library subjected to FACS -----	230
Appendix B: Supplementary material Chapter 5 – SDS-PAGE gel of purified His6-tagged CB1954 improved nitroreductase variants -----	235
Appendix C: Supplementary material Chapter 6 - Michaelis-Menten curves derived from reduction of PR-104A and SN36506 by purified His6-tagged nitroreductases -	236

Figures

Figure 1.1. Schematic illustration of VDEPT-----	8
Figure 1.2 Schematic of type 2 and type 1 reduction of a nitroaromatic substrate proceeding via either consecutive 1-electron or 2-electron steps.-----	13
Figure 1.3 Mechanism of activation and genotoxicity of metabolites of CB1954. -----	15
Figure 1.4 Direct positive selection for active nitroreductases from large-scale mutant libraries via the SOS-triggered bacteriophage λ lytic cycle. -----	22
Figure 1.5 <i>E. coli</i> SOS assays used to monitor the activity of nitroreductases with nitroaromatic prodrugs.-----	23
Figure 1.6 The SOS-GFP screen detects DNA damage within <i>E. coli</i> reporter cells.-----	25
Figure 1.7 FACS selects active nitroreductase variants from large-scale mutant libraries. -----	26
Figure 1.8 Mechanism of activation and genotoxicity of metabolites of PR-104A. -----	28
Figure 1.9 Chemical structure of the 5-nitroimidazole prodrug metronidazole-----	32
Figure 1.10 Representation of the bystander effect in vivo during virus-directed enzyme-prodrug therapy (VDEPT).-----	33
Figure 1.11 Representation of the bystander effect in vivo during bacterial-directed enzyme-prodrug therapy (BDEPT).-----	36
Figure 2.1 Plasmid map of nitroreductase expression vector pUCX.-----	44
Figure 2.2 Plasmid map of SOS-inducible GFP plasmid pANODuet-1: GFP.-----	44
Figure 2.3 Plasmid map of expression vector pET28a+, used for His6-tag protein expression and expression of multi-genomic DNA in this study.-----	45
Figure 2.4 Plasmid map of pCDF-Duet 1 used to provide spectinomycin resistance to 7NT cell strains.-----	45
Figure 3.1 Schematic of the “bacterial bystander assay” to quantify bacterial cell-to-cell transfer of genotoxic metabolites.-----	82
Figure 3.2 Identification of prodrug concentrations resulting in <20% growth inhibition of nitroreductase-expressing activator cells.-----	84
Figure 3.3 Relative GFP fluorescence of <i>nfsA</i> -expressing SOS-R4 exposed to different prodrugs.-----	85
Figure 3.4 Relative GFP fluorescence of nitroreductase null SOS-R4 recipients exposed to different prodrugs. -----	86

Figure 3.5 Microplate assay of SOS response induced by transfer of activated	88
Figure 3.6 Overlay flow cytometry histograms of test and control conditions assessing the DNA damage caused by transfer of activated prodrug metabolites from <i>nfsA</i> -expressing 7NT activator cells to nitroreductase null SOS-R4 reporter cells.	91
Figure 3.7 Mean increase in GFP signal of test condition over control condition in flow cytometry analysis.	92
Figure 3.8 Overlay histograms of test and control conditions for a 50% activator cell population in Flow cytometry analysis of DNA damage caused by transfer of activated prodrug metabolites from <i>nfsA</i> , <i>nfsB</i> or <i>yfkO</i> -expressing 7NT activator cells.	95
Figure 3.9 Mean increase in GFP signal of test condition over control condition for a 50% activator cell population in flow cytometry analysis.	95
Figure 3.10 Mean increase in GFP signal of test condition over control condition for a 10% activator cell population in flow cytometry analysis.	96
Figure 3.11 Overlay histograms of test and control conditions for a 10% activator cell population.	96
Figure 3.12 Microplate assay of SOS response induced by transfer of pre-activated prodrug metabolites to nitroreductase null SOS-R4 reporter cells.	99
Figure 3.13 Retrospective reanalysis of microplate assay of SOS response induced by transfer of pre-activated prodrug metabolites to nitroreductase null SOS-R4 reporter cells.	100
Figure 4.1 Assay design for detecting the bystander effect during FACS. (108
Figure 4.2 Chemical structure of niclosamide.	112
Figure 4.3 Validation of niclosamide as a compound to diagnose presence or absence of nitroreductase post-FACS.	113
Figure 4.4 Average percentage yield of <i>nfsA</i> -expressing activator cells for all prodrug and bystander and null bystander conditions as diagnosed using niclosamide.	117
Figure 4.5 Overlay histograms of the GFP profiles recorded in the collection gate of the bystander (yellow) and null bystander (blue) conditions.	119
Figure 4.6 Average percentage yield of <i>nfsA</i> -expressing activator clones for CB1954 10 μ M, SN27686 at 50 μ M and PR-104A at 40 μ M for both bystander and null bystander conditions as diagnosed by niclosamide.	121

Figure 4.7 Overlay histograms of the GFP profiles recorded in the collection gate of the bystander (yellow) and null bystander (blue) conditions. -----	122
Figure 4.8 Analysis of GFP profiles recorded from the controls used to set the stringency of the collection gates prior to FACS.-----	125
Figure 4.9 Average percentage of SOS-R4 cells expressing pUCX nfsA (activators) or pUCX Empty (recipients in samples taken at hourly intervals from a co-culture.-----	128
Figure 4.10 Average percentage yield of yfkO expressing cells, as diagnosed by niclosamide, recovered from FACS post challenge with 50 μ M CB1954. -----	129
Figure 5.1 Chemical structure of the pre-selection compound chloramphenicol. -----	137
Figure 5.2 Fold-GFP induction of <i>E. coli</i> expressing 7SM variants post FACS selection. 144	
Figure 5.3 Comparison of growth inhibition by 50 μ M CB1954 in 7SM variants derived from the pre-selection on solid medium under no selection pressure or positive selection pressure. -----	152
Figure 5.4 Frequency of different of amino acid categories occurring, based on general chemo-descriptive group, at the key seven active site residues in the top twenty variants derived from each screening strategy.-----	157
Figure 5.5 Michaelis-Menten curves used to calculate the kinetic parameters of the purified proteins, of the top performing variants, with CB1954. -----	161
Figure 5.6 Illustrates the colour change that can be observed in the top twenty variants from each screening strategy -----	163
Figure 5.7 HPLC analysis of reaction products of CB1954 reduction by purified nitroreductase variants-----	164
Figure 6.1 Chemical structure of the next generation prodrug SN36506. -----	175
Figure 6.2 Michaelis-Menten curves derived from reduction of SN36506 by purified His6-tagged (A). NfrA_Bs, (B). NfsA_Ec. -----	183
Figure 6.3 Chemical structures of additional mustard prodrugs tested in the bacterial bystander effect assay SN27686 and SN31609.-----	186
Figure 6.4. Microplate assay of the SOS response induced by transfer of activated prodrug metabolites from nfsA-expressing 7NT activator cells to nitroreductase null SOS-R4 reporter cells using alternative next generation prodrugs. -----	187

Figure 6.5 Microplate assay of SOS response induced by transfer of activated prodrug metabolites from *nfsA*-expressing 7KO activator cells to nitroreductase null SOS-R4 reporter cells using next generation prodrugs ----- 189

Figure 6.6 Microplate assay of SOS response induced by transfer of activated prodrug metabolites from *nfsA*-expressing 7KO activator cells to nitroreductase null SOS-R4 reporter cells using prodrugs CB1954 and nitro-CBI-DEI.----- 190

Appendices

Figure B 1 SDS-PAGE gel of purified CB1954 improved nitroreductase variants -----235

Figure C 1 Michaelis-Menten curves derived from reduction of PR-104A by purified His6-tagged *NfsA* nitroreductase candidates. (A). *NfrA_Bs*, (B). *NfsA_E*, (C). *NfsA_Es*, (D). *YcnD_Bs*----- 236

Figure C 2 Michaelis-Menten curves derived from reduction of PR-104A by purified His6-tagged *NfsB* nitroreductase candidates. (A). *NfsB_Ec*, (B). *NfsB_Vv*, (C). *NfsB_Vv* F70A/F108Y mutant (D). *Ydgl_Bs*.----- 237

Figure C 3 Michaelis-Menten curves derived from reduction of PR-104A by purified His6-tagged *NfsB* nitroreductase candidates (A). *NfsB_Nme*, (B). *YfkO_Bli*, (C). *YfkO_Bs*, (D). *YfkO_Bs* mutant 1-88, (E). *YfkO_Bs* mutant 3-62. ----- 238

Figure C 4 Menten curves derived from reduction of SN36506 by purified His6-tagged *NfsA* nitroreductase candidates. (A). *NfsA_Es*, (B). *YcnD_Bs*. ----- 239

Figure C 5 Michaelis-Menten curves derived from reduction of SN36506 by purified His6-tagged *NfsB* nitroreductase candidates. (A). *NfsB_Vv*, B. *NfsB_Vv* F70A/F108Y mutant (C). *Ydgl_Bs*, (D). *YfkO_Bs* mutant 1-88, (E). *YfkO_Bs* mutant 3-62. ----- 240

Tables

Table 1.1 Summary of Bystander Effect Efficiency (BEE) experiments in the multilayer carcinoma model and the relevant prodrug. -----	35
Table 2.1 Summary of ten wild-type nitroreductase enzymes used in this investigation.	40
Table 2.2 Summary of primers used in this investigations.-----	41
Table 2.3 Bacterial strains used in this study, key features and origins. -----	42
Table 2.4 Bacterial strains used as sources of genomic DNA in this study. -----	43
Table 2.5 Plasmids used for cloning.-----	43
Table 2.6 Liquid media used in this study. -----	46
Table 2.7 Antibiotics used in this investigation.-----	47
Table 2.8 Components for colony PCR with Biomix™Red. -----	49
Table 2.9 Thermal cycling parameters for colony PCR with Biomix™Red. -----	49
Table 2.10 Components for high-fidelity PCR with Phusion™ high-fidelity polymerase. -	50
Table 2.11 Thermal cycling parameters for high-fidelity PCR with Phusion™ high-fidelity polymerase. -----	50
Table 2.12 Components for restriction digest. -----	52
Table 2.13 Ligation protocol with T4 DNA ligase.-----	52
Table 2.14. Recipes for transformation buffers-----	56
Table 2.15 Summary of SDS-PAGE reagents and their components.-----	59
Table 2.16 Protein purification buffers.-----	63
Table 2.17 Summary of bacterial strains and relevant plasmids used in the bacterial bystander assays. -----	69
Table 4.1 Average number of recovered activator and recipient clones for bystander and null bystander conditions (as diagnosed using niclosamide) for all prodrug conditions. -----	115
Table 4.2 Average percentage of recovered nfsA-expressing activator and recipient clones for bystander and null bystander conditions. -----	116
Table 4.3 Average percentage of recovered yfkO-expressing activator and recipient cells for bystander and null bystander conditions. -----	129
Table 5.1 Summary of primary screening plates prepared from the FACS screening strategy.-----	143
Table 5.2 Top twenty nitroreductase variants, isolated by the FACS strategy. -----	146

Table 5.3 Sequence analysis of the top twenty NfsA variants from the FACS at the seven targeted amino acid sites. -----	147
Table 5.4 Summary of primary screening plates derived from pre-selection strategy.-	150
Table 5.5 Top twenty nitroreductase variants, isolated by the pre-selection strategy.	154
Table 5.6 Sequence analysis of the top twenty NfsA variants from the pre-selection strategy at the seven targeted amino acid sites. -----	155
Table 5.7 Kinetic parameters with CB1954 of the top three variants from the FACS screening strategy (3.2C, 2.2C, 3.2F) and the top two variants from the niclosamide/chloramphenicol pre-selection strategy (1.5C, 1.9C). -----	159
Table 6.1 Panel of nitroreductase candidates selected for investigation for potential CDEPT.-----	174
Table 6.2 Kinetic parameters for the reduction of PR-104A by a panel of purified His6-tagged nitroreductase candidates for investigation for a CDEPT strategy.-----	179
Table 6.3 IC ₅₀ values of prodrug PR-104A mediated growth inhibition of candidate nitroreductases.-----	180
Table 6.4 Kinetic parameters for the reduction of SN36506 by a panel of purified His6-tagged nitroreductase candidates for investigation for a CDEPT strategy.-----	182
Table 6.5 IC ₅₀ values of prodrug SN36506 mediated growth inhibition of candidate nitroreductases.-----	184

Appendices

Table A 1 Number of recovered activator and recipient cells for bystander and null bystander conditions (number of nfsA-expressing activator cells as diagnosed by niclosamide for all prodrug conditions).....	234
---	-----

List of abbreviations and definitions

5-FC	5-fluorocytosine
5-FU	5-fluorouracil
7SM	NfsA <i>E. coli</i> seven site saturation mutagenesis library
ACSRC	Auckland Cancer Society Research Centre
AKR1C3	Aldo-keto reductase 1C3
Amp	Ampicillin
BDEPT	Bacterial-directed enzyme prodrug therapy
BEE	Bystander Effect Efficiency
C10	10% of controls
CD	Cytosine deaminase
CDEPT	Clostridia-directed enzyme prodrug therapy
CYP	cytochrome P450
ddH₂O	Double-distilled H ₂ O
DMSO	Dimethyl sulfoxide
DNBM	dinitrobenzamide mustards
EDTA	Ethylenediaminetetraacetic acid (disodium salt)
epPCR	Error-prone polymerase chain reaction
FACS	Fluorescence-activated cell sorting
FMN	Flavin mononucleotide
GFP	Green fluorescent protein
GDEPT	Gene-directed enzyme prodrug therapy
gDNA	Genomic DNA
GM-CSF	Granulocyte-macrophage colony-stimulating factor
GCV	Ganciclovir
HSV-tk	Herpes simplex virus-thymidine kinase
IC₅₀	Concentration of a drug at which 50% cell growth or cell survival is detected relative to an unchallenged control.
IMAC	Immobilised metal affinity chromatography
IPTG	Isopropyl β-D-1-thiogalactopyranoside
Kan	Kanamycin
Kb	Kilobase
<i>k_{cat}</i>	Kinetic constant describing theoretical maximum rate of catalysis for a specific enzyme with a specific substrate, under the conditions tested
kDa	Kilodalton
<i>K_m</i>	Kinetic constant describing the concentration of substrate at which the rate of catalysis of a specific enzyme is exactly half of the <i>k_{cat}</i> , under the conditions tested
MCS	Multiple-cloning site
mmHg	Millimetre of mercury is a manometric unit of pressure. Defined as the extra pressure generated by a column of mercury one millimetre high.
MTD	Maximum tolerated dose
NADH	Nicotinamide adenine dinucleotide (reduced)

NADPH	Nicotinamide adenine dinucleotide phosphate (reduced)
NDT	Degenerate codon (N: adenine/cytosine/guanine/thymine; D: adenine/guanine/thymine, T: thymine)
NNK	Degenerate codon (K: guanine/thymine)
Nitro-CBI-DEI	Nitrochloromethylbenzindoline
OD₆₀₀	Optical density at 600nm wavelength
PCR	Polymerase chain reaction
PET	Positron emission tomography
Spec	Spectinomycin
VDEPT	Viral-directed enzyme prodrug therapy

1 Introduction

1.1 Obstacles for current cancer therapies

Cancer is the leading cause of death in New Zealand, accounting for nearly one third of mortalities. Around 23,000 New Zealanders per year are diagnosed with cancer, of whom 10,000 will die of their disease. Between 2007 and 2016 the incidence of cancer has risen by 21%. The incidence of cancer is predicted to surpass 50,000 per year by 2040 (NZ Ministry of Health, 2019).

Cancer incidence and mortality is also accelerating worldwide. By 2040, 22 million new cases of cancer will be diagnosed annually across the globe (WHO IARC, 2014). This acceleration is attributed to an aging population with a longer life expectancy and greater exposure to risk factors including smoking, obesity and synthetic chemicals (American Cancer Society, 2020).

Conventional cancer treatments include surgery, chemotherapy and radiation. Surgical removal is the most common and successful approach, but some tumours are inoperable or favour relapse (Duarte et al., 2012). Chemotherapy and radiation therapy for advanced cancer tend to bring remission and resistance accompanied by increased disease aggression (Breitbach et al., 2010).

Chemotherapy uses chemical agents to kill cancer cells directly by inducing DNA damage or halt the cell cycle. However, disordered tumour vasculature prevents efficient biodistribution thus promoting survival of cancer cells furthest from the vasculature (Dachs et al., 2009). Quiescent cancer stem cells rarely divide and are resistant to chemotherapies that target rapidly dividing cells (Duarte et al., 2012).

Radiation therapy directs a beam of high energy ionizing radiation, triggering localized DNA damage and apoptosis (NIH National Cancer Institute, 2019). Radioresistance is caused by metastasis and repopulation by surviving cancer stem cells (Al-Dimassi et al., 2014). Hypoxic regions in solid tumours, caused by disordered vasculature, are resistant to radiation.

Typical chemo- and radiotherapy cannot discriminate between healthy cells *versus* cancerous cells. For instance a chemotherapy, that targets rapidly dividing cancer cells, can have off-target side effects on healthy cells such as epithelial cells in the gastrointestinal tract that normally rapidly divide. This causes the severe nausea that chemotherapy patients can experience (NIH National Cancer Institute, 2015).

1.2 Targeted cancer therapies

There is a need for effective, targeted cancer therapies that eliminate cancer cells while leaving healthy cells unharmed. These therapies must be able to penetrate poorly vascularized solid tumours, retain activity under hypoxia, and overcome the DNA repair enzymes and apoptotic avoidance mechanisms that are commonly overexpressed in cancer (Al-Dimassi et al., 2014).

One solution uses naturally oncolytic and tumour-seeking bacterial or viral pathogens to launch a multi-pronged gene-directed chemotherapy on tumours. Gene therapies have been developed to selectively introduce genetic material to tumours that will direct therapy inside target cells. Such gene therapies exploit biochemical, molecular or environmental characteristics of tumours to distinguish them from normal tissues.

1.2.1 Viral cancer therapy

Oncolytic viruses can directly lyse cancer cells and activate long-term antitumor immune responses. In the early twentieth century, reports of spontaneous cancer regression coinciding with viral infection led to clinical trials of virotherapy. In 1910, the Pasteur-Roux vaccine of live attenuated rabies was used to treat cervical cancer (Fountzilias et al., 2017). These pioneering experiments were perilous, causing viral infection of healthy tissue, but they paved the way for the future of virotherapy (Cattaneo et al., 2008; Holay et al., 2017).

Naturally oncolytic viruses preferentially replicate inside of tumours, while sparing healthy cells, because the tumour environment is comparatively immune privileged and nutrient rich. Oncolytic viruses typically enter cells by binding specific cell surface receptors, which may be upregulated in certain cancers. Genetically engineering viruses for enhanced cancer specificity can increase the safety and efficacy of naturally oncolytic viruses (Cattaneo et al., 2008; Fountzilias et al., 2017).

1.2.1.1 Clinical advance in virotherapy

Significant clinical advancement of virotherapy has been made using several viruses; adenovirus, herpes simplex virus, reovirus and vaccinia virus. For example, ONYX-015, an adenovirus, was the first oncolytic virus to undergo clinical trial. ONYX-015 targets cancer cells that have a p53 mutation, based on an E1B deletion that prevents it from inhibiting the active p53 tumour suppressor in healthy cells (Taguchi et al., 2017). ONYX-015 was approved for human use in China in 2006 and is marketed under the brand name Oncorine (Fountzilias et al., 2017).

OncoVex^{GM-CSF} is a type 1 herpes simplex virus that has been engineered to express granulocyte-macrophage colony-stimulating factor (GM-CSF), which recruits dendritic cells to the tumour (Fountzilias et al., 2017). Renamed T-VEC (talimogene laherparepvec), it was approved by the US FDA in 2015 after a successful phase III trial. Branded as IMLYGIC™ it has since been approved in Europe and Australia in 2016 (Taguchi et al., 2017).

Reolysin® is a replication-competent reovirus that targets cancer cells with activated Ras signalling pathways. Active Ras oncogenes occur in about 30% of all human tumours because Ras regulates mitosis. Human reovirus requires an activated Ras signalling pathway for infection (Coffey et al., 1998). In a phase II study of Reolysin® combined with paclitaxel was promising (Bernstein et al., 2018; Fountzilias et al., 2017).

JX-594 is a recombinant Wyeth strain vaccinia virus, combining GM-CSF expression and thymidine kinase deletion (Fountzilias et al., 2017). A phase II trial of JX-594 demonstrated oncolytic and immunotherapy tumour responses and dose-related survival in liver cancer patients (Heo et al., 2013). Thymidine kinase is necessary for a virus to replicate. If the gene is deleted the virus will only be able to replicate inside of cells that express high levels of thymidine kinase such as those found in tumours (Fountzilias et al., 2017).

1.2.2 Bacterial cancer therapy

Advances in improving the specificity and efficacy of virotherapy laid the foundation for modern clinical trials and informed targeted cancer therapies with other microorganisms, such as bacteria. Potential therapeutic payloads for targeted cancer delivery include cytokines, cytotoxic agents, immunomodulators, prodrug-converting enzymes, and small

interfering RNAs (Duong et al., 2019). As with viral oncolysis, by controlling bacterial gene expression anti-cancer therapeutic payloads can be localized to tumour sites and even regulate timing of drug delivery (Duong et al., 2019).

The history of bacterial cancer therapy begins more than four millennia ago, when the ancient Egyptian priest Imohtep, used mystic poultices on his patients before cutting into their tumours. It is believed that these poultices caused bacterial infection that induced beneficial fevers. Around 2000 years later, Parmenides the Greek philosopher recognized fever as a powerful medical tool. Today we know this as raising the patient's immune response to resist disease (Hoption Cann et al., 2003).

The modern era of bacterial cancer therapy commenced in 1891, with Dr William Coley at the New York Memorial Hospital. After losing a young patient to bone cancer Coley ransacked the records of to find cases of spontaneous cancer regression. He found 47 well-documented cases of the beneficial influence of serious bacterial infections in tumour patients (Chorobik et al., 2013). In particular he discovered the case of Fred Stein, who had suffered multiple unsuccessful operations to remove a facial tumour. The surgeons were unable to close the wound and the patient contracted a *Streptococcus* infection, which caused a life-threatening fever. Coley discovered that seven years after his surgery, Stein was still cancer free. Coley determined that the bacterial infection and the resulting high fever was responsible for the cure. He went on to create vaccine of dead bacteria called "Coley's toxins" and treated ~1000 patients who had a ten-year survival rate equivalent to that of cancer patients treated today (Hoption Cann et al., 2003). Due to safety concerns regarding septic shock, radiation and chemotherapy superseded Coley's early work to become the conventional cancer therapies we are familiar with today.

However, research into bacterial cancer therapy has continued throughout the 20th century. In the last few decades, it has been shown that *Salmonella*, *Escherichia*, *Clostridium* and *Bifidobacterium* species preferentially accumulate inside tumours, and *Salmonella* and *Clostridium* species have shown antitumor effect in animal models (Forbes, 2010).

1.2.2.1 Mechanisms of target bacterial cancer therapy

Bacteria possess several characteristics that are attractive for cancer therapy. Bacteria can specifically seek out and target tumours, actively penetrate tissue, express cytotoxins or immune stimulating factors, induce cytotoxicity in response to external signals and be detected *in situ* using fluorescent reporter proteins. Furthermore, bacteria can be easily genetically manipulated to enhance these features (Forbes, 2010; Hoffman, 2011).

Forbes (2010) summarises five mechanisms that influence the accumulation of facultative anaerobes in tumours: entrapment of bacteria in tumours vasculature (Forbes, 2010); bacterial invasion of tumours following inflammation (Leschner et al., 2009); chemotaxis toward compounds produced by tumours (Kasinskas & Forbes, 2006, 2007); preferential growth in tumour-specific microenvironments (Kasinskas & Forbes, 2006; Zhao et al., 2005); and protection from clearance by the immune system (Sznol & Lin, 2000).

Mechanisms of tumour specificity are dependent on the bacterial species. Obligate anaerobes, for example, *Clostridium* and *Bifidobacterium*, cannot tolerate oxygen. Obligate anaerobes germinate only in anoxic regions. Anoxic regions are caused by rapid angiogenesis resulting in poor vasculature inside tumours. Anoxic regions are not common in healthy tissue (Carmeliet & Jain, 2000; Dang et al., 2001). In contrast, facultative anaerobes, e.g. Gram-negative *Salmonella* and *Escherichia*, accumulate inside tumours. These bacteria are self-motile and can be attracted by specific chemical resources inside tumours (Forbes et al., 2003). For example chemotactic receptors direct bacteria to tumours by sensing molecules in the tumour microenvironment such as aspartate or ribose in necrotic tissue (Hoffman, 2011).

Since bacteria can migrate far from the vasculature, bacteria can penetrate tumours to a greater degree than chemotherapeutic molecules that diffuse only passively (Hoffman, 2011). In this manner, bacteria can treat quiescent cancer stem cells that are chemoresistant or escape exposure to chemotherapy. Furthermore, tumours offer an immune-privileged environment where bacteria can replicate unobstructed by normal immune system clearance mechanisms (Forbes, 2010). Crucially bacterial infection can be controlled by antibiotics – a major advantage over viruses. This additional level of safety coupled with the ease of genetic manipulation has made bacteria an attractive option among microorganisms to treat cancer (Lehouritis et al. 2013).

1.2.2.2 Advance of oncolytic bacterial cancer therapy

Coley's legacy has continued into the twenty-first century. In 2012 a phase 1 clinical trial investigating the safety and the dosage of Coley's toxin, presently known as mixed bacterial vaccine, comprises heat-inactivated *Streptococcus pyogenes* and *Serratia marcescens*. Of the twelve patients enrolled, eleven developed fever after administration of the vaccine. This fever led to a massive induction of cytokines that likely induced tumour regression. Six of the patients had a prolonged overall survival but the results did not warrant the use of the vaccine as a monotherapy in a phase II trial (Karbach et al., 2012).

Efforts to more-directly target tumours have focused on the genera *Clostridium* and *Salmonella*, with *Bifidobacterium* and *Listeria* also explored to a lesser extent (Duong et al., 2019). Bacterial species of these genera have been shown to preferentially replicate within solid tumours when injected from a distal site (Hoffman, 2011).

Attenuated *Clostridium novyi-NT* is known for its ability to precisely germinate in and eradicate treatment-resistant hypoxic tumours in animal models (Staedtke et al., 2016). *Clostridium novyi* was identified as a superior strain for anti-neoplastic properties among anaerobic bacteria (Dang et al., 2001). A non-toxic strain, *C. novyi-NT*, was generated by eliminating a phage carrying α -toxin. In a phase I human trial, one patient received *C. novyi-NT* spores injected directly into a target tumour. The treatment resulted in extensive tumour necrosis and formation of an abscess that required surgical removal. Side-effects included an increase in white blood cell count, fever, and pain (Roberts et al., 2014). Use of attenuated *C. novyi-NT* significantly decreased treatment related toxicity, however the mechanism of toxicity and tumour destruction are necessary for an effective therapeutic outcome (Staedtke et al., 2016). Of import, clostridial infection stimulates the immune response by recruiting granulocytes and cytotoxic lymphocytes to the tumour site which significantly increases cytokines and chemokines that promote tumour elimination (Duong et al., 2019). As of 2020, a phase Ib clinical trial of *C. novyi-NT* spores in combination with chemotherapeutics is being recruited for patients with advanced solid tumours (NCT03435952).

Salmonella grows under both aerobic and anaerobic conditions, hence is able to colonize large and small tumours. *Salmonella* naturally identifies and penetrates tumours by

chemotaxis toward small molecule gradients of serine, aspartate, and ribose (Kasinskas & Forbes, 2006, 2007). A *Salmonella typhimurium* amino acid auxotroph was developed, the A1-R mutant, which is auxotrophic for leucine and arginine. These nutrients are derived from dying tumour tissue (Zhao et al., 2005). *S. typhimurium* A1-R selectively grows in necrotic areas of tumours but not normal tissue. *S. typhimurium* A1-R has been tested extensively in animal models of prostate, breast and pancreatic cancer. A1-R was able to effect cures in monotherapy on mouse models of metastatic human cancer (Hoffman, 2011).

VNP20009, a purine- dependent attenuated strain of *S. typhimurium*, showed significant toxicity against murine tumours and was studied in a phase I clinical trial; proving to be safe for use in cancer patients, inadequate tumour colonization by VNP20009 was the major limitation (Chorobik et al., 2013). Overall *Salmonella* strains tested so far have not yet demonstrated robust colonization and therapeutic benefit in preclinical studies. The reason for this is unclear, but over-attenuation has been proposed as a reason (Zhou et al., 2017).

Other individual strains of bacteria that have already been proven safe for use in human treatments have also been explored for anti-tumour activity. For example the non-pathogenic *Escherichia coli* strain Nissle 1917 has exhibited promising tumour-targeting activity in mice (Stritzker et al., 2007). As a licensed probiotic treatment for diarrhoea and colitis it has been extensively characterized and is therefore readily engineered to increase anti-tumour activity (Yu et al., 2019).

In recent years there have been profound advances in the development of viral and bacterial cancer therapies by manipulating and directing the natural oncolytic abilities of these pathogens. However the therapeutic efficacy of these treatments can also be augmented by gene-directed enzyme-prodrug therapy (GDEPT).

1.3 Gene Directed Enzyme Prodrug Therapy

GDEPT leverages the natural potential and innovative engineering of viral and bacterial cancer therapy and unites it with the paradigm of chemotherapy. It is a promising avenue for modern cancer therapy. GDEPT is a targeted cancer therapy that uses viral (VDEPT) or bacterial (BDEPT) vectors to deliver a genetically encoded therapeutic enzyme, which

drives a chemotherapeutic attack directly inside tumours. Other vectors include naked DNA, liposomes or nanoparticles to deliver the therapeutic gene (Duarte et al., 2012).

GDEPT comprises three phases. First, an inert prodrug is systemically administered. Second, viral or bacterial vectors, encoding a prodrug-activating-enzyme, are used to selectively infect tumours. In the case of VDEPT, expression of the enzyme occurs directly within the tumour cells, whereas for BDEPT the enzyme is expressed within the tumour adjacent or internalized bacteria. Third, the expressed enzyme converts the prodrug to a lethal cytotoxin, resulting in a localized chemotherapeutic effect inside the tumour (**Figure 1.1**) (Duarte et al., 2012; Portsmouth et al., 2007; Zhang et al., 2015).

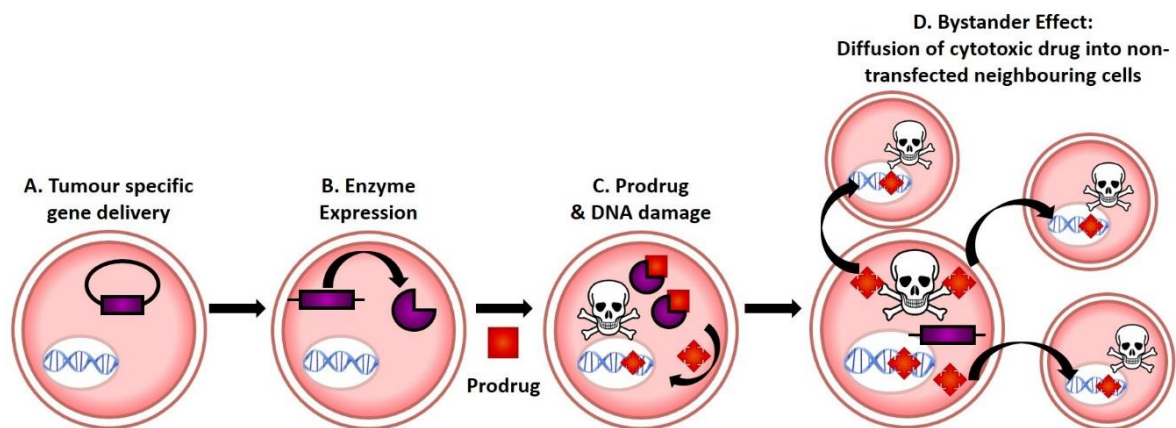


Figure 1.1. Schematic illustration of VDEPT (A) Gene (purple rectangle) delivery mediated by a tumour-tropic vector leads to (B) tumour-specific expression of the encoded enzyme (purple pacman), which is able to convert a prodrug (red square) into a highly cytotoxic form. (C) Following systemic administration, enzyme-mediated conversion of the prodrug leads to toxic effects in transfected cells. (D) Neighbouring non-transfected cells may also be killed due to a local bystander effect. Figure created by me, and first published in Williams et al., (2015).

1.3.1 The bystander effect

The bystander effect is crucial to all GDEPT systems. It occurs when an activated chemotherapeutic diffuses from the cell, expressing the prodrug activating enzyme, into neighbouring tumour cells (Dachs et al., 2009; Wilson et al., 2002). The bystander effect extends the therapeutic effect to the wider tumour environment (Dachs et al., 2009).

Research has found that gene transfer efficiencies are usually less than 10% in the target tissue in a VDEPT scenario (Dachs et al., 2009; Zhang et al., 2015). A superior bystander effect can overcome low expression of a therapeutic gene in GDEPT. Tumour cells that are

not infected by the viral vector can still experience cytotoxicity and death caused by diffusion of the active prodrug (Dachs et al., 2009; Zhang et al., 2015). The bystander effect improves GDEPT cell killing by several fold and is critical to tumour regression (Dachs et al., 2009; Zhang et al., 2015).

A local bystander effect occurs via passive diffusion or active transport of the active cytotoxic drug metabolites, through gap junctions, into neighbouring untransfected cancer cells. In the case of passive diffusion, the local bystander effect can be enhanced by increasing the lipophilicity of the prodrug metabolites (Denny, 2002).

A distant bystander effect is prompted by the natural immunogenic properties of the viral or bacterial vectors in conjunction with the release of tumour antigens from apoptosing cancer cells, raising an immune response against the cancer (Dachs et al., 2009; Zhang et al., 2015). This also known as the “vaccination effect” of GDEPT (Portsmouth et al., 2007).

1.3.2 GDEPT enzyme/prodrug partnerships

After two decades of development the most clinically advanced GDEPT systems are herpes simplex virus thymidine kinase/ganciclovir (HSV-tk/GCV), cytosine deaminase/5-fluorocytosine (CD/5-FC), cytochrome P450/oxazaphosphorines, and nitroreductase/CB1954. As yet no GDEPT product is commercially available.

1.3.2.1 Thymidine kinase/ganciclovir

A viral or bacterial vector that is not dependent on a thymidine kinase deletion for tumour specificity may be used to express the viral HSV-tk gene. HSV-tk is able to metabolize non-toxic ganciclovir (GCV) into GCV-monophosphate, after which cellular kinases convert GCV-monophosphate to GCV-triphosphate. This is an analogue of deoxy-guanosine triphosphate and is incorporated into replicating DNA, causing cell cycle arrest and apoptosis (Duarte et al., 2012; Portsmouth et al., 2007).

HSV-tk/GCV is the only GDEPT combination to have reached phase III human trials (Zhang et al., 2015). In a phase III clinical evaluation, 248 patients, diagnosed with glioblastoma multiforme were used in this study. Over a 12 month time period the HSV-tk/GCV treatment did not significantly improve survival rates compared to the standard therapeutic treatments (Rainov, 2000).

A prostate cancer phase I clinical trial using the HSV-tk/GCV GDEPT system was performed with an adenovirus expressing HSV-tk. A significant prolongation of the median serum prostate-specific antigen doubling time from 2.9 to 6.2 months was detected i.e. it took significantly longer for the tumour antigens to be detected in patients again (Nasu et al., 2007).

Several issues have impacted the advance of HSV-tk/GCV treatment including inefficient viral transfection and off-target side effects in healthy dividing cells that express thymidine kinase (Zhang et al., 2015). Moreover, GCV triphosphate is membrane insoluble, which prevents passive diffusion; transport is limited to gap junctions thereby restricting its local bystander effect (Zhang et al., 2015).

1.3.2.2 Cytosine deaminase/ 5-fluorocytosine

Cytosine deaminase (CD) is a bacterial enzyme that catalyses the hydrolytic deamination of cytosine to uracil. CD converts the prodrug 5-fluorocytosine (5-FC) to 5-fluorouracil (5-FU). Host cell enzymes metabolize 5-FU into pyrimidine antimetabolites, a nucleoside analogue, that when incorporated into DNA during synthesis halts replication. 5-FU is used as a standalone chemotherapeutic but has a low therapeutic index and toxic side-effects (Duarte et al., 2012; Portsmouth et al., 2007).

GDEPT can potentially overcome these drawbacks and has been explored clinically. In pilot tests, an attenuated *Salmonella* strain expressing the *Escherichia coli* CD gene was injected into patients and demonstrated successful colonization of the tumour site and localized CD expression (Nemunaitis et al., 2003). A phase I clinical trial consisting of prostate cancer patients used an oncolytic adenovirus containing the HSV-tk fusion gene as well as a CD gene. In combination with radiation therapy there was a significant decline in prostate specific antigen in all patients (Freytag et al., 2002).

Of note, comparing the CD/5-FC with HSV-tk/GCV systems, the two approaches have similar efficacy in hepatocellular carcinoma, but CD/5-FC was more effective than HSV-tk/GCV for treating renal carcinoma and colorectal carcinoma. The superior effect of CD/5-FC may be attributed to its greater bystander effect. The bystander effect of GCV is dependent on gap junction whereas the bystander effect of 5-FU are mediated by passive diffusion (Zhang et al., 2015).

1.3.2.3 Cytochrome P450/ oxazaphosphorines

Some cytochrome P450 (CYP) enzymes can activate oxazaphosphorine prodrugs to 4-hydroxy metabolites that are alkylating agents. The 4-OH decomposes to phosphoramidate mustards which form DNA cross-links, causing apoptosis (Portsmouth et al., 2007; Zhang et al., 2015).

A phase I clinical trial used a retroviral vector that encoded CYP2B6, in combination with chemotherapy, was used to treat advanced breast cancer or melanoma. The trial demonstrated tolerability and safety, and expression of the CYP2B6 gene in cancer cells (Braybrooke et al., 2005).

Cytochrome P450 enzymes are also capable of oxidising many other xenobiotic compounds. This includes N-oxides and furan derivatives each of which have demonstrated anti-cancer activity in a GDEPT strategy with at least one cytochrome P450 enzyme *in vivo* (Huttunen et al., 2008).

1.3.2.4 Nitroreductase/nitroaromatic prodrug

Nitroreductases are promiscuous flavin-associated oxidoreductase enzymes, defined by their ability to reduce nitro substituents. Nitroreductases convert nitroaromatic prodrugs to DNA-damaging metabolites that are cytotoxic to both quiescent and actively dividing tumour cells (Denny, 2002; Williams et al., 2015). Nitroreductase GDEPT does not rely on the use of nucleotide analogues which are only effective at killing actively dividing cells - an advantage over ganciclovir and 5-FU.

The focus of this thesis is the evaluation of bacterial nitroreductase/nitroaromatic prodrug partnerships for use in a bacterial vector. Many advances have been made using a nitroreductase/nitroaromatic prodrug partnership. These are explored in more detail in the following section.

1.4 Nitroreductases

1.4.1 Nitroreductase reduction mechanism

The nitroreductase family is divided into two classes based on their mechanisms of electron transfer to substrates. Type 1 nitroreductases are oxygen-insensitive; generating nitroso, hydroxylamine and/or amine end products under any oxygen condition. Type 2 nitroreductases are oxygen-sensitive and exclusively generate these products in the

absence of oxygen. Type 2 enzymes reduce nitro groups via successive single-electron transfers to nitro anion radical intermediates. In the absence of oxygen the intermediates are reduced all the way to the end products. However, in the presence of oxygen the nitro anion radicals are rapidly back-oxidized to the parental compound in a futile redox cycle that generates superoxide radical. In contrast, type 1 nitroreductases reduce the substrate in two-electron increments all the way to the genotoxic end products (Denny, 2002; Portsmouth et al., 2007; Williams et al., 2015).

The four- or six-electron reduction of the nitro group to a hydroxylamine (-NHOH) or an amine (-NH₂) is one of the largest possible electronic changes achieved by a single-enzyme-catalysed reaction (Denny, 2002). The parental nitro group is strongly electron-withdrawing whereas hydroxylamines or amines are electron-donating. The reduction of the nitro group pushes the electrons back into the aromatic ring. The increase in electron density around the reactive substituents allows them to form DNA adducts or crosslinks. This powerful “electronic switch” has underpinned the design of nitroaromatic prodrugs, with the diminished electron density rendering reactive substituents of the prodrug inert until bioreductive activation (**Figure 1.2**) (Siim et al., 1997).

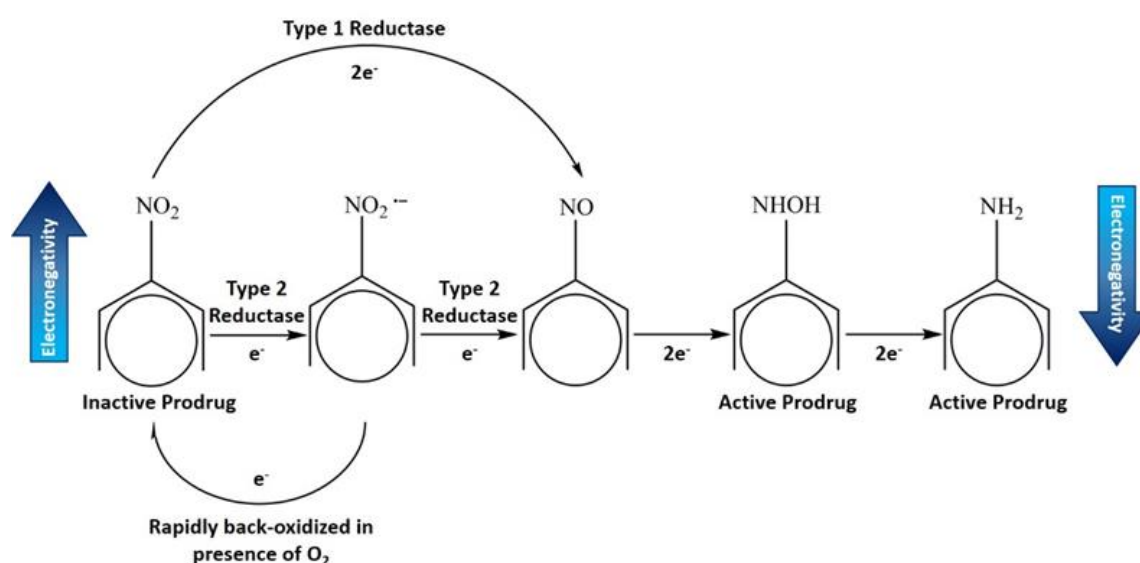


Figure 1.2 Schematic of type 2 and type 1 reduction of a nitroaromatic substrate proceeding via either consecutive 1-electron or 2-electron steps. If the first reduction is carried out by a type 2 reductase, the hydroxylamine or amine end-products can only be achieved in the absence of oxygen. In the presence of oxygen, the nitro anion radical generated by a type 2 reductase is back-oxidized, regenerating the parental compound in a futile redox cycle. A type 1 nitroreductase reduces in 2-electron increments then reduction proceeds irrespective of the oxygenation status of the environment. Reduction to a hydroxylamine or amine end-product results in a profound change in electronic effect as the nitro group is strongly electron-withdrawing, whereas the reduced hydroxylamine and amine are electron-donating. Figure created by me, and first published in Williams et al. (2015). (Reproduced from Williams et al. (2015) with permission from Portland Press).

Bacterial type 1 nitroreductases typically have a homodimeric quaternary structure. Each monomer is associated with one flavin of either flavin mononucleotide (FMN) or flavin adenine dinucleotide (FAD). Catalysis occurs via a bi-bi-ping-pong kinetic mechanism (Roldán et al., 2008). According to this mechanism, an NAD(P)H co-factor enters each active site of the homodimer. Two electrons are passed to the flavin and the oxidized nicotinic cofactor leaves the active site. A second substrate enters the same active site to accept the electron pair from the flavin. The reduced end product then dissociates from the nitroreductase. Reduction may occur once, forming nitroso derivatives, twice to form hydroxylamines, or three times to form amine metabolites. In type 1 nitroreductases the semiquinone states of the flavin are destabilized, rendering one-electron chemistry thermodynamically unfavourable (Williams et al., 2015).

Bacterial type 1 nitroreductases have been exploited for clinical GDEPT development because they can activate nitroaromatic prodrugs regardless of the oxygen status of the surrounding tissues, and therefore offer scope to target the most clinically recalcitrant hypoxic tumour zones.

1.4.2 Historic partnership: *E. coli* NfsB/CB1954

Nitroreductase GDEPT has almost exclusively focused on *E. coli* NfsB, to the extent that the field has historically referred to *E. coli* NfsB as just “bacterial nitroreductase” or “nitroreductase” (Williams et al., 2015).

NfsB *E. coli* is a type 1 nitroreductase that has been tested with many nitroaromatic prodrugs, but most extensively CB1954 a 5-aziridiny-2,4-dinitrobenzamide (Denny, 2002). CB1954 was first synthesized in the 1960s at the Chester Beatty Laboratories. When administered as a sole agent in the rat Walker 256 carcinoma model (rat breast cancer), CB1954 demonstrated complete cures with few side effects (Cobb et al., 1969). In this system, CB1954 is converted into its 4-hydroxylamine derivative by rat NQO1 (NAD(P)H quinone oxidoreductase 1). NQO1, also known as DT diaphorase, is a type 1 nitroreductase (Knox et al., 2005).

The outstanding success in rat Walker cells was not repeated in human carcinoma cells. Owing to a single amino acid substitution between rat and human NQO1, as well as differential levels of expression, CB1954 is 500–5000-fold less toxic to human cells than rat Walker cells (Boland et al., 1991). In part, this is because the rat NQO1 is 60-fold faster than the equivalent human enzyme at reducing CB1954 (Anlezark et al., 1992; Dachs et al., 2009). Furthermore, NQO1 overexpression and ineffective DNA repair mechanisms likely rendered the rat Walker 256 tumours more susceptible to CB1954 (Knox et al., 1991). The relative inactivity of human NQO1 has led to the development of alternative activating enzymes for CB1954.

1.4.2.1 Genotoxic mechanisms of CB1954

The primary activated products of nitroreductase-mediated CB1954 metabolism are 2- and/or 4-hydroxylamines. Intercellular disproportionation converts 2- hydroxylamines to 2-amine monofunctional alkylating agents that can form DNA mono-adducts but not cross-links. In contrast, the 4-hydroxylamine (4-NHOH) is processed to a 4-acetoxyamine

that is an effective DNA cross-linking agent (**Figure 1.3**) (Lehouritis et al., 2013; Williams et al., 2015). The reduction of the nitro group pushes the electrons back into the aromatic ring. The increases in electron density around the reactive substituents allows them to form DNA adducts or crosslinks. The 4-NO₂ metabolites undergo spontaneous reaction with acetyl-CoA to an alkylating agent capable of interstrand DNA cross-linking (Williams et al., 2015). Interstrand cross-links are generally more toxic than single strand or monofunctional lesions. Interstrand cross-links are poorly repaired and correlate to increased cytotoxicity by the CB1954 4-NO₂ metabolites compared to other alkylating agents (Chung-Faye et al., 2001)

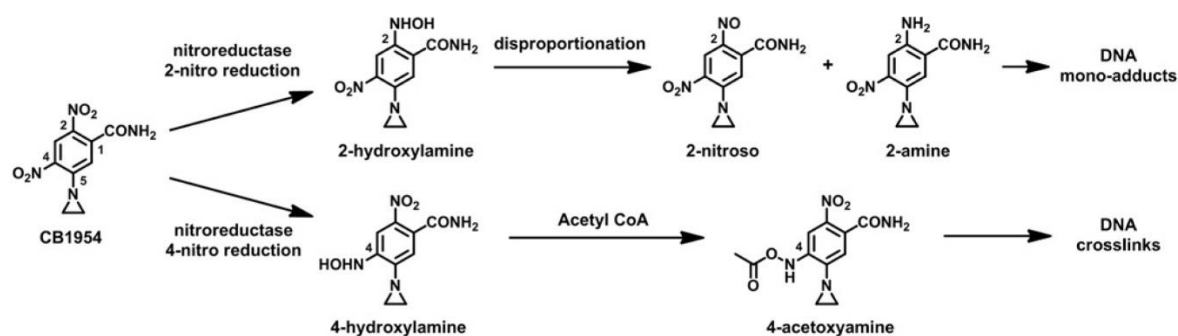


Figure 1.3 Mechanism of activation and genotoxicity of metabolites of CB1954. Mechanism of activation and genotoxicity of metabolites of CB1954. (Reproduced from Williams et al. (2015) with permission from Portland Press).

1.4.2.2 Bystander effect of CB1954

CB1954 can be enzymatically reduced at either the 2-nitro or the 4-nitro position, but not both. There are four cytotoxic extracellular metabolites of CB1954 in cultures of nitroreductase-expressing tumour cells; the 2- and 4-hydroxylamines and their corresponding amines (Helsby et al., 2004). At first the 2-NO₂ metabolites (2-amine or 2-hydroxylamine products) were considered undesirable owing to their lower cytotoxicity relative to the 4-NO₂ metabolites (4-amine or 4-hydroxylamine products) in some cell lines because unlike the 4-hydroxylamine, the 2-hydroxylamine derivative of CB1954 remains a monofunctional alkylating agent (i.e. is unable to go on to cross-link DNA (Williams et al., 2015). However, it was revealed that the 2-NO₂ metabolites are the key mediators of the CB1954 bystander effects (Helsby et al., 2004). *In vivo* the 2-amine metabolites were shown to be responsible for significant tumour growth delay when only 5% of the tumour

cells were NfsB-expressing. This is because the 2-amine metabolites are more stable and more diffusible than 4-hydroxylamine. Moreover, it was demonstrated that the 2-amine metabolites are at least as toxic as the 4-hydroxyl amines in tumour lines that contain intact nucleotide-excision repair processes (Helsby et al., 2004).

CB1954 has cell-cycle independent cytotoxicity and can treat tumours resistant to nucleotide analogues (Chung-Faye et al., 2001). This motivated discovery of more efficient nitroreductase enzymes such as *E. coli* NfsB which is 90-fold more efficient than even the rat form of NQO1 for reducing CB1954 (Anlezark et al., 1992). Unlike NQO1, *E. coli* NfsB is able to generate either the 2- or the 4-NO₂ reduction product of CB1954, and does so in an approximately equimolar ratio.

1.4.2.3 Barriers to clinical *E. coli* NfsB/CB1954

The critical clinical barrier to CB1954 is the maximum tolerated dose that can be achieved in humans. All the promising murine experiments used CB1954 doses ~20-fold higher than those achievable in humans with corrected scaling (Tang et al., 2007). Critically, the plasma concentration, using a typical 50 mg/kg CB1954 dose, in mice was 50-fold greater than that recorded in humans (Chung-Faye et al., 2001; Patel et al., 2009).

When a phase I clinical of *E. coli* NfsB/CB1954 using an adenovirus vector was performed, dose limiting toxicities of diarrhoea and hepatic toxicity were observed at doses of only ~2 mg/kg (24 mg/m²) (Chung-Faye et al., 2001); far less than 50-80 mg/kg tolerated by mice. A peak achievable serum level of CB1954 6.3 μM corresponds to a maximum achievable plasma concentration (C_{max}) that is 100-500-fold lower the *K_m* of NfsB (Chung-Faye et al., 2001; Liu et al., 2008). The serum concentration of 5.8 μM/h CB1954 achievable in patients is <1% of the *K_m* of *E. coli* NfsB. At these low serum concentrations NfsB catalysis is extremely inefficient (Williams et al., 2015).

1.4.3 Discovery of nitroreductases for GDEPT

The low achievable serum concentrations of CB1954 spurred efforts to discover more efficient nitroreductase enzymes that were catalytically efficient at lower CB1954 concentrations (Prosser et al., 2013; Williams et al., 2015). Discovery strategies have included database interrogation, using sequence, structural or functional homology, and directed evolution (Prosser et al., 2013; Swe et al., 2012) Numerous nitroreductases from

other bacterial species have been tested for activity with CB1954. Studies of particular relevance to this thesis are summarised below.

1.4.3.1 *Neisseria meningitidis* NfsB

Neisseria meningitidis NfsB was part of a panel of alternative nitroreductases assembled with the aim of finding superior CB1954-reducing enzymes and significantly outperformed *E. coli* NfsB in CB1954 murine model using a *Clostridium sporogenes* vector (Heap et al., 2014). *N. meningitidis* NfsB was reported to have a K_m of 2.47 μM with CB1954 and it was therefore concluded that it could efficiently activate CB1954 at clinically-achievable serum concentrations. In contrast with *E. coli* NfsB, *N. meningitidis* NfsB was found to exclusively reduce the 4-nitro group of CB1954 (Heap et al., 2014).

1.4.3.2 *E. coli* NfsA

The kinetic and *in vitro* performance of *E. coli* NfsA with CB1954 was far superior to that of *E. coli* NfsB (Prosser, Patterson, et al., 2010; Vass et al., 2009). *E. coli* NfsA reduces CB1954 almost entirely at the 2-nitro position. As the 2-amine metabolites are responsible for the bystander effect of CB1954, *E. coli* NfsA became a candidate for CB1954 GDEPT (Helsby et al., 2004).

A protein sequence alignment of *E. coli* NfsA and NfsB shows shared structural features; a 5-stranded anti-parallel β -sheet core and surrounding α -helices, two active sites occupying clefts at the dimer interface and presentation of the re-face of the FMN isoalloxazine ring towards the substrate pocket (Kobori et al., 2001; Lovering et al., 2001). However, *E. coli* NfsA has a more open active site than NfsB that may enable it to better accommodate CB1954 (Vass et al., 2009). In an adenovirus VDEPT model, *nfsA* expressing cells were 6.3 fold more sensitive to CB1954 than those expressing *nfsB*. Consistent with NfsA exclusively reducing the 2-nitro moiety of CB1954, a higher bystander effect was measured from cells expressing *nfsA* compared to *nfsB*. Moreover, the k_{cat}/K_m for NfsA is ~ 25 -fold higher than NfsB, which indicates that NfsA will activate CB1954 ~ 18 -fold faster than NfsB in physiological conditions (Vass et al., 2009).

Although *E. coli* NfsA demonstrated promise with CB1954, it was recognised that there might be even more naturally occurring nitroreductases to be explored for GDEPT.

1.4.3.3 Library of 47 wild-type oxidoreductases

A larger-scale study was undertaken to examine 47 enzymes spanning 11 different bacterial oxidoreductase families. The library comprised 12 NfsA and 12 NfsB family members, four representatives of each of the Nema and AzoR families, three from the YwrO family and the remaining six families were represented by one *E. coli* and one non-*E. coli* homologue, with the exception of the NQO1 family, for which there is no known orthologous *E. coli* enzyme. These 47 enzymes were examined for activity with CB1954 and a next generation prodrug PR-104A (Prosser et al., 2013). Kinetic analysis of 20 top-performing nitroreductases was performed with both CB1954 and PR-104A. This revealed eight nitroreductases with a greater k_{cat}/K_m for CB1954 than *E. coli* NfsA. All of these were from the NfsA family, and the most active was *Bacillus subtilis* YcnD followed by *Vibrio fischeri* NfsA (Prosser et al., 2013).

1.4.4 Engineering of nitroreductases for GDEPT

Most nitroaromatic prodrugs are synthetic substrates as they are designed specifically to kill cancer cells. It is therefore unlikely that a natural nitroreductase exists that is optimal for reducing man-made prodrugs. Discovery of new nitroreductases has been superseded by genetic engineering to improve enzymatic efficacy with prodrugs.

1.4.4.1 Directed evolution of nitroreductases

Directed evolution is a powerful strategy for engineering enzymes. It involves iterative rounds of mutagenesis followed by selective screening to identify enzyme variants with improved activity (Gillam et al., 2011). Mutagenesis is achieved by non-rational or semi-rational design. Whereas rational design leverages structural and mechanistic knowledge to target codons encoding amino-acids in the active site for specific point mutations, non-rational mutagenesis does not require structural or mechanistic knowledge, but rather entails low frequency random mutagenesis over the whole gene encoding the enzyme. Random mutagenesis methods include error-prone PCR, recombining gene fragments with staggered extension process PCR or random priming. Semi-rational design uses partial structural knowledge and serendipitous improvement through random variation. An example of semi-rational design is site-saturation mutagenesis, which replaces amino-acids, usually chosen based on structural information, with partially- or fully-degenerate codons. The degenerate codon permits up to 64 possible codons and hence up to 20

amino acids coded for at that specific locus (Chica et al., 2005). Promiscuous enzymes are most suitable for semi-rational engineering (Bornscheuer et al., 2012; Denny, 2002). Promiscuous enzymes have been improved by altering only a few amino acid residues using directed evolution (Tracewell & Arnold, 2009).

The mutagenesis phase creates vast gene variant libraries. The next step in a directed evolution cycle is selective screening to isolate variants with improved activity. Using non-rational design, the majority of the variants will be less-functional enzymes. Ideally it will be possible to apply a selection pressure to enrich the library for mutants above a particular threshold of activity (Tracewell & Arnold, 2009). Accurately interrogating variant libraries is the most rate limiting step in directed evolution.

Nitroreductases offer excellent targets for directed evolution because they have promiscuous activities. Nitroaromatic compounds occur rarely in nature, making it likely that nitro-reduction is itself a promiscuous activity. However, the primary biological role of most nitroreductases has not been elucidated.

Known physiological roles of nitroreductases are diverse. Some nitroreductases can act as flavin reductases, reducing FMNH₂ to power bioluminescence. For example an NAD(P)H-flavin oxidoreductase facilitates bioluminescent bacterium *Vibrio fischeri* (Zenno et al., 1994). In other bacteria, such as *Pseudomonas aeruginosa* or *Helicobacter pylori*, nitroreductases are thought to act as quinone reductases, maintaining reduced quinones for antioxidant defence (Green et al., 2014; Wang & Maier, 2004). Type 1 nitroreductase activity has also been found to reduce hexavalent chromium (Ackerley et al., 2004; Robins et al., 2013), iron (Takeda et al., 2010) and azo dyes (Rafii & Cerniglia, 1995). Type 1 nitroreductases are a versatile evolutionary starting point for bioactivation of synthetic prodrugs (Williams et al., 2015).

It has been proposed that the unique architecture of nitroreductase dimers is responsible for this functional diversity among the nitroreductase super family. The dimer structure produces a vast contact area that may provide the stabilization needed to offset the costs of insertion of the active sites between the monomers. Overall this results in versatility of the flavin cofactor and a tertiary structure that facilitates active site variability (Miller et al., 2018).

1.4.4.1.1 Directed evolution of nitroreductases for improved CB1954 reduction

A superior nitroreductase, maximising cytotoxin production at low concentrations, may overcome the low maximum tolerated dose of CB1954 in humans; which is the major clinical barrier (Chung-Faye et al., 2001; Denny, 2002). The first attempt to achieve this used the solved crystal structure of *E. coli* NfsB (Lovering et al., 2001) to inform a directed evolution by semi-rational design (Grove et al., 2003).

Nine amino acid residues in *E. coli* NfsB were randomised on an individual basis using degenerate codon mutagenesis. Residues that surround the substrate-binding pocket were targeted (Grove et al., 2003). The nine variant libraries were visually screened, by growth inhibition, for their ability to sensitize a nitroreductase-deficient strain of *E. coli* to CB1954. The top performing individual variant was F124K, with an *E. coli* IC₅₀ value 5-fold lower compared to wild-type *E. coli* NfsB (the IC₅₀ being the concentration of a drug at which 50% cell growth or cell survival is detected relative to an unchallenged control). Genes encoding the wild-type *E. coli* NfsB and F124K variant were inserted into adenovirus vectors, and transfected into carcinoma cells. In this cell background, the IC₅₀ for CB1954 was, on average, ~4-fold lower for F124K compared to *E. coli* NfsB. At 1 μM CB1954, a clinically relevant concentration, F124K was ~5-fold more potent in sensitizing the carcinoma cells to CB1954 than *E. coli* NfsB (Grove et al., 2003).

In kinetic assays with CB1954 an N71S mutant exhibited the greatest increase in k_{cat}/K_m of 5-fold compared *E. coli* NfsB. The two most beneficial mutations were therefore combined, and the N71S/F124K double mutant had a 6-fold improvement in k_{cat}/K_m . Structural analysis, by X-ray crystallography of the single and double mutants in complex with nicotinic acid, indicated that the N71S mutation affects interactions of the FMN cofactor, while mutations at T41 and F124 affect interactions with nicotinic acid. The changes to structure and substrate and cofactor interaction were likely responsible for the enhanced specificity constants and selectivity for CB1954 by these variants compared to the wild-type enzyme (Race et al., 2007). F124 mutations improve steric conditions; movement of the side-chain of residue 124 into a polar pocket away from the substrate was observed in F124N and F124K mutants, promoting increased substrate affinity (Race et al., 2007).

Further combinations of beneficial single mutants were explored by a sophisticated phage selection system that employs an SOS signal to activate the bacteriophage lambda lytic cycle (**Figure 1.4**) (Guise et al., 2007). The nitroreductase variant library was cloned into λ phages and transformed into *E. coli*. When challenged with sub-lethal CB1954 concentrations, the individual *E. coli* bacteria expressing the most improved nitroreductase mutants experienced the greatest levels of DNA damage, thereby triggering the largest SOS (DNA damage repair) responses. The SOS response induces the λ phage lytic cycle, whereupon the *E. coli* hosts release phages that encode the most active nitroreductase variants for collection.

Successive cycles of infection and CB1954 selection identified the T41Q/N71S/F124T triple mutant from a library of 6.8×10^5 clones (Guise et al., 2007; Jarrom et al., 2009). In carcinoma cells, T41Q/N71S/F124T sensitized cells 40- 80-fold to CB1954 relative to *E. coli* NfsB (Jarrom et al., 2009). Further combinations of beneficial single mutants were explored. Top candidates, identified by growth inhibition, were tested in carcinoma cells. Variants T41L/N71S and T41L/F70A, were 14–17-fold more potent than *E. coli* NfsB at sensitising cells to CB1954 (Jaberipour et al., 2010).

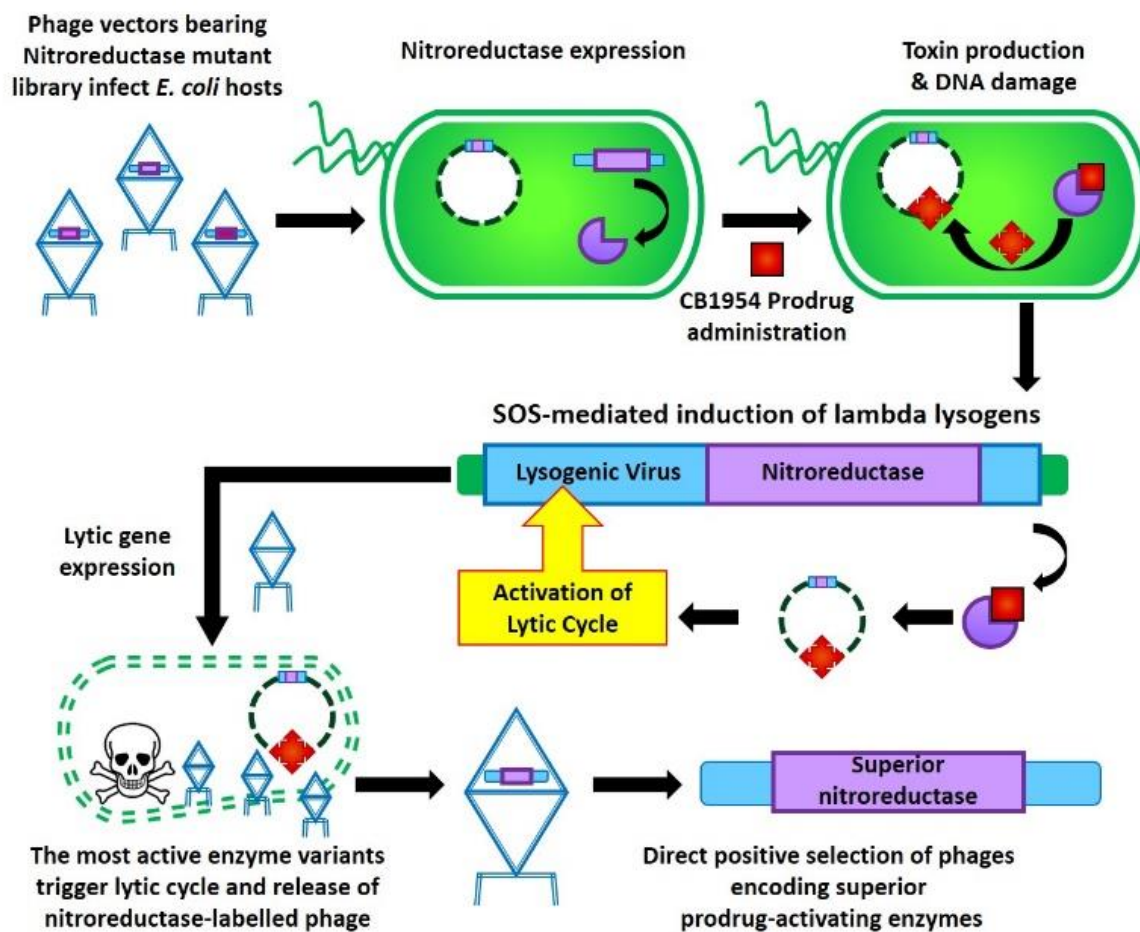


Figure 1.4 Direct positive selection for active nitroreductases from large-scale mutant libraries via the SOS-triggered bacteriophage λ lytic cycle. A nitroreductase mutant library is cloned into λ phages that are then used to infect *E. coli*. The bacteria are briefly exposed to sub-lethal concentrations of CB1954. Any *E. coli* expressing active nitroreductase convert CB1954 to DNA-damaging form, triggering the SOS response. This causes RecA activation, leading to proteolysis of the λ *ci* repressor and switching the λ phage into the lytic cycle. Phage replication occurs and subsequent lysis of the host *E. coli* releases large quantities of phage that carry the most active nitroreductase variants. Successive cycles of infection and CB1954 exposure lead to populations highly enriched for mutants that possess superior CB1954 reductase activity. Figure prepared by me, based on the work of Guise et al., (2007) and first published in Williams et al., (2015). (Reproduced from Williams et al. (2015) with permission from Portland Press).

1.4.4.1.2 Novel screens for directed evolution of nitroreductases

The SOS-triggered bacteriophage screen is labour intensive and technically challenging (Baker, 2011; Williams et al., 2015). Alternative screening strategies have been developed in specialized *E. coli* screening strains.

1.4.4.1.2.1 SOS-R2 screening strain

An *E. coli* SOS reporter strain, named “SOS-R1”, was developed to detect prodrug activation by nitroreductases (Prosser, Patterson, et al., 2010). Nitroreductase variants are cloned into a plasmid (pUCX) and over-expressed in an *E. coli* strain that contains a lacZ reporter gene under control of an SOS responsive promoter. Transformed cells are challenged with sub-lethal levels of a test prodrug, whereupon nitroreductase activity results in DNA damage, inducing the SOS response which triggers measurable production of the reporter protein β -galactosidase (**Figure 1.5**). The reporter strain was subsequently optimised by gene deletion of the endogenous nitroreductase genes *nfsA*, *nfsB*, *nemA*, and *azoR* to eliminate background activation of the prodrug. The *tolC* gene was also deleted to restrict active efflux of unreduced prodrug which increases sensitivity to the prodrug, and the final optimised screening strain was designated SOS-R2 (Prosser et al., 2013).

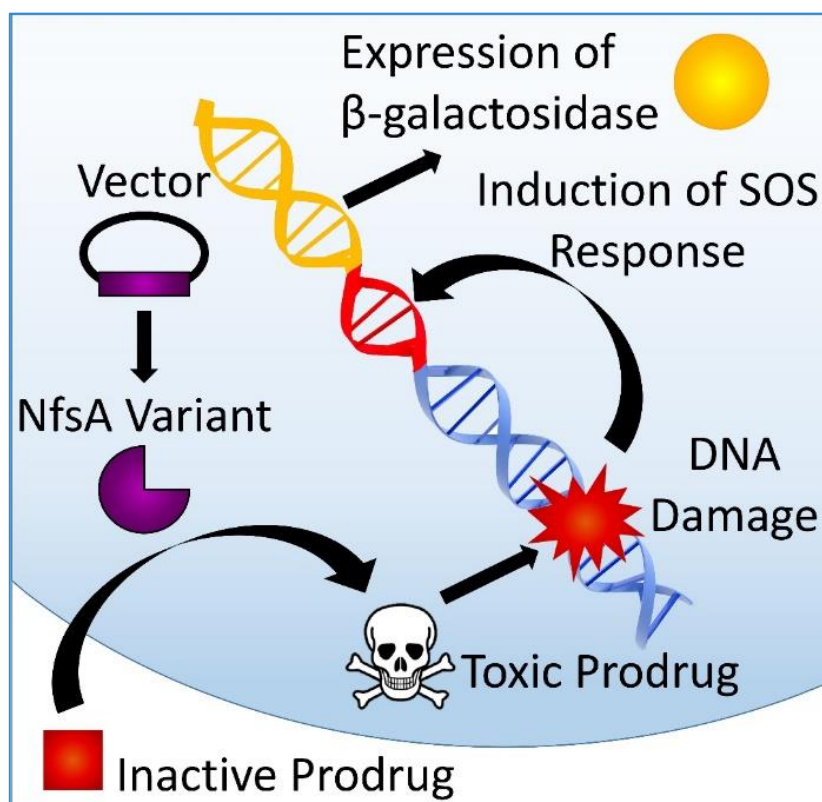


Figure 1.5 *E. coli* SOS assays used to monitor the activity of nitroreductases with nitroaromatic prodrugs. Overexpression of nitroreductases able to activate a prodrug to a genotoxic form results in DNA damage and activation of the *E. coli* SOS response. The strength of the response can then be quantified in specialized SOS reporter strains by β -galactosidase assay. Figure prepared by me, first published in Williams et al. (2015). (Reproduced from Williams et al. (2015) with permission from Portland Press).

In the 47-membered oxidoreductase library, the SOS response to CB1954 was similar between NfsA- and NfsB-expressing strains. NfsA and NfsB family members were consistently more active than any other enzymes in the library, although trace levels of activity with CB1954 were detected in the Azor and Nema families. The SOS assay was broadly predictive of the IC₅₀ in SOS-R2 cells (i.e., the concentration of prodrug at which nitroreductase-expressing cells grew to half the culture turbidity relative to an unchallenged control), and was an improvement over more labour-intensive and prodrug-consuming IC₅₀ assays. The overall top candidates by IC₅₀ were confirmed to be *B. subtilis* YcnD at 29 μM and *B. subtilis* NfrA at 46 μM. *E. coli* NfsA and NfsB each had IC₅₀s of 150 μM CB1954 (Prosser et al., 2013).

The SOS-R2 screening strain was used in a small-scale directed evolution study to enrich a variant library of *Aliivibrio fischeri* FRaseI, an NfsB homologue, for activity with CB1954. The library was generated by site-saturation mutagenesis. The top mutants recovered possessed up to 8.4-fold improvement in k_{cat}/K_m relative to wild-type FRaseI (Swe et al., 2012).

However, the SOS-R2 screen has a limited throughput rate. It depends on manual induction of a colour change of individual variant cultures in 96 well plates.

1.4.4.1.2.2 SOS-R4 screening strain

To enable greater throughput a new screening strain, expressing a GFP reporter protein in response to DNA damage, was developed. The *E. coli* strain, labelled “SOS-R4”, is a derivative of the *E. coli* strain W3110 in which seven endogenous nitroreductase genes (*nfsA*, *nfsB*, *azoR*, *nema*, *mdaB*, *yieF* and *ycaK*) were deleted as well as the *tolC* gene. The SOS-R4 strain contains a plasmid bearing a *green-fluorescent-protein-mut3* (GFP) reporter gene controlled by the SOS inducible *sfiA* promoter. This particular variant of GFP is a specialized protein derived from *Aequorea victoria* GFP with the following mutations: S65G/S72A. Most GFP expressing cassettes used by bacteriological laboratories have been optimized for immunofluorescence microscopy. For example GFP mut3 proteins reach maximal fluorescence when excited at 501 nm, corresponding to blue light (450_495 nm) which is more favourable for detection when using a fluorescence

microplate reader (Cormack et al., 1996). This is more favourable for detection. SOS-R4 cells expressing a nitroreductase convert the prodrug into DNA-damaging metabolites that trigger GFP expression (**Figure 1.6**). Superior nitroreductase variants are identified by increased fluorescence relative to a control (Copp et al., 2014).

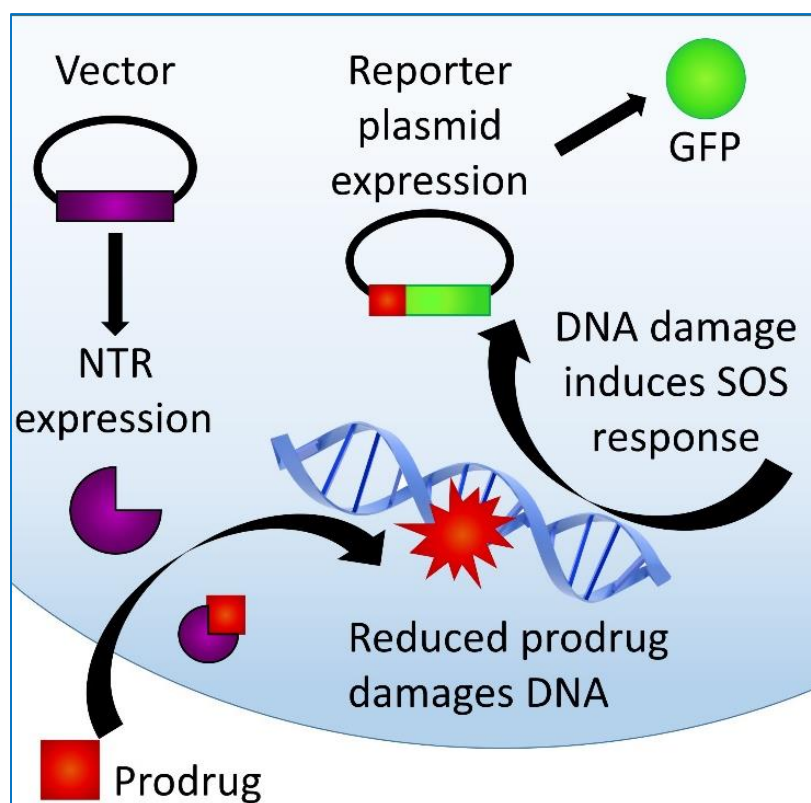


Figure 1.6 The SOS-GFP screen detects DNA damage within *E. coli* reporter cells. Nitroreductase (NTR) mediated activation of a nitroaromatic prodrug to a genotoxic form results in DNA damage (red explosion) and activation of the *E. coli* SOS response, detectable in reporter cells via induction of GFP (green circle) from a plasmid-based reporter. Prodrug activation can occur either internal (as depicted) or external to the reporter cell; in the latter scenario, the activated prodrug metabolites must be transferred into the reporter cell before induction of the SOS response will occur. Figure created by me for Chan-Hyams et al. (2018), based on Copp et al. (2014).

The high sensitivity of the GFP signal enabled miniaturization of the SOS assays into a 384-well plate format. This is even more parsimonious with prodrug stocks than SOS-R2, but still relies on challenging cultures of individual variants manually with prodrug.

1.4.4.1.2.3 High-throughput screening with SOS-R4

The true value of the GFP signal was in enabling an automated high throughput based screening method - Fluorescence Activated Cell Sorting (FACS). FACS recovers the most active nitroreductase variants, based on fluorescence, from a mixed culture of the variant

library that has been collectively challenged with a sub-lethal concentration of prodrug. The most highly fluorescent cells are selected from the pool and then individually assessed (Figure 1.7).

In a proof of principle investigation, FACS successfully enriched a model library after only a single sort. The model library consisted of cells expressing a strongly active nitroreductase (*B. subtilis* YcnD) and cells expressing a poor nitroreductase (*E. coli* YdjA) mixed at a 1:1000 starting ratio. FACS was performed, post CB1954 challenge, yielding 38% recovery rate of cells expressing *ycnD*. Two consecutive sorts, at a 1:100 000 starting ratio, yielded a 90,000-fold enrichment of *ycnD*-expressing cells (Copp et al., 2014).

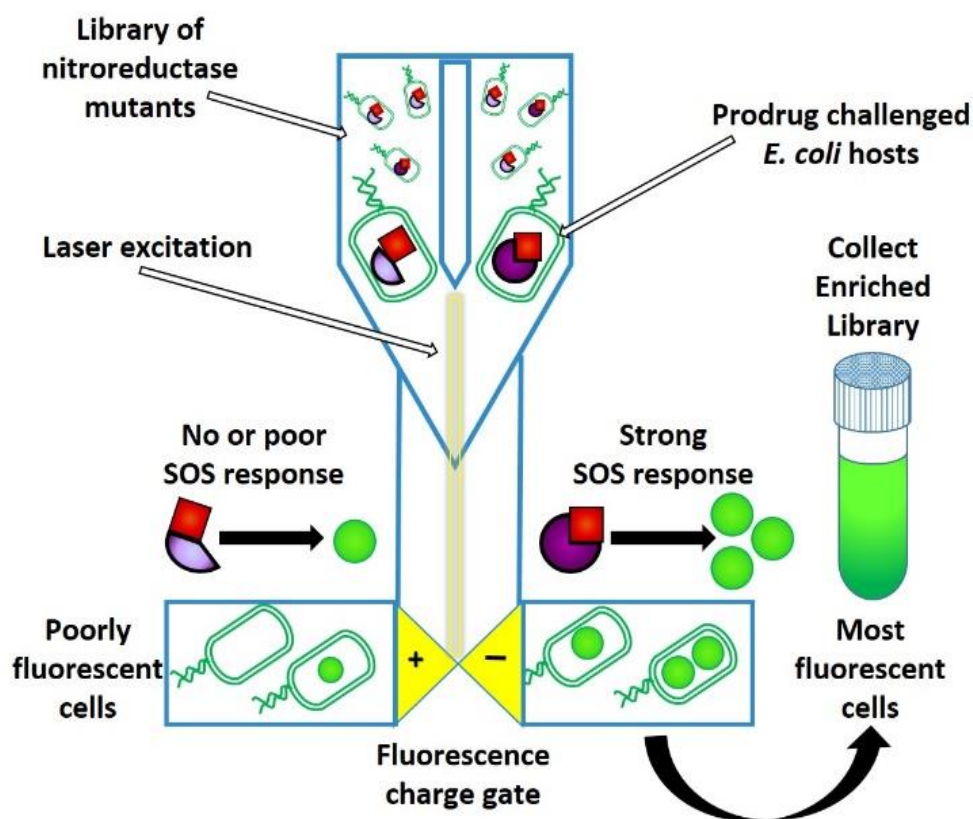


Figure 1.7 FACS selects active nitroreductase variants from large-scale mutant libraries. *E. coli* SOS reporter cells engineered to both express a bacterial nitroreductase variant and to generate GFP in response to DNA damage are pooled and exposed to the prodrug of interest. Any individual *E. coli* cells carrying active nitroreductases convert the prodrug into a DNA-damaging form and subsequently begin to make GFP. The pooled *E. coli* are then analysed by flow cytometry and the most highly fluorescent cells are selected from the pool and cultured on an individual basis for further analysis. Figure created by me and first published in Williams et al. (2015). (Reproduced from Williams et al. (2015) with permission from Portland Press).

1.5 Next generation nitroaromatic prodrugs

Owing to the limitations of CB1954 as a prodrug, in particular its low maximum tolerated dose in humans, discovery and optimization of new nitroreductase/prodrug partnerships with next generation prodrugs is paramount.

1.5.1 Hypoxia activated prodrugs

Regions of hypoxia, or low oxygen, are a common characteristic of most solid malignant tumours, contributes to therapeutic resistance and more aggressive cancer phenotypes. Hypoxia is a physiologic state where the oxygen partial pressure is below the normal physiologic range which is typically between 10-20 mmHg. Hypoxic regions develop when demand exceeds oxygen supply (Rickard et al., 2019). Poor development of vasculature in fast growing tumours can lead to regions of hypoxia. (Carmeliet & Jain, 2000; Dang et al., 2001). Regions of hypoxia vary spatial within tumours and are subject to change over time and treatment. Substantial changes in the oxygen pressure can occur within the distance of a few cell layers (Vaupel & Mayer, 2016).

Low oxygen regions are not common in healthy tissue. Hence hypoxic regions of solid tumours offer an environment unique from healthy tissue (Carmeliet & Jain, 2000; Dang et al., 2001). This differentiating characteristic can be used to selectively activate chemotherapeutics.

Prodrugs can be designed for activation by metabolic reduction under hypoxic conditions. Forerunners were quinone bioreductive drugs that are converted to alkylating agents. Next generation prodrugs are dinitrobenzamide mustards (DNBMs) that are reduced to reactive nitrogen mustard metabolites that cross-link DNA. DNBM cytotoxicity is restricted to pathologically low oxygen regions that occur exclusively in tumours. DNBMs can also be designed to possess an efficient bystander effect that kills adjacent tumour cells (Patterson et al., 2007).

1.5.1.1 PR-104A

PR-104 is a hypoxia activated DNBM “pre-prodrug” that has been repurposed for GDEPT. PR-104 is a 3, 5-dinitrobenzamide-2-mustard ([2-((2-bromoethyl)-2-[[2-hydroxyethyl] amino] carbonyl)-4, 6-dinitroanilino) ethyl methanesulfonate phosphate ester] (**Figure 1.8**). Following cleavage of the solubilising phosphates by cellular esterases, the alcohol

prodrug form PR-104A is reduced by endogenous human Type 2 nitroreductases exclusively under hypoxia (Jameson et al., 2010; Patterson et al., 2007). This bioreductive activation is facilitated, compared to structural predecessors, by the more reactive leaving groups PR bromide and mesylate (Patterson et al., 2007).

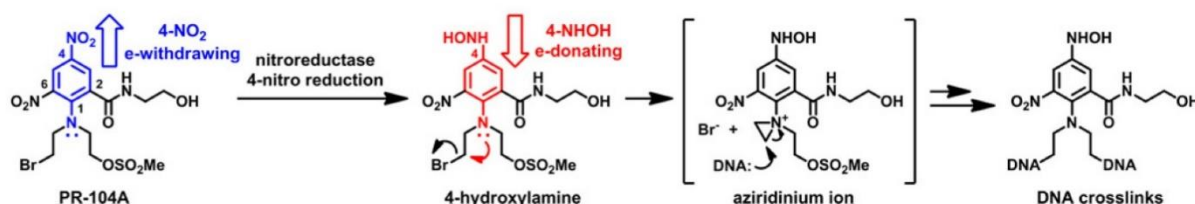


Figure 1.8 Mechanism of activation and genotoxicity of metabolites of PR-104A. The “pre-prodrug” of PR-104, is hydrolysed to the prodrug PR-104A. PR-104A is activated under hypoxic conditions by NADPH-cytochrome P450 oxidoreductases via one-electron reduction to cytotoxic metabolites PR-104H (hydroxylamine) and PR-104M (amine). (Reproduced from Williams et al. (2015) with permission from Portland Press).

PR-104H, is the major cytotoxin, causing severe interstrand DNA cross-links in a carcinoma strain defective in DNA repair. In an *in vivo* model, PR-104H is the most prevalent intracellular metabolite and was restricted to hypoxic regions (Patterson et al., 2007). However, hypoxia-independent activation of PR-104A can occur by two-electron reduction (Guise et al., 2010; Konopleva et al., 2015).

1.5.1.1.1 Clinical trials of hypoxia activated PR-104

Phase I-II clinical trials have been performed with PR-104 (Jameson et al., 2010; McKeage et al., 2011, 2012). A phase I trial of PR-104 determined the weekly maximum tolerated dose to be 675 mg/m² (~25-fold higher than CB1954). Dose limiting toxicities included thrombocytopenia and neutropenia (McKeage et al., 2011). Thrombocytopenia is a condition of low blood platelet count. Neutropenia is a low level of neutrophils. Both conditions can be measured to monitor blood-related drug toxicity. A phase IB study, in patients with advanced solid tumours, showed a maximum tolerated dose of 140 mg/m² PR-104A combined with gemcitabine or docetaxel. Granulocyte-colony-stimulating-factor raised the predicted maximum tolerated dose to >700 mg/m² by countering dose limiting toxicities (McKeage et al., 2011).

A phase I/II study was performed with leukaemia patients at 3 g/m² and 4 g/m² doses of PR-104. In comparison to the solid tumours treated by previous clinical trials a higher dose

was selected due to the nature of the cancer type to be treated i.e. leukaemia. Tumour killing was achieved but severe myelotoxicity, caused by activation in bone marrow, precluded long-term administration of PR-104 (Konopleva et al., 2015).

1.5.1.1.2 Oxic activation of PR-104

Clinical progress of PR-104 was abruptly halted by discovery that expression of five human aldo-keto reductase (AKR) family members correlated to PR-104A activation in oxygenated conditions (Guise et al., 2010). One of these, AKR1C3, was confirmed as a Type 1 (two-electron) nitroreductase of PR-104A in purified enzyme assays. AKR1C3 is expressed at high levels in healthy cells including those in the gastrointestinal tract and in CD34+ human myeloid progenitor cells in the bone marrow. Myelotoxicity may be caused by PR-104A activation in the bone marrow by AKR1C3 or by hypoxic stem cell niches (Guise et al., 2010; McKeage et al., 2011).

1.5.1.1.3 Nitroreductase activated PR-104A

PR-104 has been repurposed for GDEPT. On the premise that a highly efficient nitroreductases can activate PR-104A at very low doses, at which AKR1C3 is inefficient, investigations were launched to discover/generate such a nitroreductase. It was reasoned that via GDEPT, PR-104A might be reduced by a Type 1 nitroreductase, extending the effective range of “hypoxia activated” prodrugs into oxygenated tumour regions (Denny, 2002; Foehrenbacher et al., 2013).

Prosser et al. (2013) demonstrated that 14 nitroreductases in their 47 oxidoreductase library had a higher k_{cat}/K_m for PR-104 compared to *E. coli* NfsB. The NfsA and NfsB family members were consistently more active with PR-104 than any other enzymes in the library.

A directed evolution campaign was performed on *E. coli* NfsA to improve PR-104A reduction (Copp et al., 2017). Although it was not the most active NfsA enzyme in the collection, it offered two key advantages of having a solved crystal structure (Race et al., 2007) and being well-tolerated in transfected human cell lines (Prosser et al., 2013). Using the crystal structure of *E. coli* NfsA, twelve key residues contributing to substrate binding were chosen for individual site saturation mutagenesis using NNK (K: guanine/thymine) degenerate codons. Degenerate codons allow for semi-rational mutagenesis; where a

particular gene loci can be targeted for replacement with a select range of codons that change the identity of the corresponding amino acid in the protein. The NNK degenerate codon facilitates the replacement of a codon with any one of 32 codons that results in any of the 20 amino acids.

In parallel, FACS was performed on SOS-R4 cells expressing an *nfsA* variant library generated by error-prone PCR. A combinatorial gene library was generated to encode all possible combinations of beneficial substitutions recovered from the epPCR and/or targeted mutagenesis. Two thousand clones, representing >95% coverage of the library, were screened by SOS-R2 assay to identify beneficial substitutions at each residue.

The most active variant was variant no. 22, which had substitutions S41Y, E99G, L103M, R225P, and F227S. Variant no. 22 conferred a significant 3.8-fold improvement in IC₅₀ with PR-104A and a >25-fold greater increase in SOS challenge at 2.5 μM PR-104A compared to *E. coli* NfsA. 2.5 μM PR-104A is one-tenth of the maximum achievable plasma concentration C_{max} (Copp et al., 2017).

1.5.2 Alternative next generation prodrugs

Partnerships with other next-generation prodrugs and alternative nitroreductases have been explored (Williams et al., 2015). A brief summary of those most relevant to this thesis is provided here.

The nitroaromatic prodrug SN27686, a 3, 5-dinitrobenzamide-2- bromo mustard analogue of CB1954, was shown to be more dose potent and selective than CB1954. SN 27686 was compared to CB 1954 by determining growth inhibition (IC₅₀ values) across a panel of five human carcinoma cell lines, in which SN 27686 was on average 12.8-fold more dose potent than CB1954 against cells expressing *E. coli nfsB* (Singleton et al., 2007). The structure of SN27686 is displayed in **Table 1.1**.

Pseudomonas aeruginosa NfsB and MsuE have been assessed for activity with the next generation prodrug nitrochloromethylbenzindoline (nitro-CBI-DEI) (Green, Storey, et al., 2013). Like PR-104, nitro-CBIs were originally designed to be hypoxia-activated prodrugs. The activity of *P. aeruginosa* MsuE, a flavin-dependent oxidoreductase, was evaluated with PR-104 and nitro-CBI-DEI using the SOS-R2 screen. *P. aeruginosa* MsuE exhibited

comparable levels of activity to *E. coli* NfsB and NfsA (Green, Storey, et al., 2013). The structure of nitro-CBI-DEI is displayed in **Table 1.1**.

In a more extensive study, ten oxidoreductase enzymes from *P. aeruginosa* and *E. coli* NfsB and NfsA were assessed for activity with nitro-CBI-DEI. HCT-116 cells stably transfected with *P. aeruginosa* NfsB were significantly more sensitive to nitro-CBI-DEI than cells expressing the *E. coli* nitroreductases (Green, Syddall, et al., 2013). Of note an unprecedented bystander effect was observed in the transfer of active nitro-CBI-DEI between HCT-116 cells expressing *P. aeruginosa* NfsB and wild-type HCT-116 cells.

The bystander effect is critical to the success of nitroreductase GDEPT strategies, and substantial efforts have gone into optimizing this characteristic, as well as developing reliable methods to quantify it. Unlike SN27686 and nitro-CBI-DEI, metronidazole is a nitroaromatic prodrug that is a 5-nitroimidazole antibiotic compound (**Figure 1.9**).

The 5-nitroimidazole drug metronidazole has remained the drug of choice for treating parasitic and bacterial anaerobic infections since its development in 1959. Unlike many other antimicrobials metronidazole, is a prodrug that must be reduced at its nitro group in order to become toxic (Leitsch, 2019).

The toxic mechanism of the reduced metabolite of metronidazole is not yet well understood, however is thought to involve DNA binding and adduct formation upon reduction (Goldman et al., 1986; Ludlum et al., 1988). However, unlike the other prodrugs discussed, downstream products of this reduction are not cell-permeable and do not cause a bystander effect and as such has been used as a control for measuring the bystander effect (Bridgewater et al., 1997; Freeman et al., 1993).

Metronidazole has been investigated for use in GDEPT. Metronidazole, reduced by *E. coli* NfsB, demonstrated both apoptosis and necrosis of endothelial cell lines *in vitro* in addition to anti-vascular effects (Hunt et al., 2012). The partnership of nitroreductase/metronidazole was suggested as a candidate for anti-vascular enzyme prodrug gene therapy (Hunt et al., 2012).

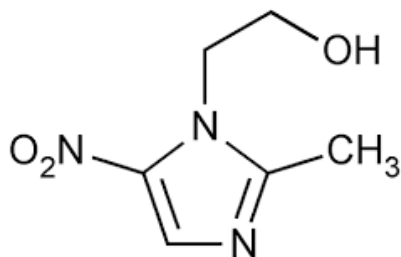


Figure 1.9 Chemical structure of the 5-nitroimidazole prodrug metronidazole

1.6 Measuring the bystander effect

The phenomenon of the bystander effect was first documented when only a fraction of a tumour mass (generated *in vitro* from mixed cell lines) was genetically modified with a prodrug activating enzyme. It was observed *in vivo* that having as few as 10% of tumour cells expressing the prodrug activating enzyme HSV-tk could lethally sensitize neighbouring tumour cells to ganciclovir (Freeman et al., 1993).

The bystander effect was first measured for the *E. coli* NfsB/ CB1954 partnership *in vitro*. Cancer cells expressing *E. coli* NfsB were challenged with CB1954, then the medium was collected and incubated with unmodified cancer cells, resulting in a 25% decrease in cell survival. This was attributed to cell permeable active metabolites of CB1954 diffusing from the NfsB expressing cells into surrounding medium and showcased that the *E. coli* NfsB /CB1954 GDEPT system does not require direct cell-to-cell contact to mediate the bystander effect. This is valuable as most tumours down-regulate gap junctions (Bridgewater et al., 1997).

1.6.1 A multilayer human carcinoma bystander effect assay

The bystander effect is essential in overcoming low transduction rates of VDEPT to achieve a therapeutic outcome (Dachs et al., 2009) (**Figure 1.10**). To enable quantification of the bystander effect, a standard assay modelling a VDEPT scenario was developed. This model measures survival of untransduced carcinoma “target” cells co-incubated with a minority (3-10%) of transduced nitroreductase expressing “activator” cells in 3D multilayers. This multilayer model was designed to mimic tissue-like cell densities to test the ability of activated metabolites to diffuse through tumour tissue (Wilson et al., 2002).

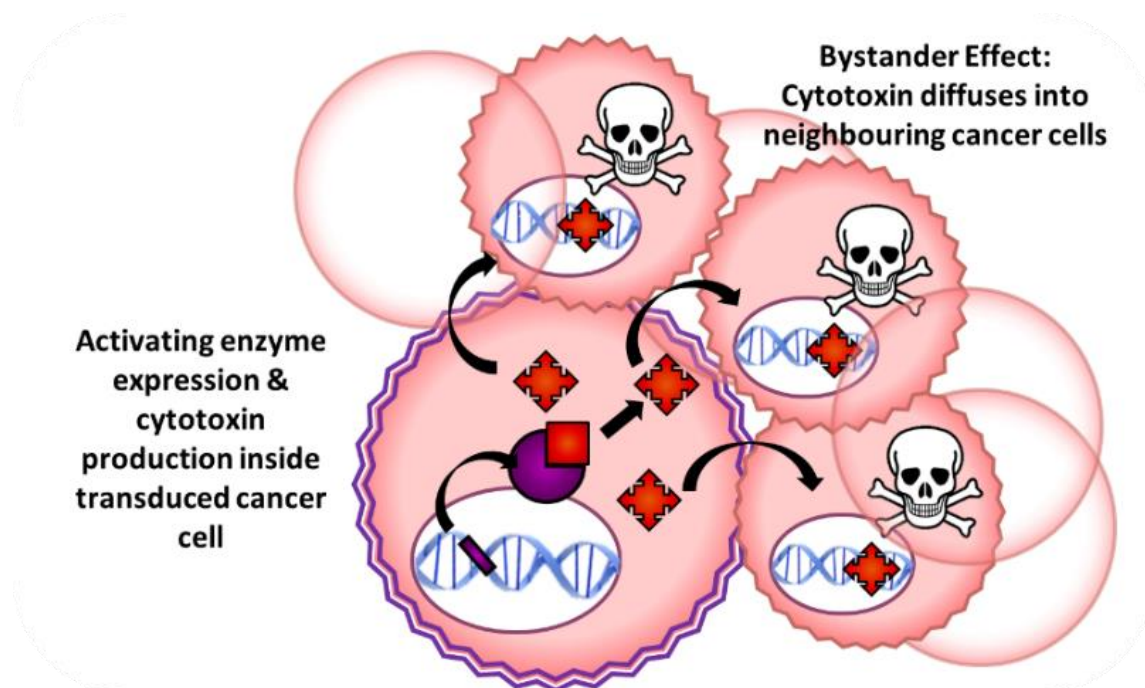


Figure 1.10 Representation of the bystander effect in vivo during virus-directed enzyme-prodrug therapy (VDEPT). Gene (purple rectangle) delivery mediated by a tumour tropic viral vector leads to tumour-specific expression of the encoded nitroreductase enzyme (purple pacman), able to convert a nitroaromatic prodrug (red square) into a genotoxic form (red star). In this scenario the bystander effect involves transfer of the genotoxin from a transduced cancer cell into neighbouring untransduced cancer cells. Figure created by me for Chan-Hyams et al. (2018).

Following challenge with a prodrug, cultures are plated to quantify the relative survival of activator and target cells. A reduction in the numbers of target cells in co-culture relative to a target cell only control indicates bystander killing. Cytotoxicity is quantified as the prodrug concentration to reduce survival to 10% relative to an unchallenged control (C10), and the magnitude of the “Bystander Effect Efficiency” (BEE) against target cells measured as the ratio of C10 values for activators versus targets. A BEE value approaching 1.0 (100%) indicates a lower concentration of prodrug is required to sensitize target cells. This multilayer carcinoma model was found to be predictive of the bystander effect *in vivo*. The multilayer carcinoma model has been used by many subsequent investigations to measure the bystander effect for potential VDEPT partnerships (**Table 1.1**).

1.6.1.1 Bystander effect of PR-104A

The bystander effect of PR-104A and a PR-104A analogue (SN34507) was quantified in the multilayer carcinoma model using HCT-116 cells wherein only 3% of the tumour cells

expressed *E. coli* NfsA. The BEE of PR-104A was 68% and the mono-nitro analogue SN34507 was 38% (Mowday, Guise, et al., 2016).

1.6.1.2 Bystander effect of CB1954 and analogues

The bystander effect of CB1954 and SN27686 was quantified in the same multilayer carcinoma model using HCT116 cells wherein only 1% of the expressed *E. coli nfsb*. The BEE of SN27686 was >3 fold greater than CB1954. SN 27686 provided a BEE of $48 \pm 9\%$ over three independent experiments, whereas the BEE value for CB 1954 was only $13 \pm 8\%$ under identical conditions (Singleton et al., 2007).

1.6.1.3 Bystander effect of nitro-CB-DEI

A three dimensional (3D) mixed cell culture assay, based on that developed by Wilson et al. (2002) was employed where activator carcinoma cells expressing the therapeutic protein are co-incubated alongside target cells that report on receipt of the activated genotoxic prodrug metabolites. This particular investigation used transfected 'activator' HCT-116 cells expressing *P. aeruginosa* NfsB equated to $5.8\% \pm 3.2\%$ of the total cells in the 3D co-culture. The overall BEE was calculated to be 89%. The target cells in this 3D co-culture were nearly as sensitive as the activators in an almost perfectly uniform transfer of toxicity (Green, Syddall, et al., 2013).

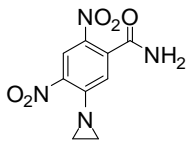
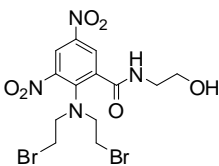
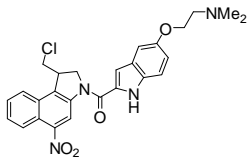
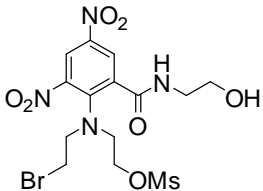
Prodrug activating enzyme	Prodrug	% Activators	BEE	Publication
<i>E. coli</i> NfsB	CB1954 	10% (9.5%)	0.4	(Wilson et al., 2002)
<i>E. coli</i> NfsB	CB1954	1%	13±8%	(Singleton et al., 2007)
<i>E. coli</i> NfsB	SN27686 	1%	48±9%	(Singleton et al., 2007)
<i>P. aeruginosa</i> NfsB	Nitro-CBI-DEI 	6%	89%	(Green, Syddall, et al., 2013)
<i>E. coli</i> NfsA	PR-104A 	3%	68%	(Mowday, Guise, et al., 2016)

Table 1.1 Summary of Bystander Effect Efficiency (BEE) experiments in the multilayer carcinoma model and the relevant prodrug. Cytotoxicity was quantified as the prodrug concentration to reduce survival to 10% of an unchallenged control (C10). The magnitude of the BEE against the target cells was measured as the ratio of C10 values for activators versus targets. A BEE value approaching 1.0 indicates a lower concentration of prodrug was required to sensitize target cells. Prodrug structures also presented here for comparison.

The multilayer carcinoma model depends on the release of activated prodrug from transfected cancer cells and the uptake by neighbouring untransfected cancer cells to measure the bystander effect. Metronidazole has also been evaluated in this system and found to have a negligible BEE (*Prof. David Ackerley, personal communication*). It should

be noted that this system provides an appropriate model for the bystander effect during VDEPT but is not a model for BDEPT.

1.6.2 Importance of bacterial bystander effect

The bystander effect is fundamental to BDEPT. The cytotoxin must be transported out of the bacterial vectors into surrounding tumour cells to be therapeutically effective (**Figure 1.11**). If the cytotoxin is unable to exit the bacteria then the vector itself may suffer DNA damage and be sterilized from the tumour thus preventing optimal activation of the prodrug.

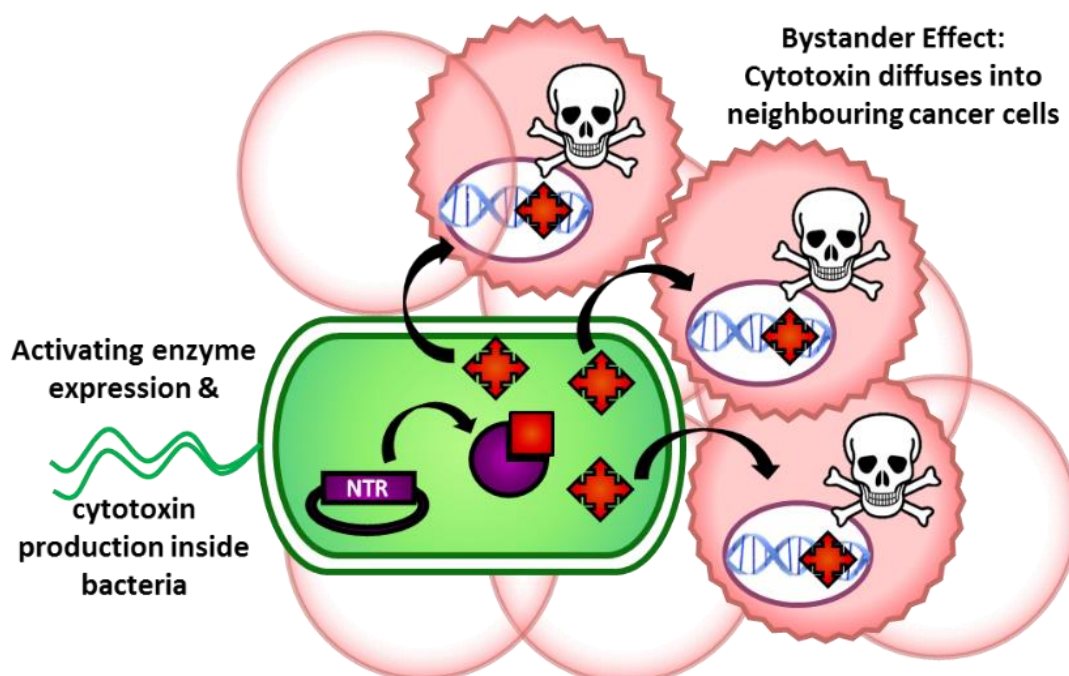


Figure 1.11 Representation of the bystander effect in vivo during bacterial-directed enzyme-prodrug therapy (BDEPT). Gene delivery mediated by a tumour tropic bacterial vector leads to expression of the encoded nitroreductase enzyme within a bacterial cell residing in infected tumour tissue. The nitroreductase is able to convert a nitroaromatic prodrug (red square) into a highly genotoxic form (red star) inside the bacterial vector. In this scenario the bystander effect involves transfer of the genotoxin from the bacterial vector into surrounding cancer cells. Figure created by me for Chan-Hyams et al. (2018).

Next generation prodrugs, with enhanced bystander effects, are the future of GDEPT. Lipophilicity accounts for >80% of nitroaromatic prodrug variance in the bystander effect in the multilayer carcinoma model (Wilson et al., 2002). Improved lipophilicity facilitates

transport across cell membranes. Prodrugs can therefore be designed to maximise lipophilicity post-reduction.

At the time the work in this thesis was initiated, there was no equivalent model for measuring the bystander effect where the cytotoxins were diffusing out of a bacterial vector rather than a transfected cancer cell. Given the increasing interest in BDEPT strategies and totally different physiology of bacterial cells relative to human tumour cells, we considered this an important oversight.

Furthermore an opportunity arose to contribute to larger collaborative research effort between the Ackerley laboratory, the Auckland Cancer Society Research Centre (ACSRC) and researchers at the Universities of Nottingham and Maastricht, to advance *Clostridia*-directed enzyme prodrug therapy (CDEPT) toward a human clinical trial. The research I performed was only a small contribution to identify the most promising wild-type bacterial nitroreductase enzymes, by enzyme kinetic analysis and IC₅₀ assays, with two next generation prodrugs under consideration for the human clinical trial; PR-104A and SN36506. This research opportunity also motivated a small investigation in to bacteria bystander effect SN36506 and other next generation prodrugs.

1.7 Thesis aims

A key aim of this thesis was to develop a standardized method for measuring the bacterial bystander effect in an appropriate model of BDEPT. A secondary goal was to explore the role of the bacterial bystander effect on the efficacy of FACS as a screen for directed evolution of bacterial nitroreductases.

1. Develop an assay to measure the bacterial bystander effect in bacterial model of BDEPT (**Chapter 3**).
2. A related aim was to discover whether bacterial cell-to-cell transfer might be impeding our ability to evolve better nitroreductases using FACS screening (**Chapter 4**).
3. Based on a surprising finding from Aim 1, that CB1954 appears to exhibit a far greater bystander effect from a bacterial activating cell than a transfected human cell, an additional aim was to evolve a better nitroreductase for application in CB1954 BDEPT (**Chapter 5**).

4. During the course of this research the opportunity arose to contribute to an ongoing CDEPT study, giving rise to an additional aim of identifying the most promising nitroreductase/prodrug combination from multiple candidates **(Chapter 6)**.

2 Methods

2.1 Chemicals and growth media

The nitroaromatic compounds metronidazole (2-(2-methyl-5-nitro-1H-imidazol-1-yl)ethanol) and niclosamide (5-Chloro-N-(2-chloro-4-nitrophenyl)-2-hydroxybenzamide) were obtained from Sigma–Aldrich (St. Louis, MO). CB1954 (5-[aziridin-1-yl]-2,4-dinitrobenzamide) was purchased from MedKoo Bioscience (Morrinsville, NC). The prodrugs PR-104A (2-((2-bromoethyl)-2-(((2-hydroxyethyl)amino)carbonyl)-4,6-nitroanilino)ethylmethanesulfonate) and its di-bromo analogue SN27686 as well as dinitrobenzamide mustards (DNBM) SN31609 and SN36506 and nitro-CBI-DEI (nitro-CBI-5-[[dimethylamino]ethoxy]indole) were synthesised in-house at the Auckland Cancer Society Research Centre (ACSRC), Auckland, New Zealand. Stock solutions of all prodrugs were made up in dimethyl sulfoxide (DMSO) and stored at -80 °C.

Restriction enzymes were purchased from New England Biolabs (NEB; Ipswich, MA, USA) and Thermo Fisher Scientific (Waltham, MA, USA). BioMix™ Red Polymerase Mastermix was purchased from Bioline (London, UK). Phusion™ high-fidelity DNA polymerase was purchased from New England Biolabs (NEB; Ipswich, MA, USA). Agilent Technologies. Bugbuster HT Protein Extraction Reagent was purchased from Merck Millipore (Billerica, Massachusetts, USA). Unless otherwise stated, all other chemicals and reagents were purchased from Sigma-Aldrich (St. Louis, MO, USA), Thermo Fisher Scientific (Waltham, MA, USA), or Total Lab Systems (Auckland, NZ).

2.2 Software

All nucleotide sequence alignments were generated using Geneious 8.0 (Biomatters Ltd; Auckland, NZ). Plasmid maps were generated using the open-source visualisation software AngularPlasmid (<http://angularplasmid.vixis.com/>; Vixis, LLC) or Genscript (<https://www.genscript.com/gensmart-design>). Graphs were generated using GraphPad Prism 7.0 (GraphPad Software Inc.; La Jolla, CA, USA). Flow cytometry data was processed using either the Flowing Software version 2.5.1 by Perttu Terho (Turku Centre for Biotechnology, Turku, Finland) or Flowjo (© FlowJo, LLC, 2013–2018; BD Biosciences San Jose, CA).

2.3 Wild-type Nitroreductases used in this study

A broad range of wild-type nitroreductases were used in this investigation. **Table 2.1** provides a summary of these enzymes where each nitroreductase is referred to using standard nomenclature followed by an underscore and a two letter abbreviation of the genus and species; for example NfA_Ec indicates the NfsA enzyme derived from *E. coli*.

Species	Enzyme	Oxidoreductase Family
<i>Bacillus subtilis</i>	NfrA_Bs	NfsA
<i>Escherichia coli</i>	NfsA_Ec	NfsA
<i>Enterobacter (Chronobacter) sakazakii</i>	NfsA_Es	NfsA
<i>Bacillus subtilis</i>	YcnD_Bs	NfsA
<i>Escherichia coli</i>	NfsB_Ec	NfsB
<i>Vibrio vulnificus</i>	NfsB_Vv	NfsB
<i>Bacillus subtilis</i>	Ydgl_Bs	NfsB
<i>Neisseria meningitidis</i>	NfsB_Nme	NfsB
<i>Bacillus licheniformis</i>	YfkO_Bli	NfsB
<i>Bacillus subtilis</i>	YfkO_Bs	NfsB

Table 2.1 Summary of ten wild-type nitroreductase enzymes used in this investigation. Each nitroreductase is referred to using standard nomenclature followed by an underscore and a two letter abbreviation of the genus and species for example NfA_Ec indicates the NfsA enzyme derived from *E. coli*.

2.4 Oligonucleotide primers

Oligonucleotide primers used in this study were supplied as lyophilised powders by Integrated DNA Technologies (IDT; Coralville, IA, USA). Primer stock solutions of 100 µM were made up in Tris-EDTA (TE; 10 mM Tris-HCl pH 8.0, 0.1 mM EDTA). Working primer solutions of 10 µM were made by diluting the 100 µM primer stocks in autoclaved and filter sterilized double distilled H₂O (MQ). Working and stock solutions were stored at -20 °C. The sequences of all primers used in this study are detailed in **Table 2.2**.

Primer name **Sequence (5'-3')**
 (underlined text indicate restriction sites used for cloning)

Plasmid specific

pmmB_Fw GGCTCGTATAATGTGTGG
pmmB_Rv GACCGCTTCTGCGTTCTGAT
pUCX_Fw GACATCATAACGGTTCTG
pUCX_Rv GTTTCACCTTCTGAGTTCG
T7_promoter TAATACGACTCACTATAGGG
T7_terminator GCTAGTTATTGCTCAGCGG
ACYCDuetUP1 GGATCTCGACGCTCTCCCT
DuetDOWN1 GATTATGCGGCCGTGTACAA

Gene specific

NfsA_Ec_Fw GGCATATGACGCCAACCATTGAAC
NfsA_Ec_Rv GGGTCGACTTAGCGCGTCGCCCAACCCTG
NfsB_Ec_Fw GGGCATATGGATATCATTCTG
NfsB_Ec_Rv GGGGAATTCTTACACTTCGGTTAAG
YfkO_Bs_Fw GGGGCATATGGCAGATCTAAAGACACA
YfkO_Bs_Rv CTAGGTCGACTTAAACCCACTTCACAACAT
YfkO_Bli_Fw GGGGCATATGACAGAGCAATCCAAG
YfkO_Bli_Rv CCCCCTCGACTTATTCGACCCATTTTC

Table 2.2 Summary of primers used in this investigations. For nitroreductase specific primers each nitroreductase is referred to using standard nomenclature followed by an underscore and a two letter abbreviation of the genus and species for example NfsA_Ec indicates the NfsA enzyme derived from *E. coli*.

2.5 Bacterial strains and plasmids

2.5.1 Bacterial strains

All *E. coli* expression and screening strains used in this study are described in **Table 2.3** and all bacterial strains used as sources of genomic DNA in this study are listed in **Table 2.4**.

For screening we employed the *E. coli* strains 7NT and SOS-R4 that were previously developed by members of the Ackerley laboratory (Copp et al., 2014). Both strains are isogenic derivatives of the *E. coli* strain W3110, which has seven endogenous nitroreductase candidate genes (*nfsA*, *nfsB*, *azoR*, *nema*, *mdaB*, *yieF* and *ycaK*) deleted to reduce background activation of nitroaromatic prodrugs together with deletion of the *tolC* efflux pump gene to restrict active ejection of unreduced prodrug. The SOS-R4 strain additionally contains a spectinomycin resistant plasmid bearing a green-fluorescent-protein-mut3 (GFP) reporter gene controlled by the SOS inducible *sfiA* promoter.

The 7KO strain, similarly to 7NT, has had the seven endogenous nitroreductase candidate genes deleted but does contain a functional *tolC* efflux pump. To enable co-incubation of 7NT or 7KO cells with SOS-R4 strains the empty plasmid pCDFDuet was transformed into the 7NT and 7KO strains to confer spectinomycin resistance.

A commercially available *E. coli* strain, from Novagen, BL21 was used to express the protein of nitroreductases under investigation.

All of the bacterial strains used in this investigation are detailed in **Table 2.3**

Strain	Relevant characteristics	Source
W3110	<i>E. coli</i> K12 F ⁺ λ ⁻ rph-1 IN(rrnD-rrnE)1	Lab stock
7KO	Δ <i>nfsA</i> , <i>nfsB</i> , <i>azoR</i> , <i>nema</i> , <i>yieF</i> , <i>ycaK</i> and <i>mdaB</i>	(Williams, 2013)
7NT	7KO Δ <i>tolC</i>	(Copp et al., 2014)
SOS-R4	7NT containing pANODuet (GFP SOS plasmid)	(Copp et al., 2014)
BL21	F- <i>ompT gal dcm lon hsdS_B</i> (r _B ⁻ m _B ⁻) λ(DE3)	Novagen

Table 2.3 Bacterial strains used in this study, key features and origins.

2.5.2 2.4.2 Bacterial sources of genomic DNA

The bacterial strains used as sources of genomic DNA in this investigation are detailed in **Table 2.4**.

Strain	Source
<i>Escherichia coli</i> W3110	Lab stock
<i>Bacillus subtilis</i> subsp. <i>subtilis</i> str. 168	Brady lab
<i>Vibrio vulnificus</i>	Lab stock

Table 2.4 Bacterial strains used as sources of genomic DNA in this study.

2.5.3 Plasmids

All plasmids used for transformation of *E. coli* cells are listed in **Table 2.5**. The plasmid maps of the vectors used for expression of bacterial nitroreductase enzymes and GFP in *E. coli* are also displayed. Plasmid maps are provided for pUCX (**Figure 2.1**), pANODuet-1: GFP (**Figure 2.2**) pET28A (**Figure 2.3**) and pCDF-Duet 1 (**Figure 2.4**).

Plasmid	Resistance	Description	Source
pUCX	Ampicillin	Nitroreductase expression vector. <i>tac</i> promoter, <i>lac</i> operator	(Prosser, Patterson, et al., 2010)
pET28A(+)	Kanamycin	Expression vector for His ₆ -tagged enzyme expression. T7 promoter, <i>lac</i> operator	Novagen
pANODuet-1 GFP	Spectinomycin	GFPmut3b expression under control of <i>sulA/sfiA</i> SOS promoter.	(Copp et al., 2014)
pCDFDuet -1	Spectinomycin	Used only to provide additional antibiotic resistance. T7 promoter, <i>lac</i> operator	Novagen

Table 2.5 Plasmids used for cloning.

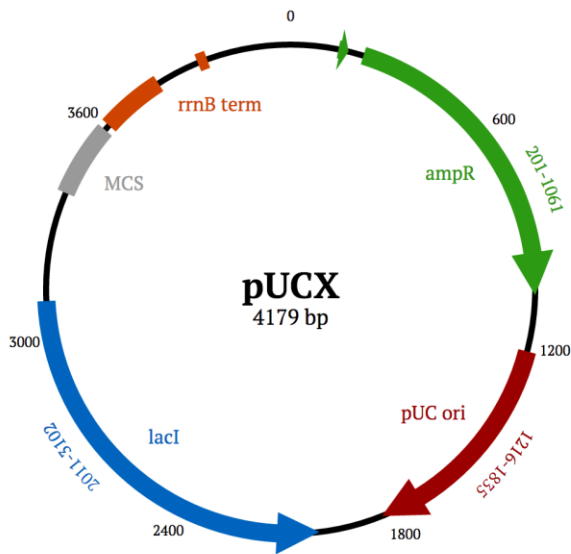


Figure 2.1 Plasmid map of nitroreductase expression vector pUCX. Numbers denote the base pair location of genes of interest. Key features of the plasmid include the ampicillin resistance cassette (green), pUC ori (red), lacI repressor (blue), multiple cloning site (includes promoter, operator and ribosome binding sites, and the rrnB terminators (orange). Reproduced with permission from (Rich (2017).

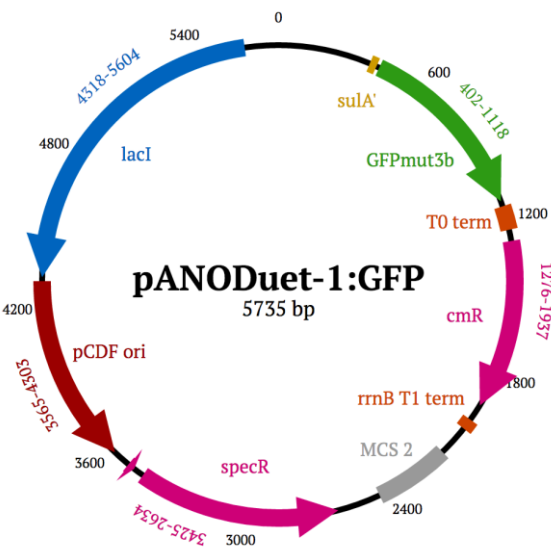


Figure 2.2 Plasmid map of SOS-inducible GFP plasmid pANODuet-1: GFP. Numbers denote the base pair location of genes of interest. Key features of the plasmid include the sulA' SOS promoter (yellow), GFPmut3b gene (green), lambda T0 and rrnB T1 terminators (orange), chloramphenicol (cm) and spectinomycin (spec) resistance cassettes (pink), MCS2 of pCDFDuet-1 (grey), pCDF ori (red), and lacI repressor (blue). Reproduced with permission from Rich (2017).

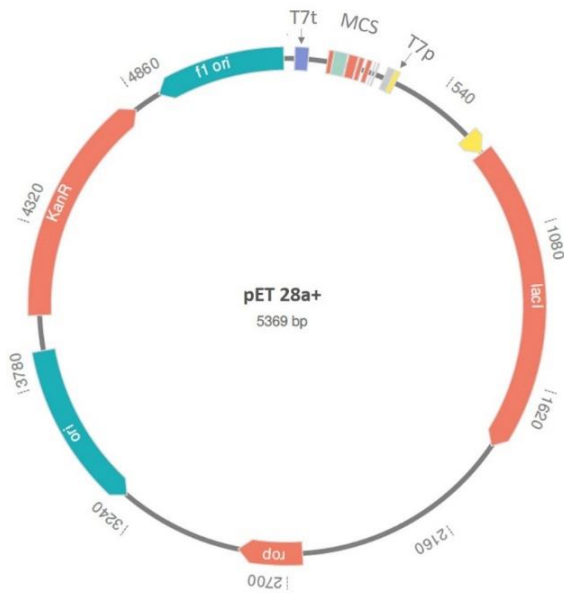


Figure 2.3 Plasmid map of expression vector pET28a+, used for His6-tag protein expression and expression of multi-genomic DNA in this study. Numbers denote the base pair location of genes of interest. Key features of the plasmid include the kanamycin resistance (Kan^R) gene cassettes, f1 origin (f1 ori), lac repressor (lacI), multiple cloning site (MCS) includes promoter, operator and ribosome binding sites) and ROP regulatory protein (rop), T7 terminator (T7t) and T7 promoter (T7p).

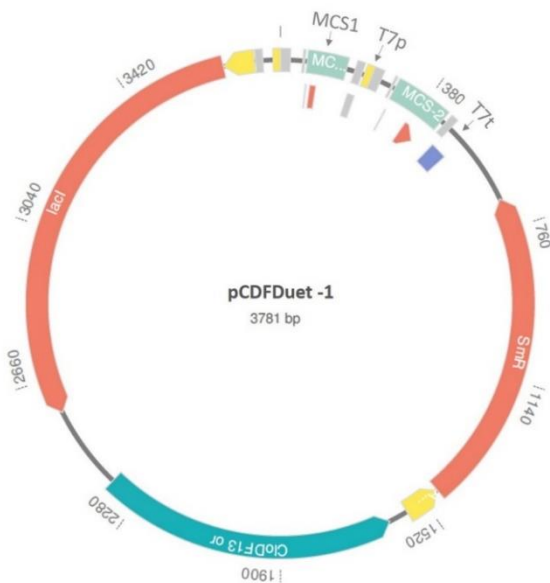


Figure 2.4 Plasmid map of pCDF-Duet 1 used to provide spectinomycin resistance to 7NT cell strains. Numbers denote the base pair location of genes of interest. Key features of the plasmid include the spectinomycin resistance (Sm^R) gene cassettes, lac repressor (lacI), multiple cloning site 1 (MCS1) includes promoter, operator and ribosome binding sites) and origin of replication (CloDF13 ori), T7 terminator (T7t) and T7 promoter (T7p).

2.6 Growth media

All growth media were made up in double distilled H₂O that were sterilised by autoclaving at 121 °C for 30 minutes. All growth media were stored at room temperature. Liquid growth media and solid growth media used in this study are detailed in **Table 2.6**.

2.6.1 Liquid media

The only type of liquid media was used in this study was Lysogeny broth (LB) that was supplemented with various additives such as antibiotics depending on the bacterial strain being cultured. The only exception was SOC media which is Superoptimal broth, when lacking Mg²⁺ ions and glucose, *extra reagents were added post-autoclave after which the media was renamed SOC. These extra reagents were filter-sterilized prior to use.

Media type	Contents	Notes
Lysogeny broth	Tryptone 10 g.L ⁻¹ Yeast extract 5 g.L ⁻¹ NaCl 5 g.L ⁻¹	Premixed LB powder was provided by Duchefa Biochemie
SOC media	Tryptone 10 g.L ⁻¹ Yeast extract 5 g.L ⁻¹ NaCl 5 g.L ⁻¹ KCl 2.5 mM MgCl ₂ 10 mM* Glucose 20 mM* MgSO ₄ 10 mM*	

Table 2.6 Liquid media used in this study.

2.6.2 Solid Media

Agar plates were exclusively used as the solid growth media in this investigation. Agar solid growth media was made by adding molecular biology-grade agar powder purchased from Duchefa Biochemie, equivalent to 1.5% (w/v) final concentration, to Luria broth followed by autoclaving. As necessary, the growth media was supplemented with antibiotics post autoclaving when the media had cooled to <50 °C to prevent denaturing of the antibiotics. The agar was poured into sterile 90 mm × 15 mm Petri dishes in a

laminar fume hood and left to solidify. Plates were stored at 4 °C for no more than two weeks prior to use.

2.6.3 Bacterial antibiotics and indication agents

Antibiotic powders were commercially purchased from Duchefa Biochemie. Autoclaved double distilled H₂O was used as the solvent for all the antibiotics used in this study as detailed in **Table 2.7**. All antibiotic working stocks were filter sterilized using a 0.22 µm filter and stored in aliquots of <1mL in -20 °C indefinitely. Final concentrations of antibiotics used to propagate plasmids in this study are also described in **Table 2.7**.

Antibiotic	Final Concentration
Ampicillin	100 µg.L ⁻¹
Kanamycin	50 µg.L ⁻¹
Spectinomycin	50 µg.L ⁻¹

Table 2.7 Antibiotics used in this investigation.

Isopropyl β-D-1-thiogalactopyranoside (IPTG) for induction of genes from the *lac* operator was made up in autoclaved double distilled H₂O to a concentration of 420 mM (10%w/v), filter sterilised using a 0.22 µM filter and stored in aliquots at -20 °C.

2.7 Growth and storage of bacterial strains and variants

Unless otherwise stated, bacteria were cultured at 37 °C in a static incubator if on solid media or at 200 revolutions per minute (rpm) if in liquid culture media. For short term storage of bacterial strains on solid media the agar plates were refrigerated at 4 °C. For long term storage of liquid cultures 40% glycerol stocks were created by mixing with autoclaved 80% (v/v) glycerol with the bacterial liquid culture in a 1:1 ratio. These bacterial glycerol stocks were stored indefinitely at -80 °C.

2.8 Cloning methods & routine molecular biology

2.8.1 Isolation of plasmid DNA

Plasmid DNA was extracted from a 3 mL overnight culture using the High-Speed Plasmid Mini Kit (*Geneaid Biotech Ltd; New Taipei City, Taiwan*) according to the manufacturer's instructions. Plasmid DNA was stored at -20 °C.

2.8.2 Polymerase chain reaction (PCR) protocol

For downstream cloning applications PCR products were generated using Phusion™ high-fidelity polymerase. In contrast for colony screening and for diagnostic PCR purposes Biomix Red™ was used. These two different protocols were used based on the greater expense of the Phusion™ high-fidelity polymerase – which being high fidelity results in less PCR errors that can introduce mutations in to PCR products. This higher quality of PCR product is not necessary for colony screening as the PCR products are not used for further research.

The melting temperature (T_m) depends on the length of the DNA molecule and its specific nucleotide sequence and GC content. When primers are ordered commercially they typically have T_m provided on the tube label by the manufacturer. If not provided this can be easily calculated using online tools and the sequence of the primers. To ensure that both primers are able to anneal correctly the T_m temperature selected for a PCR is typically set at 5°C less than the T_m of the primer with the lower T_m . For example if the T_m of the forward primer is 60°C and the reverse primer is 55°C then the T_m would be set at 50°C.

2.8.2.1 Protocol for PCR with Biomix™ Red

For colony screens and diagnostic PCRs, a 10 µL reaction consisting of 1xBiomix™ Red, 0.5 µM forward and reverse primers was used with a sample of 10 – 50 ng purified plasmid DNA or a small amount of *E. coli* colony, picked directly from an agar plate with a sterile toothpick or pipette tip. The standard PCR protocol used is shown in **Table 2.8**. The thermal cycling parameters are detailed in **Table 2.9**.

Component	Volume
Biomix™ Red	10 µL
Primer 1	1 µL
Primer 2	1 µL
Template DNA	0.2-1 µL
ddH ₂ O	To 20 µL final volume

Table 2.8 Components for colony PCR with Biomix™ Red.

Temperature (°C)	Time	
95	5 min	
95	20 sec	30-35 cycles
Lowest primer	10-30sec	
Tm-5		
72	30 sec per Kb	
72	5min	
16	Hold	

Table 2.9 Thermal cycling parameters for colony PCR with Biomix™ Red.

2.8.2.2 Protocol for PCR with Phusion™

For high-fidelity PCR, a 20 µL PCR using Phusion™ high-fidelity polymerase was performed. All gene products amplified by Phusion™ PCR and cloned into a plasmid were sequence verified before use in downstream applications. The standard PCR protocol used is shown in **Table 2.10**. The thermal cycling parameters are detailed in **Table 2.12**.

Component	Volume
5 × Phusion™ HF buffer	4 µL
10 mM dNTP mix	0.4 µL
Phusion™ high-fidelity polymerase	0.2 µL
Primer 1	1 µL
Primer 2	1 µL
Template DNA	0.2-1 µL
ddH ₂ O	To 20 µL final volume

Table 2.10 Components for high-fidelity PCR with Phusion™ high-fidelity polymerase.

Temperature (°C)	Time	
98	2 min	
98	10 sec	30-35 cycles
Lowest primer T _m -5	10-30sec	
72	30 sec per Kb DNA	
72	5 min	
16	Hold	

Table 2.11 Thermal cycling parameters for high-fidelity PCR with Phusion™ high-fidelity polymerase.

2.8.3 DNA product purification

Purification of DNA samples such as PCR products was performed using the DNA Clean and Concentrator™ kit (Zymo Research; Irvine, CA, USA), according to the manufacturer’s instructions. Products were eluted in elution buffer warmed to 70 °C and stored at -20 °C.

2.8.4 DNA quantification

Concentration in µg/mL and purity of DNA in PCR and plasmid samples was measured using a NanoDrop ND-1000 spectrophotometer (Thermo Scientific, Waltham, MA, USA), using the manufacturer’s instructions.

2.8.5 DNA Sequencing

All DNA sequencing was performed commercially by Macrogen Inc. (Seoul, South Korea) to determine the sequence of nitroreductase mutants of interest and verify correct insertion orientation and sequence of nitroreductase genes post insertion into a new plasmid.

2.8.6 Agarose gel electrophoresis

To analyse the size of PCR products, plasmid digests and other DNA samples, small volumes of 1-20 μL were run on ethidium bromide-containing 1 % agarose gels (1 % w/v agarose in 1 \times TAE buffer, 1 $\mu\text{g mL}^{-1}$ ethidium bromide), immersed in 1 \times TAE buffer in a suitable electrophoresis tank at 120-135 volts for 25-40 minutes. DNA was visualised under UV light and size determined by comparison to Hyperladder I (Bioline, London, UK).

2.8.7 Restriction digests

The composition of the restriction enzyme reactions are detailed in **Table 2.12**. Restriction digests were incubated at 37 $^{\circ}\text{C}$ in a PCR machine for 3-4 hours, prior to heat inactivation for the length of time stipulated at the temperature recommended by the manufacturer of the particular restriction enzymes used. Digested DNA was then purified using the DNA purification protocol previously outlined in 2.7.3. This was followed by analysis of 50-200 ng DNA by agarose gel electrophoresis to confirm success of restriction digest. Purified digested DNA samples were stored at 4 $^{\circ}\text{C}$ until use in ligation within 1-2 days of restriction digest. The Thermo Fisher Fast digest enzymes were used throughout this set of investigations.

Plasmid

Component	Volume per 100 μ L reaction
10 \times Restriction buffer	10 μ L
Restriction enzyme 1*	1 μ L
Restriction enzyme 2*	1 μ L
Plasmid DNA	2 μ g
ddH ₂ O	To 20 μ L final volume

*Total enzyme <4% of total digest volume

Insert DNA

Component	Volume per 20 μ L reaction
10 \times Restriction Anza buffer	2 μ L
Restriction enzyme 1*	1 μ L
Restriction enzyme 2*	1 μ L
Insert DNA	1 μ g
ddH ₂ O	To 20 μ L final volume

Table 2.12 Components for restriction digest.

2.8.8 Ligation

The quantities of components used in the DNA ligation reactions are shown in **Table 2.13**. Invitrogen T4 DNA Ligase was used for ligation reactions. Ligations were incubated overnight at 16 °C in a PCR machine before being used to transform cells. The ligation products were then used directly to transform *E. coli*.

Component	Final concentration
Linear vector DNA	> 100 ng
Insert	6:1 molar ratio over vector
10x ligase buffer	2 μ L (1x final concentration)
Ligase (1 U. μ L ⁻¹)	1 μ L per 200 ng total DNA
ddH ₂ O	Up to 20 μ L total volume

Table 2.13 Ligation protocol with T4 DNA ligase.

2.8.9 Transformation of *E. coli*

2.8.9.1 Preparation of electrocompetent cells used between 2014-2017 (Chapters 3-4)

Overnight cultures of 50mL LB, with appropriate antibiotics if required, were inoculated with a sample of the glycerol stock of the *E. coli* strain to be made competent. A 100 μ L pipette tip was used to scoop a small amount of the 40% glycerol stock kept in the -80 °C freezer and was dropped into an autoclaved 50 mL flask containing the medium. The culture was then grown overnight at 37 °C, 200 rpm. The following day, a day culture starting at 0.1 OD₆₀₀ was made by first measuring the OD₆₀₀ of the overnight culture and transferring the appropriate amount to an autoclaved 2 L flask containing 400 mL of medium. To accurately measure the OD₆₀₀ of the overnight culture a dilution was required; 200 μ L of the overnight culture was mixed with 800 μ L of LB prior to reading on a spectrophotometer. The day culture and grown at 37 °C, 200 rpm until an OD₆₀₀ of ~0.4-0.6 was reached typically 2-3 hours after initiating the day culture. The culture was then transferred into eight pre-chilled 50 mL falcon tubes a rested on ice for 1 hour prior to centrifugation at 4,000 rpm, 12 minutes at 4 °C. The supernatant was discarded and each cell pellet gently resuspended and in 50 mL of ice cold ddH₂O and centrifuged at 4,000 rpm, 12 minutes at 4 °C. Again supernatant was discarded and each cell pellet gently resuspended in 25 mL of ice cold 10% glycerol, eight tubes were combined into four 50 mL falcons and centrifuged at 4,000 rpm, 15 minutes at 4 °C. Again supernatant was discarded and each cell pellet gently resuspended in 15 mL of ice cold 10% glycerol, combine the four tubes into one pre-chilled 50 mL falcon and centrifuged at 4,000 rpm, 15 minutes at 4 °C. The supernatant was discarded and the final cell pellet resuspended in 150 μ L of 10% glycerol.

At this point, the concentration of *E. coli* was determined by measuring the OD₆₀₀ of a 1:1000 dilution of the cell preparation. The OD₆₀₀ value of 1.0 is approximately equivalent to an *E. coli* density of 2.5×10^8 cells mL⁻¹, the cell prep was adjusted to $2-3 \times 10^{10}$ cells mL⁻¹, either by the addition of extra 10 % glycerol, or by re-centrifuging and resuspending in a lower volume. The cells were then aliquoted (45-125 μ L) into sterile 1.5 mL microfuge tubes and snap frozen using a metal tube rack pre-chilled to -80 °C. Competent cell aliquots were stored at -80 °C indefinitely.

2.8.9.2 Preparation of electrocompetent cells used between 2018-2019 (Chapter 5)

A new protocol for preparation of electrocompetent cells became common practice in the Ackerley laboratory as generally higher levels of competency has been observed by other members of the group.

The bacterial strain to be made competent was streaked onto an LB agar plate and incubated overnight at 37 °C. One colony was picked, used to inoculate 4 ml LB medium and grown overnight at 37 °C, 200 rpm. The overnight culture was used to inoculate 400 ml LB medium at a 1:100 dilution. The day culture was grown at 37 °C, 200 rpm until an OD₆₀₀ of 0.4-0.7 was reached, at which point the culture was separated into eight 50 ml centrifuge tubes and incubated on ice for 30 minutes. Cells were pelleted by centrifugation at 2,600 x g, 4 °C for 10 min, the supernatant was discarded, and the pellets were gently resuspended in 50 ml ice-cold, sterile ddH₂O. The resuspended cells were pelleted by centrifugation at 2600 x g, 4 °C for 10 min, the supernatant was discarded, and the pellets were gently resuspended in 25 ml ice-cold, sterile 10% (v/v) glycerol. The resuspended cells were pooled into four 50 ml centrifuges tubes, pelleted by centrifugation at 2,600 x g, 4 °C for 10 min, the supernatant was discarded, and the pellets were gently resuspended in a total volume of 15 ml ice-cold, sterile 10% (v/v) glycerol. The resuspended cells were pooled into one 15 ml centrifuge tube, centrifuged at 2,600 x g, 4 °C for 10 min and the supernatant was discarded. The pellet was resuspended in the minimum volume of sterile 10% (v/v) glycerol necessary to generate a homogeneous liquid suspension (<500 µL). Cells were aliquoted in 45-90 µL volumes and used immediately or snap frozen for storage at -80 °C until required.

2.8.9.3 Transformation of electrocompetent cells

Aliquots of electrocompetent cells were thawed on ice. DNA to be electroporated was incubated with cells on ice for 15 min. Per 40 µL cell aliquot, ≤1 µL of a ≤10 ng/µL ligation was added, or up to 10 ng of purified plasmid DNA. Cells were transferred to a pre-chilled 0.2 mm gap electroporation cuvette and electroporated using a Bio-Rad GenePulser Xcell™ (Hercules, CA, USA). The cells were pulsed at 2.5 kV, 25 µF capacitance, 200 Ω resistance. For recovery, 960 µL of room temperature SOC medium was immediately added and the entire culture volume was transferred to a 1.5 ml microcentrifuge tube and incubated at 37 °C, 200 rpm for 45-60 min. Recovered cells were pelleted (17,000 x g, 2

min), the supernatant was discarded, and the pellet was resuspended in 200 μ L LB medium and spread onto an agar plate containing the applicable antibiotic. Agar plates were incubated at 37 $^{\circ}$ C in a static incubator overnight, for approximately 16 hours, or until colonies became visible.

2.8.9.4 Preparation of chemically competent cells 2014-2017 (Chapters 3-4)

Overnight cultures of 3mL LB supplemented with sterile 10 mM $MgCl_2$ and appropriate antibiotics (if required), were inoculated with a sample of the glycerol stock of the *E. coli* strain to be made competent. A 100 μ L pipette tip was used to scoop a small amount of the 40% glycerol stock kept in the -80 $^{\circ}$ C freezer and was dropped into a 15 mL falcon tube containing the medium. The culture was then grown overnight at 37 $^{\circ}$ C, 200 rpm. The following day, the 100 μ L of the overnight transferred into 10 mL LB + 10 mM $MgCl_2$ culture and grown at 37 $^{\circ}$ C, 200 rpm until an OD_{600} of \sim 0.4-0.6 was reached typically 2-3 hours after initiating the day culture. At this point the cells were transferred to ice for 10-15 minutes. Cells were then centrifuged at 4 $^{\circ}$ C, 4,000 rpm for 10 minutes, the supernatant was discarded and the cell pellet resuspended in 0.8 x volume of the day culture in ice-cold TFB I (**Table 2.14** for buffer recipe). Resuspended cells remained on ice for 2 hours followed by another centrifugation at 4 $^{\circ}$ C, 4,000 rpm for 10 minutes. The supernatant was discarded and the cell pellet resuspended in 0.1 volumes of ice-cold TFB II (**Table 2.14**). Cells were aliquoted (100-200 μ L) into sterile 1.5 mL microfuge tubes and snap frozen using a metal tube rack pre-chilled to -80 $^{\circ}$ C. Competent cell aliquots were stored at -80 $^{\circ}$ C indefinitely.

2.8.9.5 Preparation of chemically competent cells 2018-2019 (Chapter 5)

An overnight culture of the bacterial strain to be made competent was grown in 3 ml of LB medium supplemented with antibiotic as required at 37 $^{\circ}$ C, 200 rpm. The overnight culture was used to inoculate 100 ml LB medium at a 1:100 dilution. The culture was grown until an OD_{600} of 0.35-0.4 was reached, after which the culture was rested and chilled on ice for 10 minutes and then pelleted at 4 $^{\circ}$ C, 2,600 x g for 10 minutes. The supernatant was discarded, and the cell pellet was resuspended in 0.8 of a volume of ice cold, sterile 100 mM $MgCl_2$. The resuspended cells were pelleted at 4 $^{\circ}$ C, 2,600 x g for 10 minutes. The supernatant was discarded, and the cell pellet was resuspended in 0.8 of a volume of ice cold, sterile 100 mM $CaCl_2$. The resuspended cells were pelleted at 4 $^{\circ}$ C,

2,600 x g for 10 minutes. The supernatant was discarded, and the cell pellet was resuspended in 2 ml ice cold, sterile 85 mM CaCl₂, 15% glycerol. Cells were aliquoted in 10-100 µL volumes and immediately used or snap frozen for storage at -80 °C until required.

Component	Final concentration	Stock concentration	Volume required
TFB I*			
Potassium acetate	30 mM	1 M	1.5 mL
MnCl₂	50 mM	1 M	2.5 mL
CaCl₂	10 mM	1 M	0.5 mL
Glycerol		80%	9 mL
MQ H₂O			36.5 mL
TFB II*			
Sodium MOPS, pH 7.0	10 mM	1 M	0.25 mL
CaCl₂	75 mM	1 M	1.875 mL
KCl	10 mM	1 M	0.25 mL
Glycerol		80%	4.5 mL
MQ H₂O			22.6 mL

* TFB I & II transformation buffers were sterile-filtered (0.22 µm) prior to use. Long term storage was at 4 °C.

Table 2.14. Recipes for transformation buffers

2.8.9.6 Transformation into chemically competent cells

Chemically competent cell aliquots were removed from the -80 °C storage and thawed on ice for 5-10 minutes. For each transformation 100 µL competent cells was used. Plasmid DNA to be transformed was added (never more than 0.1 the volume of competent cells being used) to the cells and the mixture was incubated on ice for 15 minutes. Cells were then heat shocked at 42 °C for 90 seconds, typically in a heating block, and then returned to ice for 5 minutes. Then 900 µL of LB was added to each tube, followed by a recovery incubation at 37 °C for 45-60 minutes. Recovered cells were pelleted (17,000 x g, 3 min), the supernatant was discarded, and the pellet was resuspended in 200 µL LB medium and spread onto an agar plate containing the appropriate antibiotic. Agar plates were

incubated at 37 °C in a static incubator overnight, for approximately 16 hours or until colonies became visible.

2.8.10 SDS-PAGE

Preparation and running of SDS-PAGE was carried out essentially as in the Laemmli-SDS-PAGE protocol (He, 2011). 12-15 % polyacrylamide gels (1 mm thickness) were cast and run on a Bio-Rad Protean II™ apparatus, according to the manufacturer's instructions. Briefly, ~5 mL of pre-set 12-15 % stacking gel (**Table 2.15**) was applied to the gel cast and covered with ~1 mL of ddH₂O. The gel was left to set for roughly 30 minutes, followed by discarding of the ddH₂O by tipping the whole apparatus upside down and dabbing with a paper towel. Approximately 1.5 mL of pre-set 4 % loading gel was then pipetted over the top of the separating gel, a multi-well comb inserted and left to solidify for at least 1 hour. At this point the gel could be stored in paper towels soaked in 1x SDS-PAGE buffer and sealed in glad-wrap for 1-2 days. Samples to be run on SDS-PAGE were added in a 2:1 ratio to 3 × SDS-load buffer. Samples (typically 30 µL total) were boiled at 90-100 °C for 10 minutes prior to electrophoresis. Gels were run in 1 × SDS-Run buffer, at constant voltage (175 Volts) for 45-60 minutes. Protein bands in gels were stained by gentle shaking in Coomassie blue stain solution overnight on an orbital shaker. Destaining was carried out by washing the gel of all Coomassie blue stain in running tap water, followed gentle shaking in 1cm of destain solution for 30 minutes, then rinsing with tap water again. This 30 minute destain and rinse was repeated. The gel was typically left for another 2-3 hours in destain until the protein bands became clearly visible with acceptable contrast.

Component	Concentration
15 % separating gel	Per 10 mL
40 % acrylamide solution	3.65 mL
2 % Bis-acrylamide solution	2 mL
1.5 M Tris-Cl pH 8.8	2.5 mL
10 % SDS	100 μ L
ddH₂O	1.75 mL
10% APS*	100 μ L
TEMED*	6 μ L
4 % stacking gel	Per 3 mL
40 % acrylamide solution	288 μ L
2 % Bis-acrylamide solution	156 μ L
0.5 M Tris-Cl pH 6.8	750 μ L
10 % SDS	30 μ L
ddH₂O	1.77 mL
10% APS*	30 μ L
TEMED*	5 μ L
3 \times SDS-load buffer	Final concentration
Tris-Cl, pH 6.8	150 mM
SDS	6 % (w/v)
Bromophenol blue	0.3 % (w/v)
Glycerol	30 % (w/v)
β-Mercaptoethanol	300 mM
1 \times SDS-run buffer**	Per 1 L
Glycine	14.4 g
Tris	3.03 g
SDS 1 g	1 g
Coomassie blue stain	Per 1 L
Coomassie Brilliant Blue	2.5 g
100 % Ethanol	450 mL

100 % Acetic Acid	100 mL
ddH₂O	450 mL
<hr/>	
Destain	Per 1 L
<hr/>	
100 % Methanol	400 mL
Acetic acid	100 mL
ddH₂O	500 mL

*Added immediately prior to pouring gel

**SDS-run buffer was prepared as a 10 × solution, with ddH₂O used to dilute to 1

× when necessary.

Table 2.15 Summary of SDS-PAGE reagents and their components.

2.9 Protein expression culture and cell lysis

2.9.1 Long over-expression protein culture

A small amount of glycerol stock of *E. coli* BL21(DE3) harbouring pET28+:*ntr*, where *ntr* denotes any nitroreductase cloned into the multiple cloning site of pET28a(+), was used to inoculate 50 mL LB medium, in an autoclaved 200 mL glass flask, supplemented with kanamycin (50 µg mL⁻¹) to maintain the pET28+ plasmid. The culture was then incubated at 37 °C at 200rpm overnight for approximately 16 hours. The following morning in an autoclaved 2 L flask, 400 mL LB medium supplemented with kanamycin (50 µg mL⁻¹) was inoculated with overnight culture to generate a starting OD₆₀₀ of 0.1. This was typically 10-15 mL of the overnight culture. The overnight culture was measured at a one in five dilution of 200 µL of the overnight well mixed with 800 µL of LB prior to reading in the spectrophotometer. This day culture was incubated at 37 °C, 200 rpm until the OD₆₀₀ of the culture reached 0.4-0.6 which was typically 2-3.5 hours. The cultures were then rested on ice for 15 minutes before the enzyme expression was induced by adding IPTG to a 0.5 mM final concentration (this equated to 400 µL of 10% IPTG added to 400 mL of protein day culture). The flasks were then transferred to an 18 °C, 200 rpm incubator for approximated 40-45 hours. A 500 µL sample was collected of the culture prior to IPTG induction while the flasks rested on ice as well as after the 45 hour long over expression culture and was set aside and stored at -20 °C for examination by SDS-PAGE

Growing the protein expression cultures at the low temperature of 18 °C for ~45 hours allows an extended time for protein expression. The lower temperature and longer expression time promotes protein folding into the correct tertiary structure; thus is one

of the optimization techniques used to increase production of soluble protein yield. After the 18 °C incubation the cell pellets were collected by centrifugation at 4000 rpm, 4 °C, for 25 minutes. The supernatant was discarded and the cell pellets were stored overnight at -20 °C until for processing the next day or within the week. A single freeze-thaw cycle was found to increase protein yield. The freeze-thawing assists in the lysing of the cells prior to further lysis.

The majority of protein purification in this thesis was performed using the longer process but gentler French Press methods which uses pressure to lyse the cells post protein expression (French & Milner, 1950). Depending on time constraints for collaboration deadlines the faster enzymatic method of lysis, using BugBuster™, was used in some instances and use will be clearly stated henceforth. It was found that using the French Press method increased the yield of soluble protein compared to the enzymatic BugBuster™ method.

2.9.1.1 Pressure based cell lysis: French Press method

The long over-expression protein culture method 2.10.1 above was exclusively used to generate cell pellets prior to French Press lysis. The cell pellets were resuspended in a total volume of 20 mL 1 × Binding buffer (**Table 2.16**) which was equated to ~2.5 mL of buffer per pelleted 50 mL of protein expression culture. Typically a single passage of cells at a pressure of 40,000 psi was applied to achieve uniform lysis. Lysed cells were then kept on ice until further processing. Lysed cultures were centrifuged at 17,000 x rpm, 4 °C for 25 minutes to achieve separation of the insoluble and soluble fractions. Soluble fractions were decanted and placed on ice.

2.9.2 Short expression protein culture

A small amount of glycerol stock of *E. coli* BL21 (DE3) pET28+: ntr, was used to inoculate 10 mL LB medium, in a sterile 50 mL tube, supplemented with kanamycin (50 µg mL⁻¹) to maintain the pET28+ plasmid. The culture was then incubated at 37 °C at 200rpm overnight for approximately 16 hours. The following morning in an autoclaved 500 mL flask, 100 mL LB medium supplemented with kanamycin (50 µg mL⁻¹) was inoculated with overnight culture to generate a starting OD₆₀₀ of 0.1. This day culture was incubated at 37 °C, 200 rpm until the OD₆₀₀ of the culture reached 0.4-0.6. The cultures were then rested on ice for 15 minutes before the enzyme expression was induced by adding IPTG to a 0.5

mM final concentration. The flasks were then incubated at 18 °C, 200 rpm for approximated 16 hours. A 500 µL sample was collected of the culture prior to IPTG induction while the flasks rested on ice as well as after the 45 hour long over expression culture and was set aside and stored at -20 °C for examination by SDS-PAGE. After the overnight incubation the cell pellets were collected by centrifugation at in 4000 rpm, 4 °C, for 25 minutes. The supernatant was discarded at the cell pellets were stored overnight at -20 °C until for processing the next day or within the week.

2.9.2.1 Chemical cell lysis: BugBuster®

The short expression protein culture 2.10.3 above was used to generate cell pellets prior to enzymatic cell lysis. The BugBuster® protein-extraction (Novagen; Merck Millipore, MA, USA) method was performed according to the manufacturer's protocol. Cell pellets were lysed by addition of 2.5 mL BugBuster® for every 50 mL of initial culture. The pellets were resuspended and incubated at room temperature on an orbital shaker for 20 minutes prior to removal of the insoluble fraction by centrifugation. Lysed cultures were centrifuged at 17,000 x rpm, 4 °C for 25 minutes to achieve separation of the insoluble and soluble fractions. Soluble fractions were decanted and placed on ice.

2.9.3 Protein purification by Immobilised metal affinity chromatography (IMAC)

2.9.3.1 IMAC protein purification with a peristaltic pump

Purification of His₆-tagged proteins from the soluble fraction was achieved using Ni-NTA His.Bind® Resin (Merck Millipore, MA, USA), a peristaltic pump and a series of column washes with buffers of increasing imidazole content, the compositions for which are listed in **Table 2.16**. In all cases, buffers were run through the column until the buffer level was just above the top of the resin bed. Ni-NTA His.Bind® Resin (2-4 ml) was packed into a 10 ml Pierce disposable column (Thermo Fisher Scientific, Waltham, USA) and connected to the peristaltic pump and allowed to settle into a resin bed using gravity. The resin was washed with 4 ml of ddH₂O and charged by flowing through 8 ml of Charge buffer. The supernatant, containing the soluble quotient of the lysed cells, was well mixed with the charged resin and incubated on ice on an orbital shaker for 40-60 minutes to allow time for the protein to bind to the resin and increase yield.

The soluble fraction of the lysed cells was pumped through the column, followed by 10 ml Bind buffer and 8 ml Wash buffer. The pump tubing was evacuated, after which 4 ml of Elute buffer was run through the column and flow through was collected in 500 μ L fractions. The three most yellow fractions (indicative of the highest concentration of FMN-bound nitroreductase) were pooled into single volume of 1.5 mL. Resin beads were washed and stored in Strip buffer at 4 °C. At each stage of purification 50 μ L sample was set aside for later SDS-PAGE gel examination, including flow through of soluble protein, binding buffer, wash buffer and a 50 μ L sample of the pooled eluate.

Pooled nickel-purified protein fractions were incubated with excess FMN cofactor (1 mM) (15 μ L of 100 mM FMN cofactor) for a minimum of 15 minutes or up to an hour on ice. The insoluble fraction pellet was vortexed roughly with 2.5 mL of 6 M urea and incubated on the orbital shaker for 1-2 hours. An inoculation loop was used to break up the pellet prior to adding the urea. A 50 μ L sample of the insoluble fraction was set aside for later SDS-PAGE gel analysis.

Buffer	Components	pH
Charge buffer		
NiSO₄	50mM	
Binding buffer		
NaCl	500mM	
Tris-Cl	20mM	pH 7.9
Imidazole	5mM	
Wash buffer		
NaCl	500mM	
Tris-Cl	20mM	pH 7.9
Imidazole	60mM	
Elution buffer		
NaCl	500mM	
Tris-Cl	20mM	pH 7.9
Imidazole	1mM	
Strip buffer		
NaCl	500mM	
Tris-Cl	20mM	pH 7.9
EDTA	100mM	

Table 2.16 Protein purification buffers.

2.9.3.2 FMN incubation and de-salting

Buffer-exchange into 40 mM Tris-Cl pH 7.0 was carried out using a 5 ml HiTrap™ desalting column (GE Healthcare, UK) as per the manufacturer's instructions. Collected flow-through was restricted to the first 1.5 ml, as flow-through beyond 1.5 ml was likely to contain contaminating free FMN. His₆-tags were not removed at any point during protein purification as the presence of the tag has been determined not to affect nitroreductase catalytic activity (Prosser et al., 2013). A 10 µL sample of the purified protein was set aside for measuring the protein concentration. The desalted protein was then mixed 1:1 with 80 % glycerol and stored at -20 °C for use within 6 months. The presence of glycerol was found to have no detrimental effect on enzyme activity (GA Prosser private observation). Protein purity was confirmed using SDS-PAGE.

2.9.4 Purified protein quantification

The concentrations of protein samples were measured using a NanoDrop 2000 spectrophotometer (*Thermo Scientific, USA*), whereby absorbance of the sample at 280 nm was used to calculate protein concentration using the Beer-Lambert equation $A = \epsilon c l$, where A is the absorbance at 280 nm, ϵ is the theoretical molar extinction coefficient ($M^{-1}cm^{-1}$), c is the concentration (M) and l is the path length. The online tool ProtParam was used to calculate theoretical molar extinction coefficients for proteins. Division of the NanoDrop protein concentration value by the molar extinction coefficient determined the true protein concentration value. An average protein concentration was derived from the average of three replicates of 1 μ L samples of the desalted protein set aside before addition of glycerol. The blank was set using 40 mM Tris-Cl pH 7.0 buffer.

2.9.5 Protein storage

Desalted protein was mixed 1:1 with 80% glycerol and stored at $-20\text{ }^{\circ}\text{C}$ for use within 6 months.

2.10 Purified Enzyme Kinetics

Steady-state enzyme kinetics of purified nitroreductases was measured using a Helios γ UV-Vis spectrophotometer (Thermo Fisher Scientific; Waltham, USA) or the Ocean Optics USB4000 UV-VIS spectrometer (Halma PLC) as available. Reactions were performed in UVettes™ (Eppendorf, Hamburg, Germany), containing 10 mM Tris-Cl (pH 7.0), 4 % DMSO, 0.25 mM NADPH and varying substrate concentrations using a 1cm or 2 mm path length. Reactions were performed at room temperature whereby 6 μ L of an appropriate purified enzyme dilution was mixed with 54 μ L of a particular substrate concentration. When using the Helios γ UV-Vis spectrophotometer the change in absorbance was recorded for the initial 60-120 seconds. The linear change in absorbance recorded by the Helios γ UV-Vis spectrophotometer was automatically extrapolated by the spectrophotometer to a change in absorbance per minute. When using the Ocean Optics USB4000 UV-VIS spectrometer (Halma PLC) the change in absorbance was recorded as individual data points over the initial 60-120 seconds. In Microsoft Excel the linear portion of the change in absorbance was identified and the slope was recorded as the change in absorbance per second. The Ocean Optics USB4000 UV-VIS spectrometers replaced the Helios γ UV-Vis spectrophotometer and was only available from 2018 onwards.

Steady-state enzyme kinetics with purified nitroreductases were assessed spectrophotometrically at 420 nm for CB1954 (based on equal absorption of both 2- and 4-hydroxylamine reduction products of CB1954 at this wavelength. CB1954 possesses an extinction coefficient (ϵ) of $1200 \text{ M}^{-1} \text{ cm}^{-1}$. For the mustard prodrugs a wavelength of 400 nm for PR-104A $\epsilon = 600 \text{ M}^{-1} \cdot \text{cm}^{-1}$, DTP-006 (SN 36506) $\epsilon = 17400 \text{ M}^{-1} \cdot \text{cm}^{-1}$.

For each substrate concentration a minimum of three replicate measurements were performed for each enzyme. All enzyme dilutions were discarded after 20 minutes of use to prevent use of destabilized protein in the assay. All prodrug solutions were used within two hours of creation. Solubility of CB1954 and PR-104A solubility and absorbance limits prohibited analysis of the full range of concentrations for enzymes with high K_m values; maximum CB1954 concentration tested was $2000 \mu\text{M}$, maximum PR-104A concentration tested was $1000 \mu\text{M}$. Non-linear regression analyses and Michaelis-Menten curve fitting were performed using GraphPad Prism 7.0 software (GraphPad Software Inc.; La Jolla, CA, USA).

2.11 Bacterial fluorescence and growth assays

2.11.1 SOS-GFP screening assay

SOS-R4 strains transformed with pUCX: nitroreductase plasmids were individually grown overnight in $150 \mu\text{L}$ LB + Amp + Spec + 0.4 % glucose (LBASG). The outer wells surrounding the wells containing cultures, were filled with $150 \mu\text{L}$ of LB to prohibit growth advantage due to receiving extra heat in the incubator. The following day $15 \mu\text{L}$ of each overnight culture was used to inoculate $200 \mu\text{L}$ of LBASGI which contains $50 \mu\text{M}$ IPTG in 96 well plate format and grown at $30 \text{ }^\circ\text{C}$ 200 rpm for 2.5 hours. The outer wells were filled with $200 \mu\text{L}$ of LB. Following the incubation period, $30 \mu\text{L}$ of each day culture was added in duplicate to $30 \mu\text{L}$ LBASGI medium containing 2x the final prodrug concentration and up to 10% DMSO if necessary for prodrug solubility. The control, no prodrug, cultures were made by adding $30 \mu\text{L}$ of the day culture in duplicate to LBASGI medium containing an equivalent amount of DMSO if necessary in 384 well plates. The outer wells, surrounding the wells containing cultures, were filled with $60 \mu\text{L}$ of LBASGI. Cultures were then incubated for 2.5 hours at $30 \text{ }^\circ\text{C}$ 200 rpm.

GFP fluorescence (488 excitation/510 emission) and culture turbidity (OD_{600}) were then recorded using EnSpire 2300 Multilabel Reader (*Perkin Elmer; Waltham, MA, USA*). To calculate GFP fold induction values, the raw GFP value of each well was normalized against its OD_{600} reading. Fold induction was then calculated from the fold difference between the normalized GFP value of each challenged well and its respective unchallenged control.

2.11.2 Bacterial growth inhibition screening assay

The 7NT screening strains transformed with pUCX: nitroreductase plasmids were grown overnight at 30 °C, 200 rpm in 150 μ L LBAG. The following day, 15 μ L of each overnight culture was used to inoculate 200 μ L of LBAGI. Cultures were then grown for 2.5 hours at 30 °C 200 rpm. Following the incubation period, 30 μ L of each day culture was added in duplicate to 30 μ L LBASGI medium containing 2x the final prodrug concentration and up to 10% DMSO if necessary for prodrug solubility. Control no prodrug challenge cultures were made by adding 30 μ L of the day culture in duplicate to LBASGI medium containing an equivalent amount of DMSO if necessary in 384 well plates. Note that the outer wells around the wells containing cultures were filled with a protective barrier of 60 μ L of LBASGI to prohibit growth advantage due to receiving extra heat in the incubator. A T0 OD_{600} reading was taken prior to incubation. Cultures were incubated for a further 3.5 hours at 30 °C, 200 rpm, and the T3.5 OD_{600} reading was taken. Growth of each well was calculated from the difference between the T3.5 and T0 OD_{600} values. Growth inhibition was calculated from the relative difference in growth between challenged cultures and their respective unchallenged controls.

2.11.3 Bacterial IC₅₀ inhibition screening assay

The 7NT screening strains transformed with pUCX: nitroreductase plasmids were grown overnight at 30 °C, 200 rpm in 150 μ L LBAG. The following day, 15 μ L of each overnight culture was used to inoculate 200 μ L of LBAGI. Cultures were then grown for 2.5 hours at 30 °C 200 rpm. Typically require 2 x 200 μ L volume of each culture to perform the assay. Following the incubation period, 30 μ L of each day culture was added in duplicate to 30 μ L LBAG medium containing 2x the final prodrug concentration and up to 10% DMSO if necessary for prodrug solubility. The prodrugs were serially diluted in LBAGI typically with a maximal concentration of 2000 μ M depending on solubility and availability and then serially diluted to <3 μ M. Control no prodrug challenge cultures were made by adding 30

μL of the day culture in duplicate to LBAGI medium containing an equivalent amount of DMSO if necessary in 384 well plates. The outer wells, around the wells containing cultures, were filled with a protective barrier of 60 μL of LBAGI to prohibit growth advantage due to receiving extra heat in the incubator. A T0 OD₆₀₀ reading was taken prior to incubation. Cultures were incubated for a further 3.5 hours at 30 °C, 200 rpm, and the T3.5 OD₆₀₀ reading was taken.

Growth of each well was calculated from the difference between the T3.5 and T0 OD₆₀₀ values. Growth inhibition caused by prodrug activation was calculated from the difference in growth between challenged cultures and the unchallenged (0 μM) control. IC₅₀ values for each nitroreductase-expressing strain (the prodrug concentration at which growth was inhibited by 50% relative to the unchallenged control) were calculated using the non-linear regression analysis function of GraphPad Prism™.

2.12 Bacterial bystander effect assays and preparations

The following methods relate to the specific methods developed for the work regarding the bacterial bystander effect assay in Chapter 3.

2.12.1 Bacterial bystander assay

To measure the transfer of activated prodrug metabolites between bacterial cells we repurposed the SOS-GFP assay. The assay begins with inoculating three overnight cultures: 1) 7NT nitroreductase expressing activators - 7NTpUCX::nitroreductase (ampicillin resistant), pCDFDuet (spectinomycin resistant) 2) 7NT Empty control activator - 7NTpUCXEmpty (ampicillin resistant), pCDFDuet (spectinomycin resistant) 3) SOS-R4 GFP recipient cells – pUCX Empty (ampicillin resistant), pANODuet GFP reporter plasmid (spectinomycin resistant) (**Table 2.17**). The overnight cultures were 3 mL aliquots of LBASG medium (lysogeny broth supplemented with 100 μgml^{-1} ampicillin, 50 μgml^{-1} spectinomycin and 0.2% glucose (w/v) and were incubated overnight for ~16 hours, at 30 °C, 200 rpm..

The following morning, 0.5 mL of the overnight culture was used to inoculate a day culture of 10 mL of LBASGI which was then incubated at 30 °C, 200 rpm for 3 hours. Prior to prodrug challenge all cultures were diluted using LBASGI medium to the same OD₆₀₀. Subsequently, in 384 well plates, 15 μL of the 7NT activator and 15 μL of the SOS-R4

recipient day cultures were mixed with either 30 μ L control medium (LBASGI only) and 30 μ L challenge medium (LBASGI supplemented with double the challenge concentration of the prodrug). The test co-culture contains nitroreductase expressing 7NT cells hence it is the positive bystander effect condition. In the equivalent null-bystander control no nitroreductase gene is present in the co-culture of 15 μ L of the 7NT control activator and 15 μ L of the SOS-R4 recipient day cultures. All cultures were then incubated at 30 °C, 200 rpm for 3.5 hours, at which point OD₆₀₀ and GFP fluorescence (excitation 490 nm/emission 503 nm) were measured on an Enspire™ 2300 Multilabel Reader (Perkin Elmer, Waltham, MA).

Growth inhibition was also monitored as the percentage growth of prodrug challenged cultures compared to unchallenged cultures. All prodrug concentrations were optimized to prevent greater than 25% inhibition of growth in prodrug challenged cultures compared to unchallenged cultures as measured by cellular density at 600 nm. Higher levels of cell death have previously been found to reduce the measurable levels of SOS response. The final prodrug concentrations in the bacterial bystander effect assay were 50 μ M CB1954, 40 μ M PR-104A, 25 μ M SN27686, 1 μ M nitro-CBI-DEI and metronidazole at 5 μ M.

To measure the bystander effect, transfer of the active prodrug from the activators into the reporting recipient cells, we developed a simple equation to calculate the bacterial bystander assay (BAA). The percentage increase in fluorescence measured in the test bystander positive condition is calculated by converting the fluorescence of the control null-bystander effect condition into a percentage of the total fluorescence measured in the test bystander positive condition and then subtracting this value from a 100% total. The bystander effect was measured under conditions where the ratio of activators to recipient cells were equivalent (50%:50%) and at 10% activators: 90% recipients. At this 1: 9 ratio 200 μ L of the activator day culture was premixed with 1800 μ L of the recipient day culture and then plate 30 μ L of this mixture was plated into 30 μ L challenge or control medium in a 384 well microplate. This protocol has been published (Chan-Hyams et al., 2018; Chan-Hyams & Ackerley, 2020).

<i>E. coli</i> strains	Plasmid 1	Plasmid 1	Primer name	Sequence 5'→3'
	Ampicillin ^R	Spectinomycin ^R		
7NT	pUCX::Nfs	pCDFDu	NfsA_Ec_	GGCATATGACGCCAACCATTGAAC
Activator	A_Ec	et	Rv	
			NfsA_Ec_	GGGTCGACTTAGCGCGTCGCCCAA
			Fw	CCCTG
7NT	pUCX::Nfs	pCDFDu	NfsB_Ec_	GGGCATATGGATATCATTCTG
Activator	B_Ec	et	Fw	
			NfsB_Ec_	GGGGAATTCTTACACTTCGGTTAA
			Rv	G
7NT	pUCX::Yfk	pCDFDu	YfkO_Bs_	GGGGCATATGGCAGATCTAAAGAC
Activator	O_Bs	et	Fw	ACA
			YfkO_Bs_	CTAGGTCGACTTAAACCCACTTCAC
			Rv	AACAT
7NT Control	pUCX::Em	pCDFDu		
Activator	pty	et		
SOS-R4	pUCX::Em	pANODu		
Recipient	pty	et	GFP	
		reporter		

Table 2.17 Summary of bacterial strains and relevant plasmids used in the bacterial bystander assays. ^R indicates expression of antibiotic resistance for maintenance of the plasmid in the strain

2.12.2 Bacterial bystander effect flow cytometry procedures

Flow cytometry was used to quantify the levels of GFP expression in individual cells immediately following evaluation of cell-to-cell transfer of activated prodrug metabolites for the entire population by the microtitre plate method. After the OD₆₀₀ and GFP fluorescence were recorded for the 384 well plates, each set of technical replicates for each challenge condition was pooled. In individual 14 mL round-bottom polypropylene tubes, 25 µL of each challenge or control condition was diluted in 1 mL of PBS and mixed by vortexing for five seconds. Each sample was analysed on a Becton Dickinson FACSCanto II (BD Biosciences San Jose, CA), under the parameters: FSC 570, SSC 450 and GFP 555 within 2.5 h of removal from the incubator. The first sample analysed was always the unchallenged 7NT strain bearing an empty pUCX plasmid, to establish the level of background fluorescence for activator cells and allow a gate to be set immediately above this boundary. Subsequently, for each sample 30,000 fluorescent events were collected using a low flow rate of approximately 12 µL of sample per minute (BD LSR II User's Guide). A minimum of three experimental replicates were collected for each challenge condition and at least three independent biological repeats were performed for each final data set. All data sets were processed using the Flowing Software version 2.5.1 by Perttu Terho (Turku Centre for Biotechnology, Turku, Finland) and Flowjo (© FlowJo, LLC, 2013–2018; BD Biosciences San Jose, CA). To calculate the fold increase in mean population fluorescence resulting from cell-to-cell transfer of activated prodrug metabolites, the average fluorescence of each test condition was divided by the average fluorescence of the corresponding control condition. In this flow cytometry based assay, biological replicates were derived from independent overnight cultures. Technical replicates were individual microtitre cultures derived from a single overnight culture that were then pooled and dispensed into PBS for flow cytometry assessment. This protocol has been published in Chan-Hyams et al. (2018) and Chan-Hyams et al. (2020).

2.12.3 Prodrug pre-activation assay

Recombinant NfsA was expressed from plasmid pET28a(+) as an N-terminal His6 tagged enzyme and purified by nickel-affinity chromatography (Novagen, Merck, Darmstadt, Germany) with flavin reconstitution and buffer exchange as previously described (Prosser, Copp, et al., 2010). Protein concentrations were calculated using a NanoDrop

spectrophotometer and enzyme purity was confirmed by SDS-PAGE. Subsequently the purified NfsA protein was used to pre-activate 200 μ M PR-104A, 150 μ M SN27686 or 125 μ M of nitro-CBI-DEI. Reactions were performed in 60 μ L in UVettes™ (Eppendorf, Hamburg, Germany), containing 10mM Tris–Cl (pH 7.0), 4% DMSO, 3mM NAD (P)H. Reactions were initiated by addition of 6 μ L of 1 μ g/ μ L NfsA enzyme to 54 μ L of the appropriate substrate mixture, for a final concentration of 0.1 μ g/ μ L of enzyme. The reaction was monitored in a 1 cm path length, using a Helios γ UV–Vis spectrophotometer (Thermo Scientific, Middletown, VA) at 5 min intervals for 15–20 min until the reaction had gone to completion, i.e. no further change in absorbance was detected. Activation of the prodrug nitro-CBI-DEI was monitored by oxidation of the electron donating co-substrate NADPH at a wavelength of 340 nm as measured by a decrease in absorbance. For the mustard prodrugs PR-104A and SN27686 the formation of the reduced metabolite, from the parental substrate, can be detected by monitoring the decrease in absorbance at a wave length of 400 nM. At this wavelength there is no interference by reduced or oxidised NADPH co-substrate. The pre-activated prodrug metabolites were used to challenge cultures of the null-nitroreductase recipients. Overnight cultures of the SOS-R4 recipient strain were inoculated in 3 mL aliquots of LBASG medium in sterile 15 mL centrifuge tubes and incubated for 16 h at 30 °C with shaking at 200 rpm. The following morning, 0.5 mL of the overnight culture was used to inoculate a day culture of 10 mL of LBASGI which was then incubated at 30 °C, 200 rpm for 3 h. Prior to challenge with the pre-activated prodrug metabolites the SOS-R4 culture was diluted using fresh LBASGI medium to an OD₆₀₀ of 0.8. In 384 well plates eight technical replicate were created for each challenge condition. LBASGI medium was used to dilute the pre-activated prodrug metabolites to the following concentrations: 80 μ M for PR-104A, 100 μ M for SN27686 and 2 μ M for nitro-CBI-DEI in a volume of 30 μ L. The challenge culture was inoculated by addition of 30 μ L of the diluted SOS-R4 recipient strains to each of the wells; this diluted the pre-activated prodrug metabolites to the same final concentrations as used in the bystander effect assays. Control conditions for each condition were created by using a volume of 10mM Tris–Cl (pH 7.0) buffer equivalent to that of the volume of the pre-activated prodrug metabolites. Prior to incubation the OD₆₀₀ was measured on an Enspire™ 2300 Multilabel Reader (Perkin Elmer, Waltham, MA). All cultures were then incubated at 30 °C, 200 rpm for 3.5 h at which point the OD₆₀₀ and GFP fluorescence was

also recorded. To calculate the fold increase in fluorescence, resulting from transfer of activated prodrug metabolites from the medium into the SOS-R4 cells, the average fluorescence of each challenge condition was divided by the average fluorescence of the corresponding control condition. Growth inhibition was also measured at 600 nm to ensure the acceptable limit of 20% growth inhibition of challenged cultures compared to unchallenged controls was not exceeded. This protocol is also detailed in Chan-Hyams et al. (2018).

2.13 Bacterial bystander effect FACS assays and preparations

The following methods relate to the specific methods developed for the work regarding the bacterial bystander effect assay in Chapter 4. The methods of section 2.12.2 was used to prepare the bacterial cultures prior to procedure outlined in the following section.

2.13.1 Setting the collection gates and sample preparation for FACS

At the start of each FACS experiment for each prodrug condition, a collection gate was set to capture the top 10% region of the GFP profile of a positive control. This was a sample of exclusively *nfsA*-expressing activator cells challenged with the relevant prodrug. Within this gate, 50,000 individual cell GFP events were recorded. The GFP profiles of these positive controls indicated the upper limit of expected fluorescence in our model library.

After the collection gate was set, for each prodrug condition, cells were collected by FACS from the bystander condition and the null bystander condition. For the bystander condition, a pooled sample of 75 μ L of the co-incubated strains was analysed for each prodrug treatment. Individual cells that exhibited fluorescence within the collection gate were collected into 384 well microtitre plates. The null bystander condition sample for each prodrug was created by mixing the pooled activators and the pooled recipients in a 1:9 ratio. This mixture was analysed by FACS, immediately upon mixing, to prevent exchange of activated prodrug metabolites between activator and recipient cells. Samples were run through a BD FACS Vantage DiVa flow cytometer (Becton Dickinson; San Jose, CA) using the 355 nm laser and the 450/50 bandpass with ND1 filter removed from the Forward Scatter Detector.

Individual cells that exhibited fluorescence within the collection gate were collected into 384 well microtitre plates. The microtitre plates, containing the collected cells, were then

incubated for 48 hours. This allowed the collected cells to recover and establish a visually dense culture.

In addition, 50,000 individual cell GFP events were recorded, for each prodrug treatment under both the bystander and null bystander conditions, within the 10% collection gate. A minimum of 3 biological replicates, derived independent overnight cultures, and were performed for each prodrug treatment under the bystander or null bystander condition.

2.13.2 Recovery of cells post-FACS

Prior to niclosamide diagnosis, it was necessary to recover collected cells in LB microwell cultures. For each prodrug treatment, under both the bystander and null bystander conditions, the number of wells able to recover post-FACS to visual density from a 384 well plate after 48 hours was typically fewer than 120 wells per 384 microtitre plate. In each case, up to a maximum of 95 individual samples were randomly selected and stored in 40% glycerol at -80 °C. If fewer than 95 wells recovered, post-FACS, then all cells that did recover were stored.

2.13.3 Diagnosing expression of *nfsA* in samples recovered from FACS

To rapidly determine the overall yield of *nfsA*-expressing cells from FACS, we designed a bacterial growth inhibition assay using the compound niclosamide, to interrogate recovered cells for possession of a nitroreductase gene. Niclosamide is toxic to *tolC* mutant strains of *E. coli* unless reduced by a functional nitroreductase to a non-toxic state (Ackerley lab, unpublished finding). The collected cells from each FACS sort were grown in LB microplate cultures and used to perform a growth inhibition assay with a final challenge concentration of 1 µM niclosamide. See bacterial growth inhibition protocol

2.11.2.

Growth inhibition was calculated from the relative difference in growth between challenged cultures and their respective unchallenged controls. Samples containing a functional nitroreductase were able to detoxify the niclosamide and did not suffer greater than 50% growth inhibition. These were deemed to be positive hits, i.e. *nfsA*-expressing activator cells that had been correctly selected by FACS. Our modelled false hits, i.e. nitroreductase null recipient cells, suffered extreme growth inhibition (far exceeding 50%) in the presence of 1 µM niclosamide.

2.14 FACS nitroreductase library selection

The following methods relate to the specific methods developed for the work regarding the bacterial bystander effect assay in Chapter 5.

2.14.1 Preparation of 7SM library for FACS with CB1954 selection pressure

A glycerol of the NfsA *E. coli* 7SM site saturation mutagenesis library in the SOS-R4 strain was used to inoculate an overnight culture. Additionally, an overnight of SOS-R4 NfsA *E. coli* was cultured for the purpose of setting the selection gates on a positive control. No other culture was necessary to establish the collection gates.

The following day, the overnight cultures were used to inoculate day cultures in LBASGI and grown to an OD₆₀₀ of 0.8. Subsequently, 30 µL aliquots of each day culture were separately challenged with 30 µL LBASGI medium supplemented with CB1954 (to give a final challenge concentration of 50 µM) or incubated with 30 µL of control (no prodrug) medium in a 384 well microtitre plate. At least eight technical replicates were performed and incubated for 3.5 hours.

2.14.2 FACS of 7SM library under CB1954 selection pressure

The microtitre samples were then pooled for each condition and analysed using a BD FACS Vantage DiVa flow cytometer (Becton Dickinson; San Jose, CA) using the 355 nm laser and the 450/50 bandpass with ND1 filter removed from the Forward Scatter Detector. The positive control of SOS-R4 NfsA *E. coli* challenged with CB1954 was used to set the collection gates to the top 10% most fluorescent based on the GFP signal.

2.14.3 FACS of 7SM library under CB1954 selection pressure collected in 384 microtitre plates

Individual samples of the 7SM library challenged with CB1954 were then sorted and collected into 384 well microtitre plates containing LBASG medium. A further three 384 well microtitre plates were collected from the control sample of the 7SM library incubated with unamended (no prodrug) medium prior to FACS. Post-sorting, the plates were recovered for 48 hours, at 200 rpm, 30 °C incubation.

After a post-FACS recovery period of 48 hours the fifteen microtitre plates were examined to identify wells with visible culture density. From those cultures that had recovered to visible turbidity, 94 samples from each plate were randomly chosen for storage in 40%

glycerol at -80 °C. Typically only 25% of the cells recovered post-FACS per 384 well plate (2.13.2).

2.14.4 FACS of 7SM library under CB1954 selection pressure collected into microcentrifuge tubes

From the pooled sample of the 7SM library challenged with CB1954 as cells were sorted I chose to collect cells into micro-centrifuge tubes, containing LBASG recovery medium. Collecting cells from FACS into microcentrifuge tube is an alternative strategy for recovering cells post FACS that has been used previously in the Ackerley Laboratory (Copp et al., 2014). The final concentration of cells per tube was approximately 1×10^5 cells per tube. The tubes were recovered for 48 hours, at 200 rpm, 30 °C incubation. Post recover the cultures were stored in 40% glycerol at -80 °C so that at a later date individual variants recovered in this fashion could be individually interrogated for advanced activity with CB1954.

2.14.5 Screening cells collected from FACS for activity with CB1954

2.14.5.1 Making and storing primary screening plates from cells collected in 384 well plates

The glycerol plates derived from the cells collected into individual wells from FACS, were used to inoculate 150 μ L of LBASG growth medium in individual overnight cultures in a 96-well plate format. The following day the overnight cultures were used to inoculate 200 μ L LBASGI day cultures and incubated for 2.5 hours. An SOS-GFP assay was performed with as final concentration of 50 μ M CB1954 (2.11.1).

2.14.5.2 Making and storing primary screening plates from cells collected into microcentrifuge tubes

The glycerol stock of the stored cultures derived from cells collected into microcentrifuge tubes was allowed to defrost to a point where a 1 μ L volume could be taken and used in a serial dilution in LBAS medium ranging from 1×10^{-3} to 1×10^{-16} . Subsequently 50 μ L samples were plated on LBASG agar plates and incubated overnight for ~16 hours at 37 °C in static incubator. Individual colonies were picked using sterile tooth picks to inoculate individual wells in 96 well plates containing 150 μ L of LBASG medium and incubated overnight at 37 °C, 200rpm for ~ 16 hours. The following day 15 μ L of the culture was use

to inoculate 200 μ L LBASG medium in a 96 well plate and incubated at 37 °C, 200rpm for 2.5 hours to create a day culture. An SOS-GFP assay was performed with as final concentration of 50 μ M CB1954 (**2.11.1**). The remaining 135 μ L of culture was mixed with an equivalent volume of 80% glycerol and stored at -80 °C.

2.14.5.3 Creating hit plates from primary screening plates

The SOS-GFP response is calculated as the fold increase in GFP induction in the prodrug challenge culture over the no-prodrug culture (**2.11.1**). Growth inhibition is calculated as the percentage growth the prodrug challenge culture experiences compared to the no prodrug culture (**2.11.2**). The top performing variants were identified from each of the primary screening plates based on either GFP induction or growth inhibition and used to create “hit plates” for further investigation.

To create a hit plates for long term storage and analysis a sterile toothpick was used to inoculate 150 μ L of LBASG growth medium in individual overnight cultures in a 96-well plate format. The following day, typically, 15 μ L of the overnight culture was removed to perform an SOS-GFP assay. The remaining 135 μ L of culture was mixed with an equivalent volume of 80% glycerol and stored at -80 °C.

2.15 Pre-selection of nitroreductase libraries using positive selection compounds

The following methods relate to the specific methods developed for the work regarding the bacterial bystander effect assay in Chapter 5.

The niclosamide/chloramphenicol pre-selection strategy was performed with the *NfsA E. coli* 7SM site saturation mutagenesis library expressed in the screening 7NT strain. The 7NT cell strain is isogenic with SOS-R4, but does not contain a GFP plasmid to report on DNA damage so it cannot be used in FACS (**Table 2.17**).

The glycerol 7SM library in 7NT cells was allowed to defrost to a point where a 1 μ L volume could be taken and used in a serial dilution in LBAS medium ranging from 1×10^{-3} - 1×10^{-16} . Of these dilutions a volume of 100 μ L was plated in solid LBA agar medium supplemented with 0.5 mM IPTG as well as the desired concentration of the positive selection compounds niclosamide or chloramphenicol.

A 100 μL volume from each dilution was plated on both selective and non-selective plates to allow for estimation of the number of cells plated on each selection condition so that the selection pressure of niclosamide or chloramphenicol could be calculated as a percentage relative to this control.

Agar plates containing niclosamide were incubated at 37 $^{\circ}\text{C}$ overnight, whilst plates containing chloramphenicol were incubated at 37 $^{\circ}\text{C}$ for 40 hours.

Colonies that were present following incubation were picked into wells of a 96 well plate containing 150 μL of LBA medium. This plate was incubated at 37 $^{\circ}\text{C}$, 200 rpm overnight and a portion of the culture was stored in 40% glycerol at -80 $^{\circ}\text{C}$. The primary pre-selection plates were subjected to further screening with specific prodrugs using growth inhibition assays (**2.11.2**) with 50 μM CB1954. Hit plates were then created based on growth inhibition results. Hit plates were created and stored as defined in **2.14.5.3**. The hit plates were then subjected to further analysis by growth inhibition and IC_{50} analysis.

2.16 HPLC identification of CB1954 nitroreduction products

Reactions of 100 μL containing 10 mM Tris-HCl pH 7.0, 1 mM NADPH and 200 μM CB1954 were initiated by addition of ~ 35 μM purified enzyme. Reactions were incubated for 25 minutes at room temperature before being stopped by addition of one volume ice-cold 100% methanol. Samples were transferred to -80 $^{\circ}\text{C}$ for at least 1 hour to precipitate proteins after which samples were centrifuged for 10 min at 12,000 g, 4 $^{\circ}\text{C}$. The supernatant was decanted and diluted 1:20 in 45 mM formate buffer, 2.5% (v/v) methanol (pH 6.5).

A 100 μL volume of each sample was analysed by reverse phase-HPLC employing reverse phase-HPLC employing an Agilent 1100 system with an AlltimaTM C8 5 μ 150x2.1mm column (Fisher Scientific, Pittsburgh, PA). The mobile phase used for HPLC analysis was 45 mM formate buffer (pH 6.5) as aqueous and 80% acetonitrile as organic. The HPLC run parameters consisted of 4 minutes at 5% organic, a linear increase to 50% organic from 4 to 19 min and a further gradient increase to 70% organic from 19 to 21 minutes. Flow rate throughout was 1.5 $\text{ml}\cdot\text{min}^{-1}$ and the eluate was monitored at 262 nm. Elution profiles from each nitroreductase-CB1954 reaction were compared against controls reactions

including YfkO_Bs and NfsA_Ec which are known to exclusively reduce CB1954 at the 4- and 2- nitro positions respectively (Prosser et al., 2013).

The control no nitroreductase reaction was performed with all of the same components as the other reactions tested with the exception that no nitroreductase enzyme was added to the reaction. An equivalent volume of 10 mM Tris pH 7.0 buffer was added instead.

3 Evaluating the abilities of diverse nitroaromatic prodrug metabolites to exit a model Gram negative vector for bacterial-directed enzyme-prodrug therapy

3.1 Overview

Critical to the success of GDEPT strategies is the bystander effect, which occurs when an activated chemotherapeutic diffuses from the activating cell to neighbouring tumour cells (Dachs et al., 2009) **(1.3.1)**. The bystander effect has been quantified for some nitroaromatic prodrugs in mixed multilayer human cell cultures, however while these provide a good model for VDEPT they do not inform on the ability of these prodrug metabolites to exit bacterial vectors as in BDEPT.

To investigate the bacterial bystander effect I grew two *E. coli* strains in co-culture; an activator strain expressing the nitroreductase *E. coli* NfsA and a recipient strain containing an SOS-GFP DNA damage responsive gene construct. In this system, induction of GFP by reduced prodrug metabolites can only occur following their transfer from the activator to the recipient cells. I used this to investigate five clinically relevant prodrugs: metronidazole, CB1954, nitro-CBI-DEI, and two DNBM s PR-104A and SN27686.

Consistent with the bystander efficiencies previously measured in human cell multilayers, **(Table 1.1)** reduced metronidazole exhibited little bacterial cell-to-cell transfer, whereas nitro-CBI-DEI was passed very efficiently from activator to recipient cells post-reduction. However, in contrast with observations in human cell multilayers, the nitrogen mustard prodrug metabolites were not effectively passed between the two bacterial strains, whereas reduced CB1954 was transferred efficiently. Using nitroreductase enzymes that exhibit different biases for the 2- versus 4-nitro substituents of CB1954, I further showed that the 2-nitro reduction products exhibit substantially higher levels of bacterial cell-to-cell transfer than the 4-nitro reduction products, consistent with their relative bystander efficiencies in human cell culture. Overall, the data suggests that prodrugs may differ in their suitability for VDEPT versus BDEPT applications and emphasise the importance of evaluating an enzyme-prodrug partnership in an appropriate context for the intended vector.

3.1.1 Aims:

- Design an assay that can robustly detect cell-to-cell transfer of the activated prodrug metabolites in an *E. coli* model of Bacterial-Directed-Enzyme-Prodrug-Therapy.
- Determine which types of clinically relevant prodrugs generate the greatest bystander effect from a Gram negative bacterial vector into recipient bacterial cells.

3.2 Introduction

The bystander effect is of particular importance when using bacterial vectors for GDEPT, as the success of the therapy depends entirely upon transport of the activated cytotoxin out of the activating bacterial cell and into the surrounding cancer tissue (**Figure 1.11**), and failure to exit the vector may result in sterilisation of the bacteria within the tumour.

To quantify the levels of cell-to-cell transfer of the reduced metabolites of nitroaromatic prodrugs between human tumour cells, Wilson et al. (2002) developed a mixed multilayer cell culture system, comprising a small proportion of “activator” cells that had been transfected with a nitroreductase together with a large majority of untransfected “recipient” cells. This system has been used to successfully evaluate the relative bystander effect efficiency, across multiple independent publications, over a diverse range of nitroaromatic prodrug metabolites for clinical application (**Table 1.1**).

However, we considered that a strong bystander effect measured in human cell culture might not accurately predict the ability of these prodrugs to exit bacterial activator cells, owing to the different physiology. To investigate this, I adapted a previously developed *E. coli* DNA damage responsive GFP reporter strain (Copp et al., 2014) (**Figure 1.6**), to detect nitroaromatic prodrug metabolites generated by a co-cultured strain expressing a strong nitroreductase.

3.2.1 Key terminology for the bacterial bystander effect assay

- Nitroreductase-expressing activators (7NT cells)
- Nitroreductase null negative controls (7NT cells)
- Nitroreductase null recipients (SOS-R4 cells)
- Positive control (100% *nfsA*-expressing SOS-R4 cells)

- Test condition (50% activators and 50% recipients co-incubated with prodrug)
- Control condition (50% control activators and 50% recipients co-incubated with prodrug)

3.3 Results

3.3.1 Bacterial bystander effect assay design, optimization and execution

3.3.1.1 Design: Prodrugs, bacterial strains, genes and plasmids

The prodrugs selected for investigation in this chapter were metronidazole and CB1954 (both purchased from Sigma-Aldrich), PR-104A and its di-bromo analogue SN27686, and nitro-CBI-DEI, which were synthesised by our collaborators Dr Jeff Smaill and Assoc. Prof. Moana Terrel at the Auckland Cancer Society Research Centre. Nitroreductases NfsA, NfsB from *E. coli* and YfkO from *B. subtilis* were expressed from the ampicillin resistant expression plasmid pUCX as previously described (Prosser et al., 2013; Prosser, Patterson, et al., 2010).

In this assay I employed the *E. coli* strains 7NT and SOS-R4 as previously described (Copp et al., 2014) as activator and recipient cells, respectively. Both strains are isogenic derivatives of the *E. coli* strain W3110, but with seven endogenous nitroreductase candidate genes deleted as well as the efflux pump *tolC* gene as to restrict active efflux of unreduced prodrug (Copp et al., 2014, 2017). The SOS-R4 strain additionally contains a spectinomycin resistant plasmid bearing a green-fluorescent-proteinmut3 (GFP) reporter gene controlled by the SOS inducible *sfiA* promoter. To enable co-incubation of the activator and recipient strains the empty plasmid pCDFDuet was transformed into the 7NT strains to confer spectinomycin resistance.

The development of SOS-R4, a SOS (DNA damage responsive) GFP reporter strain of *E. coli*, and its utility for directed evolution to improve the bioreductive activation of nitroaromatic prodrugs by a target nitroreductase enzyme, has been previously reported (Copp et al., 2014, 2017) (**Figure 1.6**). Here, I considered that SOS-R4 might also be able to report on the ability of genotoxic prodrug metabolites to exit a nitroreductase-expressing non-reporter strain of *E. coli* in liquid co-culture and enter SOS-R4 cells. By comparing the levels of GFP expression between SOS-R4 cells co-cultured with either a

nitroreductase-expressing or a nitroreductase null 7NT strain (Figure 1.2), I reasoned that the fold difference in GFP signal between the test and control conditions is a measure of the extent of bacterial cell-to-cell transfer of nitroreductase-activated prodrug metabolites.

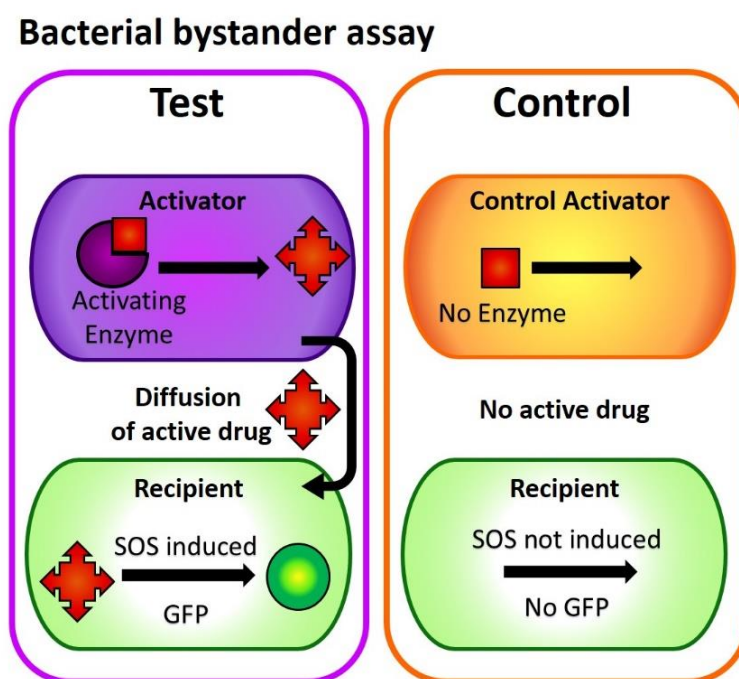


Figure 3.1 Schematic of the “bacterial bystander assay” to quantify bacterial cell-to-cell transfer of genotoxic metabolites. In the test condition the nitroreductase-expressing 7NT activator cells (purple cell) convert the prodrug into a genotoxic product. The bacterial bystander assay monitors the efficiency of transfer of the genotoxin from the activator cells into co-cultured SOS-R4 recipients (green cell). The recipients quantify receipt of the genotoxin via GFP expression induced by DNA damage. The background level of toxicity caused by unconverted prodrug, or prodrug activated by other endogenous enzymes present in the activator or recipient cells, is measured using a nitroreductase-null 7NT control activator strain (orange cell) co-cultured with SOS-R4 recipients. The fold difference in GFP signal between the test and control conditions is a measure of the extent of bacterial cell-to-cell transfer of nitroreductase-activated prodrug metabolites.

3.3.1.2 Optimizing the bacterial bystander effect assay

3.3.1.2.1 Selecting prodrug concentrations for bacterial bystander microtitre plate assay

I selected *E. coli* NfsA as the prodrug-converting enzyme, as previous studies have shown that this enzyme is an excellent generalist nitroreductase that has high-level activity across a range of nitroaromatic substrates (Valiauga et al., 2017; Zenno et al., 1996). Prodrugs were selected for this investigation to span a range of chemical structures and

on the basis of their bystander effects having previously been evaluated in mixed multilayer cell culture models.

Metronidazole was selected as a nil bystander control. The next-generation prodrugs PR-104A and SN27686 are both nitroaromatic mustards that have proven to have a high bystander effect in a mixed multi-layer carcinoma cell model of VDEPT. Nitro-CBI-DEI has the highest recorded bystander effect of any nitroaromatic prodrug in this same carcinoma model (Green, Syddall, et al., 2013). CB1954 is a first-generation prodrug that has a poor bystander effect in carcinoma cells and was selected as a comparative standard. The chemical structures of these prodrugs are presented in **Table 1.1** and **Figure 1.9**.

In order of ascending bystander effect in these models the selected prodrugs were: metronidazole, negligible bystander effect (Bridgewater et al., 1997; Hunt et al., 2012); CB1954, low bystander effect (Singleton et al., 2007; Wilson et al., 2002, 2007); PR-104A and its more lipophilic di-bromo mustard analogue SN27686, medium to high bystander effects (Foehrenbacher et al., 2013; Mowday, Ashoorzadeh, et al., 2016; Singleton et al., 2007) and nitro-CBI DEI, maximal bystander effect (Green, Syddall, et al., 2013; Wilson et al., 2009). It should be noted that as the different studies that I refer to employed substantially different proportions of activator cells in their mixed multilayer cell culture models (**Table 1.1**), it is not possible to directly compare the calculated bystander effect efficiencies of the different prodrug metabolites, and hence I have employed qualitative terms to describe their relative bystander efficiencies.

3.3.1.2.2 Selecting appropriate prodrug concentrations for the bacterial bystander assays in 384 well microtitre plates

I next sought to identify test concentrations for each prodrug that would enable meaningful comparisons to be made between the different molecules. It is known that different nitroaromatic prodrug metabolites can exhibit markedly different dose potencies (Williams et al., 2015). It was previously found that a greater than 20% decrease in culture turbidity in response to prodrug challenge, relative to an unchallenged control, can cause a reduction in output from SOS reporter gene assays (Prosser, Copp, et al., 2010). I therefore empirically selected concentrations of each prodrug that could elicit

comparable levels of GFP expression in an SOS-R4 reporter strain expressing *nfsA*, without causing more than 20% growth inhibition of that strain.

Pilot studies resulted in selection of the following test prodrug concentrations: 5 μ M metronidazole, 50 μ M CB1954, 40 μ M PR-104A, 50 μ M SN27686, and 1 μ M nitro-CBI-DEI. At these selected prodrug concentrations growth inhibition was in the allowable range for all bacterial strains used. I observed that at these concentrations the reduction in culture turbidity relative to an unchallenged control was similar for both 7NT and SOS-R4 strains expressing *nfsA* (and in all cases <20%), and that nitroreductase null 7NT and SOS-R4 strains exhibited little to no growth inhibition (**Figure 3.2**).

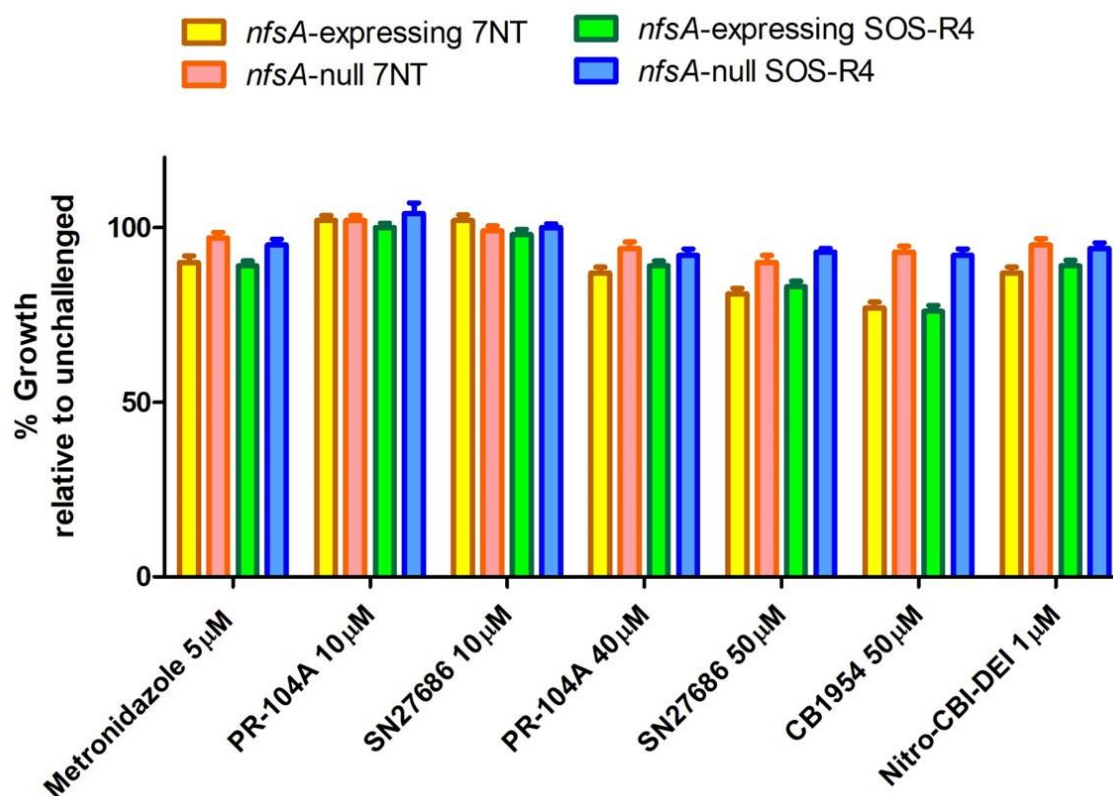


Figure 3.2 Identification of prodrug concentrations resulting in <20% growth inhibition of nitroreductase-expressing activator cells. Empirical testing identified promising prodrug concentrations of 5 μ M metronidazole, 50 μ M CB1954, 1 μ M nitro-CBI-DEI, and either 10 μ M or 40 μ M PR-104A, and 10 μ M or 50 μ M SN27686. The effect of these prodrug concentrations on growth inhibition was tested for different strains used in this study: *nfsA*-expressing 7NT activators (yellow bars), nitroreductase null 7NT control (pink bars), nitroreductase null SOS-R4 recipients (blue bars), and an additional positive control of *nfsA*-expressing SOS-R4 (green bars). Data were derived from six biological replicates, each comprising a minimum of four technical replicate cultures grown in a 384 well microtiter plate. Error bars represent standard deviation of the average growth (OD_{600} represented as a percentage relative to unchallenged control cultures) across the six biological replicates.

The relative levels of GFP expression in the *nfsA*-expressing SOS-R4 strain were similar for all prodrugs at these concentrations (**Figure 3.3**), however I additionally noted that the dinitrobenzamide mustard prodrugs PR-104A and SN27686 caused a statistically significant induction of GFP in a nitroreductase null strain of SOS-R4 at the selected test concentrations of 40 μ M and 50 μ M respectively compared to the no prodrug control (**Figure 3.4**). This indicates that at these concentrations the two prodrugs were causing a significant SOS DNA damage response despite the absence of an activating nitroreductase.

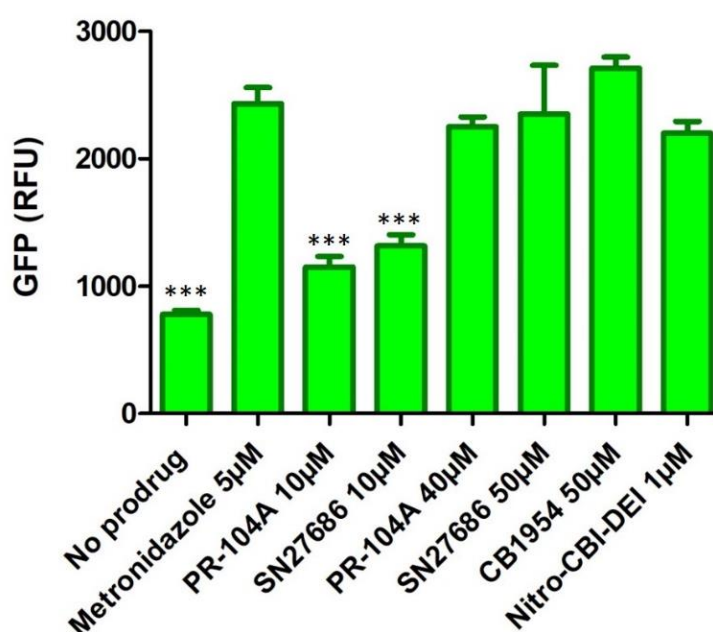


Figure 3.3 Relative GFP fluorescence of *nfsA*-expressing SOS-R4 exposed to different prodrugs. Levels of GFP fluorescence were measured following 3.5 h incubation of *nfsA*-expressing SOS-R4 challenged with each prodrug at 30 °C, 200 rpm. Data were derived from six biological replicates, each comprising a minimum of four technical replicate cultures grown in a 384 well microtiter plate. Error bars represent standard deviation of the average GFP (RFU) across the six biological replicates. *** indicates $p < 0.001$ (one-way repeated measures ANOVA with Tukey's post-hoc test) GFP signal is significantly different from that measured for the nil-bystander prodrug metronidazole.

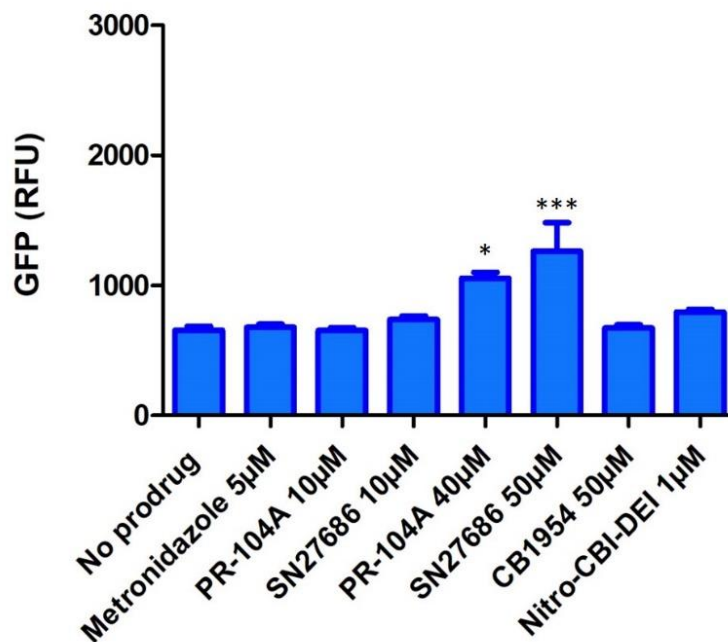


Figure 3.4 Relative GFP fluorescence of nitroreductase null SOS-R4 recipients exposed to different prodrugs. To evaluate the basal levels of genotoxicity for each prodrug in the absence of *NfsA*, SOS-R4 cells containing an empty plasmid were exposed to each prodrug, with data collected and presented as for Panel C. Error bars represent standard deviation of the average GFP (RFU) across the six biological replicates. * indicates $p < 0.05$ and *** indicates $p < 0.001$ (one-way repeated measures ANOVA with Tukey's post-hoc test) GFP signal is significantly different from no prodrug control.

To allow for the possibility that this low-level background might influence assay results, I therefore also tested PR-104A and SN27686 at 10 µM apiece throughout this work. After retesting the *nfsA*-expressing SOS-R4 strain at these lower prodrug concentrations, I found that the PR-104A and SN27686 at 10 µM generated significantly lower GFP signals than the metronidazole control (**Figure 3.3**) but did not induce a statistically significant SOS DNA damage response in the absence of a nitroreductase (**Figure 3.4**). The particulars of the experimental procedure are outlined in section **2.12**.

3.3.2 SOS and bacterial bystander assays in 384 well microtitre plates

Evaluation of cell-to-cell transfer of activated prodrug metabolites in *E. coli* liquid cultures was performed in microtitre plates. Overnight and day cultures of a nitroreductase expressing 7NT activator strain, a nitroreductase null 7NT control strain, and the SOS-R4 recipient strain were inoculated and incubated as described in section **2.12.1**. Prior to prodrug challenge, all cultures were diluted to ensure equivalent number of activators and recipients be present in the co-culture. In 384 well plates, pairs of wells were filled with either control medium or challenge medium supplemented with twice the desired final challenge concentration of the prodrug. A 50:50 ratio of activator to recipient cells was established by addition of equivalent volumes of either the nitroreductase-expressing 7NT activator or the nitroreductase null 7NT control day cultures added to each pair of wells, followed by addition of an equivalent volume of the SOS-R4 recipient strain and then incubated. The 10: 90 ratio of activators to recipients was established in a similar manner using different proportions of each day culture. Individual controls of each test strain were also grown in both control and challenge media to enable background levels of growth inhibition and GFP expression to be monitored. These background levels of fluorescence in individual strains were not used to normalize the data. Instead the co-culture control condition was used.

To calculate the fold increase in fluorescence resulting from cell-to-cell transfer of activated prodrug metabolites, the average fluorescence of each test condition (i.e., using the nitroreductase-expressing 7NT activator strain) was recorded post-incubation and divided by the average fluorescence of the corresponding control condition (i.e., using the nitroreductase null 7NT control strain).

3.3.2.1 Results of the bacterial bystander microtitre assay

I first evaluated the ability of the activated prodrug metabolites to be transferred from activator to recipient cells in a microtitre plate assay format. Nitroreductase null SOS-R4 recipient cells were co-cultured at a 1:1 ratio with either *nfsA*-expressing 7NT activator cells (test condition) or nitroreductase-null 7NT cells (control condition). Following exposure to each prodrug, cell-to-cell transfer of genotoxic metabolites was quantified by monitoring the mean fold-increase in fluorescence for the test condition relative to the control (**Figure 3.5**)

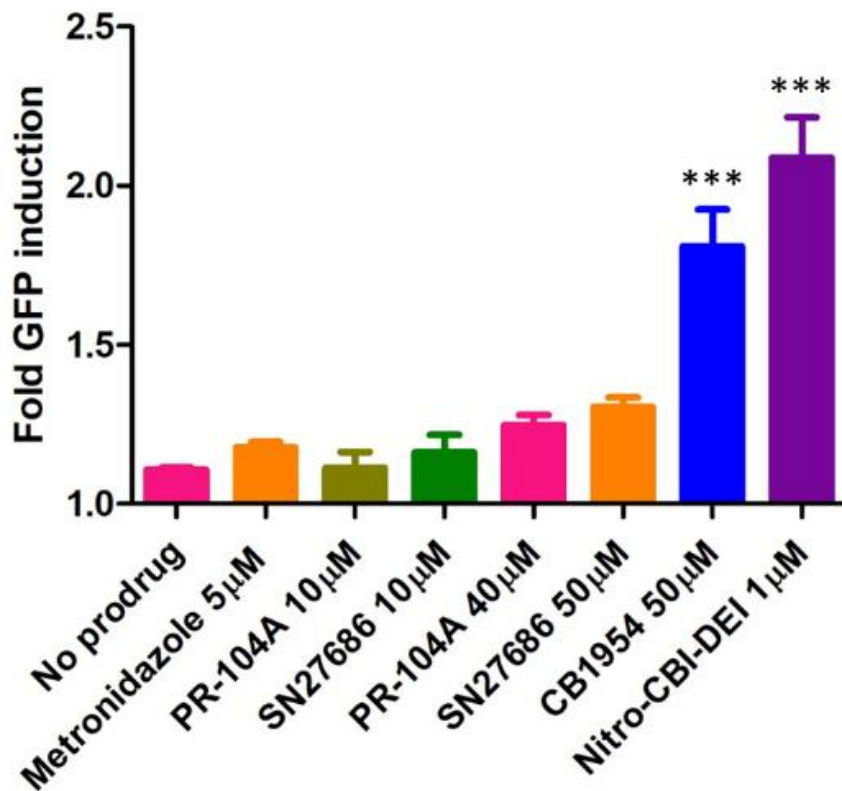


Figure 3.5 Microplate assay of SOS response induced by transfer of activated 50:50 mixed cultures of *nfsA*-expressing 7NT activator cells and SOS-R4 recipients were incubated with either 5 µM metronidazole, 50 µM CB1954, 1 µM nitro-CBI-DEI, 10 µM or 40µM PR-104A, or 10 µM or 50µM SN27686 for 3.5 h, at which point GFP fluorescence (excitation 490 nm/emission 530 nm) was measured. The bacterial bystander effect was measured by the fold increase in GFP expression of the test condition over the control condition. Six biological replicates were performed each comprising eight technical replicates for test and control conditions. Error bars represent standard deviation of the average fold increase in GFP induction across the six biological replicates. *** indicates $p < 0.001$ (one-way repeated measures ANOVA with Tukey's post-hoc test) relative to no prodrug control.

Consistent with the bystander effects previously observed in human tumour mixed multilayer cell culture models, reduction of metronidazole by *nfsA*-expressing 7NT activator cells did not induce significant levels of GFP in SOS-R4 recipients, whereas nitro-CBI-DEI caused a significant ($p < 0.001$) increase in fluorescence. Surprisingly, CB1954 also caused a significant ($p < 0.001$) increase in fluorescence, despite having exhibited only a weak bystander effect in human cell models (Singleton et al., 2007; Wilson et al., 2002, 2009).

In contrast, the dinitrobenzamide mustard prodrugs, which exhibited substantially higher bystander effects than CB1954 in human cell models, induced only slightly higher levels of GFP in the SOS-R4 recipients than metronidazole. The bystander effects of the mustard prodrugs were not significantly different from metronidazole irrespective of whether the 10 μ M or higher challenge concentration was applied. Relative to PR-104A ($\log P = 1.0$) the more lipophilic (di-bromo-mustard) analogue SN27686 ($\log P = 2.3$) appeared to induce higher levels of GFP in SOS-R4 cells, however this difference was not significant.

3.3.3 Bacterial bystander assays in flow cytometry

Flow cytometry was used to quantify the levels of GFP expression in individual cells immediately following evaluation of cell-to-cell transfer of activated prodrug metabolites for the entire population by the microtitre plate method. After the OD_{600} and GFP fluorescence were recorded for the 384 well plates, each set of technical replicates for each challenge condition was pooled. In individual polypropylene tubes, a portion of each challenge or control condition was analysed by flow cytometry. The particulars of the experimental procedure are outlined in section 2.14.2.

To calculate the fold increase in mean population fluorescence resulting from cell-to-cell transfer of activated prodrug metabolites, the average fluorescence of each test condition was divided by the average fluorescence of the corresponding control condition. In this flow cytometry based assay, biological replicates were derived from independent overnight cultures. Technical replicates were individual microtitre cultures derived from a single overnight culture that were then pooled and dispensed into PBS for flow cytometry assessment.

3.3.3.1 Results of the bacterial bystander flow cytometry assay

Whereas plate reader assays measure the mean fluorescence of an entire population of cells, flow cytometry approaches can provide additional information on the variance between individual cells in that population. Here, *nfsA*-expressing 7NT activator cells or nitroreductase null 7NT cells were mixed 1:1 with SOS-R4 recipient cells, exposed to prodrug, and analysed by flow cytometry. For each prodrug, fluorescence histograms were derived from gated reads of 30,000 recipient cells apiece for the test and control conditions.

When paired histograms were overlaid, no clear differences could be observed between the test and control for either the no prodrug control or for 5 μ M metronidazole (**Figure 3.6**). It was also evident that although there was substantial variation in the fluorescence of individual SOS-R4 recipient cells, at a population level the distribution of fluorescence was highly consistent. For the remaining prodrugs, the histogram overlay plots were also congruent with the plate reader data: 50 μ M CB1954 and 1 μ M nitro-CBI-DEI both caused strong shifts in SOS-R4 fluorescence, indicating high levels of cell-to-cell transfer of activated prodrug metabolites, whereas PR-104A and SN27686 caused minimal shifts in SOS-R4 fluorescence at either challenge concentration (**Figure 3.6**).

The fluorescence histograms confirmed that 40 μ M PR-104A and 50 μ M SN27686 were causing activation of GFP expression in SOS-R4 cells even in the absence of the *nfsA*-expressing activator strain (as previously observed in microplate assays (**Figure 3.5**)). However, this high GFP background does not appear to have been the reason for the failure to detect cell-to-cell transfer of the activated metabolites of these prodrugs, given the lack of background yet minimal fluorescence shift when each dinitrobenzamide mustard was tested at 10 μ M (**Figure 3.6**).

At present this assay design is not sensitive enough to differentiate the bacterial bystander effect signal above the background fluorescence of non-nitroreductase activated prodrug at lower concentrations of the mustard prodrugs PR-104A and SN27686. In preliminary experiments, concentrations greater than 10 μ M but less than 50 μ M of PR-104A and SN27686 generated a background fluorescence in the nitroreductase null SOS-R4 recipient cells that were significantly higher than that of the positive control nitroreductase expressing SOS-R4 cells (data not shown).

The mean population fluorescence for each condition across all repeats is summarised in **Figure 3.7**. As in the microplate assay, CB1954 and nitro-CBI-DEI were the only prodrugs that induced statistically significant ($p < 0.001$) increases in GFP induction compared to the null bystander effect metronidazole condition.

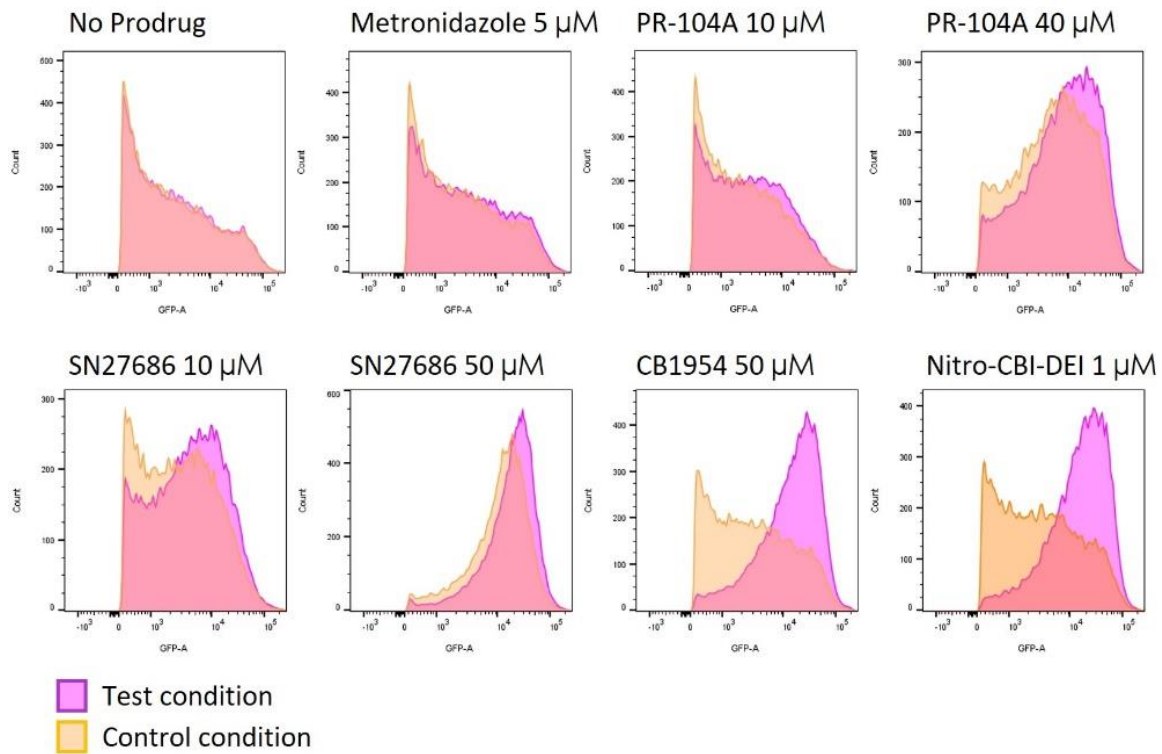


Figure 3.6 Overlay flow cytometry histograms of test and control conditions assessing the DNA damage caused by transfer of activated prodrug metabolites from *nfsA*-expressing 7NT activator cells to nitroreductase null *SOS-R4* reporter cells. 50:50 mixed cultures of *SOS-R4* recipients and either nitroreductase null 7NT control cells or *nfsA*-expressing 7NT activator cells were incubated with either 5 μM metronidazole, 50 μM CB1954, 1 μM nitro-CBI-DEI, 10 μM or 40 μM PR-104A, or 10 μM or 50 μM SN27686 for 3.5 h in eight technical replicates apiece. The eight replicates were then pooled and 25 μL of each pooled sample measured for GFP fluorescence using flow cytometry. The collection gate was set at the GFP region above the background fluorescence of the nitroreductase null 7NT control strain under no prodrug conditions. Overlay histograms are representative technical replicates that indicate the population fluorescence of 30,000 events for the mixture containing the nitroreductase null 7NT strain (Control condition; orange) or the *nfsA*-expressing 7NT activator cells (Test condition; pink).

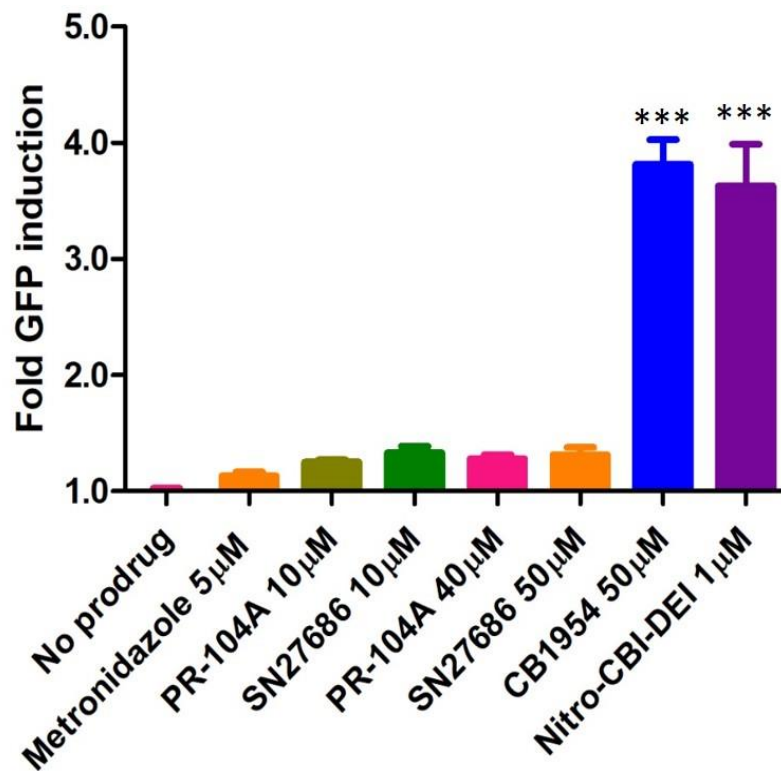


Figure 3.7 Mean increase in GFP signal of test condition over control condition in flow cytometry analysis. Six biological replicates were performed for each condition. For each, the GFP geomean of at least three technical replicates was averaged and the bacterial bystander effect was quantified as the average fold increase in GFP fluorescence for the test condition over the control condition. Error bars represent standard deviation of the average fold increase in GFP induction across the six biological replicates, and *** indicates $p < 0.001$ (one-way repeated measures ANOVA with Tukey's post-hoc test).

3.3.4 The bystander effect of CB1954 is dependent on the reduction product(s)

The ability of the reduced metabolites of CB1954 to exit the *nfsA*-expressing 7NT activator strain and induce GFP expression in the SOS-R4 recipient strain was substantially stronger than expected based on previous studies of bystander effect in human carcinoma 3D mixed multicellular models (Singleton et al., 2007; Wilson et al., 2002, 2007). One possible explanation for this was my choice of NfsA as the prodrug-converting nitroreductase, in contrast to the NfsB enzyme that was used in the 3D cell culture studies. Whereas NfsB can reduce either the 2-NO₂ or the 4-NO₂ groups of CB1954, in an approximately equimolar ratio (Anlezark et al., 1992; Helsby et al., 2004), NfsA reduces CB1954 exclusively at the 2-NO₂ position (Prosser, Copp, et al., 2010; Vass et al., 2009). It has been shown in human cervical cancer (SiHa) cells expressing *nfsB* that the products of reduction at the 4-NO₂ position exhibit a substantially lower bystander effect than the 2-NO₂ reduction products (Helsby et al., 2004). Consistent with this, untransfected ovarian carcinoma (SKOV3) cells were found to be more sensitive to CB1954 when co-cultured with *nfsA*-expressing cells than when they were co-cultured with *nfsB*-expressing cells (Vass et al., 2009).

I therefore sought to compare the effects of using *nfsA* versus *nfsB* as the prodrug converting nitroreductase gene in our 7NT activator cells. To enable a more precise assessment of the ability of the 2-NO₂ versus 4-NO₂ reduction products of CB1954 to activate the SOS response in SOS-R4 recipient cells, I also generated a third activator strain, 7NT cells expressing the nitroreductase gene *yfkO* from *Bacillus subtilis*. It has previously been shown that Yfko is an efficient nitroreductase that reduces CB1954 exclusively at the 4-NO₂ position (Prosser, Patterson, et al., 2010) and that the *nfsA*, *nfsB*, and *yfkO* genes all express protein at similar levels from plasmid pUCX in *E. coli* (Prosser et al., 2013).

7NT activator cells expressing *nfsA*, *nfsB* or *yfkO* or nitroreductase-null 7NT cells were mixed 1:1 with SOS-R4 recipient cells, challenged with 50 µM CB1954, and analysed by flow cytometry. There was little to no difference in GFP profiles between the overlay histograms for the *nfsA* and *nfsB* expressing activator strains (**Figure 3.8, Figure 3.9**). Although NfsA and NfsB induced levels of GFP that were significantly greater ($p < 0.01$ and

$p < 0.05$ respectively) than YfkO, the two *E. coli* derived nitroreductases were not significantly different from each other (**Figure 3.9**).

Thus, the strong induction of GFP expression in the CB1954 assays could not be attributed to our selection of NfsA over NfsB as the prodrug converting nitroreductase. In contrast, the *yfkO*-expressing activator strain caused only a small increase in SOS-R4 population fluorescence relative to the nitroreductase-null control (**Figure 3.8, Figure 3.9**), confirming that the 4-NO₂ reduced metabolites of CB1954 exhibit poor cell-to-cell transfer in bacteria as well as cultured human cells (**Figure 3.9**).

I considered that these results may also have been consistent with the 4-NO₂ reduction products may have been received by the reported strain and for some reason not induced an SOS-DNA damage response i.e. a good bystander effect but poor activity in bacteria. However, this is unlikely given the established higher toxicity of the 4-NO₂ metabolite than the 2-NO₂ metabolite (Helsby et al., 2004) . Furthermore it has been shown that strains expressing nitroreductases that exclusively generate 4-NO₂ metabolites (e.g., YfkO_Bs) are known to experience strong SOS responses and IC₅₀s (*Prof. David Ackerley private communication*).

To further investigate whether the lack of substantial difference between the *nfsA* and *nfsB* expressing activator strains may have been due to saturation of fluorescence in the SOS-R4 recipients, I reduced the ratio of activator to recipient cells in our assay co-cultures from 1:1 to 1:9. As expected the overall levels of fluorescence for each co-culture greatly decreased, reflecting the reduced number of nitroreductase expressing cells in the assay (**Figure 3.11, Figure 3.10**). Under these conditions there was a significant difference between the NfsA and YfkO conditions ($p < 0.01$) but not between NfsB and YfkO (**Figure 3.10**).

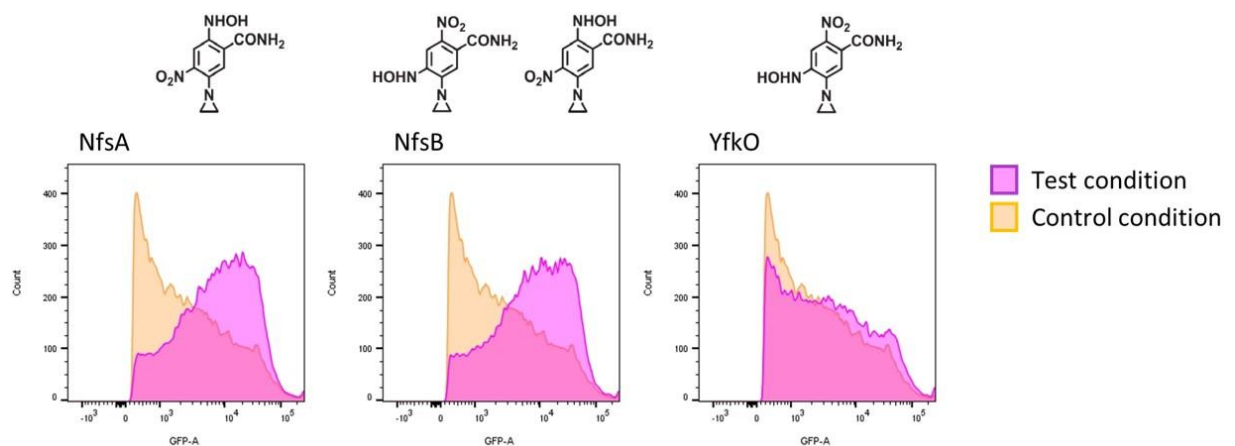


Figure 3.8 Overlay histograms of test and control conditions for a 50% activator cell population in Flow cytometry analysis of DNA damage caused by transfer of activated prodrug metabolites from *nfsA*, *nfsB* or *yfkO* -expressing 7NT activator cells. 50:50 mixed cultures of SOS-R4 recipients and either nitroreductase null 7NT control cells or *nfsA*, *nfsB* or *yfkO* -expressing 7NT activator cells were incubated with either no prodrug or 50 μ M CB1954 for 3.5 h in eight technical replicates apiece. The eight replicates were then pooled and 25 μ L of each pooled sample measured for GFP fluorescence using flow cytometry. Overlay histograms indicate the population fluorescence of 30,000 events for the mixture containing the nitroreductase null 7NT strain (Control condition; orange) or the *nfsA*, *nfsB* or *yfkO* -expressing 7NT activator cells (Test condition; pink).

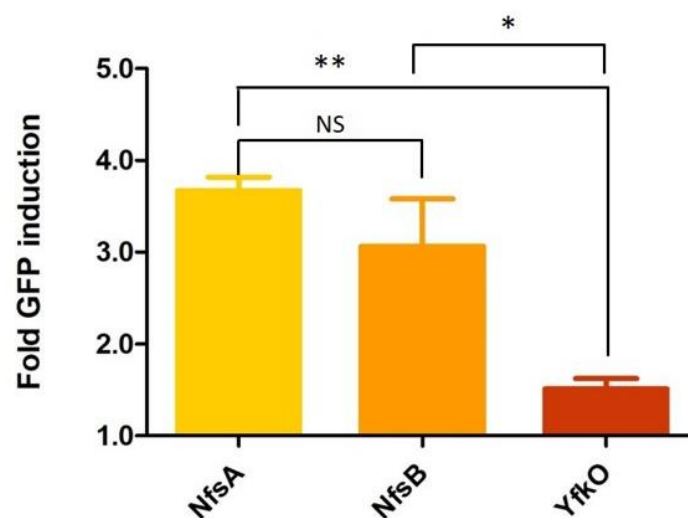


Figure 3.9 Mean increase in GFP signal of test condition over control condition for a 50% activator cell population in flow cytometry analysis. Three biological replicates were performed each comprising a minimum of three technical replicates for each test and control condition indicated in Panel A. For each, the GFP geomean of the three technical replicates was averaged and the bacterial bystander effect was quantified as the average fold increase in GFP fluorescence for the test condition over the control condition. A fold induction of GFP approaching one indicates a poor bacterial bystander effect. Error bars represent standard deviation of the average fold increase in GFP induction across the three biological replicates, and ** indicates $p < 0.01$ (one-way ANOVA Tukey test) GFP signal is significantly different from *YfkO*

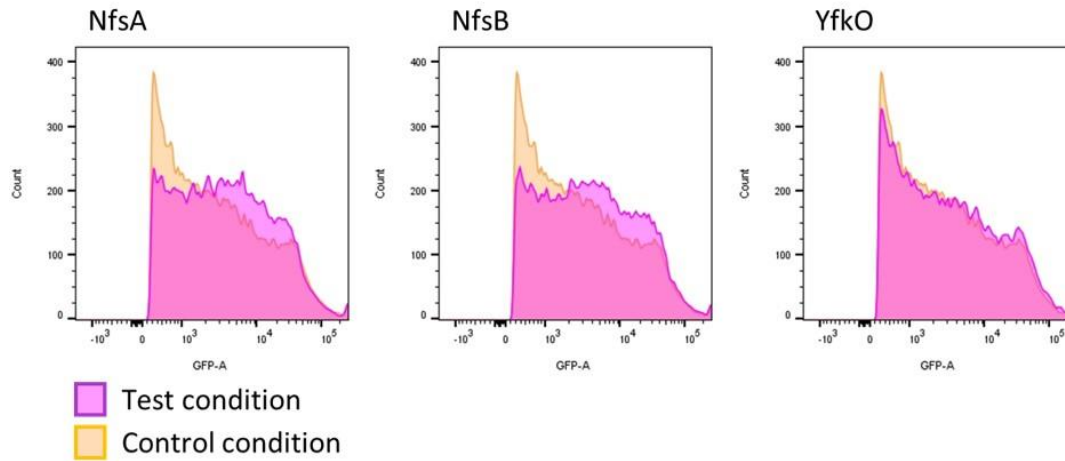


Figure 3.11 *Overlay histograms of test and control conditions for a 10% activator cell population.* As per Figure 3.8, but with 90:10 mixed cultures of SOS-R4 recipients and either nitroreductase null 7NT control cells or *nfsA*, *nfsB* or *yfkO*-expressing 7NT activator cells.

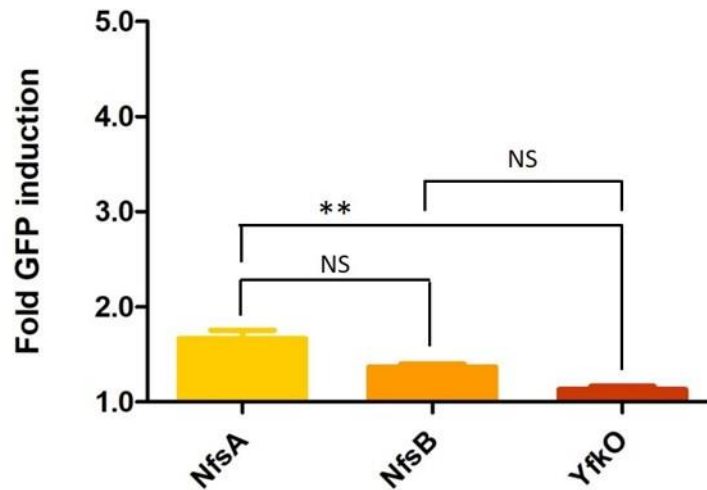


Figure 3.10 *Mean increase in GFP signal of test condition over control condition for a 10% activator cell population in flow cytometry analysis.* As per Figure 3.9, but with 90:10 mixed cultures of SOS-R4 recipients and either nitroreductase null 7NT control cells or *nfsA*, *nfsB* or *yfkO*-expressing 7NT activator cells. ** indicates $p < 0.01$ (one-way repeated measures ANOVA with Tukey's post-hoc test) GFP signal is significantly different from *YfkO*.

3.3.5 Prodrug pre-activation assay

To test that the lack of GFP induction by the activated metabolites of the two dinitrobenzamide mustard prodrugs was indeed due to inability to exit the 7NT activator cells, we incubated each prodrug with purified NfsA enzyme and NADPH in vitro, then added the mixture 1:1 to a culture of SOS-R4 cells.

First the purified NfsA protein was used to pre-activate 200 μM PR-104A, 150 μM SN27686 or 125 μM nitro-CBI-DEI. Reactions were initiated by addition of the purified NfsA enzyme to appropriate substrate mixture. The reaction was monitored, using a spectrophotometer until the reaction had gone to completion i.e. no further change in absorbance was detected. The pre-activated prodrug metabolites were used to challenge cultures of the null-nitroreductase recipients. The pre-activated prodrug metabolites were diluted so that by addition of an equal volume of SOS-R4 recipient strains the pre-activated prodrug metabolites would be at the same final concentrations as that used in the bystander effect assays. Control conditions for each condition were created by using a volume of Tris-Cl buffer equivalent to that of the volume of the pre-activated prodrug metabolites. After incubation the OD_{600} and GFP fluorescence was also recorded. To calculate the fold increase in fluorescence, resulting from transfer of activated prodrug metabolites from the medium into the SOS-R4 cells, the average fluorescence of each challenge condition was divided by the average fluorescence of the corresponding control condition. The particulars of the experiment are outlined in section **2.12.3**.

A significant ($p < 0.001$) SOS DNA damage response, was observed, in the nitroreductase null SOS-R4 recipients incubated with pre-activated mustard prodrugs as well as pre-activated nitro-CBI-DEI compared to the no prodrug controls (**Figure 3.12**). This observation ruled out the possibility of compound-specific neutralisation in the LB growth medium or inability of the dinitrobenzamide mustards to penetrate the SOS-R4 recipient cells.

However, retrospectively it was considered that a no prodrug control condition may not have been the ideal control for comparison of the preactivated prodrug samples. A more relevant control condition would have been a culture SOS-R4 nitroreductase null reporter cells co-incubated with the same concentration of the prodrug that the pre-activation conditions were set at. As there was no opportunity to repeat the experiment with a new

control condition, a retrospective reanalysis of the data was performed using the data from **Figure 3.4**. This is an appropriate use of existing data as all of the conditions used to generate Figure 3.4 would be the same as those if the pre-activation assay were to be repeated using this more relevant control.

A two-tailed unpaired t-test was used to re-analyse the data. A significant SOS DNA damage response, was observed, in the nitroreductase null SOS-R4 recipients incubated with pre-activated mustard prodrug SN27686 and nitro-CBI-DEI compared to the historic data of prodrug challenged controls SOS-R4 nitroreductase null reporter cells. The prodrug SN27686 had a p value of 0.0411 and nitro-CBI-DEI has a p value of 0.0003. However the pre-activated prodrug PR-104A condition did not indicate that significant SOS DNA damage response compared to the historic data of SOS-R4 reporter cells challenged with the same concentration of PR-104A (p value 0.0950) (**Figure 3.13**).

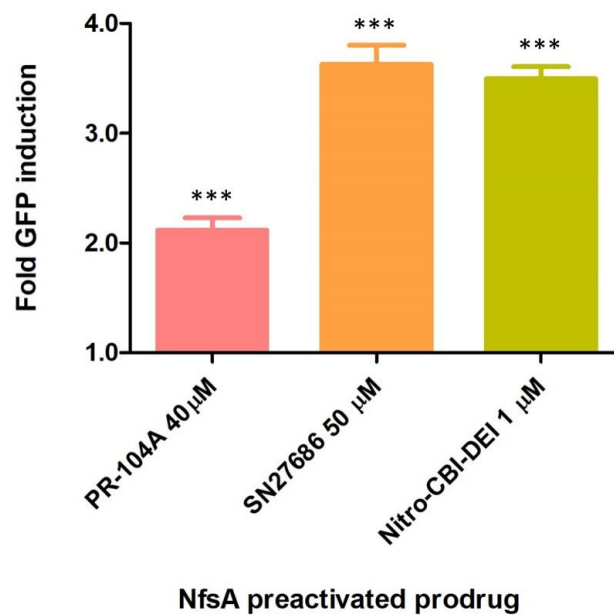


Figure 3.12 Microplate assay of SOS response induced by transfer of pre-activated prodrug metabolites to nitroreductase null SOS-R4 reporter cells. Demonstrates transfer of pre-activated prodrugs compared to a control of an unchallenged control condition of SOS-R4 nitroreductase null reporter cells. 30 μ L cultures of SOS-R4 recipients were incubated with either 40 μ M PR-104A, 50 μ M SN27686 or 1 μ M nitro-CBI-DEI that had been pre-activated by incubation in vitro with purified NfsA enzyme and excess NADPH, after which GFP fluorescence was measured. The transfer of the pre-activated prodrug metabolite from the surrounding medium into the SOS-R4 recipients was detected by the fold increase in GFP expression relative to an unchallenged control condition. A minimum of three biological replicates were performed (each comprising at least four technical replicates), and error bars represent standard deviation across the three biological replicates. *** indicates $p < 0.001$ (one-way repeated measures ANOVA with Tukey's post-hoc test) relative to the unchallenged control.

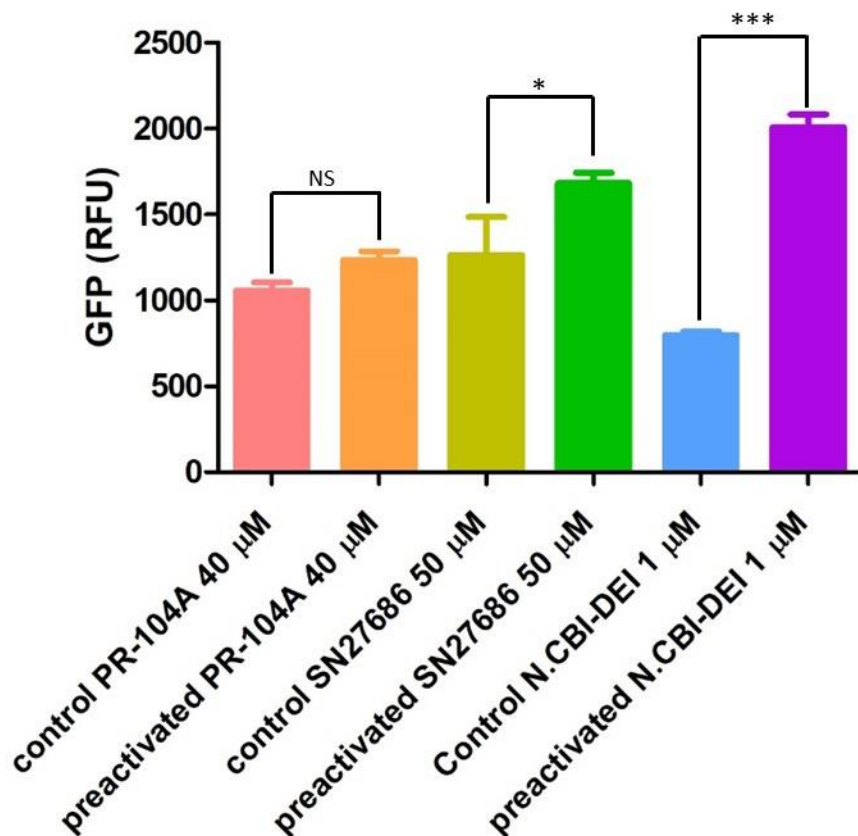


Figure 3.13 Retrospective reanalysis of microplate assay of SOS response induced by transfer of pre-activated prodrug metabolites to nitroreductase null SOS-R4 reporter cells. Demonstrates transfer of pre-activated prodrugs compared to historic data of prodrug challenged control condition of SOS-R4 nitroreductase null reporter cells. 30 μ L cultures of SOS-R4 recipients were incubated with either 40 μ M PR-104A, 50 μ M SN27686 or 1 μ M nitro-CBI-DEI that had been pre-activated by incubation *in vitro* with purified NfsA enzyme and excess NADPH, after which GFP fluorescence was measured. The transfer of the pre-activated prodrug metabolite from the surrounding medium into the SOS-R4 recipients was detected by a significant increase in GFP expression relative to a prodrug challenge control condition consisting of SOS-R4 nitroreductase null reporter cells. A minimum of three biological replicates were performed (each comprising at least four technical replicates), and error bars represent standard deviation across the three biological replicates. *** indicates $p < 0.001$ (unpaired two-tailed t-test) relative to the historical data of prodrug challenged control SOS-R4 nitroreductase null reporter cells. Note that N.CBI-DEI represents an abbreviation for Nitro-CBI-DEI.

3.4 Discussion

The bystander effects of diverse nitroaromatic prodrug metabolites have previously been evaluated in mixed multilayer carcinoma cell models, comparing the survival of untransduced target cells in the presence or absence of co-incubated nitroreductase-expressing activator cells. This multilayer model simulates tissue-like cell densities and can explicitly test the ability of activated metabolites to diffuse through tumour tissue (Wilson

et al., 2002). These qualities make the model highly appropriate for modelling VDEPT scenarios, where infected human cells yield prodrug products from intracellular catalytic processes. However, the physiology of bacterial cells differs substantially from human cells, and we considered that the same prodrug metabolites might vary in their relative abilities to exit a bacterial activator cell. To establish a more relevant model for cell-to-cell transfer of activated prodrug metabolites in BDEPT I adapted a GFP-SOS reporter strain of *E. coli* to monitor the transfer of genotoxic prodrug metabolites from a co-cultured activator strain, rather than activation of prodrugs by an endogenous nitroreductase as previously described (Copp et al., 2014, 2017).

I recognise that my experimental model employs a large liquid to cell volume ratio, which may not reproduce the potentially close association of bacterial vectors to cancer cells in clinical BDEPT. However, studying the effects of prodrug activation by bacterial activator cells in co-culture with target carcinoma cells would be confounded by the naturally oncolytic nature of bacteria, which would cause death of the target cells by numerous prodrug independent mechanisms (Forbes, 2010; Prosser et al., 2013). The model developed here is robust and easily implemented, and importantly it does inform on the relative abilities of prodrug metabolites to exit bacterial activator cells. Moreover, as I have shown, addition of prodrug metabolites activated by a purified nitroreductase *in vitro* can be used to control for the possibility that these metabolites might be unstable and neutralised by components of the culture medium, or fail to penetrate the SOS-R4 reporter cells.

As my model employs *E. coli* activator cells I consider that it is most relevant to *E. coli* and *Salmonella* vectors for BDEPT, rather than obligate anaerobes such as *Clostridium* or *Bifidobacteria*, owing to the inherent differences between Gram negative and Gram positive cell walls. For example, it is possible that the Gram positive cell wall might pose less of a barrier to the activated metabolites of dinitrobenzamide mustard prodrugs such as PR-104A and its analogues. Maintenance of an active TolC outer-membrane efflux channel might improve the ability of Gram negative bacterial vectors to redistribute these activated metabolites, but because PR-104A is itself rapidly effluxed by TolC (Prosser et al., 2013), this would necessitate substantially higher concentrations of prodrug to render

BDEPT effective, likely exceeding the dose that can be safely administered to patients (only 270 mg/m² for PR104, the pre-prodrug form of PR-104A) (McKeage et al., 2011).

I note it is also possible that the surprisingly poor cell-to-cell transfer I detected for the activated metabolites of PR-104A and SN27686 stems from a more generic feature of prokaryotic genome architecture. Unlike in a human activator cell, bacterial DNA is not coiled around histones or compartmentalised in a nucleus, and thus is more exposed to a cytoplasm-activated genotoxin. This may cause it to act as a sink for the activated mustards, which exhibit particularly high levels of alkylating reactivity (Helsby et al., 2003), restricting cell-to-cell transfer relative to the less reactive metabolites of nitro-CBI-DEI and (2-nitro reduced) CB1954. In particular, mustard prodrugs contain charged groups in their activated state unlike CB1954 and nitro-CBI-DEI. This indicates that they are designed to react faster i.e. to bind their target molecule DNA. Therefore PR-104A and SN27686 are more likely become permanently bound to the bacterial DNA.

In future the pro-prodrug preactivation assay should be repeated with the more relevant control of SOS-R4 nitroreductase null reporter cells. Repetition of this assay may shed more light on the ability of activated drug metabolites to enter surrounding cells. Using historic data of SOS-R4 empty recipients is a useful for reconsidering the ability of the activated drugs to enter cells. However because of its very nature of being historic, and not a true control performed on the day at the same time as the pre-activation assay, I cannot draw definite conclusions. In particular, further investigation in to the movement of PR-104A metabolites is warranted and may require spectroscopic analysis.

Future collaborative efforts using mass spectroscopy to analyse the activated prodrug metabolites in the culture medium surrounding the reporter cells as well as the activated prodrug metabolites inside of the cells would be ideal to confirm the ability or inability of mustard prodrugs to exit bacterial cells such as the *E. coli* used here. However mass spectroscopic analysis of activated prodrug metabolites inside of cells will not be able to discern those prodrug metabolites that have successfully bound to DNA.

Overall, a moderate interpretation of this data must be taken in the context of the assay design. In this particular assay design, the specialized *E. coli* screening strain SOS-R4 was not sensitive enough to detect a bacterial bystander effect signal above the background

fluorescence, experienced by the cells in the absence of a nitroreductase, at lower concentrations of the mustard prodrugs PR-104A and SN27686. This led to the exploration of the role of multi-drug efflux pumps in my bacterial bystander effect assay. This investigation is presented later alongside other next generation prodrugs in Chapter 6.

The relative absence of a bystander effect exhibited by 4-nitro reduced (i.e., YfkO activated) CB1954 was consistent with previous studies in human carcinoma multicellular layers (Helsby et al., 2004), I observed surprisingly high levels of cell-to-cell transfer for 2-nitro reduced CB1954, approaching those of reduced nitro-CBI-DEI. In contrast, NfsB activated CB1954 exhibits only a weak bystander effect in human multicellular layers (Mowday, Ashoorzadeh, et al., 2016; Singleton et al., 2007; Wilson et al., 2002). The data therefore suggests that CB1954 may be a more effective prodrug for BDEPT applications (those employing Gram negative vectors, at least) than it has previously indicated in clinical VDEPT trials (Chung-Faye et al., 2001; Patel et al., 2009).

Based on this, I consider that CB1954 in combination with NfsA (or variants engineered for superior efficacy at the concentrations of this prodrug that are achievable in patients) may be worthy of further investigation in engineered *Salmonella* or *E. coli* BDEPT systems, leveraging the previous clinical development of this prodrug. Above all else, my results highlight the importance of evaluating enzyme-prodrug combinations in models relevant to the intended GDEPT vector, as there can evidently be profound differences in efficacy in different settings. Taking into account the fundamental physiological differences associated with different gene-delivery systems will facilitate the identification of optimal enzyme-prodrug combinations for each setting.

The work described in this chapter has been published in Biochemical Pharmacology (JVE Chan-Hyams, JN Copp, JB Smaill, AV Patterson, DF Ackerley (2018). Evaluating the abilities of diverse nitroaromatic prodrug metabolites to exit a model Gram negative vector for bacterial-directed enzyme-prodrug therapy. Biochemical Pharmacology 158:192-200). All experimental work described in that paper and in this chapter was performed by Jasmine Chan-Hyams.

4 Assessing the impact of the bystander effect on directed evolution of nitroreductases via SOS-GFP selection

4.1 Overview

Interrogating vast libraries of enzyme variants is frequently the rate limiting step in the directed evolution process. Optimization of high-throughput and accurate screening methods can address this limitation. One such selective screening method is fluorescence activating cell sorting (FACS). SOS-R4 is a SOS (DNA damage responsive) GFP reporter strain of *E. coli* that has utility for FACS selection during directed evolution to improve the bioreductive activation of a nitroaromatic prodrug by a target nitroreductase enzyme. In this system a functional nitroreductase converts a nitroaromatic prodrug to a genotoxic metabolite. The genotoxin then causes DNA adducts that trigger the SOS-DNA damage response, quantified via GFP expression. Thus the most efficient nitroreductase variants can be isolated, from a library of functional and non-functional variants, by selecting the most fluorescent clones. However, as demonstrated in Chapter 3, the activated metabolites of some nitroaromatic prodrugs are able to transfer efficiently between *E. coli* cells, causing DNA damage in cells that do not express an efficient nitroreductase. Here I modelled the impact of this bacterial bystander effect on the enrichment of a variant library for functional nitroreductases using FACS.

Based on my evaluation of prodrug bacterial bystander capabilities in Chapter 3, I predicted a negative correlation between the yield of active nitroreductases, from FACS, and the cell-to-cell transfer potential of each prodrug tested. I observed that significantly fewer *nfsA*-expressing cells were recovered from FACS when using CB1954 and nitro-CBI-DEI when the bystander effect was given time to occur, as compared to a control in which the bystander effect was given no time to occur. This was consistent with the high bacterial bystander effect recorded for these two prodrugs in Chapter 3. In comparison, at the preferred 10 μ M challenge concentrations, the mustard prodrugs PR-104A and SN27686 did not yield significantly lower proportions of *nfsA*-expressing cells under bystander conditions. This was not unexpected as at this low concentration I did not

previously observe a significant bystander effect. However, it was noted that at a higher challenge concentration of 50 μM , SN27686 did yield significantly fewer *nfsA*-expressing cells recovered from FACS, a potentially artefactual phenomenon that was attributed to the higher fluorescence gate boundaries required under that specific prodrug condition.

4.1.1 Aims:

- Design and perform an assay that can monitor the impact of the bystander effect on the efficiency of FACS for enriching a model nitroreductase variant library.
- Determine which types of nitroaromatic prodrug result in the most efficient library enrichment using FACS.

4.2 Introduction

Directed evolution is a powerful and successful approach for improving enzyme efficiency via iterative rounds of mutagenesis and selection. Accurately and quickly interrogating vast libraries of enzyme variants is frequently a rate limiting step in the directed evolution process (Copp et al., 2014; Currin et al., 2015). Fluorescence Activated Cell Sorting (FACS) is a high throughput screening method that has proven to be a successful screening approach for directed evolution of numerous enzymes including nitroreductases (Copp et al., 2017; Ruff et al., 2012; Tu et al., 2011).

As described in section 1.6.3.3, Copp et al (2014) showcased the ability of FACS to enrich a model nitroreductase library for functional activity with the first-generation nitroaromatic prodrug CB1954. The most efficient nitroreductase variants can be isolated and collected by setting stringent fluorescence-based collection gates (**Figure 1.8**). This strategy was later implemented to successfully evolve an NfsA *E. coli* nitroreductase for enhanced activity at low concentrations of the prodrug PR-104A (Copp et al., 2017).

Next generation nitroaromatic prodrugs, with enhanced bystander effects, are the leading therapeutic agents in GDEPT clinical trials (Williams et al., 2015). In one seminal study, increased lipophilicity accounted for upwards of 80% of the bystander effect in a human carcinoma model of GDEPT (Wilson et al., 2002). Consequently, there is strong motivation to engineer nitroreductase enzymes that are highly efficient at activating these synthetic nitroaromatic prodrugs. However, over recent years the Ackerley lab has waged several

unsuccessful campaigns to evolve nitroreductases for improved activity with other prodrugs that, based on their lipophilicity, were expected to exhibit very high bystander effects (*Prof. David Ackerley, personal communication*).

Based on these past difficulties, we hypothesised that prodrugs that exhibit high levels of bacterial cell-to-cell transfer post-activation might confound FACS selection. If during preparation for FACS, the activated prodrug metabolite can enter cells that contain non-functional nitroreductase variants, inducing the SOS response, this would generate false positives (**Figure 4.1**). This would result in a diminished level of library enrichment from FACS, such that fewer of the recovered cells express a functional nitroreductase let alone variants of improved enzymatic efficiency. This poor quality yield would ultimately encumber the rate of genetic gain in a directed evolution campaign for improved nitroreductases for GDEPT.

We predicted that prodrugs exhibiting a high bacterial bystander effect would confound selection of nitroreductase-expressing cells during FACS. To test this I designed a bystander and a null bystander treatment. I expected that if the bystander effect impairs FACS enrichment, then significantly fewer nitroreductase-expressing cells will be yielded from the bystander condition compared to the null bystander condition. To investigate, a model library was developed of *E. coli* SOS-R4 activator cells that express a nitroreductase and *E. coli* SOS-R4 recipient cells that do not express a nitroreductase (**Figure 4.2**). These two strains were co-cultured together in the presence of a range of clinically relevant prodrugs. The co-culture was then subjected to FACS to simulate a nitroreductase library undergoing screening during a directed evolution campaign. The cells recovered post-FACS were interrogated to determine their nitroreductase expression status.

4.2.1 Key Terminology

- Nitroreductase-expressing activators (SOS-R4 cells)
- Nitroreductase null recipients (SOS-R4 cells)
- Bystander condition (10% activators and 90% recipients co-culture incubated with prodrug)

- Null bystander condition (activators and recipient mono-cultures are separately incubated with prodrug and then mixed immediately prior to FACS in a 10%:90% ratio)
- Positive control (mono-culture of 100% *nfsA*-expressing activator cells)

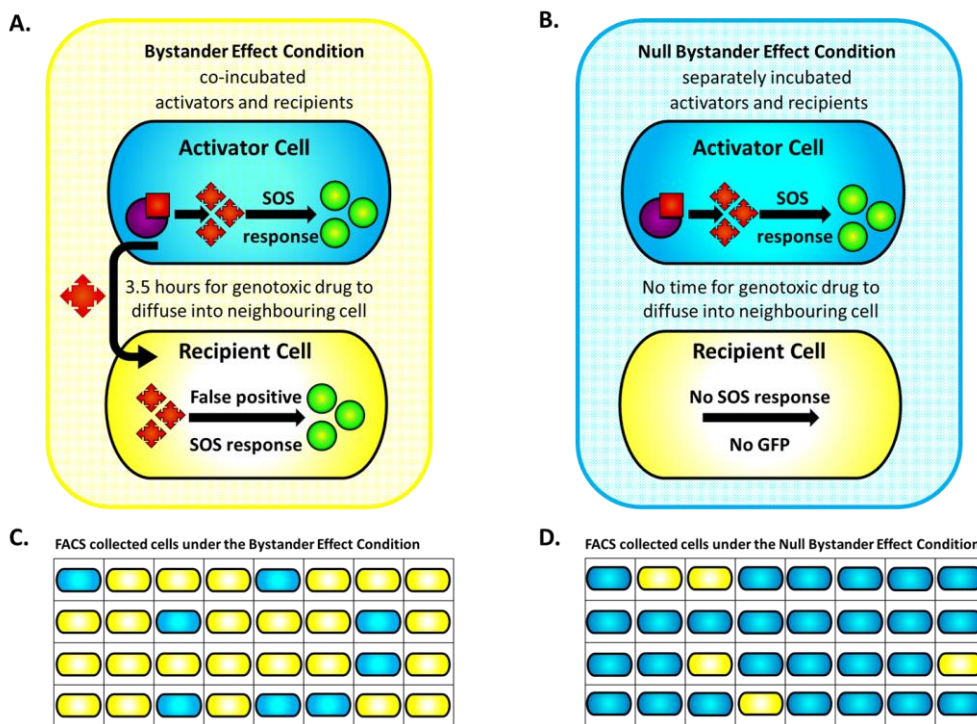


Figure 4.1 Assay design for detecting the bystander effect during FACS. (A). Bystander condition: nitroreductase expressing activator cells and nitroreductase null recipient cells are co-cultured with the prodrug. During a 3.5 hour prodrug challenge incubation period the activated prodrug has time to diffuse from the activators (blue cells) to the recipients (yellow cells). Consequently these recipient *E. coli* also have potential to experience and report DNA damage. **(B). Null bystander condition: nitroreductase expressing activator cells and nitroreductase null recipient cells are separately incubated with the prodrug in monoculture.** Activators (blue cells) and recipients (yellow cells) are separately incubated with the prodrugs and only mixed together immediately prior to FACS. In this scenario the bystander effect has no time to occur and the genotoxin cannot reach the recipient cells (yellow cells) to mask the absence of a nitroreductase from FACS. **(C). Example ratio of activators (blue cells) to recipients (yellow cells) recovered from the bystander condition.** If recipient *E. coli* receive activated prodrug from a neighbouring activator, via the bystander effect, then they will be selected by FACS as positive hits despite absence of a prodrug activating enzyme. We hypothesise that for a high-bystander prodrug FACS enrichment of nitroreductase-expressing cells will be significantly impaired, which will be quantifiable as a poor yield of nitroreductase expressing cells compared to a greater number of nitroreductase null recipients. **(D). Example ratio of activators (blue cells) to recipients (yellow cells) recovered from the null bystander condition.** We predict, in the absence of any bystander effect, a significantly greater number of nitroreductase expressing cells will be yielded from FACS compared to nitroreductase null recipients.

4.3 Results

4.3.1 Designing an assay to measure the impact of the bystander effect on FACS enrichment

To simulate the impact of the bystander effect on FACS I modelled a nitroreductase variant library undergoing directed evolution. A major point of difference to the bacterial bystander assay, developed in Chapter 3, is that all cells in this model bear the SOS-DNA-damage GFP reporter plasmid. A small proportion of these cells also express a highly active nitroreductase, while the remaining cells are nitroreductase null, representing the non-functional variants that are commonly generated by the mutagenesis process. A perfect FACS selection would exclude these non-functional variants from selection.

To date, all reported nitroreductase evolution studies have involved at least a component of targeted mutagenesis, probing specific codons by site-saturation mutagenesis (Copp et al., 2017; Grove et al., 2003; Guise et al., 2007; Jaberipour et al., 2010). Targeted mutagenesis libraries usually contain a much higher proportion of enhanced or active enzymes compared to libraries generated by random mutagenesis (Copp et al., 2014). To represent this scenario in my model library I initially used 10% *E. coli* SOS-R4 ***nfsA*-expressing activator cells** (expressing *E. coli nfsA*) while the remaining 90% of cells were *E. coli* SOS-R4 **nitroreductase null recipients** (empty plasmid control cells) that express no nitroreductases. This experimental design was similar to that used by Copp et al. (2014), who employed a mixture of 10% highly CB1954 active YcnD-expressing cells and 90% inactive YdjA-expressing cells.

To test our hypothesis, that prodrugs exhibiting a high bacterial bystander effect would impair selection of nitroreductase-expressing cells during FACS, I designed a bystander and a null bystander treatment. The **bystander condition** was simulated by co-incubating the activators and recipients together with prodrugs. During this co-incubation period the bystander effect has time to occur by diffusion of the genotoxin from the activators into the recipients (**Figure 4.1A**). The bystander condition contained 10% activators and 90% recipients co-incubated with a prodrug and then screened with FACS. I predicted that the FACS enrichment of this model library would be significantly impaired compared to that of a null bystander condition. In the **null bystander** condition the activators and recipients were separately incubated with the prodrugs and only mixed together in 1: 9 ratio

immediately prior to FACS (**Figure 4.1B**). In this scenario the bystander effect has no time to occur, i.e. the genotoxin cannot reach the recipient cells to induce an SOS response that would mask the absence of a nitroreductase from FACS.

I predicted that if the bystander effect impairs FACS enrichment, then significantly fewer nitroreductase-expressing cells will be yielded from the bystander condition (**Figure 4.1C**) compared to the null bystander condition (**Figure 4.1D**). In Chapter 3, I demonstrated that NfsA-mediated activation of the prodrugs CB1954, PR-104A, SN27686 and nitro-CBI-DEI generated genotoxic metabolites that had a range of bystander potentials. I therefore performed FACS at prodrug concentrations previously optimized, for growth inhibition of SOS-R4 cells, with the exceptions of 2 μ M metronidazole and CB1954 at both 10 and 50 μ M. Initially metronidazole was tested at a concentration of 5 μ M, as used in Chapter 3, however a pilot test revealed that a concentration of 2 μ M resulted in greater recovery of cells post-FACS. We also tested 10 μ M CB1954 to permit more direct comparisons with the lower concentrations of the mustard prodrugs also tested at 10 μ M. Particulars of the experimental procedure are detailed in section **2.13**.

A prodrug challenge incubation time of 3.5 hours was selected due to previous optimization in microplate based assays with the screening strain SOS-R4. Typically 3-4 hours of prodrug challenge time with nitroaromatic prodrugs and an NfsA *E. coli* activating enzyme is necessary to stimulate a measurable GFP fluorescence signal from the specialized SOS-R4 screening strain. Less than 3 hours prodrug challenge incubation is not enough time for sufficient GFP expression to be detectable i.e. not enough prodrug has been activated to trigger the SOS-DNA response in the majority of SOS-R4 cells. At greater 4 hours incubation, if too much DNA damage has occurred then the SOS-R4 cells will suffer from drug toxicity and thus will not be optimally expressing GFP. Longer incubation times can be selected depending on the toxicity of the active prodrug as well as the efficiency of the prodrug activating enzyme. For instance if the activating enzyme is inefficient then a longer incubation time of 5-6 hours may be used. However, a 3.5 hour prodrug challenge incubation has been extensively tested and observed with prodrugs such as CB1954, PR-104A and analogues thereof with an NfsA nitroreductases activating enzyme by myself and other members of the Ackerley laboratory.

4.3.1.1 Setting the collection gates and sample preparation for FACS

At the start of each FACS experiment for each prodrug condition, a collection gate was set to capture the top 10% region of the GFP profile of a positive control. This was a sample of exclusively *nfsA*-expressing activator cells challenged with the relevant prodrug. Within this gate, 50,000 individual cell GFP events were recorded. The GFP profiles of these positive controls indicated the upper limit of expected fluorescence in our model library.

After the collection gate was set, for each prodrug condition, cells were collected by FACS from the bystander condition and the null bystander condition. For the bystander condition, a pooled sample of 75 μ L of the co-incubated strains was analysed for each prodrug treatment. Individual cells that exhibited fluorescence within the collection gate were collected into 384 well microtitre plates. The null bystander condition sample for each prodrug was created by mixing the pooled activators and the pooled recipients in a 1:9 ratio. This mixture was analysed by FACS, immediately upon mixing, to prevent exchange of activated prodrug metabolites between activator and recipient cells. Individual cells that exhibited fluorescence within the collection gate were collected into 384 well microtitre plates. The microtitre plates, containing the collected cells, were then incubated for 48 hours. This allowed the collected cells to recover and establish a visually dense culture.

In addition, 50,000 individual cell GFP events were recorded, for each prodrug treatment under both the bystander and null bystander conditions, within the 10% collection gate. Details of the experimental procedure can be found in section **2.13.1**. A minimum of 3 biological replicates, derived from independent overnight cultures, and were performed for each prodrug treatment under the bystander or null bystander condition.

4.3.1.2 Recovery of cells post-FACS

After FACS, it was necessary to recover collected cells in LB microwell cultures. For each prodrug treatment, under both the bystander and null bystander conditions, the number of wells able to recover post-FACS to visual density from a 384 well plate after 48 hours was typically fewer than 120 wells per 384 microtitre plate. In each case, up to a maximum of 95 individual samples were randomly selected and stored in 40% glycerol at -80 °C. If fewer than 95 wells recovered, post-FACS, then all cells that did recover were stored. This is described in section **2.13.2**.

4.3.1.3 Diagnosing expression of *nfsA* in samples recovered from FACS

To rapidly determine the overall yield of *nfsA*-expressing cells from FACS, we designed a bacterial growth inhibition assay using the compound niclosamide, to interrogate recovered cells for possession of a nitroreductase gene. Niclosamide is toxic to *tolC* mutant strains of *E. coli* unless reduced by a functional nitroreductase to a non-toxic state (Ackerley lab, unpublished finding) (**Figure 4.2**). The collected cells from each FACS sort were grown in LB microplate cultures and used to perform a growth inhibition assay with a final challenge concentration of 1 μM niclosamide as described in section **2.13.3**. Additionally samples of the cells from each FACS sort were stored in 40% glycerol at -80°C .

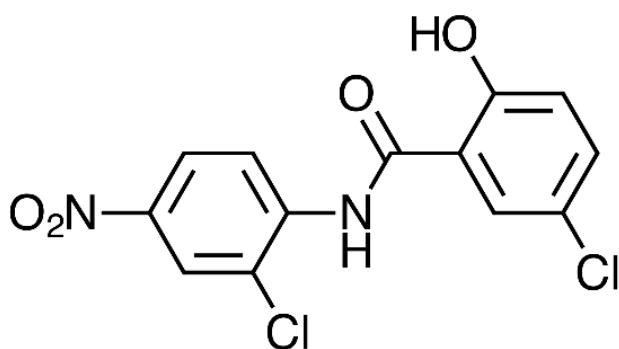


Figure 4.2 Chemical structure of niclosamide.

Growth inhibition was calculated from the relative difference in growth between challenged cultures and their respective unchallenged controls. Samples containing a functional nitroreductase were able to detoxify the niclosamide and did not suffer greater than 50% growth inhibition. These were deemed to be positive hits, i.e. *nfsA*-expressing activator cells that had been correctly selected by FACS. In the modelled false hits, i.e. nitroreductase null recipient cells, suffered extreme growth inhibition (far exceeding 50%) in the presence of 1 μM niclosamide (**Figure 4.3A**). An example of niclosamide diagnosis of nitroreductase expression in cells, from a single 384 well plate collected from FACS, under the bystander and null bystander conditions for 50 μM CB1954 demonstrates the general distribution of *nfsA*-expressing cells recovered post-FACS under a prodrug treatment (**Figure 4.3B**).

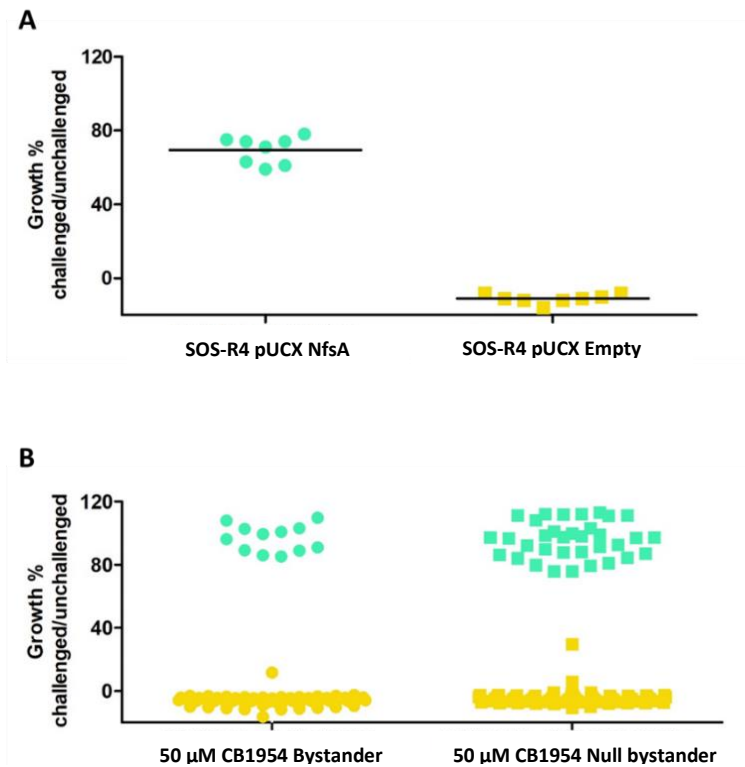


Figure 4.3 Validation of niclosamide as a compound to diagnose presence or absence of nitroreductase post-FACS. Niclosamide is toxic to *tolC* mutant strains of *E. coli* unless reduced by a functional nitroreductase to a non-toxic state. **(A). Proof of principle for use of niclosamide to diagnose nitroreductase expression.** Strains of SOS-R4 pUCX *nfsA* (green) or SOS-R4 pUCX Empty (yellow) were used to perform a growth inhibition assay with a final challenge concentration of 1 μM of niclosamide. Growth inhibition was calculated from the relative difference in growth between challenged cultures and their respective unchallenged controls. Samples containing a functional nitroreductase were able to detoxify the niclosamide and did not suffer greater than 50% growth inhibition. **(B). An example of niclosamide diagnosis of presence or absence of nitroreductase in cells, from a single 384 well plates collected from FACS, under the bystander and null bystander conditions for CB1954 at 50 μM .** Samples expressing *nfsA* were able to detoxify the niclosamide and did not suffer greater than 50% growth inhibition. These were deemed to be positive hits; *nfsA*-expressing activator cells that had been correctly selected by FACS whereas false hits were nitroreductase null recipient cells that suffered >50% growth inhibition.

4.3.2 Yield of *nfsA*-expressing clones recovered from FACS using prodrugs of a high bacterial bystander effect potential

As stated above, primary analysis focused on the prodrug concentrations previously observed to be optimal for flow cytometry analysis as described in section 3.3.1.2 (i.e. 1 μ M nitro-CBI-DEI, 50 μ M CB1954, and 10 μ M SN27686 or PR-104A), with the exception that 2 μ M metronidazole was used in preference to 5 μ M. A two-way ANOVA with a *Bonferroni* post hoc test was used to determine if the yield of *nfsA*-expressing cells from the null bystander condition was significantly different to the yield from the bystander condition for a specific prodrug (**Figure 4.4**).

Not all prodrug treatments consistently resulted in recovery of at least 95 wells. This rate of recovery was attributed to the inherent stress of the FACS procedure and the toxicity of both active and inert prodrug. This variability is evident in the standard deviation for the total number of wells recovered and subsequently tested with niclosamide (**Table 4.1**). Full data is available in **Appendix Table A 1**. This variability in recovery prevented direct comparison of raw numbers, making percentage recovery of *nfsA*-expressing clones the most appropriate way to compare different prodrug treatments. The average percentage yield of *nfsA*-expressing activator cells was calculated from a minimum of three biological replicates for each prodrug and bystander and null bystander condition (**Table 4.2**).

Average number of clones recovered														
	Bystander Condition						Null Bystander Condition							
	Activators		Recipients		Total cells		Activators		Recipients		Total cells			
No Prodrug	5	± 3	89	± 2	94	± 2	7	± 3	88	± 3	95	± 1		
2 µM metronidazole	9	± 5	78	± 12	87	± 14	8	± 2	87	± 2	95	± 0		
10 µM CB1954	7	± 3	87	± 5	94	± 2	16	± 5	75	± 10	92	± 6		
10 µM PR-104A	4	± 2	86	± 4	90	± 5	10	± 3	81	± 10	91	± 8		
10 µM SN27686	8	± 4	87	± 4	95	± 1	12	± 2	80	± 5	91	± 4		
1 µM nitro-CBI-DEI	10	± 1	80	± 7	90	± 8	25	± 6	64	± 15	89	± 10		
50 µM CB1954	12	± 2	83	± 2	95	± 0	27	± 5	68	± 5	92	± 4		
40 µM PR-104A	13	± 5	73	± 12	86	± 13	23	± 6	62	± 13	84	± 15		
50 µM SN27686	18	± 3	76	± 3	94	± 1	39	± 11	53	± 8	92	± 4		

Table 4.1 Average number of recovered activator and recipient clones for bystander and null bystander conditions (as diagnosed using niclosamide) for all prodrug conditions.

The average number of activator and recipient clones was calculated from a minimum of three biological replicates for each prodrug and bystander or null bystander condition.

Average percentage yield of <i>nfsA</i> -expressing activator cells				
	Bystander condition		Null bystander condition	
	Activators	N	Activators	N
No Prodrug	5 ± 3	4	7 ± 3	3
2 μM metronidazole	10 ± 4	3	8 ± 2	3
10 μM CB1954	7 ± 3	3	18 ± 7	3
10 μM PR-104A	4 ± 2	3	11 ± 1	3
10 μM SN27686	8 ± 4	3	13 ± 3	3
1 μM nitro-CBI-DEI	11 ± 1	3	29 ± 10	3
50 μM CB1954	13 ± 2	3	29 ± 5	2
40 μM PR-104A	15 ± 5	3	27 ± 6	3
50 μM SN27686	19 ± 3	3	42 ± 10	3

Table 4.2 Average percentage of recovered *nfsA*-expressing activator and recipient clones for bystander and null bystander conditions.

The average percentage yield of activator and recipient clones was calculated from a minimum of three biological replicates for each prodrug and bystander effect condition.

I observed, that under the prodrugs treatments 50 μM CB1954 and 1 μM nitro-CBI-DEI, the yield of *nfsA*-expressing cells from FACS was significantly less under the bystander condition compared to the null bystander condition (*p* values < 0.01 and < 0.001 for CB1954 and nitro-CBI-DEI respectively) in a two-way ANOVA with a *Bonferroni* post hoc test (**Figure 4.4**). This was consistent with the hypothesis that prodrugs exhibiting a high bacterial bystander effect would impair selection of nitroreductase-expressing cells during FACS.

There was no statistically significant difference in yield, between bystander and null bystander conditions, under the no prodrug, 2 μM metronidazole, 10 μM PR-104A and 10 μM SN27686 treatments (*p* values > 0.05) (**Figure 4.4**). These results also aligned with the predictions based on the results of Chapter 3; i.e., that prodrugs conditions exhibiting a low bacterial bystander effect will not impair the yield of *nfsA*-expressing activator cells from FACS.

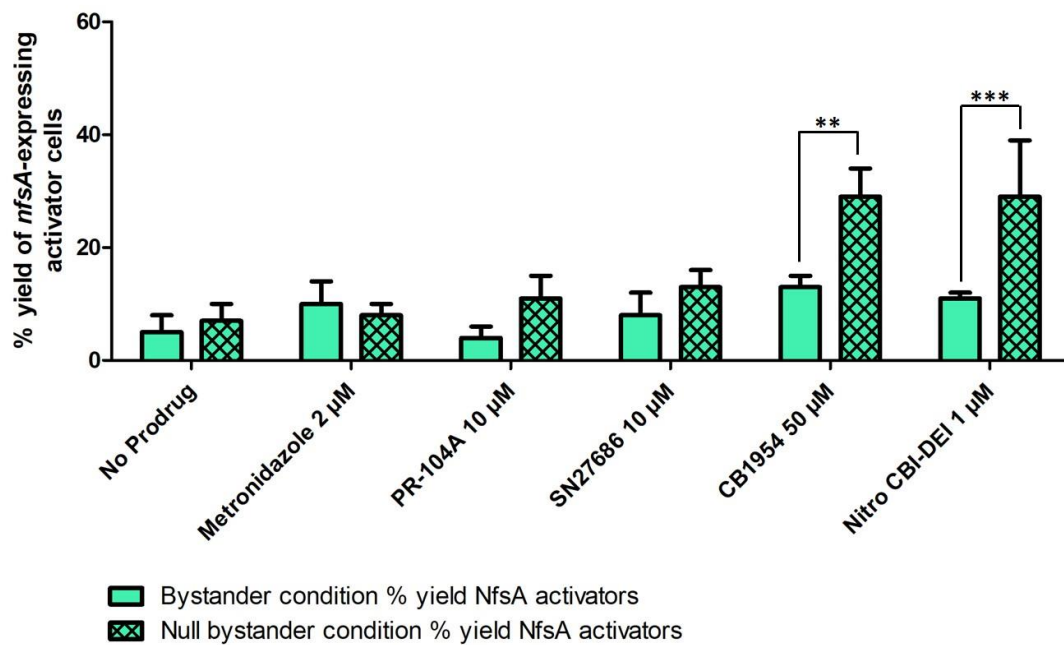


Figure 4.4 Average percentage yield of *nfsA*-expressing activator cells for all prodrug and bystander and null bystander conditions as diagnosed using niclosamide. The average number of *nfsA*-expressing activator cells for each biological replicate was normalized as a percentage out of the total number of cells recovered for each condition to allow for a fair comparison across different conditions. The average percentage yield of activator cells was calculated from a minimum of three biological replicates for each prodrug and bystander effect condition. *** indicates a p value < 0.001 , ** indicates a p value < 0.001 and * indicates a p value < 0.05 in a two-way ANOVA with a Bonferroni post hoc test was used to determine if there was a significant difference between the bystander and null bystander conditions in the yield of *nfsA*-expressing activator cells from FACS for each prodrug.

4.3.3 4.3.6 GFP profiles of bacterial populations in the collection gate under different conditions

The overlap of the GFP profiles in the collection gate, between the bystander and null bystander conditions for a prodrug, visually indicate the degree to which the nitroreductase null recipients are masked from FACS. A high degree of similarity indicates a strong influence by the bystander effect in selection. A low degree of overlay indicates a weak influence.

Overlay histograms, of data recorded within the collection gate, compare examples of the bystander and null bystander conditions from a single biological replicate for each prodrug (**Figure 4.5**). I observed less overlap under the no prodrug control and the nil-bystander effect prodrug metronidazole as well as the mustard prodrugs tested at 10 μ M (**Figure 4.5 A-D**) compared to the high degree of similarity between the GFP profiles of the null bystander and bystander conditions under 50 μ M CB1954 within the collection gate (**Figure 4.5E**). This supports the results of the niclosamide diagnosis whereby the bystander effect had raised the GFP signal of the recipients, during FACS, to such a high degree that they were included in the collection gate and thus selected as false hits. Although 1 μ M nitro-CBI-DEI generated modest overlapping histograms (**Figure 4.5F**) I observed a strong influence of the bystander effect on FACS selection.

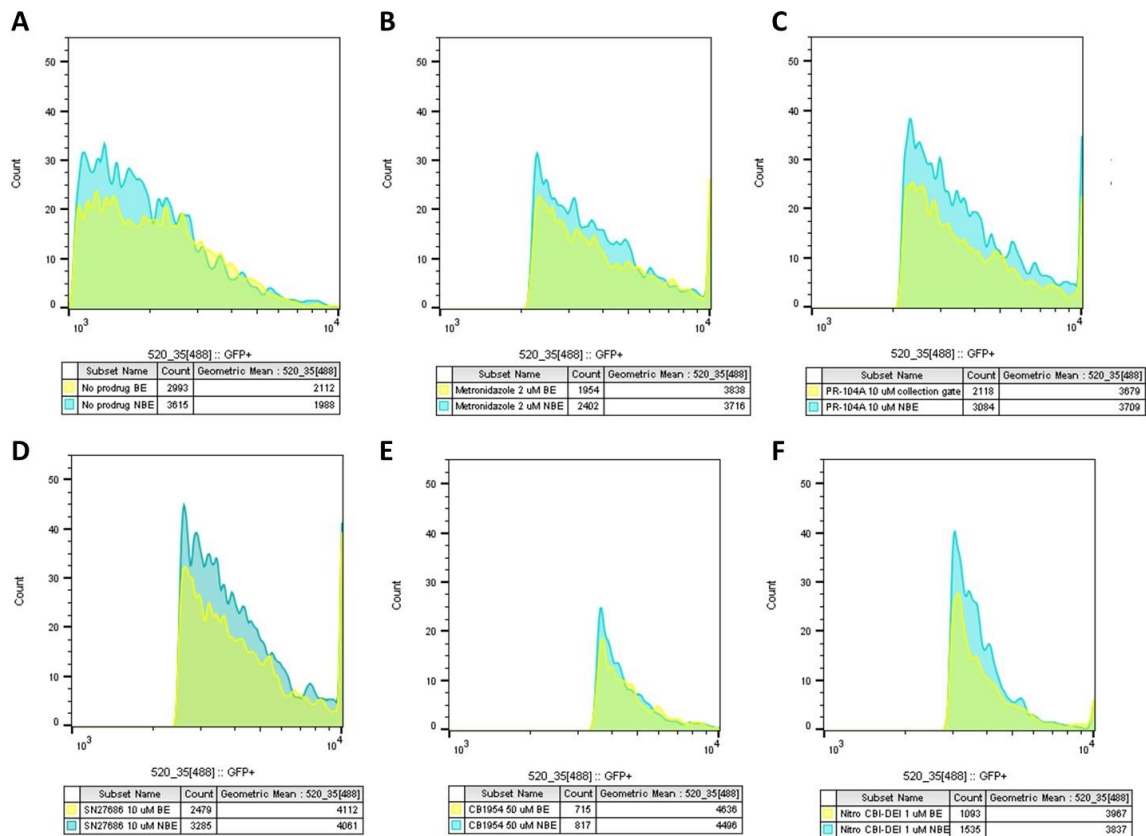


Figure 4.5 Overlay histograms of the GFP profiles recorded in the collection gate of the bystander (yellow) and null bystander (blue) conditions. 50,000 individual cell GFP reads were recorded for each condition within the 10% collection gate. Representative examples of the GFP signal were displayed as overlay histograms for the bystander and null bystander conditions for each prodrug. (A). No prodrug control. (B). metronidazole 2 μ M. (C). PR-104A 10 μ M. (D). SN27686 10 μ M. (E). 50 μ M CB1954 (F). 1 μ M nitro-CBI-DEI.

4.3.4 Yield of *nfsA*-expressing clones recovered from FACS using alternative concentrations of prodrugs

A portion of this research was performed simultaneously to that of the investigation in Chapter 3. Prior to the final optimization of the prodrug challenge concentration to 10 μ M for the mustard prodrugs in the bacterial bystander effect assay a portion of the FACS experiments had already been performed at the higher concentration of 50 μ M SN27686 and 40 μ M PR-104A. These were the concentrations that were optimized for growth inhibition rather than equivalent induction of the SOS-GFP expression in the recipient and activator strains. As a further point of investigation 10 μ M CB1954 was also used as a

prodrug treatment prior to FACS. This allowed us to directly compare the results of 10 μ M CB1954 to 10 μ M SN27686 and 10 μ M PR-104A.

In contrast to the 10 μ M data (**Figure 4.4**), treatment with SN27686 at 50 μ M significantly reduced the yield of *nfsA*-expressing cells from FACS in the bystander condition with *p* value < 0.001. PR-104A at 40 μ M also impaired recovery of *nfsA*-expressing clones, however this was not statistically significant with a *p* value > 0.05 (**Figure 4.6**). This outcome was unexpected given the results of our previous investigation in Chapter 3; where these two mustard prodrugs generated only a modest bystander effect at these same concentrations.

There was also a small but statistically significant difference in yield of *nfsA*-expressing cells detected at 10 μ M CB1954 (*p* value < 0.05). This was not surprising given the results of Chapter 3 where exclusive reduction of the 2-nitro substituent of CB1954 by NfsA resulted in a significant bystander effect even when only 10% of the bacterial population expressed NfsA (**3.3.4**).

The high degree of similarity between the GFP profiles of the null bystander and bystander conditions for 50 μ M SN27686 within the collection gate give further evidence for a strong influence by the bystander effect during FACS (**Figure 4.7E**). A smaller degree of similarity can be observed in 10 μ M CB1954 and 40 μ M PR-104A treatments (**Figure 4.7C and D**) indicating a weaker influence of the bystander effect during FACS.

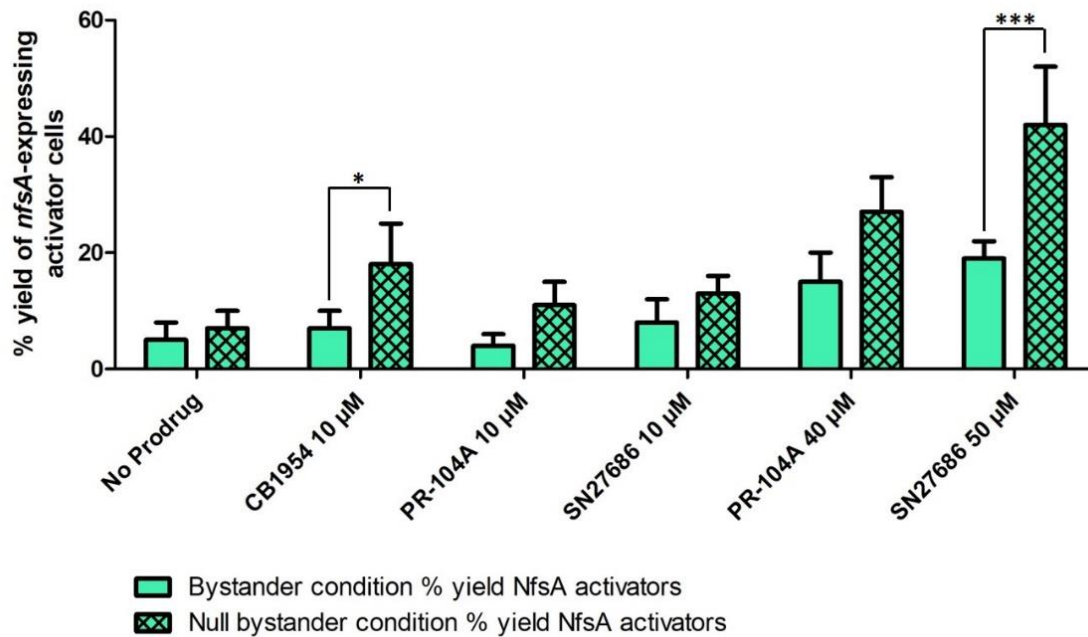


Figure 4.6 Average percentage yield of *nfsA*-expressing activator clones for CB1954 10 μ M, SN27686 at 50 μ M and PR-104A at 40 μ M for both bystander and null bystander conditions as diagnosed by niclosamide. The average number of *nfsA*-expressing activator cells for each biological replicate was normalized as a percentage out of the total number of cells recovered for each condition to allow for a fair comparison across different conditions. The average percentage yield of activator cells was calculated from a minimum of three biological replicates for each prodrug and bystander effect condition. *** indicates a *p* value < 0.001 in a two-way ANOVA with a Bonferroni post hoc test was used to determine if there was a significant difference between the bystander and null bystander conditions in the yield of *nfsA*-expressing activator cells from FACS for each prodrug.

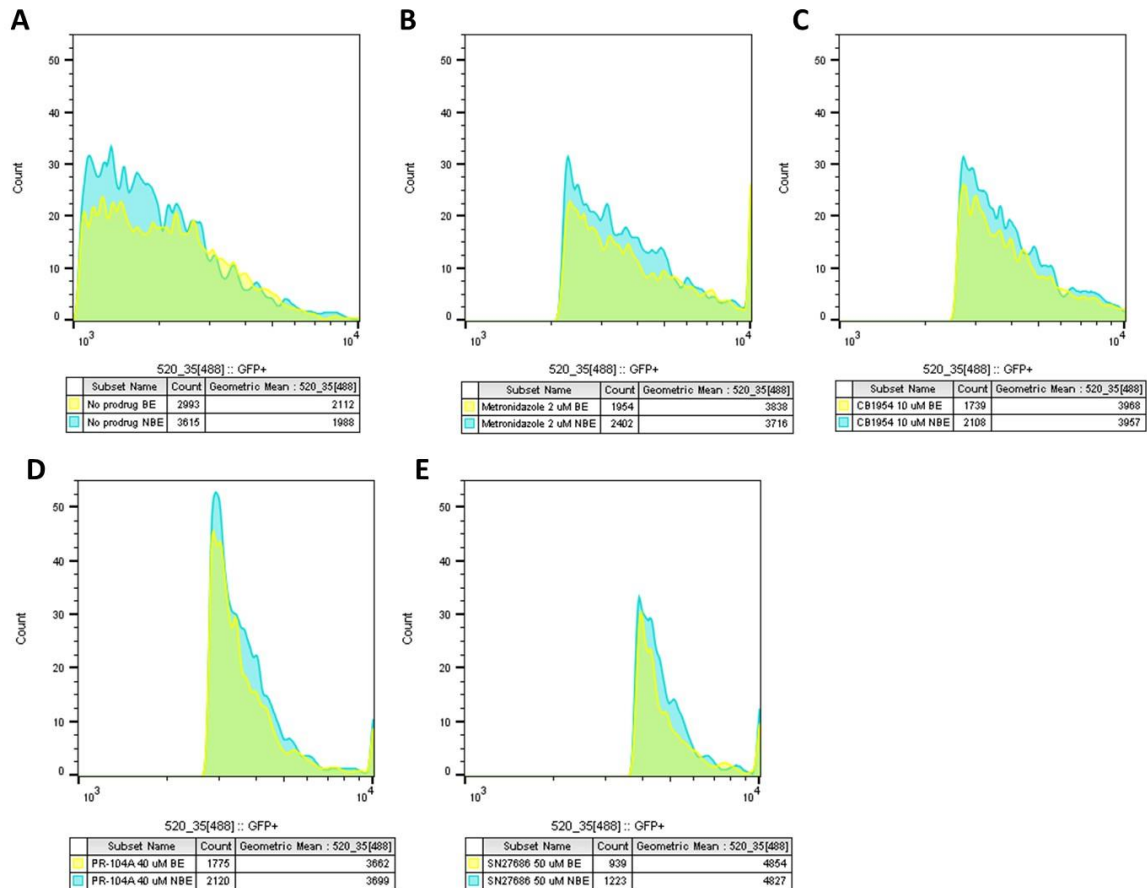


Figure 4.7 Overlay histograms of the GFP profiles recorded in the collection gate of the bystander (yellow) and null bystander (blue) conditions. 50,000 individual cell GFP reads were recorded for each condition within the 10% collection gate. Representative examples of the GFP signal were displayed as overlay histograms for the bystander and null bystander conditions for each prodrug. (A). No prodrug control. (B). 2 μ M metronidazole. (C). CB1954. (D). 40 μ M PR-104A. (E). 50 μ M SN27686.

4.3.4.1 Evidence for artefactual inflation of the influence of the bystander effect on FACS under the 50 μ M SN27686 treatment

At 50 μ M SN27686 we observed the highest yield of *nfsA*-expressing cells, in the null bystander condition (Table 4.1), compared to all other prodrugs treatments. It is important to note that the selection gate was unintentionally set more stringently (i.e., higher fluorescence cut-off for collection of cells) for the higher concentrations of the two mustard prodrugs, a consequence of the higher SOS-responses elicited by the activated metabolites of these prodrugs. This phenomenon is demonstrated in Figure 4.8. This may have resulted in more rigorous selection pressure by FACS for the cells challenged with the mustard prodrugs. Under this more strict selection pressure it is possible that SOS-R4

recipients may not receive enough of the activated prodrug, via the bystander effect, to achieve a level of GFP production that meets the threshold of the collection gate. I propose that additional stringency during gate selection unintentionally led to artificially exacerbating the size of the bystander effect during FACS for the mustard prodrugs compared to the non-mustards.

Of the GFP profiles recorded when setting the collection gates, the 50 μM SN27686 treatment (**Figure 4.8**) generated the highest average GFP signal compared to any other prodrug treatment and was significantly greater than that recorded for 50 μM CB1954 (p value < 0.05) - the only other prodrug tested at 50 μM . Furthermore, the mean fluorescence of events recorded when setting the collection gate for 50 μM CB1954, PR-40 μM 104A and 50 μM SN27686 were significantly higher on average than those recorded for the 2 μM metronidazole treatment (**Figure 4.8**). This indicates that the threshold of GFP expression required for bacterial cells to be collected by FACS under these four prodrug treatments was significantly higher than that required under the 2 μM metronidazole treatment. These observations may explain why we recovered overall more *nfsA*-expressing cells from 50 μM CB1954, 40 μM PR-104A and 50 μM SN27686, regardless of bystander status, compared to the results of 10 μM CB1954, PR-104A and SN36506 (**Table 4.1**).

We also examined the fluorescence of the 50,000 cells collected from the positive controls used to set the collection gate for 2 μM metronidazole (**Figure 4.8B**) and 50 μM SN36506 (**Figure 4.8C**) in a histogram format. We observe that the collection gate for 2 μM metronidazole is much wider and therefore less stringent compared to the narrow collection gate for 50 μM SN36506. This indicates that the lower boundary to enter the collection gate for 50 μM SN36506 is much higher i.e. more stringent than that of 2 μM metronidazole.

The stringency of the gating can also be observed in the overlay histograms of the GFP profiles of the cells collected from the bystander and null bystander conditions for each prodrug treatment (**Figure 4.5 and Figure 4.7**). The overlay histograms of 50 μM CB1954 (**Figure 4.5E**), 40 μM PR-104A (**Figure 4.7D**), and 50 μM SN27686 (**Figure 4.7E**), are narrower compared to their respective 10 μM counterparts (**Figure 4.5C-D**). This indicates that fewer cells in the samples met the lower threshold of fluorescence to fall within the

collection gates under these prodrug treatments at higher concentrations. It seems likely that a higher proportion of these more-fluorescent cells, which did fall within the boundaries of the collection gate, were *nfsA*-expressing activators.

I propose that the highly reactive metabolites of the mustard prodrug may bind to the DNA of the host bacterial *nfsA*-expressing activators more readily compared to other prodrugs. I suggest that the *nfsA*-expressing cells in the positive control used to set the collection gate, challenged with mustard prodrugs, experience a higher level of DNA damage compared to their counterparts under non-mustard prodrug treatments at the same concentration. Thus leading to unintentionally setting the increasing the stringency of the collection gates set during FACS.

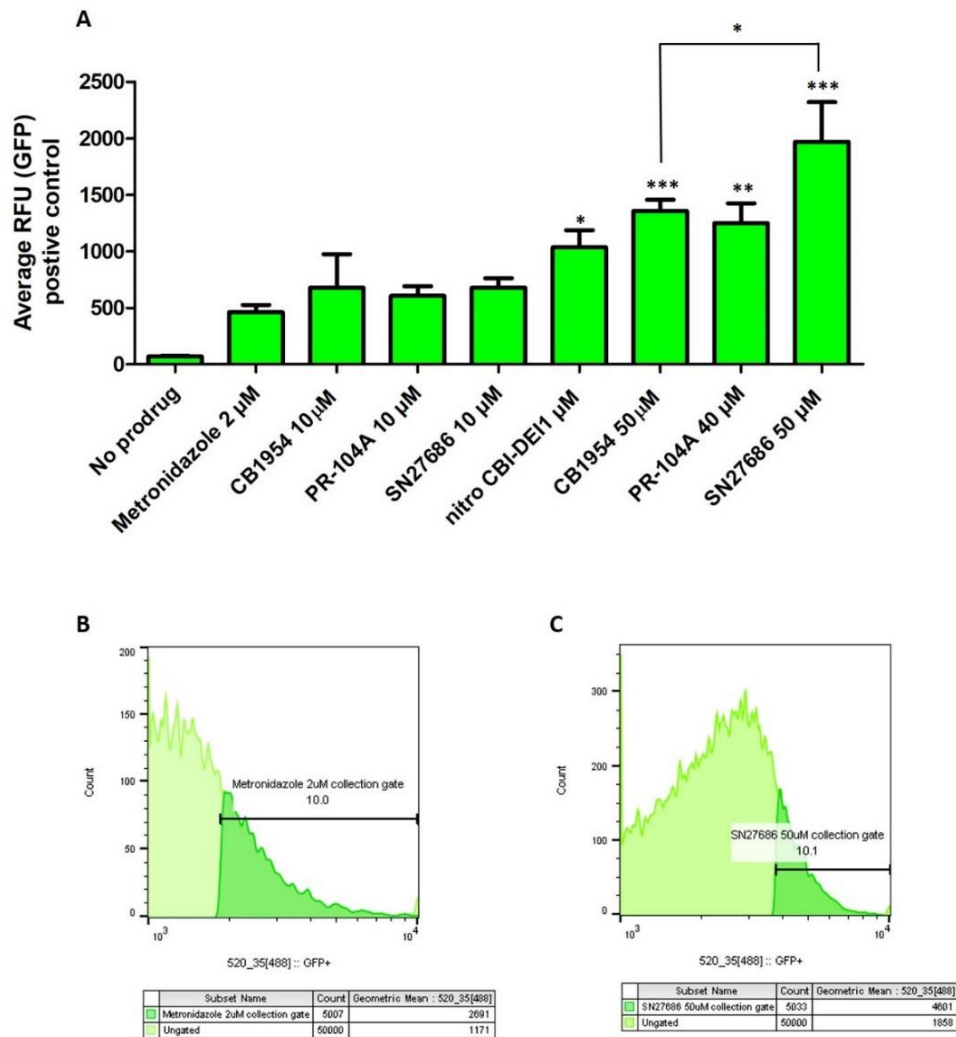


Figure 4.8 Analysis of GFP profiles recorded from the controls used to set the stringency of the collection gates prior to FACS. The positive control samples consist exclusively of *nfsA*-expressing activator cells challenged independently with each prodrug. (A). The average GFP signal recorded as the Raw Fluorescence Units (RFU) in the collection gate (top 10%). A repeated measures one-way ANOVA with a Bonferroni post-hoc test was used to determine if there was a significant difference in the RFU recorded in the collection gate between the nil-bystander control prodrug metronidazole at 2 μM compared to all other prodrug conditions where * indicates a p value < 0.001, ** indicates a p value < 0.01 and * indicates a p value < 0.05. A small but significant difference was also detected between the only two prodrugs tested at 50 μM . (B). Repetitive example of GFP signal recorded while setting the collection gate under the 2 μM metronidazole treatment. The dark green portion of the histogram indicates the top 10% most fluorescent events recorded from that population. (C). Representative example of GFP signal recorded while setting the collection gate under the 50 μM SN27686 treatment. Dark green portion of the histogram indicates the top 10% most fluorescent events recorded from that population.**

4.3.4.2 *Exogenous protein expression inhibits growth of nfsA-expressing activators*

One serious concern was that the enrichment of our model library for nitroreductase-expressing cells was substantially less than that observed previously by Copp et al. (2014) who demonstrated the ability of the FACS screening platform to enrich a model nitroreductase library for a nitroreductase that can activate the prodrug CB1954. A key difference in experimental design between Copp et al. (2014) and this investigation was that all of the cells in the model library developed by Copp et al. (2014) expressed an exogenous nitroreductase gene. The YcnD enzyme, from *Bacillus subtilis*, was chosen as a positive control for its proven ability to activate CB1954 (Prosser et al., 2013). The enzyme YdjA, from *E. coli*, was chosen as a negative control as despite being published as a “minimal nitroreductase” (Choi et al., 2008), it possesses no apparent ability to activate CB1954. With a starting proportion of 1:10 *ycnD: ydjA* expressing cells, an enrichment of 9.2 fold of the *ycnD* expressing cells was achieved under a selection pressure of 100 μM CB1954 (Copp et al., 2014).

In contrast, the enrichment of *nfsA*-expressing cells never exceeded 5-fold for any prodrug treatment (1.8 fold enrichment for 10 μM CB1954, 1.1 fold for 10 μM PR-104A, 1.3 fold for 10 μM SN27686, 2.9 fold for 1 μM nitro-CBI-DEI, 2.9 fold for 50 μM CB1954, 2.7 fold for 40 μM PR-104A and 4.2 fold for 50 μM SN27686) (**Table 4.1**).

I hypothesized that this disparity in library enrichment between these two studies was due to the metabolic load of high-level expression of NfsA placing the activator cells at a growth disadvantage compared to the nitroreductase null recipients during the co-culture and prodrug challenge stages. This would result in the number of *nfsA*-expressing cells available for FACS collection to be far less than the intended 10% under the bystander condition, where the *nfsA*-expressing activators and nitroreductase null recipients are co-incubated, compared to the null-bystander condition where the strains are separately incubated. Under this hypothesis there would be relatively more *nfsA*-expressing activators available for collection in the null bystander condition, which may lead to an over-estimation of the influence of the bystander effect in FACS enrichment under any prodrug treatment.

To investigate whether the pUCX: *nfsA* cells were experiencing a substantial metabolic burden relative to the empty plasmid control cells I performed a competition growth assay

in LBASGI medium. The starting proportions were 50:50 SOS-R4 *nfsA*-expressing activators to SOS-R4 nitroreductase null recipients. The individual strain cultures were grown to an OD₆₀₀ of 0.8 prior to mixing and incubated **(2.12.2)**. At hourly intervals, samples were taken, diluted and plated on LBAS agar. After overnight incubation 60 colonies, per time point, were randomly selected and used to inoculate overnight microwell cultures for a niclosamide growth inhibition assay **(2.13.3)** for diagnosis of nitroreductase expression. Three biological replicates were performed for this experiment.

The proportion of *nfsA*-expressing cells diagnosed, per time point and treatment, was expressed as a percentage of the total number of cells screened with niclosamide **(Figure 4.9)**. I observed that over the four hour incubation period the proportion of activators to recipients varied from the starting 50:50 ratio. By two hours the proportion of *nfsA* expressing activator cells was significantly less than the number of nitroreductase null recipient cells with a *p value* < 0.01. This general trend was maintained at the three and four hour time points.

From this I inferred that the proportion of *nfsA*-expressing cells in the bystander condition was substantially less than the intended 10% at the point when the co-cultured sample was introduced to the FACS machine. In contrast, the proportion of *nfsA*-expressing cells in the null bystander condition would have remained at 10% at the time of FACS; as the sample was mixed from independently cultured activators and recipients immediately prior to FACS.

These data indicate that the differences in percentage recovery of activator cells relative to the previous study of Copp et al. (2014) were likely due in large part to the comparison of pUCX: *nfsA* activator cells *versus* a pUCX empty recipient control, with the latter strain exhibiting a substantial growth advantage over the activator cells in liquid co-culture.

Nitroreductases are promiscuous enzymes that have the potential to interfere with core metabolic pathways of the *E. coli* host cells SOS-R4 (Copp et al., 2017). When these nitroreductases are over-expressed at high levels the *E. coli* host cells subsequently may experience metabolic interference and thus suffer greater growth inhibition relative to nitroreductase- null cells.

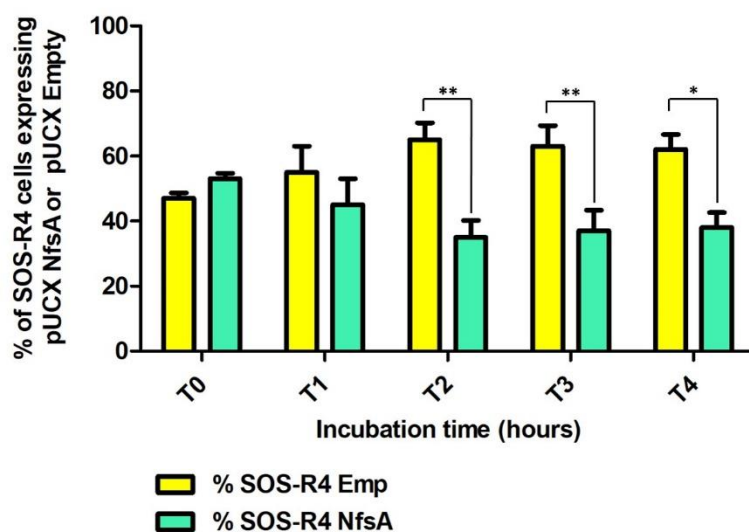


Figure 4.9 Average percentage of SOS-R4 cells expressing pUCX nfsA (activators) or pUCX Empty (recipients) in samples taken at hourly intervals from a co-culture. A 50:50 ratio of activator to recipient cells was grown in LBASGI medium as detailed for the no prodrug control and co-incubated for 4 hours at 30 °C, 200 rpm. Samples of 10 µL were taken at hourly intervals, diluted and a portion was plated on solid agar medium to give clearly distinct colonies. The niclosamide growth inhibition test for nitroreductase expression was used to determine the number of colonies expressing nfsA. The average percentage number of activator cells or recipient cells was calculated from a minimum of three biological replicates. A two-way ANOVA with Bonferroni post-tests was performed. A p value of ** indicates a p value < 0.01 and * indicates a p value < 0.05.

4.3.5 Results of diagnosing expression of *YfkO* in samples recovered from FACS

I also investigated the use of *yfkO*-expressing activators in our experimental design. In Chapter 3 we explored the use of *YfkO* as a CB1954 activating enzyme that exclusively reduces the 4-nitro substituent, yielding lower bystander metabolites than *NfsA* (which exclusively reduces the 2-nitro substituent). Using the same experimental design as before except that *yfkO*-expressing activators were used instead of *nfsA*-expressing activators (**section 2.13**). Three biological replicates were performed. The total number of cells recovered post-FACS correlated to what was observed in the *nfsA* based FACS experiments whereby only 100-120 cells in each 384 well plate recovered to visible density. I observed no significant difference in the yield of *yfkO*-expressing cells between the bystander and null bystander conditions in a two-way ANOVA with a *Bonferroni post hoc* test (**Figure 4.10 and Table 4.3**), thus the bystander effect did not impair selection by FACS of *yfkO*-expressing cells. This is consistent with what I observed in **Figure 3.10** whereby *YfkO* activation of CB1954 generated a bystander effect significantly smaller than

NfsA when only 10% of the cells in the bacterial population expressed a prodrug-activating enzyme.

Average percentage yield *yfkO*-expressing cells

	Bystander condition			Null bystander condition		
	YfkO activators	stdev	N	YfkO activators	stdev	N
No Prodrug	2	1	3	2	1	3
50 μ M CB1954	10	2	3	15	5	3

Table 4.3 Average percentage of recovered *yfkO*-expressing activator and recipient cells for bystander and null bystander conditions. The average percentage yield of activator cells and recipient cells was calculated from a minimum of three biological replicates for each prodrug and bystander effect condition.

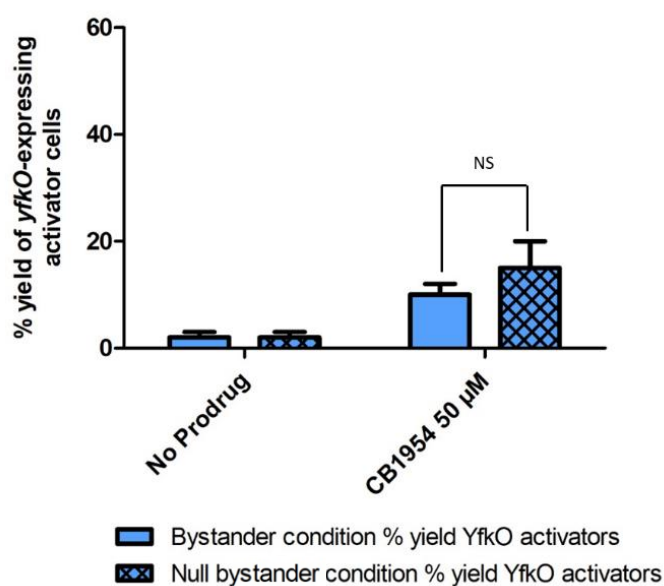


Figure 4.10 Average percentage yield of *yfkO* expressing cells, as diagnosed by niclosamide, recovered from FACS post challenge with 50 μ M CB1954. The average number of *yfkO* expressing cells for each biological replicate was normalized as a percentage out of the total number of cells recovered. The average percentage yield of activator cells was calculated from a minimum of three biological replicates for each prodrug and bystander condition. NS $p > 0.05$ in a two-way ANOVA with a Bonferroni post hoc test. We observed that at 50 μ M CB1954 the yield of *yfkO* expressing activator cells was not significantly less when the bystander effect was in play prior to FACS compared to the null bystander effect control.

4.4 Discussion

The research described in this chapter sought to determine the impact of the bystander effect on the efficiency of FACS for enriching a model nitroreductase variant. The Ackerley laboratory had, at the time of designing this investigation, waged several unsuccessful directed evolution campaigns using FACS as a screening method for selection of nitroreductase variants with advanced activation of next generation prodrugs. We hypothesised that prodrugs that exhibit high levels of bacterial cell-to-cell transfer post-activation confound FACS selection. I designed and performed an experiment, that measured the transfer of the activated prodrug metabolite from cells expressing a functional nitroreductase (activators) into cells contain non-functional nitroreductase variants (recipients). I observed that prodrugs possessing a high bacterial bystander effect induced an SOS response to such a high extent that the fluorescence profile of the recipients was raised above the lower threshold of the collection gate. This resulted in the collection of false positives that diminished library enrichment by FACS.

I observed that significantly fewer *nfsA*-expressing cells were recovered from FACS when using CB1954 and nitro-CBI-DEI when the bystander effect was given time to occur, as compared to a control in which the bystander effect was given no time to occur. This was consistent with the high bacterial bystander effects reported for these two prodrugs in Chapter 3. In contrast, the relative yield of *nfsA*-expressing cells was higher for the mustard prodrugs PR-104A and SN27686 at the preferred 10 μ M challenge concentrations established in Chapter 3, again consistent with the bystander effects reported in Chapter 3. A somewhat surprising result was that the mustard prodrug SN27686 yielded significantly fewer *nfsA*-expressing cells recovered from FACS when a 50 μ M challenge concentration was applied. This appears to have been an artefact of the higher stringency of gate selection during FACS with 50 μ M SN27686 compared to the other prodrug conditions tested.

A moderate view must be taken when assessing the data presented in Figure 4.4. The difference in yield between the bystander condition and the null bystander condition 50 μ M CB1954 and 1 μ M and CBI-DEI is statistically significant. However, not all of this statistical difference can be solely attributed to the influence of the bacterial bystander effect. I must consider that there is a confounding factor in my assay design. The activator

cells suffer growth inhibition relative to the recipients even without the presence of prodrug (**Figure 4.9**). This likely resulted in the number of activator cells in my starting library prior to FACS was less than 10% in the bystander effect conditions. In comparison the null-bystander effect condition does start at 10% activators due to separate incubation of the two cells strains. This difference in the number of activators prior to FACS artificially raises the difference in enrichment between the null-bystander and bystander conditions.

Although this work was able to compare the effects of different prodrugs on the proportion of *nfsA*-expressing cells recovered, a major limitation is that in absolute terms there was no strong enrichment of *nfsA*-expressing cells observed using any prodrug, contrasting with the previous observations of Copp et al. (2014) and Copp et al. (2017).

A major reason for this appears to have been our selection of an empty plasmid control for the null nitroreductase strain, rather than a strain expressing an inactive nitroreductase at high levels, as was utilised by Copp et al. (2014). Competition assays comparing our *nfsA*-expressing activator strain to the null nitroreductase strain revealed that the latter had a significant growth advantage in unamended LBASGI medium – and it must be considered that this growth advantage might have been even more profound under prodrug challenge conditions, where the *nfsA*-expressing strain would have also accrued higher levels of prodrug-mediated damage.

In future work to establish the absolute recovery rates for FACS enrichment under different prodrug challenge conditions, one would ideally choose a variant of *nfsA* that was verified as catalytically inert, but shown to impose an equivalent metabolic load to wild type *nfsA*. Nevertheless an important finding from this work was that cells bearing an empty plasmid exhibit a profound growth advantage relative to *nfsA*-expressing cells, to an extent that may confound directed evolution campaigns. It must therefore be considered that a poorly constructed directed evolution library that contains a high proportion of empty plasmid may prove very difficult to interrogate by FACS to recover the most active nitroreductase variants. This emphasises the importance of high-quality library construction for future nitroreductase evolution work in the Ackerley lab.

It should also be noted that in a genuine FACS procedure, for a directed evolution campaign, the collection gates are typically set based on the activation of the prodrug in question with the wild-type nitroreductase progenitor of the variant library. Hence we could not justify setting the collection gate parameters using only one prodrug in the present work. Based on our observations with the higher (50 μ M) challenge concentration of SN27686 it may be that a more stringent selection gate than top 10% will result in superior enrichment, and even perhaps eliminate any significant influence of the bystander effect on FACS. Accepting that any recipient cells, reporting DNA damage because of the bystander effect, are inherently less fluorescent than activator cells, then setting very strict collection gates may exclude the recipient cells altogether.

However, setting the collection gates too strictly may also result in poor recovery of cells post-FACS due to excessive DNA damage by prodrug activation. An additional complication is that it has been shown that GFP is inherently toxic to our *E. coli* SOS-R4 screening strain and that this also influences the recovery of cells post-FACS collection (Rich 2017). It should therefore be considered that cells that express the most effective nitroreductase variants may express such a high degree of GFP that they may not recover post FACS. A balance must be achieved between choosing high enough prodrug concentrations, which induce a stringent selection pressure to generate satisfactory library enrichment, versus low enough prodrug concentrations where the *E. coli* hosts, expressing most efficient nitroreductase variants, are not killed during the FACS process. It is this dichotomy of constraints that has ultimately led to the use of alternative screening strategies, in our laboratory, for the directed evolution of nitroreductases.

With hindsight, this investigation would ideally be re-performed using a model library where all the cells express a catalytically active *versus* a catalytically inactive nitroreductase variant in conjunction with a non-toxic DNA damage reporter protein. However this was prevented by the high cost of performing the FACS procedures under contract from the Malaghan Institute of Medical Research and the limited availability of the mustard prodrugs and nitro-CBI-DEI, as well as time constraints.

Although manual screening of nitroreductase variant libraries by individual prodrug challenge is very laborious - costly in both time and prodrug (Copp et al., 2014) – it may yet prove to be the best option for accurately screening variant libraries. FACS is a high-

throughput screen that has already demonstrated significant power for evolving therapeutic nitroreductase enzymes (Copp et al., 2017; Rich, 2017) but it is still fraught with issues. Optimizing screening strategies, for directed evolution of nitroreductases with prodrugs of greater bystander effect, is an investment towards accelerating development of nitroreductase powered GDEPT with the most potent nitroaromatic prodrugs. In the next chapter we investigate two different screening approaches for directed evolution of NfsA *E. coli* with the commercially available prodrug CB1954.

5 Chapter 5: Comparison of a manual positive pre-selection method to an automated FACS screening method for recovery of *E. coli* NfsA variants improved in CB1954 activation

5.1 Overview

Following the investigation into the influence of the bystander effect on FACS recovery of active nitroreductases, I set out to compare the evolutionary outcomes arising from a manual pre-selection method versus the automated FACS approach. I wanted to determine if one method was superior to the other in selecting for activity with a high-bystander prodrug, by assessing the level of enzymatic improvement versus the cost and time investment to achieve these outcomes.

For the pre-selection strategy I used the positive selection compounds niclosamide and chloramphenicol. As each of these nitroaromatic antibiotics can be detoxified by nitroreduction, this pre-selection strategy, on supplemented solid medium, eliminates inactive nitroreductase variants from a mutant library. By reducing the size of the variant library to only *E. coli* cells expressing a functional nitroreductase, far fewer variants need to undergo individual interrogation for activity with a specific substrate.

In this investigation I used a pre-existing (“7SM”) library, a site directed mutagenesis library derived from *E. coli nfsA* that was created by previous Ackerley lab postdoctoral fellows Dr Copp and Dr Williams. The prodrug CB1954 was selected for this study because it exhibited an unexpectedly high bacterial bystander effect following NfsA-mediated activation and therefore has potential use in BDEPT. Moreover, CB1954 has the advantages of being commercially available, and having previously undergone Phase I/II safety evaluation to establish achievable dosing levels in patients (Chung-Faye et al., 2001; Onion et al., 2009; Patel et al., 2009).

For the pre-selection strategy I used a glycerol stock of 7NT cells expressing the 7SM library and grew colonies in the presence of niclosamide or chloramphenicol. I then tested individual variants for activity with CB1954. In parallel, I performed a single FACS

procedure on SOS-R4 cells expressing the 7SM library that had been challenged with CB1954 and then collected variants were individually tested for activity with CB1954.

I recovered a similar number of clones from both the positive pre-selection and FACS strategies. I analysed the variants captured by these two different strategies for their abilities to sensitise their *E. coli* host cells to CB1954. Despite the strong bacterial bystander effect exhibited by NfsA-reduced CB1954, the FACS strategy yielded a higher proportion of clones exhibiting enhanced CB1954 sensitivity, including the most active variant overall.

We considered that there was potential for the FACS-selected NfsA variants to have switched their nitro-reducing specificity from the 2-NO₂ to the 4-NO₂ substituent of CB1954, and that FACS selection might have been biased toward selection of clones where the bystander effect was diminished. However, although HPLC profiles of the reduced metabolites produced from the top five variants recovered from each strategy showed that it was possible for a variant to gain the ability to convert a small portion of CB1954 to the 4-NO₂ metabolite, the major end-metabolite in every case was still the 2-hydroxylamine.

Overall the results of this investigation were inconclusive after just a single round of directed evolution, but there is some evidence that the FACS strategy was more effective than niclosamide/chloramphenicol pre-selection in enriching for superior CB1954-reducing variants.

5.1.1 Aims:

- Primary aim: To compare automated FACS-based screening with manual pre-selection methods for the recovery of enhanced CB1954-activating nitroreductases.
 - Compare the most active variants from each strategy.
- Secondary aim 1: To evolve NfsA variants that are more efficient at activating CB1954.
- Secondary aim 2: To identify whether any of the selected NfsA variants had gained the ability to reduce the 4-nitro substituent of CB1954.

- Determine if FACS preferentially selects NfsA variants that reduce one nitro substituent or the other.

5.2 Introduction

It has already been demonstrated that FACS can be used as a high throughput screening tool to successfully identify variants of *E. coli* NfsA that are more efficient at activating the mustard prodrug PR-104A (Copp et al., 2017). The work of Copp et al. (2014) and Copp et al. (2017) informed subsequent investigations with variant libraries of bacterial nitroreductases in the Ackerley laboratory. These libraries were expressed in SOS-R4 cells, thus the results of this directed evolution campaign may have suffered from the deleterious interference of GFP toxicity discussed in Chapter 4. Yet these directed evolution campaigns still bore valuable nitroreductase variants with advanced activity for next generation prodrugs.

FACS is an automated screen that can quickly assess and segregate thousands of variants in a short period of time. For example, in their preliminary validation work Copp et al. (2014) used an average sort rate of 4000 events per second to screen a model nitroreductase library. This is a major advantage over manually screening vast variant libraries. Even targeted mutagenesis libraries, which are far smaller than random mutagenesis libraries, typically contain millions of unique variants depending on the size of the target gene and the number of amino acid sites targeted for mutation. I considered it possible that any disadvantages stemming from impairments to FACS enrichment efficiency, whether by the bacterial bystander effect, growth inhibition by metabolic burden of exogenous protein expression, or GFP toxicity, may be outweighed by the relatively high-throughput nature of the FACS process.

In parallel to the advance of FACS, an alternative screening method for nitroreductase evolution has been developed in the Ackerley laboratory using positive pre-selection compounds (Little 2015, Rich 2017). This pre-selection method uses two different nitroaromatic antibiotics. The first is the nitroaromatic drug niclosamide, introduced in where it was used for its binary ability to diagnose the expression of an active nitroreductase **(4.3.1.3)**.

It has been demonstrated in the Ackerley laboratory that pre-selection of a nitroreductase site saturation mutagenesis library, on solid medium supplemented with 0.5 μM niclosamide, resulted in variants that were more active with the prodrug metronidazole than variants picked from solid media not supplemented with niclosamide (Little 2015, Rich 2017). This positive selection was attributed to the ability of a nitroreductase to reduce niclosamide to non-toxic state, such that all surviving cells were expressing functional nitroreductase variants.

Bearing in mind that a mutagenesis library contains both functional and non-functional variant, using a screening method that removes non-functional variants is highly advantageous. This radically reduces the number of variants to be individually interrogated for activity with a specific substrate of interest.

The second antibiotic is chloramphenicol (**Figure 5.1**), one of the rare naturally occurring nitro-compounds, which is made by different bacterial species including *Streptomyces venezuelae* (Fernández-Martínez et al., 2014). It was the first broad-spectrum antibiotic, introduced to the market in 1949, and is toxic to a range of both Gram-positive and Gram-negative bacteria (Feder et al., 1981). A more recent investigation demonstrated that a NfsB nitroreductase was able to reduce chloramphenicol to a non-toxic state and attributed one mechanism of chloramphenicol antibiotic resistance to bacterial nitroreductases (Crofts et al., 2019). Recent results from nitroreductase directed evolution campaigns undertaken in the Ackerley laboratory have shown that chloramphenicol can be used as positive selection tool in the same manner as niclosamide (Rich, 2017).

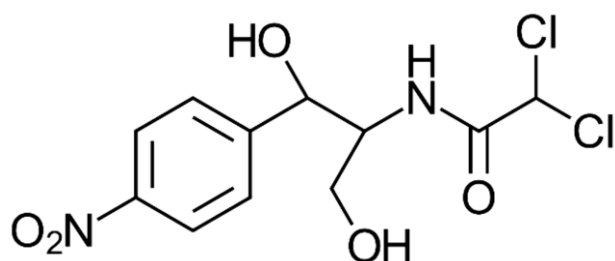


Figure 5.1 Chemical structure of the pre-selection compound chloramphenicol.

By pre-selecting variants from the 7SM library with either niclosamide or chloramphenicol I sought to reduce the bias of evolution towards activity with one of the pre-selection

compounds. We wanted to prevent a genetic bottleneck that might, for example, select for variants that are excellent at detoxifying niclosamide but are unable to reduce the target prodrug substrate. It is important to note that pre-selection does not guarantee that the variants captured in this manner will have advanced activity with a prodrug.

5.2.1 Choosing the prodrug CB1954 for this investigation

CB1954 was chosen as a prodrug for this study owing to the strong bacterial bystander effect that was demonstrated in Chapter 3, and the potential for that to impair FACS selection during directed evolution, as reported in Chapter 4. The key advantages of CB1954 over nitro-CBI-DEI (which exhibits a similarly strong bacterial bystander effect) are that it is commercially available and has been evaluated in Phase I/II clinical trials (Chung-Faye et al., 2001; Onion et al., 2009; Patel et al., 2009), whereas nitro-CBI-DEI is a bespoke ACSRC compound for which only very limited quantities were available, and did not proceed to human clinical trials owing to prohibitively high toxicity in late-stage preclinical models (*Prof. David Ackerley, personal communication*). We therefore reasoned that engineered NfsA variants exhibiting superior CB1954 activity would hold the greatest potential for application in future BDEPT trials. Moreover, the Ackerley laboratory has a long history of using CB1954 to optimize and standardize experimental procedures including methods for directed evolution using FACS (Copp et al., 2014).

5.2.2 NfsA *E. coli* site saturation mutagenesis library

The *E. coli* NfsA 7SM site saturation mutagenesis library was designed by Drs Copp and Williams, based on empirical observations that mutations at seven different amino acid positions had potential to improve activity with a variety of prodrug substrates; S41, F42, F83, K222, S224, R225, and F227 (*Dr Williams, personal communication*). The 7SM library was generated using NDT degenerate triplets (N: adenine/cytosine/guanine/thymine; D: adenine/guanine/thymine, T: thymine) at six of the target codons within the *nfsA* gene. Each NDT codon specifies 12 possible amino acids (Arg, Asn, Asp, Cys, Gly, His, Ile, Leu, Phe, Ser, Tyr, Val) that collectively provide a balanced representation of large and small, polar and nonpolar, aliphatic and aromatic, and negatively and positively charged side chains (Reetz et al., 2008), while also allowing for the inclusion of the wild-type amino acid at any of these sites. The seventh position was the codon encoding K222 in wild type *nfsA*; because lysine could not be coded for with NDT, the degenerate codon NNK (K:

guanine/thymine) was utilised instead, which allows for 32 codons and all 20 proteinogenic amino acids (Rich, 2017).

The 7SM library contains nearly 96 million possible codon combinations, and was previously ordered by Drs Copp and Williams as synthetic DNA cloned into the vector pUCX: empty by GenScript (Piscataway, New Jersey, USA), which guaranteed a total library size of 10 million unique variants. The lyophilised library was re-suspended in TE buffer and a portion was transformed into SOS-R4 cells or 7NT cells and plated on LB agar supplemented with the appropriate antibiotics to maintain the pUCX plasmid (and in the case of SOS-R4 cells the GFP-DNA-damage reporter plasmid). The agar plates were scraped and stored as glycerol stocks (Rich, 2017).

5.2.3 Key terminology

- FACS screening approach – automatically screens the nitroreductase library en masse for activity with the prodrug of interest
 - Individual variants that are recovered from FACS are then individually interrogated for advanced activity with the prodrug of interest.
- Niclosamide or chloramphenicol pre-selection of the nitroreductase library on solid media (LB agar) before individually interrogating variants for activity with the prodrug
 - Individual colonies that survive the pre-selection are individually interrogated for activity with the prodrug of interest
- 7SM library refers to a nitroreductase library created by site-saturation mutagenesis of NfsA *E. coli* at seven specific amino acid locations.
 - 7SM SOS-R4 library – variants expressed in an *E. coli* strain with GFP reporter plasmid so can be subjected to FACS.
 - 7SM 7NT library – variants expressed in an *E. coli* strain with no GFP reporter plasmid so cannot be subjected to FACS but can be subjected to niclosamide or chloramphenicol pre-selection.

5.3 Results

5.3.1 Results of FACS screening the 7SM library to recover superior CB1954-activating variants

5.3.1.1 Preparation of 7SM library for FACS with CB1954 selection pressure

A glycerol of the NfsA *E. coli* 7SM site saturation mutagenesis library in the SOS-R4 strain was used to inoculate an overnight culture. Additionally, an overnight of SOS-R4 NfsA *E. coli* was cultured for the purpose of setting the selection gates on a positive control. No other culture was necessary to establish the collection gates.

The experimental procedure for preparing the 7SM library for FACS is detailed in section 2.16.1. The following day, 30 μ L aliquots of each day culture were separately challenged with 30 μ L LBASGI medium supplemented with CB1954 (to give a final challenge concentration of 50 μ M) or incubated with 30 μ L of control (no prodrug) medium in a 384 well microtitre plate.

At least eight technical replicates were performed and incubated for 3.5 hours. The microtitre samples were then pooled for each condition and analysed using a FACS (BD INFLUX (BD Biosciences-CA) using a 70 μ m nozzle with a 200 mW laser line of 488 nm wavelength and filter band pass of (520/35). The positive control of SOS-R4 NfsA *E. coli* challenged with CB1954 was used to set the collection gates to the top 10% most fluorescent based on the GFP signal.

5.3.1.2 FACS of 7SM library under CB1954 selection pressure collected in 384 microtitre plates

Individual samples of the 7SM library challenged with CB1954 were sorted and collected into twelve separate 384 well microtitre plates containing LBASG medium. A further three 384 well microtitre plates were collected from the control sample of the 7SM library incubated with unamended (no prodrug) medium prior to FACS. Post-sorting, the plates were recovered for 48 hours.

The fifteen microtitre plates were examined to identify wells with visible culture density. From those cultures that had recovered to a visible level of turbidity, 94 samples from each plate were randomly chosen for storage in glycerol at -80 °C. Typically only 25% of the cells recovered post-FACS per 384 well plate (**2.14.3-2.14.5**).

5.3.1.3 FACS of 7SM library under CB1954 selection pressure collected into microcentrifuge tubes

Collecting cells from FACS into microcentrifuge tube is an alternative strategy for recovering cells post FACS that has been used previously in the Ackerley Laboratory (Copp et al., 2014). Collecting individual cells into microtitre plates using FACS is extremely time consuming compared to mass collecting cells into micro-centrifuge tubes. Additionally, it is theorized that collecting individual cells into individual microtitre wells may also be more stressful and contribute to poor recovery of cells post FACS. For these reasons I chose to collect a larger number of pooled cells into three microcentrifuge tubes containing LBASG recovery medium in addition to the 15 microtitre plates that were described above.

Section **2.14.4** details the making and storing primary screening plates from cells collected into microcentrifuge tubes. The final concentration of cells per tube was approximately 1×10^5 cells per tube. The tubes were recovered for 48 hours. Post recovery the cultures were stored in glycerol at -80°C until the next stage of screening where individual variants were interrogated for activity with CB1954. A portion of the recovered culture was plated onto LBASGI agar medium and incubated overnight. Resulting colonies were picked into twelve 96 well microtitre plates for storage and subsequent analysis.

5.3.1.4 Screening cells collected from FACS for activity with CB1954

In total there were twenty-seven primary screening plates (96 well plate format) generated from the FACS screening strategy and stored as glycerol plates. Twelve were derived from a culture of the 7SM library that was challenged with CB1954 medium and three were derived from challenge with unamended (no prodrug) medium collected directly into 384 well microtitre plates during FACS. A further twelve 96 well plates were derived from the same culture of the 7SM library challenged with CB1954 but that were instead collected into microcentrifuge tubes during FACS. This is summarized in **Table 5.1**.

The wells from the 27 primary screening plates were used to inoculate 150 μL of LBASG growth medium in individual overnight cultures in a 96-well plate format. The following day 30 μL of each day culture was used to inoculate 30 μL of either LBASGI growth medium (no prodrug) or LBASGI supplemented with CB1954 for a final prodrug challenge

concentration of 50 μ M CB1954. Duplicates were performed for both the no prodrug and prodrug challenge cultures **(2.14.5.1)**.

These data sets collected were used to calculate the fold-increase in SOS response (GFP induction) generated by CB1954 challenge relative to an unchallenged duplicate plate, while ensuring that the growth inhibition of any individual CB1954-challenged culture did not exceed 20% (as noted in Chapter 3 the cell death associated with >20% culture growth inhibition has potential to result in artefactually lowered SOS calculations).

The SOS-GFP response was calculated as the fold increase in GFP induction in the prodrug challenge culture over the no-prodrug culture. Growth inhibition was calculated as the percentage growth the prodrug challenge culture experiences compared to the no prodrug culture.

	FACS Collection method	Media incubated with 7SM prior to FACS
Plate 1	384 well plate	CB1954 50 μ M
Plate 2	384 well plate	CB1954 50 μ M
Plate 3	384 well plate	CB1954 50 μ M
Plate 4	384 well plate	CB1954 50 μ M
Plate 5	384 well plate	CB1954 50 μ M
Plate 6	384 well plate	CB1954 50 μ M
Plate 7	384 well plate	CB1954 50 μ M
Plate 8	384 well plate	CB1954 50 μ M
Plate 9	384 well plate	CB1954 50 μ M
Plate 10	384 well plate	CB1954 50 μ M
Plate 11	384 well plate	CB1954 50 μ M
Plate 12	384 well plate	CB1954 50 μ M
Plate 13	384 well plate	LBASGI medium only
Plate 14	384 well plate	LBASGI medium only
Plate 15	384 well plate	LBASGI medium only
Plate 16	microcentrifuge tube	CB1954 50 μ M
Plate 17	microcentrifuge tube	CB1954 50 μ M
Plate 18	microcentrifuge tube	CB1954 50 μ M
Plate 19	microcentrifuge tube	CB1954 50 μ M
Plate 20	microcentrifuge tube	CB1954 50 μ M
Plate 21	microcentrifuge tube	CB1954 50 μ M
Plate 22	microcentrifuge tube	CB1954 50 μ M
Plate 23	microcentrifuge tube	CB1954 50 μ M
Plate 24	microcentrifuge tube	CB1954 50 μ M
Plate 25	microcentrifuge tube	CB1954 50 μ M
Plate 26	microcentrifuge tube	CB1954 50 μ M
Plate 27	microcentrifuge tube	CB1954 50 μ M

Table 5.1 Summary of primary screening plates prepared from the FACS screening strategy. Plates 1-15 were 384 microtitre plates into which bacteria were collected from FACS and recovered for 48 hours. The cultures that had grown to visible density were then picked into 96 well microtitre plates for further analysis. Plates 16-27 are derived from variants that were captured from FACS into microcentrifuge tubes, recovered for 48 hours, subsequently a portion of the culture was grown on agar plates. Colonies were picked into 96 well microtitre plates for further analysis.

5.3.2 Selection pressure: evaluating the effects of CB1954 challenge on variants during FACS

During FACS, twelve plates derived from CB1954 challenged cells and three derived from unchallenged cells were collected, recovered and stored. An initial evaluation of the effectiveness of the FACS procedure was performed using the SOS-GFP assay on a small

selection of variants captured by FACS. The aim was to confirm that the FACS procedure had successfully enriched for variants exhibiting higher levels of activity with CB1954. If this had not been the case then further optimization of the FACS procedure, such as making the collection gates more stringent, would have been considered.

To assess this, I compared the SOS activities (*i.e.*, GFP fluorescence post challenge with 50 μ M of CB1954 in 96-well plates) of 94 challenged variants with those of 94 variants from the unchallenged control. These were primary screening plates 1 and plate 13 derived from cells collected directly into 384 well microtitre plates. **Figure 5.2** illustrates the mean population increase in GFP signal from the CB1954-challenged variants (**Figure 5.2 orange circles**) *versus* the unamended medium (no prodrug) control (**Figure 5.2 blue squares**). Under a two-tailed t-test the *p-value* was 0.0001, indicating a significant difference between the fluorescence of the variants collected from the no prodrug versus the 50 μ M CB1954 condition. Overall, this suggested that the conditions used in the FACS resulted in positive enrichment for nitroreductases having improved activity with CB1954.

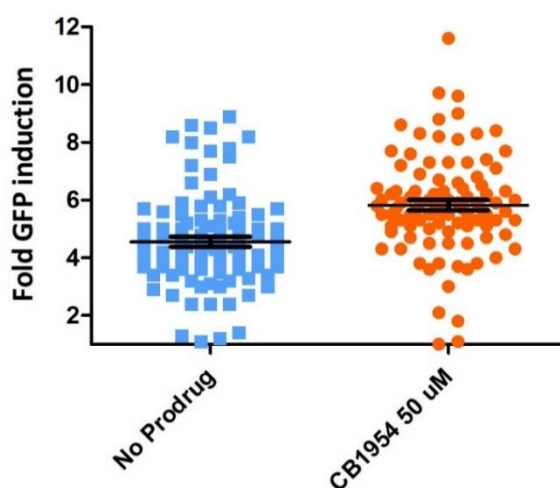


Figure 5.2 Fold-GFP induction of *E. coli* expressing 7SM variants post FACS selection. The effect of CB1954 challenge prior to FACS relative to the unchallenged control was evaluated by growing 94 cultures from each condition and examining the fold-increased in GFP induced in each population by 50 μ M CB1954 challenge. The light blue squares indicate variants collected under no prodrug selection pressure. The orange circles indicate variants collected under 50 μ M CB1954 selection pressure. A two-tailed t-test (Mann-Whitney test) was performed comparing the two conditions ($p < 0.001$).

5.3.3 Identifying the top twenty nitroreductase variants from the FACS strategy

From the 27 primary screening plates the top performing variants with CB1954 were chosen for further examination in 'Hit Plates' to undergo a secondary screening round. The top performing variants were identified from each of the primary screening plates based on either GFP induction (section 2.13.1) or growth inhibition (section 2.13.2) and used to create nine 96 well microtitre Hit Plates for further investigation. The method for generating hit plates for storage and analysis is described in 2.16.3.3.

All the primary screening plates were screened for growth inhibition and SOS-GRP response at 50 μ M CB1954. From here 10-15 variants were selected from each of the primary screening plates to contribute a hit plate. These top performing variants were chosen based on GFP inductions and growth inhibition values relative to each other within a primary screening plate rather than for improvement relative the progenitor enzyme NfsA *E. coli*. Variants for the first four hit plates were selected from the primary screening plates 1-15 (those collected as individual cells from FACS). Hit Plates 1 and 2 were selected based on GFP induction, while variants for Hit Plates 3 and 4 were based on growth inhibition. A further five hit plates were selected from the primary screening plates 16-27 (derived from variants collected into microcentrifuge tubes during FACS). Variants for Hit Plates 5-7 were selected based on GFP induction while Hit Plates 8-9 were chosen based on growth inhibition.

Twenty top variants were identified from these two collections using a combination of GFP plate assays and growth inhibition assays. The twenty top variants were minipreped and the plasmids used to transform 7NT cells.

5.3.3.1 Characterisation of the top twenty nitroreductase variants from the FACS strategy

Following transformation of 7NT cells, the strains expressing the top twenty nitroreductase variants were then subjected to IC₅₀ assays with a maximum concentration of 1000 μ M CB1954 (2.11.3).

I identified seven variants that outperformed the parental NfsA. The top performing variant 3-2C was significantly (1.7 fold) more active with CB1954 than NfsA *E. coli* (Table 5.2)

5.3.3.1.1 IC_{50} analysis of the top twenty variants isolated by the FACS strategy

Variant	Average IC_{50} CB1954 μ M			Fold improve ment	T-test vs. NfsA	Lineage
3-2C	148	± 10		1.7	≤ 0.05*	384 well plate
2-2C	172	± 43		1.4	≤ 0.05*	384 well plate
3-2Fi	184	± 57		1.3	0.20	384 well plate
2-7C	203	± 25		1.2	0.10	384 well plate
3-2F	228	± 64		1.1	0.50	384 well plate
2-10C	235	± 72		1.0	0.50	384 well plate
3-10G	237	± 38		1.0	0.35	384 well plate
NfsA_Ec	247	± 32				
8-2E	252	± 79				microcentrifuge tube
3-11C	284	± 120				384 well plate
8-2C	304	± 99				microcentrifuge tube
9-2E	313	± 44				microcentrifuge tube
7-11D	334	± 128				microcentrifuge tube
9-2Ei	369	± 43				microcentrifuge tube
2-11B	432	± 153				384 well plate
9-2B	452	± 16				microcentrifuge tube
3-8E	470	± 28				384 well plate
9-2G	484	± 69				microcentrifuge tube
8-3F	639	± 80				microcentrifuge tube
3-5C	729	± 140				384 well plate
9-5G	>1000	±				microcentrifuge tube
pUCX Empty	>1000	±				

Table 5.2 Top twenty nitroreductase variants, isolated by the FACS strategy.

IC_{50} assays were performed with a maximum concentration of 1000 μ M CB1954. The average IC_{50} value was calculated from three biological replicates. The variants are ordered in the table from the variant with the lowest IC_{50} value to the highest. A one-tailed t-test (Mann-Whitney test) was performed against NfsA for the top seven performing variants. * indicates a significant difference between the average IC_{50} value of a variant and NfsA_Ec wherein the p-value less than 0.05. The lineage column indicates what type of collection method that the variant was derived from using FACS. 384 well plate indicates that variant was collected directly from FACS. Microcentrifuge tube indicates the variant was derived from the culture collected into a microcentrifuge tube from FACS and subsequently individually picked from an agar plate.

5.3.3.1.2 Sequence analysis of the top twenty variants isolated by the FACS strategy

Amino acid substitution position in NfsA <i>E. coli</i> gene							
Variant ID	S41	F42	F83	K222	S224	R225	F227
Improved variants relative to NfsA_Ec							
3-2C	R			Y	D	H	S
2-2C	N	L		C	Y		S
3-2F	V		L	V	N	L	G
2-7C	N	L	L	G	V	S	D
2-10C	H		R	N	D	N	H
3-10G	N		Y	A	H	V	I
Not improved variants relative to NfsA_Ec							
8-2E	N	Y	L	N		H	G
3-11C	N	L		T		D	R
8-2C	R			F	L	L	C
9-2E	N	Y		S	H	S	L
7-11D	H		V	T		N	H
2-11B	C	L		V	C	H	S
9-2B	L	L		D	V	L	N
3-8E	I			M	R	C	L
9-2G	R			D	G	F	H
8-3F	R	L		A	D	D	R
3-5C	H	Y		V	V	G	C
9-5G	Y		L	L	R	N	H

Amino acid	Letter code	Description	Amino acid	Letter code	Description
Glycine	G	Small	Phenylalanine	F	Aromatic
Alanine	A		Tyrosine	Y	
Serine	S	Nucleophilic	Tryptophan	W	
Threonine	T		Aspartic acid	D	Acidic
Cysteine	C		Glutamic acid	E	
Valine	V	Hydrophobic	Asparagine	N	Amide
Leucine	L		Glutamine	Q	
Isoleucine	I		Histidine	H	Basic
Methionine	M		Lysine	K	
Proline	P		Arginine	R	

Table 5.3 Sequence analysis of the top twenty NfsA variants from the FACS at the seven targeted amino acid sites. Colour coding of the different amino acid side chains is explained in the key below. White spaces indicate the wild type residue was retained at that position. Mutations did not occur at any other sites in the protein sequence.

The top twenty variants did not contain any mutations outside of the seven amino acid sites targeted for mutagenesis (**Table 5.3**). At residue position 41 there was a noticeable trend for an amide (asparagine) or basic (arginine, histidine) amino acid substitution of

the nucleophilic serine. At positions 42 and 83 there was a clear preference to retain the wild type residue, however semi-conservative leucine (and at position 83, tyrosine) substitutions were also common. In contrast, at the four positions at the C-terminal end of the amino acid sequence there was no clear preference for specific residues, however there were a number of substitutions to small (yellow) or acidic (orange) amino acids which are considerably different in structure from the native amino acids at positions K222, R225 and F227 in particular.

Among the top performing variants there was no consistent pattern in the amino acid substitutions that may have contributed to their more advanced activity with CB1954 over NfsA *E. coli*.

Design of the 7SM library was informed in large part by the previous work of Copp et al. (2017), who used SOS-GFP FACS screening to evolve variants of *E. coli* NfsA that were more active with PR-104A. As PR-104A shares a core dinitrobenzamide structure with CB1954, we considered that there might be value in comparing the trends in observed amino acid substitutions. Copp et al. (2017) found that the single residue variants S41Y, R225A, R225G, R225P and F227S all contributed to greater activity with PR-104A in an IC₅₀ assay compared to the wild-type NfsA *E. coli*. Based on a speculative assessment of a solved NfsA crystal structure (PDB 1F5V), Copp et al., 2017 proposed that their S41Y substitution might enable planar stabilization and substrate stacking between the flavin mononucleotide (FMN) isoalloxazine and tyrosine rings, whereas the substitutions F227S and R225A/G/P were predicted to enlarge the active site pocket.

These comparisons suggest that variants of NfsA selected by FACS for activity with CB1954 may have benefited from enlarging the active site through mutation at R225 and F227. In contrast, the tyrosine stabilization at position 41 may be less of an influencing factor for CB1954 than was the case for PR-104A.

5.3.4 Results of the niclosamide and chloramphenicol pre-selection of the 7SM library for variants exhibiting superior activation of CB1954

It has been previously observed in our laboratory that expression of GFP is deleterious to growth of prodrug-activating *E. coli* cells and it has been proposed that this may lead to diminished survival of the most promising variants in our SOS-R4 screening strain (Rich

2017). To investigate the niclosamide or chloramphenicol pre-selection strategy we therefore chose to express the *NfsA* *E. coli* 7SM site saturation mutagenesis library in the 7NT strain. The 7NT cell strain is isogenic with SOS-R4, but does not contain a GFP plasmid to report on DNA damage so it cannot be used in FACS.

Aliquots of the 7SM library in 7NT cells were diluted in growth medium, plated on solid media (LB agar) supplemented with either niclosamide or chloramphenicol, and incubated overnight. I empirically determined that agar supplemented with concentrations of 10 μ M and 20 μ M niclosamide or 1, 2 and 2.5 μ g/mL chloramphenicol allowed selective screening. The optimal conditions were 10 μ M niclosamide or 2 μ g/mL chloramphenicol. At these concentrations the nitroreductase null 7NT cells were unable to grow, whereas nitroreductase expressing 7NT cells expressing were able to form more colonies relative to the other concentrations tested. At 1 μ g/mL chloramphenicol some nitroreductase null 7NT cells colonies were able to grow but at >2 μ g/mL chloramphenicol none were able to.

The following day, I handpicked colonies into 96 well plates that contained LBASG growth medium and grew them overnight. Two wells per plate were allocated as controls for 7NT pUCX *nfsA* or 7NT pUCX Empty. A total of 21 plates were picked from colonies grown on either niclosamide or chloramphenicol supplemented agar plates (primary screening plates 1-21). A further three 96 well plates (screening plates 22-24) were inoculated with colonies from solid medium that had not been supplemented with any pre-selection agent as a control to monitor the selective power for CB1954 activity of the individual pre-selection compounds. These conditions and the primary screening plates derived from them are summarized in **Table 5.4**.

The following day the overnight cultures were used to inoculate day cultures. The remaining portion of the overnight culture was stored in 40% glycerol at -80 °C.

Pre-selection primary screening plate summary

	Agar media supplement	
Plate 1	Niclosamide	10, 20 μ M
Plate 2	Niclosamide	10, 20 μ M
Plate 3	Niclosamide	10, 20 μ M
Plate 4	Niclosamide	10, 20 μ M
Plate 5	Chloramphenicol	1, 2 μ g/ mL
Plate 6	Chloramphenicol	1, 2 μ g/ mL
Plate 7	Niclosamide	10, 20 μ M
Plate 8	Niclosamide	10 μ M
Plate 9	Niclosamide	10 μ M
Plate 10	Niclosamide	10 μ M
Plate 11	Niclosamide	10 μ M
Plate 12	Niclosamide	10 μ M
Plate 13	Chloramphenicol	2 μ g/ mL
Plate 14	Chloramphenicol	2 μ g/ mL
Plate 15	Chloramphenicol	2 μ g/ mL
Plate 16	Chloramphenicol	2 μ g/ mL
Plate 17	Chloramphenicol	2 μ g/ mL
Plate 18	Niclosamide	10 μ M
Plate 19	Niclosamide	10 μ M
Plate 20	Niclosamide	10 μ M
Plate 21	Chloramphenicol	1, 2.5 μ g/ mL
Plate 22	LBAGI medium only	
Plate 23	LBAGI medium only	
Plate 24	LBAGI medium only	
Plate 25	LBAGI medium only	

Table 5.4 Summary of primary screening plates derived from pre-selection strategy. A portion of the 7SM library in 7NT cells was plated on agar supplemented with either niclosamide or chloramphenicol. Colonies were picked into 96 well microtitre plates for further analysis. Plates 1-21 were derived either LBAGI agar media supplemented with either 10-20 μ M of niclosamide or 1-2.5 μ g/ mL of chloramphenicol. Plates 22-25 were derived from colonies grown on LBAGI agar medium only.

Note that plates 1-7 and 21 in **Table 5.4** were picked from multiple agar plates because fewer than 94 colonies were available from a single agar plate supplemented with a single pre-selection agent concentration. For example, plate 21 was created by picking colonies from two different chloramphenicol supplemented agar plates; 1 or 2.5 μ g/ mL chloramphenicol.

The primary screening plates were subsequently subjected to a growth inhibition assay of 50 μ M CB1954 in 384 well plates (**2.11.3**). The twenty variants from the niclosamide and

chloramphenicol pre-selected plates that exhibited the most sensitivity to CB1954 were chosen as lead enzyme candidates.

The effect of pre-selection with niclosamide or chloramphenicol was evaluated by comparing the growth inhibition values at 50 μ M CB1954 of 120 variants randomly selected from plates 1-2 (derived from niclosamide 10, 20 μ M pre-selection) and plates 5-6 (derived from chloramphenicol 1,2 μ g/ mL pre-selection) (**Table 5.4**). A two-tailed t-test (Mann-Whitney test) was performed comparing the two conditions. The p-value for niclosamide was 0.0002, indicating a significant difference between the growth inhibition of the variants collected under no selection pressure (**Figure 5.3 blue squares**) and those under niclosamide selection pressure (**Figure 5.3 yellow circles**). In contrast, the p-value for variants collected under chloramphenicol pre-selection (**Figure 5.3 orange triangles**) was not significant ($p = 0.28$).

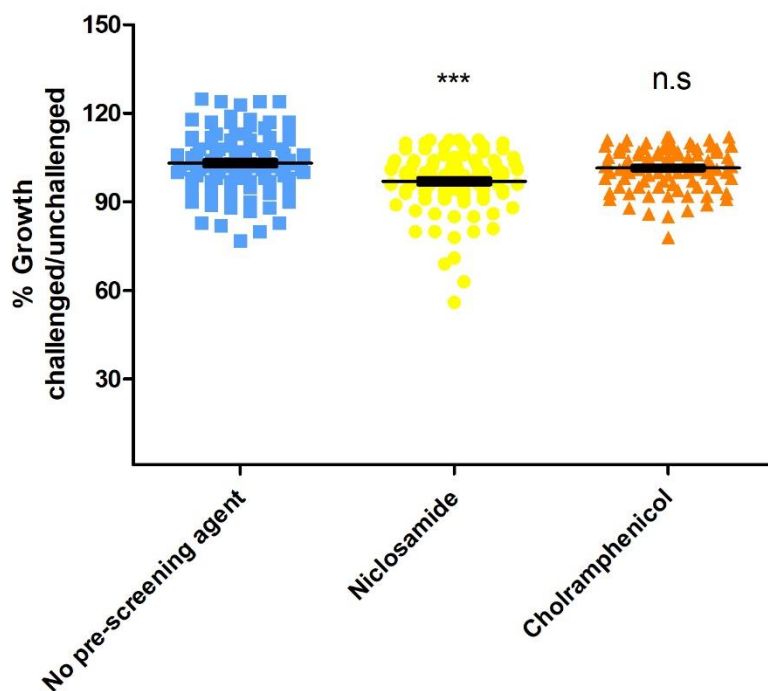


Figure 5.3 Comparison of growth inhibition by 50 μ M CB1954 in 7SM variants derived from the pre-selection on solid medium under no selection pressure or positive selection pressure. The light blue squares indicate variants randomly picked from solid agar medium containing no selection pressure. The yellow circles indicate variants randomly picked from solid agar media containing niclosamide selection pressure at 10-20 μ M. The orange triangles indicate variants randomly picked from solid agar medium containing chloramphenicol selection pressure at 1-2 μ g/mL. Variants that experienced greater growth inhibition indicate advanced activity for CB1954 activation. A two-tailed t-test (Mann-Whitney test) was performed comparing the two conditions. The p-value for niclosamide compared to the control was 0.0002 indicating a significant difference between the growth inhibition of the variants collected from under no selection pressure and niclosamide selection pressure. The p-value for chloramphenicol pre-selected variants was not significant.

5.3.4.1 Analysing the top twenty nitroreductase variants from the niclosamide/chloramphenicol pre-selection strategy

The top twenty nitroreductase variants were then subjected to IC_{50} assays in 7NT cells with a maximum concentration of 1000 μ M CB1954. Three biological replicates were performed (**Table 5.5**).

The top performing variant 1-5C was 1.3 fold more active with CB1954 than NfsA *E. coli*. This was the only variant, identified by the pre-selection approach, which outperformed

its progenitor NfsA *E. coli* (**Table 5.5**), and this was significant with p value of 0.05 in a one-tailed T-test (Mann-Whitney). The IC_{50} of the cells expressing variant 1.9C was not significant ($p = 0.35$) in a one-tailed T-test (Mann-Whitney).

5.3.4.1.1 *IC₅₀ analysis of top twenty variants from pre-selection strategy*

Variant	Average IC ₅₀ CB1954 μM			Fold improvement	T-test compared to NfsA	Lineage	
1-5C	214	±	26	1.3	≤ 0.05*	Chloramphenicol	2 μg/ mL
1-9C	279	±	32	1.0	0.5	Chloramphenicol	2 μg/ mL
NfsA_Ec	286	±	11				
1-5B	340	±	60			Niclosamide	10 μM
1-9B	341	±	8			Niclosamide	10 μM
1-3C	517	±	83			Chloramphenicol	2 μg/ mL
1-7C	614	±	17			Chloramphenicol	2 μg/ mL
1-4D	649	±	39			Chloramphenicol	1-2.5 μg/ mL
1-6B	707	±	233			Niclosamide	10 μM
1-4C	723	±	64			Chloramphenicol	2 μg/ mL
1-11B	733	±	99			Chloramphenicol	2 μg/ mL
1-10C	761	±	48			Niclosamide	10 μM
1-6C	781	±	193			Chloramphenicol	2 μg/ mL
1-3B	785	±	206			Chloramphenicol	1-2 μg/ mL
1-2C	884	±	136			Chloramphenicol	2 μg/ mL
1-11C	917	±	78			Niclosamide	10 μM
1-8B	933	±	25			Niclosamide	10 μM
1-3D	955	±	26			Niclosamide	10 μM
1-8C	>1000	±				Chloramphenicol	2 μg/ mL
1-2B	>1000	±				Niclosamide	10-20 μM
1-7B	>1000	±				Niclosamide	10 μM
pUCX Empty	>1000	±					

Table 5.5 Top twenty nitroreductase variants, isolated by the pre-selection strategy.

*IC₅₀ assays were performed with a maximum concentration of 1000 μM CB1954. The average IC₅₀ value was calculated from three biological replicates. The variants are ordered in the table in ascending order from the variant with the lowest IC₅₀ value to the highest. A one-tailed t-test (Mann-Whitney test) was performed against NfsA for the top performing variant. * indicates a significant difference between the average IC₅₀ value of a variant and NfsA_Ec wherein the p-value less than or equal to 0.05. The lineage column indicates the origin of the variant i.e. the concentration of the pre-selection agent in the agar plate that the variant was picked from.*

5.3.4.1.2 Sequence analysis of top twenty variants from pre-selection strategy

Variant ID	S41	F42	F83	K222	S224	R225	F227
Improved variants relative to NfsA_Ec							
1-5C	H	Y		L	V	N	L
1-9C	N	L		R	H	C	S
1-5B	H		N	P	L	H	S
1-9B	N		N	G	F	H	H
1-3C	Y			T		N	N
Not Improved variants relative to NfsA_Ec							
1-7C	C			D	R	Y	R
1-4D	N	L		C	Y		S
1-6B	H	N	L	L	F	C	D
1-4C	F		L	S	D	F	H
1-11B	Y	Y		Q	V	V	D
1-10C	F	L	N	R	D	V	N
1-6C	H			M	D	D	C
1-3B	Y	L	L	D	H	H	H
1-2C	H		Y	N	L	N	I
1-11C	F	N		L	H	Y	D
1-8B	H	L	L	S	G	H	D
1-3D	R			Y	D	H	S
1-8C	H	L		C	L	L	S
1-2B	H	H		T		C	C
1-7B	Y	L	Y	S	C	L	H

Amino acid	Letter code	Description	Amino acid	Letter code	Description
Glycine	G	Small	Phenylalanine	F	Aromatic
Alanine	A		Tyrosine	Y	
Serine	S	Nucleophilic	Tryptophan	W	
Threonine	T		Aspartic acid	D	Acidic
Cysteine	C		Glutamic acid	E	
Valine	V	Hydrophobic	Asparagine	N	Amide
Leucine	L		Glutamine	Q	
Isoleucine	I		Histidine	H	Basic
Methionine	M		Lysine	K	
Proline	P		Arginine	R	

Table 5.6 Sequence analysis of the top twenty NfsA variants from the pre-selection strategy at the seven targeted amino acid sites. Colour coding of the different amino acid groups in the key. White spaces indicate the wild type residue was retained in that variant. Mutations did not occur at any other sites in the protein sequence.

While none of these top performing variants contained any mutations outside of the seven amino acid sites targeted for mutagenesis, there were some similarities to the variants selected by the FACS screening method (**Table 5.6, Figure 5.4**). At the residue 41 position we again observed a predominance of substitutions to amide (asparagine) or basic (arginine, histidine) amino acids. However, we also detected more substitutions to the aromatic amino acids phenylalanine or tyrosine at position 41 than were observed following the FACS screening. We also observed a similar trend towards retention of the wild type residue with occasional substitution by leucine or tyrosine at positions 42 and 83 (with several asparagine substitutions also observed at position 83). Any pattern at the remaining four positions was harder to discern.

Moreover, in the four top performing variants (1.5C, 1.9C, 1.9B and 1.3C) there was no consistent pattern in the amino acid substitutions. As per the FACS-selected variants, it is possible that there was a general trend toward enlargement of the active site (as previously postulated by Copp et al. (2017) when evolving NfsA for more efficient PR-104A activity). Given that only one of the variants recovered by the pre-selection strategy was significantly improved over wild type *E. coli* NfsA, we did not consider it meaningful to analyse specific sequence trends that might have resulted in improved CB1954 activation.

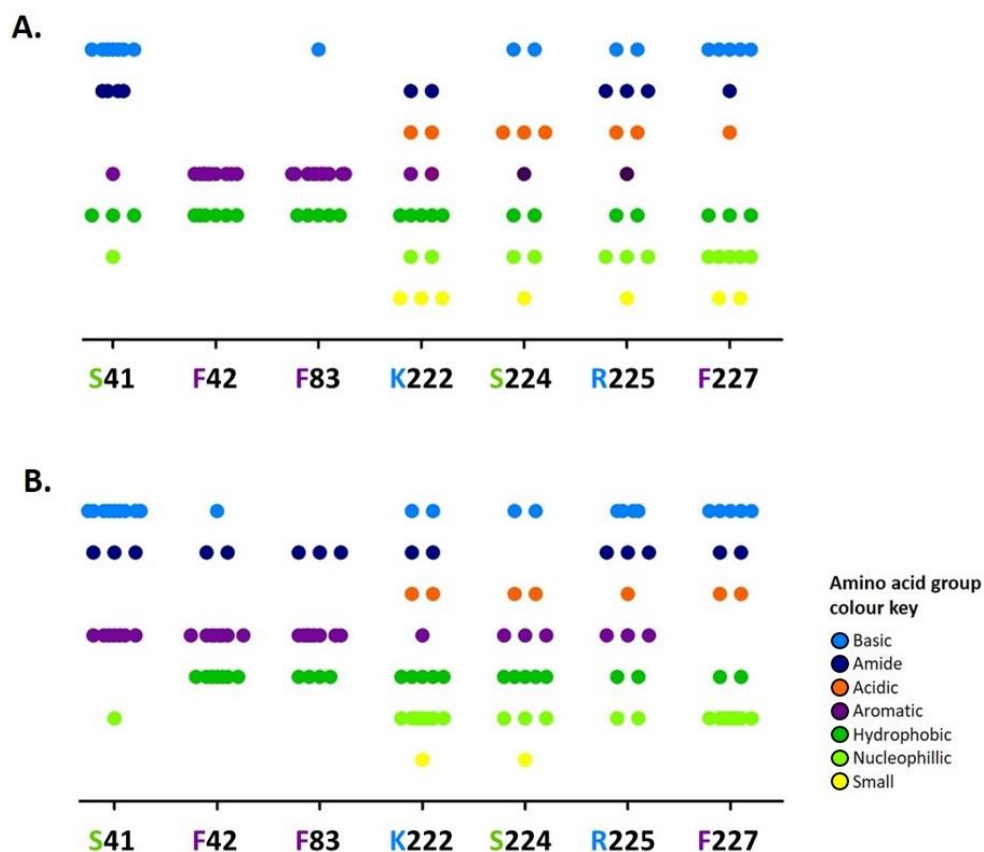


Figure 5.4 Frequency of different of amino acid categories occurring, based on general chemo-descriptive group, at the key seven active site residues in the top twenty variants derived from each screening strategy. The coloured letter on the x axis indicates the wild-type amino acid at that position and what category of amino acid it belonged to. The frequency of occurrence indicated by the dots also records if the original amino acid was retained at that position. **(A).** illustrates frequency of an amino acid category occurring at each of the seven target residues recovered from the FACS screening approach with 7SM under 50 μ M CB1954 selective screening pressure. **(B).** Illustrates frequency of an amino acid category occurring at each of the seven target residues recovered from the pre-selection strategy with niclosamide or chloramphenicol with 7SM under 50 μ M CB1954 selective screening pressure.

The complete set of amino acid substitutions in the top twenty variants recovered by: (A) the FACS screening approach; or (B) pre-selection strategy; is summarised in **(Figure 5.4)**. This figure does not reveal any obvious trends in amino acid substitutions beyond those already discussed in **5.3.3.1.2**.

In total, ~2540 variants were screened from the FACS selection strategy and ~2260 variants from the niclosamide/chloramphenicol pre-selection strategy (owing to a calculation error, three additional 96-well plates were collected and screened for the FACS-sorted cells versus the niclosamide or chloramphenicol pre-selected cells). It is

possible that a greater sample size from both strategies may have generated more discernible trends in the sequence data.

5.3.5 CB1954 enzyme kinetics with purified protein of the top five variants from each screening approach

The top three variants from the FACS screening strategy, 3.2C, 2.2C and 3.2F, and the top two variants from the pre-selection strategy, 1.5C and 1.9C, were ligated into pET28a+ and used to transform BL21(DE3) cells for His₆-tagged protein expression and nickel affinity protein purification (section 2.11) using a short expression culture (section 2.10.3) and enzymatic cell lysis (section 2.10.4). A His₆-tagged version of the wild-type *E. coli* NfsA enzyme was also purified. The concentrations of the final purified proteins were measured in triplicate (section 2.11.3). The presence of a pure nitroreductase protein band was confirmed visually by SDS-PAGE gel (section 2.9) (**Appendix B 1**). Proteins were stored in 40% glycerol at -20°C for up to three months (2.11.4).

I performed enzyme kinetic analysis of the protein variants with CB1954, within one month of purifying the proteins, using an Ocean Optics USB4000 UV-VIS spectrometer (Halma PLC) (methods in **2.10**). Buffered reactions containing CB1954, co-substrate (NAD(P)H) and purified enzyme were set up and monitored for CB1954 reduction by measuring the rate of change in absorbance of the reaction mixture at 420 nm wavelength. The apparent K_m and k_{cat} values were measured at 0.25 mM NAD(P)H. A minimum of three technical replicates were performed for each prodrug concentration analysed. The kinetic parameters were calculated using GraphPad Prism 7.0 (GraphPad Software Inc.; La Jolla, CA, USA) and are summarized in **Table 5.7**.

The rationale for presenting apparent K_m and k_{cat} values is described by Prosser (2011). Affinity (K_m) and catalytic (k_{cat}) constants for each of the enzymes with CB1954 were extrapolated from reaction rate data (triplicate reactions) obtained over a range of CB1954 concentrations. *E. coli* NfsA enzymes have previously been determined to catalyse substrate reduction via a bi-bi ping pong mechanism of action. As a result, the kinetic parameters measured are dependent on the concentration of the co-factor NAD(P)H that is used in the reaction. For this reason, the co-substrate concentration of NAD(P)H was kept constant at 0.25mM throughout these experiments.

The dependency on co-substrate concentration does not affect the ratio of k_{cat} : K_m . Therefore, the specificity constant (k_{cat}/K_m), that provides an accurate measure of relative enzyme activity towards prodrugs such as CB1954.

	K_m^a μM		k_{cat}^a s^{-1}		k_{cat}/K_m $\text{M}^{-1}\text{s}^{-1}$		$E_{[T]}^b$ μM
NfsA	60	± 12	8.2	± 0.33	140000	± 27000	0.4
3.2C	14	± 5.8	1.3	± 0.07	91000	± 38000	4.3
2.2C	30	± 18	2.2	± 0.23	73000	± 44000	1.8
3.2F	81	± 31	3.5	± 0.30	43000	± 3700	0.7
1.5C	20	± 9.2	1.0	± 0.03	50000	± 24000	2.1
1.9C	27	± 15	1.3	± 0.12	49000	± 29000	1.4

Table 5.7 Kinetic parameters with CB1954 of the top three variants from the FACS screening strategy (3.2C, 2.2C, 3.2F) and the top two variants from the niclosamide/chloramphenicol pre-selection strategy (1.5C, 1.9C). A minimum of three technical replicates were performed for each prodrug concentration analysed. a. Apparent K_m and k_{cat} values as measured at 0.25 mM NAD(P)H in triplicate reactions. b. total amount of enzyme available in the reaction. Standard errors calculated using GraphPad Prism 7.0 (GraphPad Software Inc.; La Jolla, CA, USA).

In terms of catalytic efficiency (k_{cat}/K_m), none of the evolved variants outperformed wild type *E. coli* NfsA. We have previously observed this phenomenon; where activities with a prodrug substrate in vitro, e.g. kinetic analysis with purified protein, are inconsistent with in vivo host sensitivity data, e.g. IC₅₀ assays performed in our bacterial screening strains, for both wild type (Prosser et al., 2013) and evolved (Copp et al., 2017; Sharrock, 2019) nitroreductases. In particular, evolved variants typically have both reduced k_{cat} and K_m relative to the parental enzyme, as was observed in **Table 5.7**. The Michaelis-Menten curves used to calculate the kinetic parameters of the purified proteins, of the top performing variants, with CB1954 are summarized in **Figure 5.5**.

We attribute this incongruity to a particular evolutionary direction; whereby the improved in vivo activation of CB1954 by variants is driven by heightened specificity for the prodrug over competing intracellular substrates rather than an increase in substrate turnover rate. These competing intracellular substrates include quinones. Top variants from other directed evolution campaigns with prodrugs from the Ackerley laboratory have been tested for activity with quinones. It has been demonstrated that, relative to parental NfsA,

these top performing variants have substantially heightened activity with the prodrug of interest over quinones (Copp et al., 2017; Sharrock, 2019).

Thus *in vitro*, in the presence of the competing metabolites, the top performing variants from this study such as 3.2C and 1.5C are more efficient at activating CB1954 compared to the wild-type *E. coli* NfsA. Yet, *in vitro* kinetic analysis with purified protein, the absence of the competing metabolites likely explains the diminished specificity constant observed in the top performing variants compared to *E. coli* NfsA.

The variant 3.2C presented the highest specificity constant among the variants tested, yet was still lower than that of *E. coli* NfsA. Of interest the V_{\max} value of 3.2C was the highest k_{cat}/K_m of the variants at $91000 \pm 38000 \text{ M}^{-1}\text{s}^{-1}$ which approaches that of *E. coli* NfsA at $140000 \pm 27000 \text{ M}^{-1}\text{s}^{-1}$ (**Figure 5.5**). Taken together, the kinetic parameters of 3.2C and the IC_{50} indicate that 3.2C may hold some promise for future directed evolution projects for improved NfsA nitroreductase activity with the prodrug CB1954.

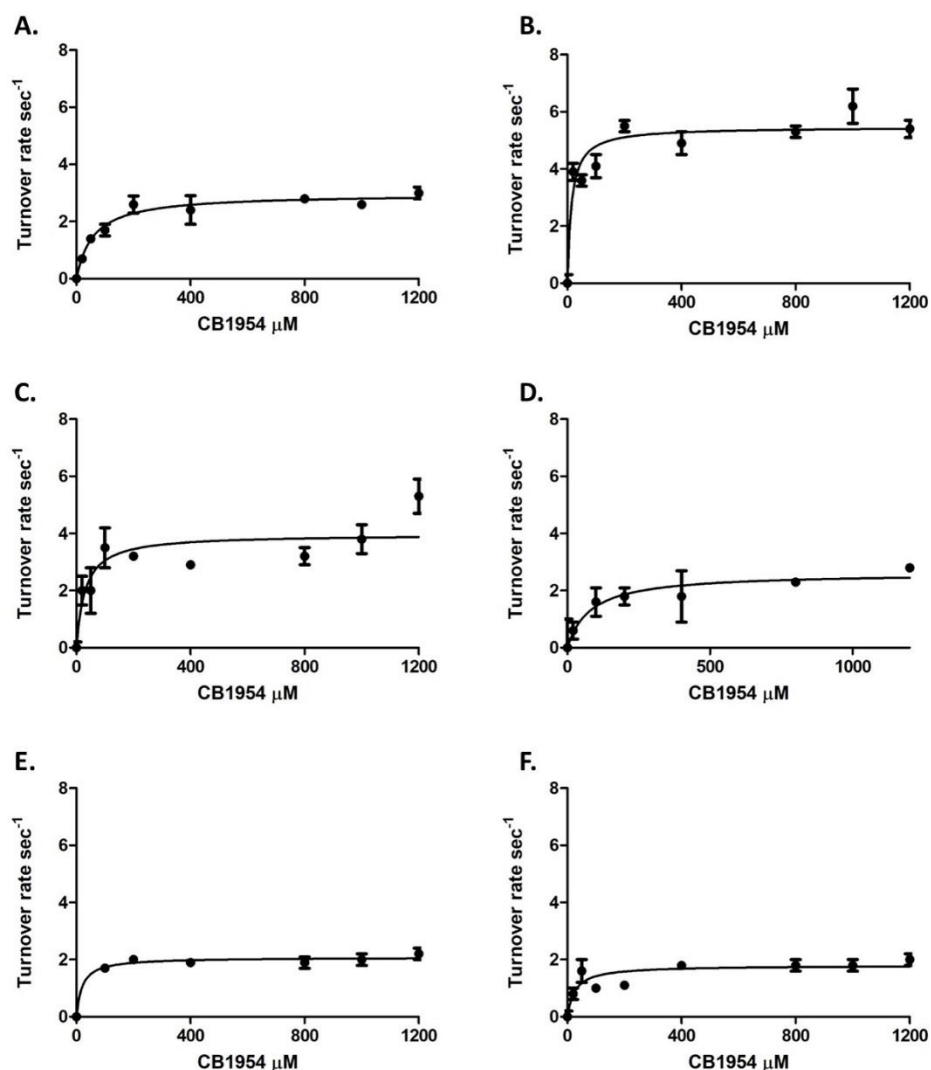


Figure 5.5 Michaelis-Menten curves used to calculate the kinetic parameters of the purified proteins, of the top performing variants, with CB1954. (A). *E. coli* NfsA; wild-type progenitor, (B). 3.2C, (C). 2.2C, (D). 3.2F; the top three variants from the FACS screening strategy, (E). 1.5C and (F). 1.9C; the top two variants from the pre-selections strategy. The kinetic parameters were recorded from three technical replicates and averaged for each CB1954 concentration.

5.3.6 HPLC analysis of the reduced metabolites from the top five variants

We considered that there was potential for the FACS-selected NfsA variants to have switched their nitro-reducing specificity from the 2-NO₂ to the 4-NO₂ substituent of CB1954. We theorized that FACS selection might have been biased toward selection of clones where the bystander effect was diminished - clones that produce the 4-NO₂ substituent.

Dr Michelle Rich, a previous Ackerley lab member, observed that in the process of performing IC₅₀ assays of different nitroreductase variants that some of the resulting

cultures were of lighter or darker colour after static incubation overnight at room temperature subsequent to the performing a CB1954 IC₅₀ assay. She proposed that this might be due to switching of specificity between 2-NO₂ and 4-NO₂ reduction. Based on this I showed that *B. subtilis YfkO* expressing cultures, when challenged with CB1954, turn a pale yellow colour post incubation, compared to *E. coli NfsA* expressing culture that turn a darker orange (**Figure 5.6A**). I therefore considered that it might be possible to visually detect a switch from exclusive 2-NO₂ reduction to partial or complete 4-NO₂ reduction, by incubating my top twenty variants from the FACS screening and pre-selection in the presence of CB1954 overnight, and observing culture colouration relative to cells expressing wild type *E. coli NfsA*.

Growth inhibition assays of the top twenty variants from the FACS screening (**Figure 5.6B**) and pre-selection strategy (**Figure 5.6C**) were performed at CB1954 500 µM and 1000 µM (methods **2.11.2**). In addition to the typical growth inhibition method, the cultures were then statically incubated at room temperature over-night for >16 hours to enable colour development.

By eye, it did not appear that any of the variants had switched specificity from 2-NO₂ reduction to predominantly 4-NO₂ reduction (**Figure 5.6**).

To further investigate, and for the sake of completeness, each of the top five variants that had already been purified for kinetic analysis was incubated with CB1954 and the reduction products analysed by HPLC, compared to *NfsA* and *YfkO* reduced metabolites (previously shown to be exclusively the 2-hydroxylamine and 4-hydroxylamine, respectively; (Prosser, Copp, et al., 2010) as standards.

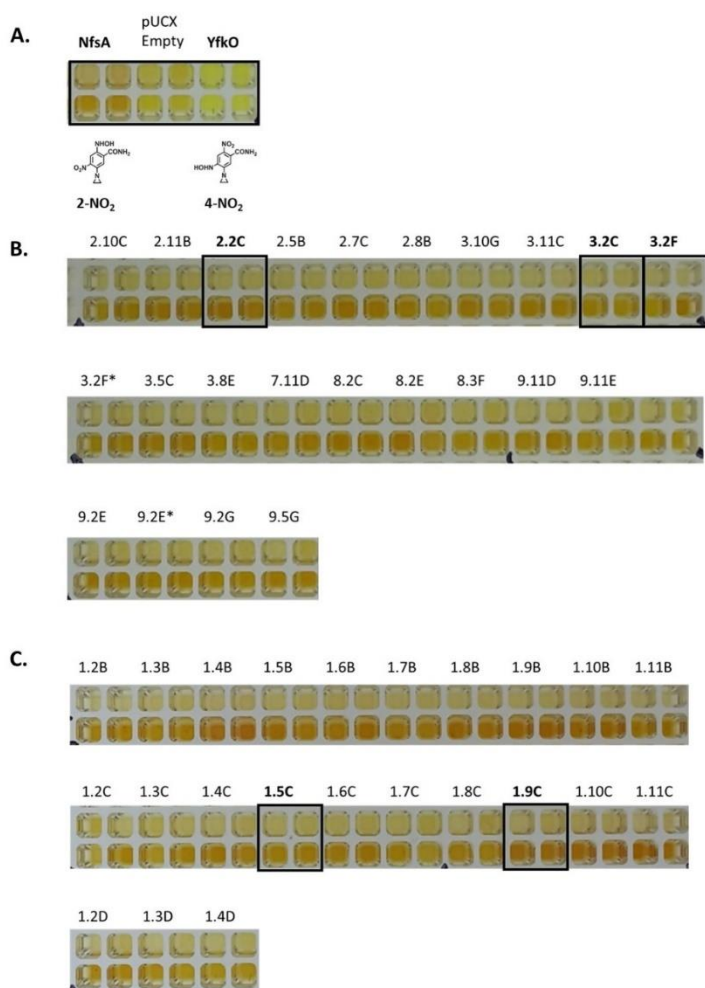


Figure 5.6 Illustrates the colour change that can be observed in the top twenty variants from each screening strategy when challenged with 500 μM of CB1954 (first row of each line) or 1000 μM of CB1954 (second row of each line) in duplicate (performed horizontally in adjacent wells). The variants were challenged in a growth inhibition assay and incubated for 3.5 hours at 30 °C after which the microtitre plate was left statically at room temperature overnight >16 hours. (A). Illustrates the NfsA positive control for production of the 2-NO₂ metabolite as a dark orange. (row 1 500 μM , row 2, 1000 μM technical duplicates columns 1 and 2) pUCX empty as a negative control for no reduction of CB1954 and YfkO was used as positive control for the production of the 4-NO₂ metabolite as a pale yellow. (B). illustrates the colouration of the top twenty variants derived from the FACS screening strategy. (C). illustrates the colouration of variants derived from the pre-selection strategy. Black squares outline the top variants from each strategy that were already had already been protein purified for kinetic analysis. These five protein purifications were used in the subsequent HPLC experiment.

Analysis of reduction metabolites by HPLC was performed as detailed in section 2.16. In brief, 100 μl reactions containing 200 μM CB1954, Tri-Cl buffer and NAD(P)H co-factor were initiated by addition of ~ 35 μM purified enzyme (the no nitroreductase control was performed with an equivalent volume of Tris-Cl buffer) and incubated at room

temperature until the reaction was stopped by addition of ice-cold methanol. Samples were transferred to $-80\text{ }^{\circ}\text{C}$ to precipitate proteins. The supernatant of the reaction was collected and diluted in formate buffer and analysed by reverse phase-HPLC employing an Agilent 1100 system with an AlltimaTM C8 5μ $150\times 2.1\text{mm}$ column (Fisher Scientific, Pittsburgh, PA). The eluate was monitored at 262 nm, and elution profiles were compared against standards of each potential metabolite produced by either NfsA or YfkO reduction of CB1954.

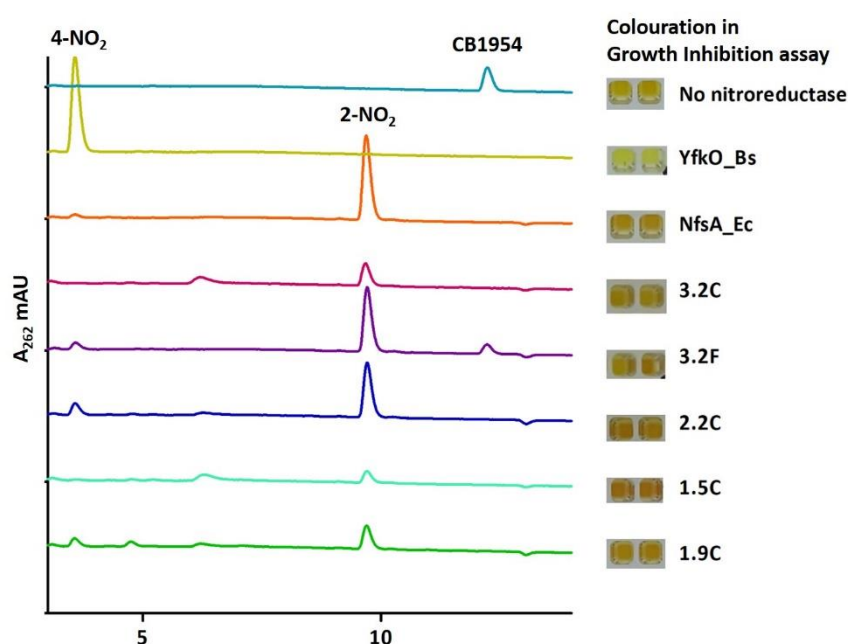


Figure 5.7 HPLC analysis of reaction products of CB1954 reduction by purified nitroreductase variants Reactions containing individual purified nitroreductase, $200\text{ }\mu\text{M}$ CB1954 and 1 mM NAD(P)H were incubated for 10–30 min at room temperature prior to chromatographic separation. Eluates were monitored at 262 nm. Peaks corresponding to the 2-NO₂ and 4-NO₂ metabolites and unreduced CB1954 are as indicated. The colouration in growth inhibition assay at $1000\text{ }\mu\text{M}$ CB1954 (Right). This key indicates the identity of each HPLC spectrum and also displays the colouration of the top variants and the wild-type enzyme standards from Figure 8.7. In vertical order the spectra are: no nitroreductase control (turquoise) unreduced CB1954, YfkO_Bs standard (yellow) for 2-NO₂ metabolite production. The NfsA standard (orange) for 4-NO₂ metabolite production, the top three variants from the FACS screening strategy 3.2C (pink), 2.2C (purple) and 3.2F (blue) and the top two variants from the pre-selection strategy 1.5C (light green) and 1.9C (green).

Figure 5.7 summarises the HPLC results. The no nitroreductase control demonstrated a clear peak of unreduced CB1954 after 10 minutes. In contrast the elution profile for YfkO, the standard used for 4-NO₂ production, demonstrated a clear

HPLC peak at 3-4 minutes representing 4-NO₂ production and no unreduced prodrug. Similarly, the NfsA_Ec elution profile, the standard used for 2-NO₂ production, demonstrated a clear peak at 9-10 minutes that represented 2-NO₂ production as expected (Prosser et al., 2013).

In comparison the elution profile of the 3.2C, the top performing variant derived from FACS, variant had a single peak of interest that indicated 2-NO₂ production. No 4-NO₂ peak was observed. The other two variants, from the FACS screening strategy, 2.2C and 3.2F produced peaks indicating 2-NO₂ production as well as very minor amount 4-NO₂. Variant 3.F also displayed a small amount of unreduced CB1954. Similarly, the top two variants derived from the pre-selection strategy, 1.5C and 1.9C produced peaks indicating 2-NO₂ production. Variant 1.9C also had a minor peak indicating 4-NO₂ production.

Although standards were not available for the potential 2-NH₂ and 4-NH₂ end-products, it is possible that the additional peaks visible in 3.2C, 1.5C and 1.9C, at the ~7 minute mark in **Figure 5.7** represent these end-products. Helsby et al. (2004) show that these primary metabolites 2-hydroxylamine and 4-hydroxylamine typically elute between 10-12 minutes and 6-8minutes respectively. However, it should be noted that this is quite speculative, as Helsby et al. (2004) used a different HPLC system (an Agilent 1100 (Agilent, Waldbronn, Germany) with an Alltech Altima 3.2x150 mm C8 5μ column (Alltech Associates Inc., Deerfield, IL, USA)).

5.4 Discussion

5.4.1 Outcomes of directed evolution of 7SM library for activity with CB1954

The aim of this investigation was to compare the evolutionary outcomes of using FACS; an automated high-throughput screening method, to a pre-selection strategy with a pre-selection agent for active nitroreductases; a manual low throughput screening strategy. In this study I chose to use the 7SM variant library derived from *E. coli* NfsA and select for variants with improved CB1954 activity.

No outstanding variants were identified from either of the screening approaches after a single round of directed evolution. The most improved variant was 3.2C, derived from the FACS screening approach, yet it was only 1.7 fold more active with CB1954 than the wild-type progenitor in IC₅₀ assays. Enzyme kinetic analysis demonstrated that this advanced activity with CB1954 was not maintained once the enzyme was isolated from the cell where the k_{cat}/K_m was smaller than that of the wild-type progenitor *E. coli* NfsA. This phenomenon of poor enzyme kinetic values recorded *in vitro* has been observed in multiple directed evolution campaigns with nitroreductases and alternative prodrugs in the Ackerley laboratory (Copp et al., 2017; Sharrock, 2019).

Analysis of sequence trends and frequency of substitution to amino acids based on chemical characteristics did not show any substantial patterns that differentiated the top twenty variants of FACS screening approach compared to pre-selection strategy. Further sequencing of a greater number of variants captured from each strategy would facilitate statistical analysis.

Overall the results of this investigation were inconclusive after just a single round of directed evolution, but there is some evidence that the FACS strategy was more effective than niclosamide/chloramphenicol pre-selection in enriching for superior CB1954-reducing variants. There were more variants derived from FACS screening that demonstrated improved activity with CB1954 compared to the wild-type NfsA in IC₅₀ assays. However, these improved variants ranged only in 1.1-1.7 fold improvement in activity with CB1954 compared to NfsA.

5.4.2 Considerations in comparing FACS to pre-selection strategies for directed evolution of nitroreductases

In comparing the physical attributes of each strategy I conclude that the FACS screening approach has many advantages in terms of scale, time and resource consumption (including prodrug) that may outweigh drawbacks of cost and accuracy of selection. Moreover, these drawbacks may be overcome by using a non-toxic reporter protein and prohibition of the bystander effect which will be discussed further in the final chapter in section **7.3.1**.

FACS is an automated and high-throughput and thus is capable of rapidly screening libraries on a much larger scale, it is also less labour intensive in time as well as being more parsimonious with prodrug consumption. However FACS is presently costly to our lab in terms of technician and equipment hire. It also requires purchase and use of unused 384-well microtitre plates for collection. Given that only single cells are collected it is important to use microtitre plates with guaranteed sterility.

In contrast pre-selection strategies with agents such as niclosamide or chloramphenicol, are very labour intensive and require mass random picking of individual colonies. These colonies are then tested for activity with the prodrug of interest in a growth inhibition assay. The prodrug of interest can be in scarce supply, possibly because it has been synthesized in-house by a collaborator, consequently randomly picking colonies with any level of a functional nitroreductase can rapidly consume prodrug to capture only a few variants worthy of further interrogation. However, shrinking a variant nitroreductase library size to only active nitroreductases is extremely valuable - particularly to a directed evolution campaign based on random mutagenesis or semi-rational library creation through processes such as error prone PCR or step-wise PCR respectively.

Perhaps the bacterial bystander effect, and its influence on the accuracy of selection, is the most important factor for comparing FACS and pre-selection methods. As presented in the discussion of Chapter 4, the accuracy of FACS may be negatively influenced by both the toxicity of GFP as well as the bacterial bystander effect. In contrast the pre-selection strategy, requires manual individual screening of variants with some able to detoxify the pre-selection agent. This may provide a higher degree of accuracy for selecting variants

with advanced activity as it is not subject to the influence of the bystander effect or GFP toxicity.

Future investigation with FACS, CB1954 and the 7SM library would benefit from secondary screening methods. In just two FACS iterations Copp et al. (2014) was able to achieve a 90 000-fold enrichment of a functional prodrug-activating nitroreductase from model library. This was done by collecting a tube of cells from FACS (as opposed to single cells in a microtitre plate), culturing of those variants together and then subjecting the culture to a secondary prodrug challenge and FACS. However, a secondary round of FACS on the tubes collected in this investigation would have made it harder to compare against the pre-selection strategy in any meaningful manner.

Of interest none of the top five performing variants with CB1954 from the FACS strategy were all derived from variants collected into a microcentrifuge tube during FACS. Instead they were all derived from variants collected into individual wells in a microtitre plate. This may indicate future FACS screening may benefit from exclusively collected cells into microtitre plates for post-FACS recovery despite additional stress of recovery from a single cell. Perhaps growth competition as a result of co-collection of cells into a microcentrifuge tube may be the underlying cause of this. I theorize that bacteria that experienced greater DNA damage, due to expression of a more efficient nitroreductase, negatively suffer from growth competition with bacterial cells that suffered less DNA damage during the post-FACS recovery period.

6 Evaluating a panel of nitroreductases for potential applications in *Clostridia*-directed enzyme prodrug therapy

6.1 Overview

The work presented here contributed to a larger collaborative research effort between the Ackerley laboratory, the ACSRC and researchers at the Universities of Nottingham and Maastricht, to advance *Clostridia*-directed enzyme prodrug therapy (CDEPT), targeting a human clinical trial with a *Clostridia sporogenes* vector. This short project identified the most promising wild-type bacterial nitroreductase enzymes with the two next generation prodrugs PR-104A and SN36506, under consideration for the human clinical trial, via kinetic analyses and IC₅₀ assays.

At the time of performing this research, four different *nfsB*-family nitroreductases had been tested by our collaborators for expression in *C. sporogenes*. Of the NfsB nitroreductases examined, the kinetic parameters and IC₅₀ analysis indicated that a variant of *Vibrio vulnificus* NfsB was the most promising candidate for activity with PR-104A as well as SN36506. *B. subtilis* YdgI displayed a low level of activity at the purified protein level with SN36506 however *V. vulnificus* NfsB and a previously-engineered *V. vulnificus* NfsB F70A/F108Y variant were the only NfsB family members to have an IC₅₀ value less than 1000 µM. It was concluded that *Vibrio vulnificus* NfsB and mutants thereof are of most interest for future directed evolution projects contributing to this collaborative research effort.

The next generation prodrug SN36506 was also tested in the bacterial bystander effect assay. As with its analogue PR-104A, SN36506 did not display a significant bacterial bystander effect. A small panel of prodrugs were used in a modified bacterial bystander effect assay using activator cells that possessed a functional TolC efflux pump. The presence of this pump did not increase the bacterial bystander effect of next generation prodrugs.

6.1.1 Aims:

- To interrogate a panel of promising bacterial nitroreductases for activity with the next generation prodrugs
 - PR-104A
 - SN36506
- To test SN36506 in the bacterial bystander effect assay
 - As a secondary objective to test two additional analogues of PR-104A in the bystander effect assay
 - As a third objective the bacterial bystander effect of SN36506 and the two PR-104A analogues were also assessed in the bacterial bystander effect assay using activators with a functional TolC efflux pump

6.2 Introduction

The work presented here contributed to a larger collaborative research effort between the Ackerley laboratory, the Auckland Cancer Society Research Centre (ACSRC) and researchers at the Universities of Nottingham and Maastricht, to advance *Clostridia*-directed enzyme prodrug therapy (CDEPT) toward a human clinical trial. The wider research collaboration is funded by a grant from the Dutch Cancer Society which dictated a strict research timeline. The research I performed was only a small contribution, which took place over a period of three months, to identify the most promising wild-type bacterial nitroreductase enzymes with two next generation prodrugs under consideration for the human clinical trial; PR-104A and SN36506. The objective was to identify which wild-type bacterial nitroreductase, from a panel of promising candidates previously identified by the collaborative team, were the most active with either of these prodrugs as determined by enzyme kinetic analysis and IC_{50} assays. The aim was for the most promising wild-type bacterial nitroreductase to be chosen as the starting point for a directed evolution campaign to further improve activity for this CDEPT collaboration.

As a continuation of my research into the bacterial bystander effect, I also wanted to investigate the bystander effect potential of alternative next generation prodrugs,

including SN36506 and other PR-104A analogues, using my plate based bacterial bystander assay developed in Chapter 3.

6.2.1 Expressing nitroreductases in *Clostridium*

The *Clostridium* species are infamously difficult to work with using standard genetic modification techniques (Minton, 2003). Yet, our collaborators at the University of Nottingham have overcome these barriers by developing new methods to achieve chromosomal integration of nitroreductase genes in *C. sporogenes* (Heap et al., 2007; Kuehne & Minton, 2012).

Despite these advances, at the time this work was conducted our collaborators had been unable to engineer *C. sporogenes* to express a member of the *nfsA* nitroreductase family. It should be noted that each nitroreductase in this chapter is referred to using standard nomenclature followed by an underscore and a two-letter abbreviation of the genus and species, for example NfrA_Bs indicates the NfrA enzyme derived from *Bacillus subtilis* (**Table 6.1** - summary of abbreviations). At the time this work was performed, attempts had failed to express functional NfsA_Ec (NfsA derived from *E. coli*), NfrA_Bs, or YcnD_Bs (YcnD derived from *Bacillus subtilis*) enzymes in *C. sporogenes* in pilot studies. Although the biological reason for the failure of NfsA family nitroreductases to express had not been identified, it was theorized that their promiscuous activities might be detrimental to *C. sporogenes* metabolism.

In contrast, all of the NfsB nitroreductase family members that had been tested by our collaborators at this stage had been successfully expressed by *C. sporogenes*. These were NfsB_Ec (NfsB derived from *E. coli*), NfsB_Nme (NfsB derived *Neisseria meningitides*), NfsB_Vv (NfsB derived from *Vibrio vulnificus*), YfkO_Bs (YfkO derived from *Bacillus subtilis*) and YfkO_Bli (YfkO derived from *Bacillus licheniformis*). Based on this, we prioritised nitroreductase candidates belonging to the NfsB family as potential candidates for the CDEPT human clinical trial. As a consequence, the panel tested in this work included several engineered variants of NfsB family enzymes that other researchers in the Ackerley lab had developed for possible CDEPT applications.

6.2.2 Selecting panel of nitroreductase enzymes

The investigation was in some respects an extension of previous work performed in the Ackerley laboratory that was published in Prosser et al. (2013). Eight wild-type nitroreductase enzymes were selected from the panel of those tested by Prosser et al. (2013) that previously displayed promising activity with PR-104A. Four of these nitroreductase enzymes are representative members of the NfsA nitroreductase family that had previously been considered as CDEPT candidates prior to *nfsA* expression issues being encountered. The remaining four were members of the NfsB nitroreductase family. Two additional enzymes have since been identified and were included here; YfkO derived from *B. licheniformis* and Nme derived from *N. meningitides* (**Table 6.1**).

Three further engineered variants from NfsB_Vv and YfkO_Bs were also included that were engineered for improved activity with other prodrugs or imaging agents. The first was a variant of NfsB_Vv, which contains the amino acid substitutions F70A and F108Y and was shown to exhibit substantially greater SN33623 activation than any previous NfsB-family nitroreductase (Rich, 2017). SN33623 is a 5-nitroimidazole PET probe that was designed to be used as an imaging agent in combination with GDEPT strategies to monitor location and progress of therapy. Positron emission tomography (PET) uses positron emitting probes to visualize cancer therapy in a patient in a non-invasive fashion. It was of central interest to the Maastricht project as a possible means of imaging the location of nitroreductase-labelled *C. sporogenes* in patients. SN33623 is a particularly attractive imaging agent for this purpose because it has a decreased one-electron reduction potential, rendering it less susceptible to activation by endogenous human one-electron reductases, even in the absence of oxygen, than other nitroimidazole probes. This limits SN33623 activation to those cells expressing the activating nitroreductase enzyme (Anderson et al., 2014).

The NfsB_Vv F70A/F108Y sequence was ordered as a synthetic gene (gBlock) from Integrated DNA Technologies (IDT; Coralville, IA, USA) and expressed in an *E. coli* 7NT expression strain. Cloning and preliminary testing of this construct was carried out by Dr Rich, who demonstrated that introduction of the F70A and F108Y substitutions rendered NfsB_Vv capable of SN33623 activation, whilst maintaining its capability to activate SN36506 (Rich, 2017).

Two further variants of a different nitroreductase enzyme, YfkO_Bs, were included in the panel based on a directed evolution project performed by Dr Rich that yielded significant improvements of up to 2.4-fold over wild-type YfkO_Bs in sensitising *E. coli* 7NT cells to SN33623 (Rich, 2017). The variants selected were 3-62, bearing two point mutations, F82L/M110I; and 1-88, with five amino acid substitutions, F14L/F82L/K94T/T122M/L133H. It was hoped one of these YfkO_Bs variants would offer a dual activation; of both the prodrug payload in the CDEPT medicament and a complementary imaging agent, such as SN33623, to monitor therapeutic outcome *in situ*. Dr Rich provided preliminary evidence that *E. coli* 7NT cells expressing variants 1-88 and 3-62 were ~2-fold less sensitive to SN36506 but up to 4-fold more sensitive to SN33623 than cells expressing the NfsB_Vv variant F70A/F108Y (Rich, 2017).

Thus these three engineered NfsB variants YfkO_Bs 1-88 and 3-62 variants and the NfsB_Vv variant F70A/F108Y, were included in the panel for direct comparison to other nitroreductase candidates of interest to the CDEPT collaboration. Genes encoding these three engineered nitroreductases were provided by Dr Sharrock (NfsB_Vv F70A F108Y) and Dr Rich (the two YfkO_Bs variants).

Species	Enzyme	Nitroreductase Family	Expression in <i>C. sporogenes</i>
<i>Bacillus subtilis</i>	NfrA_Bs	NfsA	No
<i>Escherichia coli</i>	NfsA_Ec	NfsA	No
<i>Enterobacter (Chronobacter) sakazakii</i>	NfsA_Es	NfsA	Untested
<i>Bacillus subtilis</i>	YcnD_Bs	NfsA	No
<i>Escherichia coli</i>	NfsB_Ec	NfsB	Yes
<i>Vibrio vulnificus</i>	NfsB_Vv	NfsB	Yes
	NfsB_Vv F70A F108Y		Yes
<i>Bacillus subtilis</i>	Ydgl_Bs	NfsB	Untested
<i>Neisseria meningitidis</i>	NfsB_Nme	NfsB	Yes
<i>Bacillus licheniformis</i>	YfkO_Bli	NfsB	Yes
<i>Bacillus subtilis</i>	YfkO_Bs	NfsB	Yes
	YfkO_Bs 1-88		Untested
	YfkO_Bs 3-62		Yes

Table 6.1 Panel of nitroreductase candidates selected for investigation for potential CDEPT. The panel consists of six wild-type NfsB nitroreductase representatives of which (at the time this work was conducted) five had been expressed in the proposed CDEPT vector *C. sporogenes*. Four NfsA representatives were also included based on their high efficiency for activating prodrugs PR-104A and CB1954 compared to NfsB enzymes (Prosser *et al.*, 2013). Three additional engineered NfsB variants included were NfsB_Vv F70A/F108Y, YfkO_Bs 1-88 and YfkO_Bs 3-62 owing to their abilities to efficiently activate SN36506 and/or the imaging agent SN33623 (Rich 2017). Each nitroreductase is referred to using standard nomenclature followed by an underscore and a two letter abbreviation of the genus and species for example NfA_Ec indicates the NfsA enzyme derived from *E. coli*. Grouping of enzymes into families was based on the degree of shared sequence identity with the closest *E. coli* representative for all families.

6.2.3 Prodrug candidates for CDEPT

PR-104A has already been introduced in this thesis as a key nitroaromatic prodrug in the development of GDEPT. The underlying issues of off-target activation by human aldo-keto reductase 1C3 were discussed in Chapter 1 (1.5.1.1.2). At this stage in the CDEPT collaboration, the prodrug PR-104A was still considered a candidate for the *Clostridium* clinical trial on the basis that a significantly lower dose, that maintained a therapeutic effect, could be safely used in conjunction with a highly efficient nitroreductase. A highly efficient nitroreductase could avoid off-target activation by raising the therapeutic index

to a threshold where the minimum effect dose of PR-104A would result in such a low plasma concentration of the prodrug that aldo-keto reductase 1C3 could not effectively activate it.

Subsequent to the development of PR-104A and its initial success for hypoxia activated prodrug therapy, many derivations of PR-104A have been engineered by the ACSRC. One of these next generation prodrugs was designated SN36506.

The chemical structure of SN36506 is shown in **Figure 6.1**. SN36506 is a nitrobenzamide mustard, hypoxia-activated prodrug that upon reduction is converted to a highly cytotoxic, cell permeable metabolite. This permeability enables ablation of adjacent, more oxygenated tumour cells through the bystander effect. SN3506 was specifically designed to avoid off-target activation by the endogenous human aldo-keto reductase 1C3, as well as having increased solubility and oral bioavailability relative to PR-104A (Niemans et al., 2017). SN36506 was characterised by mass spectrometry and ¹H NMR to determine purity and provided for use in this study by Dr Jeff Smaill (University of Auckland, New Zealand).

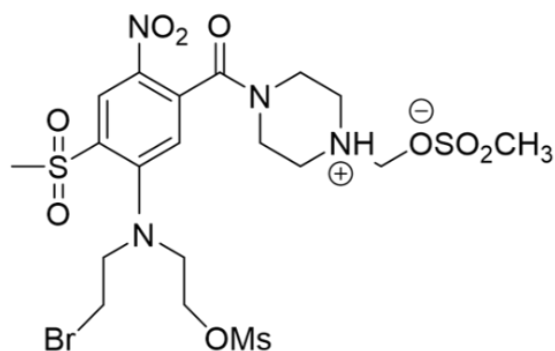


Figure 6.1 Chemical structure of the next generation prodrug SN36506.

When the present investigation was initially proposed, the next generation prodrug SN36506 was the lead prodrug candidate under consideration for the CDEPT collaboration. Before this work was conducted, SN36506 had never been broadly assessed for activity with a panel of bacterial nitroreductases because it had only recently been developed. Performing this activity assessment was the primary focus of this investigation, with consideration also given to PR-104A as an alternative prodrug possibility that had previously undergone Phase I/II safety evaluation in human clinical trials (McKeage et al., 2011, 2012).

It is also important to note that when this work was performed, concerns around the mustard prodrugs possibly being unsuitable for BDEPT applications, due to an inability to efficiently exit bacterial activator cells as per Section 3.4, had not yet been raised. Moreover, it remains possible that the underperformance of the mustard prodrugs relative to CB1954 or nitro-CBI-DEI in bacterial bystander assays (**Figure 3.5** and **Figure 3.7**) was a consequence of the Gram-negative bacterial cell wall, and that *C. sporogenes* (a Gram-positive bacterium) might prove a more suitable vector for BDEPT with mustard prodrugs.

6.3 PR-104A Analysis

6.3.1 Protein purification and steady state enzyme kinetics

Recombinant nitroreductases were expressed from pET28a+ as N-terminal His₆ tagged enzymes and purified by nickel-affinity chromatography (**2.9.4**). Protein concentrations were calculated using a NanoDrop spectrophotometer (**2.9.4**) and enzyme purity was confirmed by SDS-PAGE (**2.8.10**). Protein fractions were stable at -20 °C when stored in 40% glycerol up to six months.

Steady-state enzyme kinetics with purified nitroreductases were assessed spectrophotometrically at 400 nm for PR-104A. This was chosen based on Prosser et al. (2013) which determined that a wavelength of 400 nm captured the maximal absorption relative to the para-hydroxylamine reduction product of PR-104A, with an extinction coefficient of 6000 M⁻¹ cm⁻¹. A Helios g UV-vis spectrophotometer (Thermo Scientific, Middletown, VA) was used as described in section **2.10**.

As in section 5.3.3 the apparent K_m and k_{cat} values at 0.25 mM NADPH are presented here. Affinity (K_m) and catalytic (k_{cat}) constants for each of the enzymes with PR-104A were extrapolated from reaction rate data (triplicate reactions) obtained over a range of PR-104A concentrations from 0-1500 μM PR-104A (**Appendix C Figure C 3- Figure C 4**). *E. coli* NfsA and NfsB enzymes have previously been determined to catalyse substrate reduction via a bi-bi ping pong mechanism of action (Zenno et al., 1996). As a result the kinetic parameters measured are dependent on the concentration of the co-factor NADPH that is used in the reaction. For this reason the starting co-substrate concentration of NADPH was kept constant at 0.25 mM throughout these experiments.

The dependency on co-substrate concentration does not affect the ratio of $k_{cat}: K_m$. Therefore, the specificity constant (k_{cat}/K_m) provides an accurate measure of relative enzyme efficiency with prodrugs such as PR-104A and SN36506.

6.3.2 PR-104A steady-state kinetic parameters

The results of enzyme kinetic analysis are summarised in **Table 6.2**. The Michaelis-Menten curves of the average reaction rates can be found in **Appendix C**. In general the members of the NfsA nitroreductase family were more active overall with PR-104A than those belonging to NfsB. The only exception was NfsB_Vv and the NfsB_Vv F70A/F108Y variant, which had k_{cat}/K_m values with PR-10A that exceeded those of any of the NfsA nitroreductases. Notably the NfsB_Vv F70A/F108Y variant outperformed the wild-type progenitor NfsB_Vv ten-fold, as well as outperforming the other NfsB candidates (**Appendix C Figure C 1**).

The kinetic parameters observed for PR-104A generally correlated to those recorded by Prosser et al. (2013) as shown by comparing the k_{cat}/K_m values in **Table 6.2**. However the k_{cat}/K_m of Ydgl_Bs was ten-fold lower than that recorded by Prosser et al. (2013) (**Appendix C Figure C 2**). Furthermore NfsB_Nme also produced a very low k_{cat}/K_m with a high level of error. This was likely due to a low yield of protein (**Appendix C Figure C 3**).

The first preparation of the enzymes NfsB_Vv F70A/F108Y variant, NfsB_Nme, YcnD_Bs, YfkO_Bli and Ydgl_Bs using a chemical cell lysis method (**2.9.2.1**) yielded relatively poor concentration of the proteins. As a precaution all five enzymes were purified again. This second independent batch of purified protein was used to generate the data presented here (**Table 6.2**). There was some concern that the purified protein stock was contaminated by residual chemicals from the purification process. These contaminants may have interfered with an accurate measurement of the protein concentration. Although contamination is an unlikely root cause of the issue given that protein concentration measured by NanoDrop and SDS-PAGE were low. Therefore I opted to maximise protein expression.

Optimisation strategies used to increase protein yield included; a longer incubation of a greater volume of the bacterial culture to increase the amount protein expressed prior to purification (**2.9.1**) as well as using the French Press - a mechanical method of cell lysis

(2.9.1.1). The French Press method consists in forcing a liquid suspension at high pressure through a very fine aperture, which causes the disruption of the cells (French & Milner, 1950). The French Press method limits damage to the tertiary structure of protein by providing a single pass through the point of maximum shear force instead of repeated shearing generated by other mechanical means of cell lysis such as sonication. It has been observed by multiple members of the Ackerley Laboratory that the French Press method has generally yielded a higher concentration of nitroreductase protein compared to chemical lysis methods.

The enzymes NfsB_Vv F70A/F108Y variant, NfsB_Nme, YcnD_Bs, YfkO_Bli and Ydgl_Bs were re-purified using these tools. The protein yield was increased four-eight fold for each of these proteins. The new preparations of enzymes demonstrated *in vitro* enzyme activity that was more consistent with that previously reported (Prosser et al., 2013). The exception being Ydgl_Bs, which remained relatively inactive despite using these additional protein purification strategies. Notably NfsB_Nme and YfkO_Bli, were also relatively inactive with PR-104A (**Appendix C Figure C 4**). However, these two enzyme were not previously tested with PR-104A.

It would have been informative to repeat the purification and enzyme kinetic analysis of Ydgl_Bs, and NfsB_Nme and YfkO_Bli but due to time constraints of the CDEPT collaboration this was not possible. Instead, each enzyme was progressed to evaluation in *E. coli* expression assays.

Enzyme	Nitroreductase Family	K_m		k_{cat}		PR-104A		$[E]_{tot}$ (μM) ^c	Prosser et al. (2013) k_{cat}/K_m ($\text{M}^{-1}\text{s}^{-1}$) ^b
		(μM) ^a		(s^{-1}) ^a		k_{cat}/K_m ($\text{M}^{-1}\text{s}^{-1}$) ^b			
NfrA_Bs	NfsA	45	± 16	5.5	± 0.46	120000	± 45000	0.039	400000 \pm 61000
NfsA_Ec	NfsA	86	± 28	17	± 1.5	200000	± 66000	0.020	120000 \pm 14000
NfsA_Es	NfsA	66	± 8.7	14	± 0.440	210000	± 29000	0.039	220000 \pm 45000
NfsB_Ec	NfsA	740	± 250	13	± 1.9	18000	± 6500	0.054	13000 \pm 7800
YcnD_Bs	NfsA	11	± 3.2	11	± 0.430	980000	± 280000	0.031	480000 \pm 51000
NfsB_Vv	NfsB	15	± 7.2	3.5	± 0.27	230000	± 110000	0.65	100000 \pm 13000
NfsB_Vv F70A/F108Y	NfsB	7.2	± 1.9	15.	± 0.67	2100000	± 580000	0.021	
Ydgl_Bs	NfsB	20	± 6.4	0.24	± 0.014	12000	± 4100	0.86	140000 \pm 16000
Nme	NfsB	950	± 460	1.9	± 0.050	2000	± 990	0.3	
YfkO_Bli	NfsB	910	± 410	4.8	± 1.2	5300	± 2700	0.17	
YfkO_Bs	NfsB	600	± 280	6.70	± 1.4	11000	± 5800	0.08	
YfkO_Bs 1.88		260	± 110	8.40	± 1.2	32000	± 14000	0.049	
YfkO_Bs 3.62		330	± 130	16	± 2.3	48000	± 21000	0.024	

Table 6.2 Kinetic parameters for the reduction of PR-104A by a panel of purified His6-tagged nitroreductase candidates for investigation for a CDEPT strategy. a. Apparent K_m and k_{cat} values as measured at 0.25 mM NADPH in triplicate reactions. b. Standard errors calculated using GraphPad Prism 7.0 (GraphPad Software Inc.; La Jolla, CA, USA). c. total amount of enzyme available in the reaction. Rate of reduction at varying concentrations of PR-104A and a fixed concentration of excess NADPH (0.25 mM) were monitored by decrease in absorbance at 400 nm, rates measured in quadruplicate reactions. Apparent K_m and k_{cat} derived using GraphPad Prism 7.0 (GraphPad Software Inc.; La Jolla, CA, USA). The extinction coefficient used was $6000 \text{ M}^{-1} \text{ cm}^{-1}$.

6.3.3 PR-104A IC₅₀ assay

IC₅₀ assays were performed using *E. coli* 7NT cells expressing each candidate nitroreductase from plasmid pUCX, and compared to cells containing an empty plasmid control (“Empty”). The maximum PR-104A concentration used was 2000 μM in a two-fold dilution series (see section 2.13.3 for method details). The average IC₅₀ value was determined from three biological replicates and is summarized in **Table 6.3**.

Overall, the members of the NfsA nitroreductase family were more active with PR-104A than those belonging to NfsB by approximately two-fold as indicated by the average IC₅₀ values (**Table 6.3**). The only NfsB family enzymes to approach these levels of host-cell sensitivity to PR-104A were Ydgl_Bs, which displayed an IC₅₀ value near to that of NfsA_Ec,

and the wild type and the NfsB_Vv F70A/F108Y variant which appeared slightly less active than the least-active NfsA family member, NfsA_Es.

Enzyme	Nitroreductase Family	IC ₅₀ value PR-104A μ M	
NfrA_Bs	NfsA	380	\pm 63
NfsA_Ec	NfsA	436	\pm 42
NfsA_Es	NfsA	499	\pm 53
YcnD_Bs	NfsA	384	\pm 72
NfsB_Ec	NfsB	641	\pm 125
NfsB_Vv	NfsB	587	\pm 83
NfsB_Vv F70A/F108Y		536	\pm 127
Ydgl_Bs	NfsB	469	\pm 45
NfsB_Nme	NfsB	713	\pm 160
YfkO_Bli	NfsB	666	\pm 135
YfkO_Bs	NfsB	680	\pm 150
YfkO_Bs 1_88		689	\pm 158
YfkO_Bs 3_62		676	\pm 50
Empty		836	\pm 197

Table 6.3 IC₅₀ values of prodrug PR-104A mediated growth inhibition of candidate nitroreductases. Compound-dependent growth inhibition in *E. coli* 7NT cells was monitored by measuring strain turbidity (OD₆₀₀) pre- and post-3.5 hour incubation with a two-fold dilution series of PR-104A (top concentration of 2000 μ M). Percentage growth relative to unchallenged controls was determined and used to calculate the concentration at which 50% growth inhibition was seen using GraphPad Prism 7.0. Data are the average of at least 3 biological replicates \pm SD. IC₅₀ values are colour coded green to yellow to red based on the activity of the nitroreductase with the compound (red = highly active, yellow = moderate activity, green = low activity).

The enzymes NfrA_Bs and YcnD_Bs displayed the lowest IC₅₀ values across three biological replicates of the nitroreductases tested (**Table 6.3**). This correlates with the relatively higher k_{cat}/K_m values shown in **Table 6.2** for these two enzymes. Likewise, the low IC₅₀ value of NfsA_Ec was reflected in the high k_{cat}/K_m value of $197000 \pm 66300 \text{ M}^{-1}\text{s}^{-1}$. In comparison, Ydgl_Bs displayed a low IC₅₀ value, approaching that of NfsA_Ec, but the k_{cat}/K_m value was only $12400 \pm 4070 \text{ M}^{-1}\text{s}^{-1}$. This may be further evidence that a poor purification was responsible for the low kinetic parameters measures for Ydgl_Bs.

6.4 SN36506 Analysis

The same protein preparations used for PR-104A kinetic analysis were used for SN36506. These protein fractions were stable at -20 °C when stored in 40% glycerol up to six months. Steady-state enzyme kinetics with purified nitroreductases were assessed spectrophotometrically at 400 nm. The extinction co-efficient had previously been determined to be 174000 M⁻¹ cm⁻¹ by Dr Williams.

6.4.1 SN36506 steady-state kinetic parameters

As with PR-104A, the members of the NfsA nitroreductase family were relatively more active with SN36506 than the NfsB representatives. The only exception was NfsB_Vv F70A/F108Y, which displayed measurable activity. In contrast, the NfsB_Vv wild-type progenitor displayed only trace activity with SN36506 (insufficient to enable derivation of kinetic parameters). Of the other members of the NfsB nitroreductase family tested, only Ydgl_Bs displayed a measurable level of enzymatic activity, albeit far lower than for NfsB_Vv F70A F108Y. All other NfsB nitroreductases tested either had no activity or such low activity that kinetic parameters could not be determined (**Appendix C and Table A 1**).

Enzyme	Nitroreductase Family	K_m		k_{cat}		SN36506 k_{cat}/K_m		[E]tot (μM) ^c
		(μM) ^a		(s^{-1}) ^a		($\text{M}^{-1}\text{s}^{-1}$) ^b		
NfrA_Bs	NfsA	9.4	± 3.2	1.5	± 0.064	160000	± 54000	0.039
NfsA_Ec	NfsA	700	± 170	1.5	± 0.20	2200	± 600	0.081
NfsA_Es	NfsA	240	± 41	0.63	± 0.040	2700	± 490	0.16
YcnD_Bs	NfsA	420	± 69	0.74	± 0.047	1800	± 310	0.25
NfsB_Ec	NfsB	No activity detected						
NfsB_Vv	NfsB	Trace activity						
NfsB_Vv F70A/F108Y		2100	± 380	3.8	± 0.45	1800	± 390	0.16
Ydgl_Bs	NfsB	220	± 79	0.087	± 0.0096	410	± 150	0.86
NfsB_Nme	NfsB	No activity detected						
YfkO_Bli	NfsB	No activity detected						
YfkO_Bs	NfsB	No activity detected						
YfkO_Bs 1.88		Trace activity						
YfkO_Bs 3.62		Trace activity						

Table 6.4 Kinetic parameters for the reduction of SN36506 by a panel of purified His6-tagged nitroreductase candidates for investigation for a CDEPT strategy. a. Apparent K_m and k_{cat} values as measured at 0.25 mM NADPH in triplicate reactions. b. Standard errors calculated using GraphPad Prism 7.0 (GraphPad Software Inc.; La Jolla, CA, USA). c. total amount of enzyme available in the reaction. Rate of reduction at varying concentrations of SN36506 and a fixed concentration of excess NADPH (0.25 mM) were monitored by decrease in absorbance at 400 nm, rates measured in quadruplicate reactions. Apparent K_m and k_{cat} derived using GraphPad Prism 7.0 (GraphPad Software Inc.; La Jolla, CA, USA). The extinction coefficient used was 17,400 $\text{M}^{-1}\text{cm}^{-1}$.

The *in vitro* enzyme activity observed with the panel of nitroreductase candidates was overall considerably lower with the prodrug SN36506 compared to the activity detected with PR-104A. The k_{cat}/K_m values did not exceed 4000 $\text{M}^{-1}\text{s}^{-1}$, with the exception of NfrA_Bs, which generated a calculated k_{cat}/K_m value of 156000 \pm 53600 $\text{M}^{-1}\text{s}^{-1}$ (Table 6.4) - exceeding the activity of NfrA_Bs with PR-104A (Table 6.2). It should be considered that this relatively high activity of NfrA_Bs has potential to be inaccurate, as the high calculated activity is primarily due to the very low K_m calculated for this enzyme (Figure 6.2). The full set of Michaelis-Menten curves for the enzymes tested with SN36506 can be found in Appendix C.

Notably, the total enzyme concentration required to generate a measurable enzymatic activity for NfsA_Es, YcnD_Bs, NfsB_Vv F70A/F108Y variant and Ydgl_Bs was tenfold

higher than that required by NfrA_Bs and NfsA_Ec (**Table 6.4**). These total enzyme concentrations also far exceeded the levels required to assay activity with PR-104A for the enzymes NfsA_Es, YcnD_Bs, NfsB_Vv F70A/F108Y variant and Ydgl_Bs (**Table 6.2**).

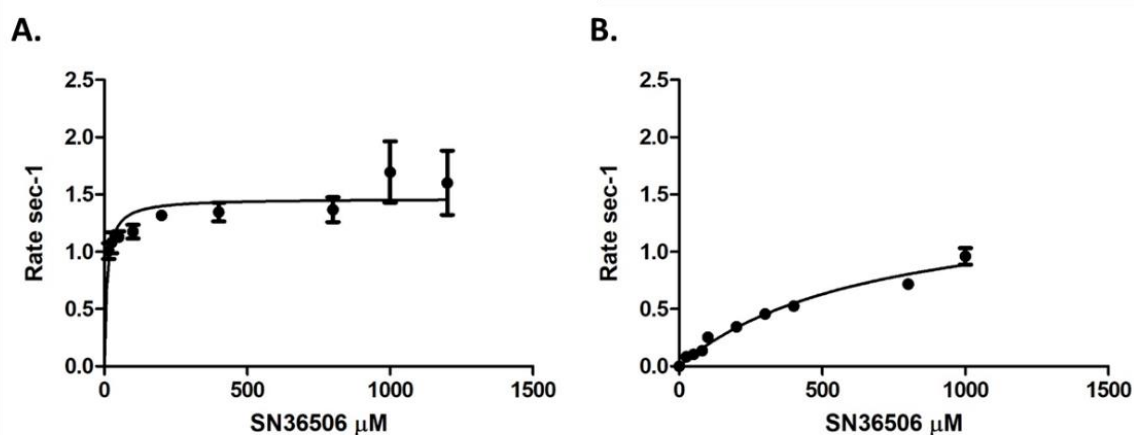


Figure 6.2 Michaelis-Menten curves derived from reduction of SN36506 by purified His6-tagged (A). NfrA_Bs, (B). NfsA_Ec. Rate of reduction at varying concentrations of SN36506 and a fixed concentration of excess NADPH (0.25 mM) were monitored by decrease in absorbance at 400 nm, rates measured in quadruplicate reactions. Apparent K_m and k_{cat} derived using GraphPad Prism 7.0 (GraphPad Software Inc.; La Jolla, CA, USA). The extinction coefficient used was 17, 400 M⁻¹ cm⁻¹. The data has been normalized according the total concentration of the enzyme (μM) and represents average of at least three biological replicates. Each biological replicate has at least three technical repeats for each substrate concentration.

6.4.2 SN36506 IC₅₀ assay

IC₅₀ assays for the prodrug SN36506 were performed using the same *E. coli* 7NT strains as those used in the PR-104A IC₅₀ assays. To preserve the limited stock of the prodrug SN36506, IC₅₀ assays were performed using a maximum concentration of only 1000 μM across a two-fold dilution series (**2.11.3**). Typically for nitroaromatic prodrugs, such as PR-104A and analogues thereof, a maximum concentration of 2000 μM is used to perform IC₅₀ analysis. In addition due to a previously observed phenomenon whereby it was seen that SN36506 can be actively effluxed from even *tolC* mutant 7NT cells (*Dr Williams, personal communication*), a final concentration of 10 μM of the efflux pump inhibitor phenylalanine-arginine beta-naphthylamide (PaβN) (Lomovskaya et al., 2001) was included in the media used to perform the IC₅₀ assays with SN36506. PAβN has been previously used in the Ackerley laboratory for this purpose (Rich, 2017). The average IC₅₀ value was determined from three biological replicates and summarized in **Table 6.5**.

Overall, the members of the NfsA nitroreductase family were again more active with SN36506 than those belonging to the NfsB family (**Table 6.5**). Of the nitroreductase candidate panel expressed in *E. coli* 7NT cells, those over-expressing the NfsA enzyme YcnD_Bs were most sensitized to the prodrug SN36506, displaying the lowest IC₅₀ value of 600 ± 45 µM.

Enzyme	Family	IC ₅₀ value	
		SN36506 µM	
YcnD_Bs	NfsA	600	± 45
NfsB_Vv	NfsB	671	± 135
NfsA_Es	NfsA	746	± 49
NfrA_Bs	NfsA	767	± 94
NfsB_Vv			
F70A/F108Y	NfsB	800	± 6
NfsA_Ec	NfsA	991	± 108
NfsB_Ec	NfsB	1000	
Ydgl_Bs	NfsB	1000	
NfsB_Nme	NfsB	1000	
YfkO_Bli	NfsB	1000	
YfkO_Bs	NfsB	1000	
YfkO_Bs 1_88	NfsB	1000	
YfkO_Bs 3_62	NfsB	1000	
Empty		1000	

Table 6.5 IC₅₀ values of prodrug SN36506 mediated growth inhibition of candidate nitroreductases. Compound-dependent growth inhibition in *E. coli* 7NT cells was monitored by measuring strain turbidity (OD₆₀₀) pre- and post-3.5 hour incubation with a two-fold dilution series of SN3506 (top concentration of 1000 µM and 10 µM PA8N included in challenge medium) and two-fold dilution series of PR-104A (top concentration of 2000 µM). Percentage growth relative to unchallenged controls was determined and used to calculate the concentration at which 50% growth inhibition was seen using GraphPad Prism 7.0. Data are the average of at least 3 biological replicates ± SD. IC₅₀ values are colour coded green to yellow to red based on the activity of the nitroreductase with the compound (red = highly active, yellow = moderate activity, green = low activity).

Most of the members of the NfsB nitroreductase family displayed IC₅₀ values greater than 1000 µM. This indicates either a low level of prodrug activation or relatively poor cytotoxicity for the activated drug within *E. coli* cells. The former scenario was consistent with the trace activity or no activity detected when measuring kinetic parameters. The exception to this was NfsB_Vv and its F70A F108Y substituted variant, the IC₅₀ values were

similar to members of the NfsA nitroreductase family. This was generally consistent with the kinetic parameters presented in **Table 6.4**.

The one profound exception to this trend was NfrA_Bs, which was only the fourth most active nitroreductase by IC₅₀ assays. This observation suggests that the kinetic parameters for SN36506 may indeed have previously been over-estimated for this enzyme (**Table 6.5**).

In summary the enzymes belonging to NfsA nitroreductase family generally outperformed those of the NfsB family in both IC₅₀ assays with PR-104A and kinetic analysis. This was consistent with the previous observations of Prosser et al. (2013).

The NfsB_Vv F70A/F108Y variant is of particular interest as it displayed the highest catalytic efficiency with PR-104A reported thus far for any nitroreductase as well as a ten-fold improvement over its progenitor according to the k_{cat}/K_m value. However the IC₅₀ values were very similar between NfsB_Vv and the NfsB_Vv F70A/F108Y mutant at 587 ± 83 and 536 ± 127 μ M PR-104A. Considering that the NfsB_Vv F70A/F108Y variant was purified using the French press method, while the NfsB_Vv wild-type was purified using the chemical cell lysis method, the IC₅₀ results could indicate that the difference in kinetic parameters may have been exaggerated by a difference in purification methods and not be exclusively due to improvement in activity with PR-104A.

Overall, the enzymes belonging to the NfsA nitroreductase family outperformed those of the NfsB family in both IC₅₀ assays and kinetic analysis with SN36506. None of the thirteen enzyme examined by IC₅₀ assay displayed any stand-out activity with SN36506.

6.5 Alternative mustard prodrugs tested in bacterial bystander assays

With SN36506 being the lead prodrug candidate for the CDEPT collaboration, we considered it important to test its bacterial bystander capabilities in the assay system that was developed as described in Chapter 3. Although we recognised that any bystander effect measured might be specific to our Gram negative bacterial model and not necessarily reflective of the ability of the activated drug to exit Gram positive *C. sporogenes*, we nevertheless considered that our bacterial system is likely to be a more appropriate model for CDEPT than a model that uses only human cells. Our model provides at least some simulation of the ability of the activated drug to exit a bacteria.

In addition to SN36506, we took the opportunity to compare the bacterial bystander capabilities of two other dinitrobenzamide mustard prodrugs that Dr Copp, a previous Ackerley laboratory researcher, had shown to be efficiently activated by NfsA_Ec. The purpose of this comparison was to determine whether further enhanced lipophilicity might make PR-104A analogues better able to exit *E. coli* activator cells.

Specifically, we sought to test a next-generation prodrug SN31609, an analogue of SN27686 which bears an additional methyl substitution, and compare the results to the bacterial bystander effect previously measured for SN27686 (**Figure 3.5 and Figure 3.7**). SN31609 is identical in structure to SN27686 apart from the additional methyl side group on the alcoholic side chain (**Figure 6.3**).

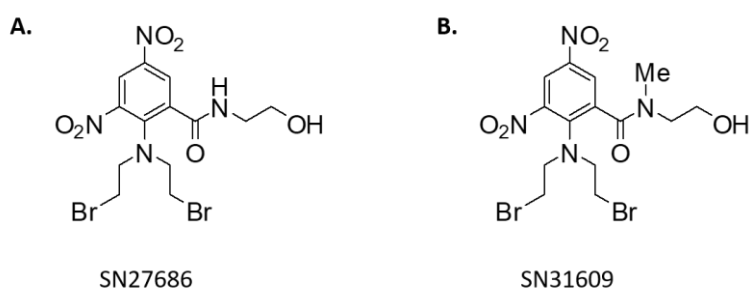


Figure 6.3 Chemical structures of additional mustard prodrugs tested in the bacterial bystander effect assay SN27686 and SN31609. A. SN27686 - a di-bromo analogue of PR-104A. B. SN31609 - an analogue of SN27686 with an additional methyl group designed to increase lipophilicity.

6.5.1 Testing next generation prodrugs in the bacterial bystander effect assay

Following the methods and nomenclature developed in Chapter 2, I evaluated the ability of the SN31609 and SN36506 prodrug metabolites to be transferred from activator to recipient cells in a microplate assay. Nitroreductase null SOS-R4 recipient cells were co-cultured at a 1:1 ratio with either *nfsA*-expressing 7NT activator cells (test condition) or nitroreductase-null 7NT cells (control condition). After incubation with an empirically optimised concentration of prodrug, cell-to-cell transfer of genotoxic metabolites was quantified by monitoring the mean fold-increase in fluorescence for the test condition relative to the control (**2.12.1**).

The growth inhibition and GFP values in the control cultures were found to be optimal at 25 μ M SN31609 (data not shown). At this concentration SN31609 activated by *nfsA*-

expressing activator cells was able to induce significantly more GFP induction from SOS-R4 recipient cells in the bystander assay than the no prodrug control (**Figure 6.4**, $p = 0.05$; in a one-way repeated measures ANOVA with Tukey's post-hoc test). This was a small improvement over the mustard prodrugs 40 μM PR-104A and 50 μM SN27686 but was still substantially less than that previously observed with either 50 μM CB1954 or 1 μM nitro-CBI-DEI as reported in Chapter 3 and published in Chan-Hyams et al. (2018).

At 25 μM SN36506 was unable to generate a bystander effect. At the higher concentration of 50 μM SN36506 there was no observable bystander effect even though growth inhibition values were still within the acceptable range (**Figure 6.4**) (<20% growth inhibition of challenged cultures compared to unchallenged controls was not exceeded).

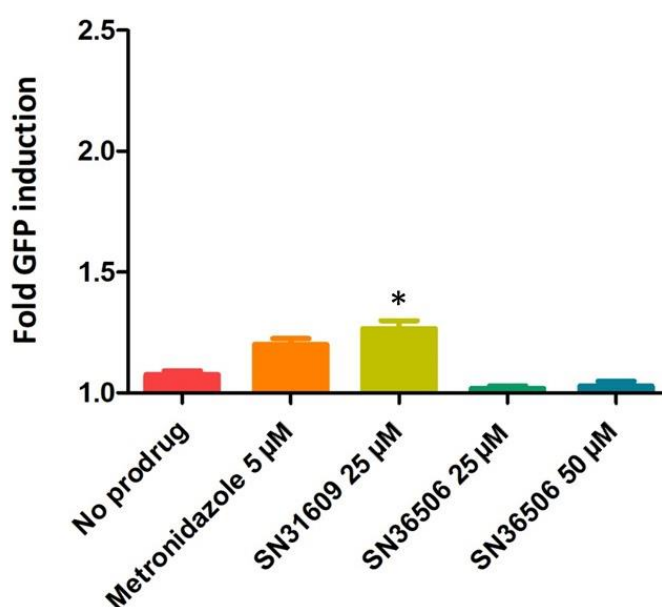


Figure 6.4. Microplate assay of the SOS response induced by transfer of activated prodrug metabolites from *nfsA*-expressing 7NT activator cells to nitroreductase null SOS-R4 reporter cells using alternative next generation prodrugs. 50:50 mixed cultures of *nfsA*-expressing 7NT activator cells and SOS-R4 recipients were incubated with either no prodrug, 5 μM metronidazole, 25 μM SN31609, 25 μM SN36506 or 50 μM SN36506 for 3.5 h, at which point GFP fluorescence (excitation 490 nm/emission 530 nm) was measured. The bacterial bystander effect was measured by the fold increase in GFP expression of the test condition over the control condition. Three biological replicates were performed each comprising eight technical replicates for test and control conditions. Error bars represent standard deviation of the average fold increase in GFP induction across the three biological replicates. *** indicates $p < 0.001$ (one-way repeated measures ANOVA with Tukey's post-hoc test) relative to no prodrug control.

6.5.2 Activator strain with functional TolC efflux pump

At this point I also sought to investigate the influence of a functional efflux pump on the bystander effect of the mustard prodrugs. The TolC efflux pump transports molecules across the outer membrane and is involved in the export of antibiotics, bile salts and organic solvents (Sulavik et al., 2001). To develop effective bacterial screening strains, for nitroreductase directed evolution, the *tolC* efflux pump gene was eliminated from *E. coli*; enhancing screening sensitivity by reducing the ejection of the active drug metabolite from the bacteria (Prosser et al., 2013). We theorized that this may inhibit the bystander effect by limiting the transport of the cytotoxic drug metabolite out of the activators. To investigate this possibility, I performed the bacterial bystander effect assay (2.12.1) with the *tolC* competent 7KO strain (otherwise isogenic with 7NT) as activators and SOS-R4 recipients in 1:1 ratio of activators to recipients in a microtitre plate. The 7KO activator strain was transformed with pUCX expressing *E. coli nfsA* which has ampicillin antibiotic resistance as well as an empty pCDF duet plasmid to provide spectinomycin antibiotic resistance equivalent to that of the SOS-R4 recipients. Thus, by expressing plasmids with the same antibiotic resistance genes that two strains could be co-cultured as in section 3.3.2.

6.5.2.1 Retesting PR-104A and analogues with a *tolC* expressing activator strain

At the same mustard prodrug concentrations found to be optimal for the previous assays, i.e., 40 μ M PR-104A, 50 μ M SN27686 or 50 μ M SNS36506 and 25 μ M SN31609, I did not observe a significant bystander effect in the presence of the *tolC* competent 7KO activators (**Figure 6.5**). Furthermore, at a higher concentration of 100 μ M PR-104A, SN27686 and SN31609 did not induce a significant bacterial bystander effect (**Figure 6.5**).

Evidently the potential for increased transport of the activated drugs did not compensate for the lowering of intracellular prodrug levels via the action of the TolC efflux pump. It is likely that insufficient activated drug was generated in the assay to generate a significant outcome for any compound. Notably at the higher concentration of 100 μ M, for any of the four prodrugs tested, growth inhibition was still within acceptable parameters for 7KO activator cells (<20% growth inhibition of challenged cultures compared to unchallenged controls was not exceeded). In comparison using 7NT activator cells, in the bacterial

bystander effect assay, a concentration of 100 μM resulted unacceptable levels of growth inhibition that interfered with the accuracy of the bacterial bystander effect assay.

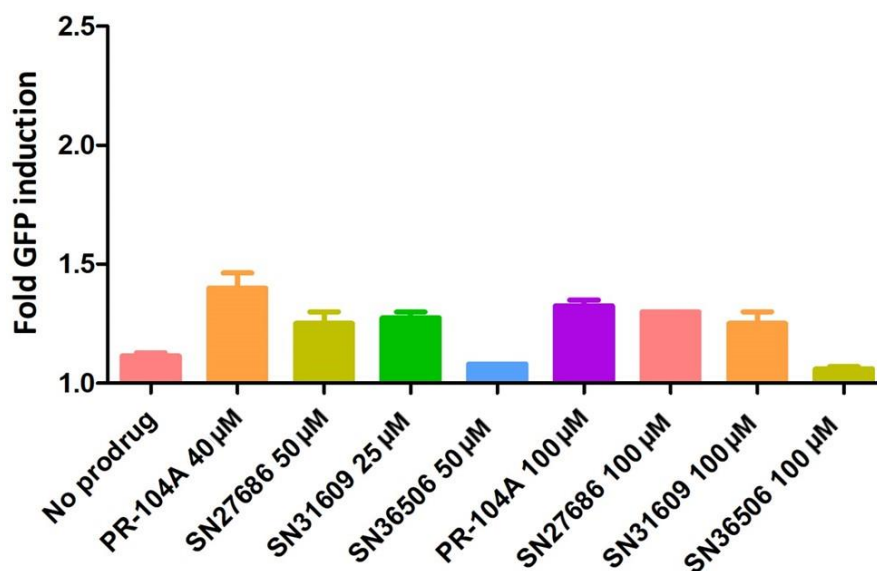


Figure 6.5 Microplate assay of SOS response induced by transfer of activated prodrug metabolites from *nfsA*-expressing 7KO activator cells to nitroreductase null SOS-R4 reporter cells using next generation prodrugs. 50:50 mixed cultures of *nfsA*-expressing 7KO activator cells and SOS-R4 recipients were incubated with either no prodrug, 40 μM PR-104A, 50 μM SN27686, 25 μM SN31609 50 μM SN36506, 100 μM PR-104A, SN27686, SN31609 and SN36506 for 3.5 h, at which point GFP fluorescence (excitation 490 nm/emission 530 nm) was measured. The bacterial bystander effect was measured by the fold increase in GFP expression of the test condition over the control condition. Three biological replicates were performed each comprising eight technical replicates for test and control conditions. Error bars represent standard deviation of the average fold increase in GFP induction across the three biological replicates. In a one-way repeated measures ANOVA with Tukey's post-hoc test the GFP signal was not significant under any of these prodrug conditions.

6.5.2.2 Retesting CB1954 and nitro-CBI-DEI with a *tolC* functional activator strain

Out of interest I also tested the bacterial bystander effect of 50 μM CB1954 as well as 1 μM nitro-CBI-DEI with the *tolC* competent 7KO activators. I observed no bystander effect at 1 μM or 5 μM nitro-CBI-DEI. At 10 μM nitro-CBI-DEI I observed a significant bystander effect with a modest *p* value of 0.05 (one-way repeated measures ANOVA with Tukey's post-hoc test). However, 50 μM CB1954 produced a significant bystander effect similar to that induced with 7NT activators with a *p* value of 0.001 (**Figure 6.6**). At these selected concentrations growth inhibition was still within acceptable parameters (<20% growth inhibition of challenged cultures compared to unchallenged controls was not exceeded).

Overall, this suggests that the nitro-CBI-DEI may be actively effluxed by TolC in the 7KO activators before reduction to the active metabolite can take place. This is consistent with a functional TolC efflux pump impairing the effectiveness of the bacterial bystander assay. In comparison, CB1954 was unaffected by the functional TolC efflux pump; consistent with previous observations by Prosser et al. (2013) that CB1954 is not a substrate for TolC, but that PR-104A is.

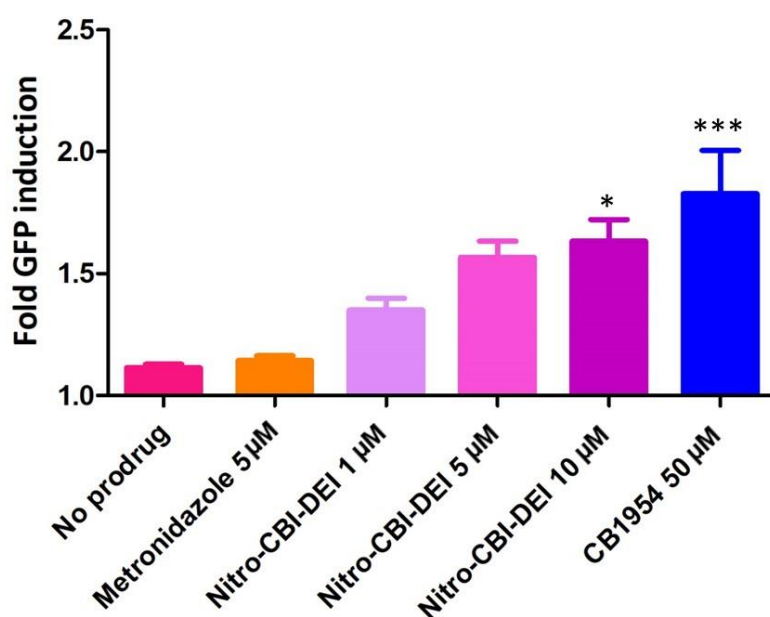


Figure 6.6 Microplate assay of SOS response induced by transfer of activated prodrug metabolites from *nfsA*-expressing 7KO activator cells to nitroreductase null *SOS-R4* reporter cells using prodrugs CB1954 and nitro-CBI-DEI. 50:50 mixed cultures of *nfsA*-expressing 7KO activator cells and *SOS-R4* recipients were incubated with either no prodrug 5 μ M metronidazole, 1 μ M, 5 μ M, 10 μ M nitro-CBI-DEI or 50 μ M CB1954 for 3.5 h, at which point GFP fluorescence (excitation 490 nm/emission 530 nm) was measured. The bacterial bystander effect was measured by the fold increase in GFP expression of the test condition over the control condition. Three biological replicates were performed each comprising eight technical replicates for test and control conditions. Error bars represent standard deviation of the average fold increase in GFP induction across the three biological replicates. *** indicates p value < 0.001, * indicates p < 0.05 (one-way repeated measures ANOVA with Tukey's post-hoc test) GFP signal is significant relative to the no prodrug control.

6.6 Discussion

6.6.1 Evaluation of PR-104A and SN36506 activity across a panel of nitroreductases

The results of this brief investigation into the activity of a select panel of promising nitroreductase candidates, with the prodrugs PR-104A and SN36506, provided data that informed the selection of nitroreductase candidates for future directed evolution campaigns for the CDEPT collaboration. As shown by Prosser et al. (2013) the enzymes belonging to NfsA nitroreductase family outperformed those of the NfsB family in both IC₅₀ assays with PR-104A and *in vitro* enzyme activity. The NfsA enzymes NfrA_Bs, NfsA_Ec, NfsA_Es all produced similarly high k_{cat}/K_m values and low IC₅₀ values. The most outstanding candidate was YcnD_Bs, which displayed the highest k_{cat}/K_m and an IC₅₀ value similar to that of NfrA_Bs, NfsA_Ec, and NfsA_Es.

Subsequent to the work of Prosser et al. (2013) a directed evolution campaign to improve the activity of NfsA_Ec with PR-104A was successfully performed and published by Copp et al. (2017). The top variant identified for PR-104A activity, by Copp et al. (2017), was variant no. 22, which deviated from wild-type NfsA_Ec by five mutations (S41Y/E99G/L103M/R225P/F227S). When screened by PR-104A growth inhibition, variant no. 22 possessed an IC₅₀ of $136 \pm 2 \mu\text{M}$ PR-104A. This was a significant 3.8-fold improvement ($p = 0.006$; Student's t test) in PR-104A sensitivity over *E. coli* cells expressing the wild-type progenitor NfsA_Ec, and also a substantial improvement over any of the nitroreductases evaluated here.

YcnD_Bs has also been the focus of directed evolution campaigns, including improving activity with the PET imaging probe SN33623 (Rich 2017). Although the *ycnD* gene does not appear to express well in *C. sporogenes*, it is possible that it would be a good candidate for directed evolution to improve activity with next-generation mustard prodrugs for other systems. Likewise, NfsA_Bs and NfsA_Es could be considered in directed evolution campaigns for improved activity with PR-104A.

In terms of NfsB nitroreductases the NfsB_Vv F70A/F108Y variant was of particular interest as it displayed the highest catalytic efficiency with PR-104A reported thus far. It also had a ten-fold improvement over its wild type, despite not having been engineered specifically for this activity. As yet, an NfsB_Vv variant library has not been explored for

PR-104A activity. As NfsB_Vv has been successfully expressed in *C. sporogenes*, this was a finding of particular interest to the CDEPT collaboration, as was the relative proficiency of this NfsB family variant with SN36506. At last update, this was one of the priority nitroreductase variants being progressed for further testing in the *C. sporogenes* background.

Overall, the enzymes belonging to the NfsA nitroreductase family outperformed those of the NfsB family in both IC₅₀ assays and kinetic analysis with SN36506. None of the thirteen enzyme examined by IC₅₀ assay displayed any stand-out activity with SN36506. Although NfrA_Bs displayed a high level of catalytic potential in the enzyme kinetics analysis, some caution around this finding may be merited given the finding is driven by a very low K_m that is likely to be hard to measure accurately, and that NfrA_Bs was less active than several other nitroreductases in the IC₅₀ assays.

Of the NfsB enzymes successfully expressed in *C. sporogenes* only the NfsB_Vv F70A/F108Y variant displayed any measureable activity with SN36506 in steady state enzyme kinetics assays. The NfsB_Vv F70A/F108Y variant with SN36506 exceeded that of the progenitor which displayed only trace activity. Moreover, NfsB_Vv and the NfsB_Vv F70A/F108Y variant were the only NfsB family members to have an IC₅₀ value less than 1000 μ M SN36506.

Ultimately, these results paired with the successful expression of the NfsB_Vv F70A/F108Y variant by *C. sporogenes* supported the use of the NfsB_Vv F70A/F108Y variant as a starting point for directed evolution with SN36506 for the CDEPT collaboration. The subsequent directed evolution campaign was performed by Dr Sharrock in the Ackerley laboratory and was published in Sharrock (2019).

Dr Sharrock generated a site saturation mutagenesis library of the NfsB_Vv F70A/F108Y protein that targeted five amino acid positions; S40, V41, N71, E72 and F124. These residues were chosen based on their position relative to the active site, activity assays that had identified residues in NfsB_Ec for activity with the imaging agent SN33623 performed by previous members of the Ackerley Laboratory, and residues in other NfsB family enzymes that had been identified as affecting activity with dinitrobenzamide prodrugs similar in structure to SN36506 (Jaberipour et al., 2010). Ultimately, the most

active variant Dr Sharrock recovered was 1.2 fold improved over the starting NfsB_Vv F70A/F108Y template, and possessed the additional mutations S40A/F41T/N71Q/F124V (Sharrock, 2019).

The research described in this chapter also reinforced the importance of standardizing purification methods when aiming to compare kinetic parameters of different enzymes with a prodrug. In the future the French Press method with a larger volume of protein expression culture and longer incubation time should be used as the standard method of protein purification for all enzymes being compared in a single investigation. This will accommodate those enzymes that typically produce low protein yields even when comparing it to those enzymes that do typically express well in *E. coli* hosts.

I also recognize that activity with a prodrug such as PR-104A is not predictive of equivalent activity with another derived analogue SN36506. However, IC₅₀ assays and *in vitro* enzymatic activity can potentially be used as general indicators of potential activity with prodrugs of similar base structure. These measurements of activity may provide rational starting points for further investigation as new prodrugs become available in the field of GDEPT.

6.6.2 Bacterial bystander effect assays with next generation prodrugs using activator strains that express a functional TolC efflux pump

Use of an activator strain expressing a *tolC* efflux pump gene did not improve the bystander effects of the prodrug analogues PR-104A, SN27686 and SN31609. Even when re-tested at a higher concentration of 100 μ M, none were able to induce a significant bacterial bystander effect. It is likely that the functional TolC efflux pump in the *tolC*-intact 7KO activator strain caused more of the unreduced prodrug to be ejected from the activator cells before it could be activated. This is supported by growth inhibition being within acceptable parameters even at higher prodrug concentrations with 7KO cells compared to 7NT cells. Consistent with this the prodrug nitro-CBI-DEI also exhibited a decreased bacterial bystander effect with 7KO activators compared to 7NT activators. Only by raising the concentration of nitro-CBI-DEI ten-fold was I able to detect a bacterial bystander effect in this system.

The results of the using a Tolc functional efflux pump, in the activator strain of my bystander effect assay, suggest that when designing a bacterial vector for BDEPT that the choice to maintain or knock out efflux pumps must be considered in relation to the prodrug and efficiency of the activating enzyme. Whether or not the prodrug is a substrate for particular bacterial efflux pumps and the speed at which the prodrug can be activated by the prodrug-activating enzyme will influence the bystander effect potential of the therapy. This is especially likely to be true for *Salmonella* BDEPT vectors, which share a highly conserved TolC efflux machinery to that present in *E. coli*. For example, alignment of the *E. coli* and *Salmonella enteritidis tolC* efflux pump genes (accession numbers HQ833340.1 and U25178.1 respectively) that indicated an 84% shared sequence identity.

7 Key findings, conclusions and future directions

7.1 Research motivation

The research performed and presented in this thesis sought to achieve further understanding of the bystander effect in BDEPT. Prior to this research, there was no suitable model for measuring the ability of activated genotoxic prodrug metabolites to exit a bacterial vector and enter surrounding cells.

Previous models exclusively focused on the bystander effect as it occurs during VDEPT (**Figure 1.10**). The bystander effect of multiple prodrugs has been evaluated in a mixed multilayer carcinoma cell model (Wilson et al., 2002). This particular model compares the survival of untransduced cancer cells (target cells) in the presence or absence of nitroreductase-expressing cancer cells (activator cells). The multilayer model simulates tissue-like cell densities and can explicitly test the ability of prodrug metabolites to diffuse through tumour tissue. Likewise, in VDEPT the bystander effect occurs when the prodrug is activated inside transfected cancer cells and is then transported into neighbouring untransfected cancer cells.

The bystander effect is critical to the success of both VDEPT and BDEPT. VDEPT is typically limited by low viral transfection rates of the target tumour. This can be overcome by a high bystander effect that disseminates the genotoxin beyond the cancer cells transfected by the virus. The bystander effect similarly augments the therapeutic effect of BDEPT. The bystander effect ensures that the genotoxin is accessible to the cancer cells adjacent to the bacteria as well as neighbouring cancer cells.

However, a key difference is that whereas nil-bystander prodrugs such as metronidazole have been considered to still have potential value for VDEPT (Hunt et al., 2012), for BDEPT to achieve any therapeutic outcome it is essential that the activated genotoxin exits the bacterial vector to access the target cancer cells. The prodrugs utilized in nitroreductase GDEPT are cytotoxic to both cancer cells and bacterial cells once they are activated to a toxic state; as the active metabolites are effective at cross-linking carcinoma cell DNA and bacterial DNA. Hence the bacterial vector itself is susceptible to the genotoxic effect of the activated prodrug. As such, a poor bystander effect during BDEPT may result in the sterilization of the bacteria.

Lipophilicity accounts for >80% of nitroaromatic prodrug variance in the bystander effect in the multilayer carcinoma model (Wilson et al., 2002). Improved lipophilicity facilitates transport across cell membranes. A poor bystander effect is therefore caused by low lipophilicity of the prodrug and /or the active drug metabolite. Next-generation prodrugs have been designed to maximise lipophilicity post-reduction to facilitate their transport outside of the bacterial vector in BDEPT but also their transport out of transfected cancer cells in VDEPT. In contrast, it was observed here that the bystander effect during BDEPT may be strongly influenced by the ability of the bacterial vector to actively transport the cytotoxic metabolites out of itself via transmembrane pumps such as TolC.

Many prodrugs have demonstrated promising genotoxicity via *in vivo* and *in vitro* models of VDEPT but have yet to be considered for BDEPT. To advance BDEPT, a method to measure a bystander effect from a bacterial vector is necessary. Such a method could reanalyse prodrugs that have already been clinically advanced for VDEPT or have a high bystander effect in VDEPT models. This was the motivation for developing a bacterial bystander effect assay in the research performed and presented here.

Furthermore, the Ackerley laboratory was interested in the potential impact of the bacterial bystander effect on certain directed evolution screening strategies. These screening strategies were designed to select nitroreductase variants that are most efficient at activating prodrugs for GDEPT. Specialized *E. coli* screening strains were purpose-built for these screening strategies by previous members of the Ackerley laboratory. It was originally hypothesised that this approach might be confounded by high-bystander prodrugs causing activation of the SOS response in *E. coli* cells that do not themselves express an effective nitroreductase variant.

The first objective of this research was to investigate the bacterial bystander effect by developing a robust *in vitro* assay using bacteria expressing a prodrug activating enzyme. The second objective was to measure the bacterial bystander effect of a panel of clinically relevant prodrugs. A third objective was to investigate the influence of the bacterial bystander effect on the efficiency of directed evolution strategies using bacterial screening strains. Subsequent objectives of engineering superior NfsA_Ec variants for CB1954 activation and evaluating a panel of promising nitroreductase variants for their BDEPT potential presented themselves as the work progressed.

7.2 Summary of key findings

7.2.1 Evaluating the abilities of diverse nitroaromatic prodrug metabolites to exit a model Gram-negative vector for bacterial-directed enzyme-prodrug therapy

I developed a robust and sensitive method for measuring the bacterial bystander effect in a microplate based assay that was validated by flow cytometry. To model cell-to-cell transfer of activated prodrug metabolites during BDEPT I grew two *E. coli* strains in co-culture; a non-fluorescent *E. coli* activator strain expressing the nitroreductase *E. coli* NfsA and an *E. coli* reporter strain containing an SOS-GFP DNA damage responsive gene construct.

In this model the reporter strain is acting as a target cell for the genotoxin to affect. Induction of GFP by the active prodrug metabolites can only occur following their transfer from the activator to the reporter cells i.e. via the bystander effect. I showed that this assay is sensitive, and initially used it to investigate five clinically relevant prodrugs: metronidazole, CB1954, nitro-CBI-DEI, and two dinitrobenzamide mustard prodrug analogues, PR-104A and SN27686, in both a microplate and flow cytometry assay format. Consistent with the bystander efficiencies previously measured in human cell multilayers, reduced metronidazole exhibited little bacterial cell-to-cell transfer, whereas the active metabolites of nitro-CBI-DEI were passed very efficiently from activator to reporter cells post-reduction. However, in contrast with observations in human cell multilayers, as described in Table 1.1 Summary of Bystander Effect Efficiency (BEE) experiments in the multilayer carcinoma model and the relevant prodrug, the nitrogen mustard prodrug metabolites were not effectively passed between the two bacterial strains, whereas reduced CB1954 was transferred efficiently.

Using nitroreductase enzymes that exhibit different biases for the 2-nitro versus 4-nitro substituents of CB1954, I further showed that the 2-nitro reduction products (NfsA-activated) exhibit substantially higher levels of bacterial cell-to-cell transfer than the 4-nitro reduction products (YfkO-activated). These results were consistent with the relative bystander efficiencies of the 2-NO₂ versus 4-NO₂ metabolites in human cell culture (Helsby et al., 2004).

Another surprising result was that the high levels of cell-to-cell transfer for 2-nitro reduced CB1954 approached that of reduced nitro-CBI-DEI. This was unexpected as the prodrug nitro-CBI-DEI has the highest published bystander effect in a three dimensional mixed cell cultures model of VDEPT (Green, Syddall, et al., 2013). In comparison CB1954 exhibited only a weak bystander effect in human multicellular layers when activated by NfsB (Wilson et al., 2002).

CB1954 is a relatively old prodrug that has undergone an immense amount of pre-clinical development for various types of GDEPT that can be leveraged specifically for BDEPT. Given my discovery that CB1954 generates a high bacterial bystander effect, rivalling the maximum achieved in a VDEPT model, CB1954 may be a more effective prodrug for BDEPT applications than it has previously indicated in clinical VDEPT trials (Chung-Faye et al., 2001; Patel et al., 2009). In particular BDEPT strategies employing Gram-negative vectors, such as *E. coli*, warrant further investigation.

7.2.2 Assessing the impact of the bystander effect on directed evolution of nitroreductases using a SOS-GFP screening strain

FACS can isolate the most efficient nitroreductase variants from a variant library of nitroreductase enzymes expressed in SOS-R4 cells. FACS employs fluorescence-based selection gates to segregate the most fluorescent clones for further analysis. Notionally, these highly fluorescent clones express nitroreductase variants that are efficient at reducing the target prodrug to a DNA-damaging genotoxin. However, the bacterial bystander effect assay demonstrated that activated prodrug metabolites can be transferred between *E. coli* cells and cause DNA damage in SOS-R4 cells not expressing a nitroreductase.

To investigate whether this bystander effect might confound selection of the most active variants, I designed a bystander and a null bystander treatment of a model nitroreductase variant library. The model library consisted of two fluorescent screening strains; SOS-R4 activator cells that express a nitroreductase and SOS-R4 recipient cells that do not express a nitroreductase. The two strains were either co-cultured under a prodrug selection pressure together (bystander condition) or placed under selection pressure separately (null bystander condition) and subsequently subjected to FACS. I predicted that if the bystander effect impairs FACS enrichment, then significantly fewer nitroreductase-

expressing cells would be yielded from the bystander condition compared to the null bystander condition.

I observed that significantly fewer *nfsA*-expressing cells were recovered from FACS when using CB1954 and nitro-CBI-DEI under the bystander condition compared to the null bystander condition. This was consistent with the high bacterial bystander effect observed in the bacterial bystander effect assay of these two prodrugs. I also observed that prodrugs CB1954 and nitro-CBI-DEI induced an SOS response to such a high extent that the fluorescence profile of the recipients was raised above the lower threshold of the selection gate. This resulted in the collection of false positives i.e. SOS-R4 recipients. The bystander effect diminished effective nitroreductase library enrichment by FACS using these two prodrugs.

The mustard prodrugs PR-104A and SN27686 did not yield significantly lower proportions of *nfsA*-expressing cells under bystander conditions at the preferred 10 μ M challenge concentrations. This was not unexpected as at this concentration I did not previously observe a significant bystander effect in the bacterial bystander effect assay. However, SN27686 did yield significantly fewer *nfsA*-expressing cells recovered from FACS when a 50 μ M challenge concentration was applied. This appears to have been an artefact of the higher stringency of the fluorescence selection gate during FACS with 50 μ M SN27686 compared to the other prodrug conditions tested.

This investigation offered insight into optimizing FACS for a range of clinically relevant nitroaromatic prodrugs. The results indicated that FACS enrichment of nitroreductase enzymes with activity for high-bystander effect drugs is diminished by the bacterial bystander effect.

7.2.3 Comparing a manual pre-selection method to FACS for recovery of *E. coli* NfsA variants improved in CB1954 activation

This research continued the investigation into the influence of the bystander effect on FACS. I compared the evolutionary outcomes arising from screening a nitroreductase variant library using the automated FACS approach, in which the bystander effect can occur, in parallel to a manual pre-selection method of individual clones during which the bystander effect has no opportunity to occur.

The prodrug CB1954 was selected for this study, prompted by my surprising discovery that it exhibited a high bacterial bystander effect following NfsA-mediated activation. As such, I chose to use a large *nfsA* nitroreductase variant library “7SM”; a site directed mutagenesis library derived from *E. coli nfsA* that was already available in the Ackerley lab, having been created by previous postdoctoral fellows.

For the pre-selection strategy I used the positive selection compounds niclosamide and chloramphenicol which can be detoxified by nitro-reduction. Pre-selection, on supplemented solid medium, eliminates inactive nitroreductase variants from a mutant library thereby reducing the size of the variant library to be screened for activity with a specific substrate. Colonies of *E. coli* cells expressing the 7SM library were grown in the presence of niclosamide or chloramphenicol. I then tested individual variants for activity with CB1954. In parallel, I performed a single FACS procedure on SOS-R4 cells expressing the 7SM library that had been challenged with CB1954. I analysed the variants captured by these two different strategies for their abilities to sensitise their *E. coli* host cells to CB1954.

Despite the strong bacterial bystander effect exhibited by NfsA-reduced CB1954, the FACS strategy yielded a higher proportion of clones exhibiting enhanced CB1954 sensitivity. However, no outstanding variants were identified from either of the screening approaches after a single round of directed evolution. The most improved variant from the FACS screening approach was 3.2C. This was 1.7-fold more active more active with CB1954 than the wild-type progenitor in by IC₅₀ assay. Enzyme kinetic analysis demonstrated that this advanced activity with CB1954 was not maintained once the enzyme was isolated from the cell. The frequency of substitution to alternative amino acids, based on chemical characteristics, did not reveal any distinct evolutionary patterns in either screening approach.

We considered that the FACS-selected NfsA variants may have switched their nitro-reducing specificity from the 2-NO₂ to the 4-NO₂ substituent of CB1954, and that FACS selection may have been biased toward selection of clones where the bystander effect was diminished. However, although HPLC profiles of the reduced metabolites, produced by the top five variants recovered from each strategy, showed that it was possible for a

variant to gain the ability to convert a small portion of CB1954 to the 4-NHOH metabolite, the major end-metabolite in every case was still 2-NHOH.

Overall the results of this investigation were inconclusive after just a single round of directed evolution, but there is some evidence that the FACS strategy was more effective than niclosamide/chloramphenicol pre-selection in enriching for superior CB1954-reducing variants. Overall, there were slightly more variants derived from FACS screening that demonstrated improved activity with CB1954 compared to the wild-type NfsA in IC₅₀ assays.

7.2.4 Evaluating a panel of nitroreductases for potential applications in *Clostridia*-directed Enzyme Prodrug Therapy

This investigation contributed to a collaborative research effort between the Ackerley laboratory, the ACSRC and researchers at the Universities of Nottingham and Maastricht, seeking to advance *Clostridia*-directed enzyme prodrug therapy (CDEPT) towards a human clinical trial.

This short project identified the most promising wild-type bacterial nitroreductase enzymes from a panel of candidates with the two next generation prodrugs PR-104A and SN36506, under consideration for the human clinical trial, via *in vitro* purified protein kinetics and IC₅₀ assays. The panel of nitroreductases was selected based on the successful expression of several NfsB nitroreductases in *C. sporogenes* and the demonstrated *in vitro* activity of NfsA nitroreductases and select NfsB variants with similar prodrugs.

The enzymes belonging to NfsA nitroreductase family outperformed those of the NfsB family in both IC₅₀ assays and *in vitro* kinetics assays with PR-104A. The most outstanding candidate was *Bacillus licheniformis* YcnD which displayed the highest k_{cat}/K_m and a low IC₅₀ value.

The *Vibrio vulnificus* NfsB F70A/F108Y variant is of particular interest as it displayed the highest catalytic efficiency with PR-104A reported thus far compared to any other nitroreductase. It also had a ten-fold improvement over its wild type. As yet, a *V. vulnificus* NfsB variant library has not been explored for PR-104A activity, however my results suggest that this might be a worthwhile line of enquiry.

Compared to the activity with PR-104A, kinetic parameters for enzymes in the panel were considerably lower with SN36506. The enzymes belonging to the NfsA nitroreductase family generally outperformed those of the NfsB family in both IC₅₀ assays and *in vitro* enzyme activity (**Table 6.5**). None of the thirteen enzyme examined by IC₅₀ assay displayed any stand-out activity; the top performing nitroreductase with SN36506, by IC₅₀ assay, was YcnD_Bs with an IC₅₀ of 600± 45 μM SN36506. *V. vulnificus* NfsB and the *V. vulnificus* NfsB F70A/F108Y variant were the only NfsB family members to produce IC₅₀ values approaching those of the NfsA family members. In contrast, the IC₅₀ value of *V. vulnificus* NfsB was 670±140 μM SN36506, and *V. vulnificus* NfsB F70A/F108Y produced a poorer IC₅₀ value of 800± 6 μM SN36506. However, of the NfsB enzymes only the *V. vulnificus* NfsB F70A/F108Y variant displayed any activity with SN36506 at the purified protein level. The *V. vulnificus* NfsB progenitor displayed only trace activity.

These results guided the subsequent selection of *V. vulnificus* NfsB F70A/F108Y variant as a starting point for directed evolution with SN36506 for the CDEPT collaboration; which was performed by Dr Sharrock in the Ackerley laboratory. The most active variant was 1.2 fold improved in IC₅₀ over the starting variant (Sharrock, 2019). As the *V. vulnificus* NfsB F70A/F108Y variant has since been successfully expressed in *C. sporogenes* by our collaborators, this new variant may also offer promise for CDEPT.

As a continuation of my research into the bacterial bystander effect, I investigated the bystander effect potential of alternative next generation prodrugs, including SN36506 and other PR-104A analogues, using my microplate based bacterial bystander effect assay. None of the PR-104A analogues including SN36506 displayed a significant bacterial bystander effect from *E. coli* 7NT activator cells. This same panel of SN36506 and PR-104A analogues was then used in a modified bacterial bystander effect assay using activator cells (7KO) that possessed a functional TolC efflux pump. The presence of this pump did not increase the bacterial bystander effect of the PR-104A analogue prodrugs. However, I went on to make the interesting discovery that the prodrug nitro-CBI-DEI displayed a decreased bacterial bystander effect when using activator cells that possessed a functional TolC efflux pump, whereas CB1954 was unaffected by TolC. Overall, a consistent message from my research is the importance of evaluating enzyme-prodrug pairings in models that bear precise relevance to their intended GDEPT vector.

7.3 Critical evaluations of methods used in this research

7.3.1 Development of the bacterial bystander model

Overall, a moderate interpretation of this data must be taken in the context of the assay design. In this particular assay design, the specialized *E. coli* screening strain SOS-R4 was not sensitive enough to detect a bacterial bystander effect signal above the background fluorescence, experienced by the cells in the absence of a nitroreductase, at lower concentrations of the mustard prodrugs PR-104A and SN27686. In future, more sensitive *E. coli* strains might be developed for a bystander effect assay and may consider the role of multi-drug efflux pumps as well as the efficacy of the prodrug activating enzyme.

The current bacterial bystander effect model employs a large liquid to cell volume ratio, which likely does not adequately simulate the proximity of bacterial vectors to cancer cells in clinical BDEPT. An ideal *in vitro* model of BDEPT would involve co-incubation of bacterial vectors with human carcinoma cells. However, studying the effects of prodrug activation by bacterial activator cells in co-culture with target carcinoma cells is confounded by the naturally oncolytic nature of bacteria.

Exploration of and development of such a model by the Ackerley laboratory was further prohibited by the use of communal cell culture facilities. Purposefully infecting carcinoma cultures with an active bacterial strain would have placed undue risk of contamination on the work of other researchers using the facilities.

We considered the use of attenuated bacterial vectors in an *in vitro* model of BDEPT. In this scenario, a bacterial strain expressing the prodrug activating enzyme would be incubated with a prodrug and then attenuated by a method such as heat inactivation. The attenuated bacteria could then be used in a communal cell culture facility with a lower risk of cross-contamination. The attenuated bacteria could be co-incubated with human carcinoma cells which report on receipt of the active genotoxic drug. A major drawback of this model is that the bystander effect would exclusively occur by passive diffusion out of the bacteria. Attenuation of the bacteria would prevent active transport for instance by drug efflux pumps. Therefore this model would also not be an accurate simulation of the bacterial bystander effect. Furthermore, heat treatment may have resulted

confounding factors such as increased production of extracellular vesicles that can influence the bystander effect (Bewicke-Copley et al., 2017).

Obviously, an *in vivo* test of the bacterial bystander effect of a prodrug is the most accurate measurement possible for a BDEPT medicament. In such an animal cancer model, bacterial vectors expressing the prodrug activating enzyme are administered intravenously, the prodrug is then administered and the tumour-site is monitored for regression (Heap et al., 2014). Although *in vivo* models are critical to the advance of a BDEPT medicament, these types of experiments are resource demanding in time, money and prodrug. Models to quickly assess the potential bacterial bystander effect can guide precise prodrug design in the context of BDEPT before testing *in vivo*. Assessing the bystander effect in an *in vivo* microtitre assay is parsimonious with a limited supply of developmental prodrugs. It can also potentially compare an array of analogues of a prodrug in a context relevant to the intended vector.

The *in vitro* model I developed is robust and easily implemented, and importantly it does inform on the relative abilities of prodrug metabolites to exit Gram-negative bacterial activator cells. As a microtitre assay it consumes less prodrug than a human carcinoma cell models.

To address the concern that the genotoxin product of prodrug activation might be inactivated in the liquid culture before it penetrates the reporter cells, I developed an assay that demonstrated addition of prodrug metabolites, pre-activated by a purified nitroreductase, resulted in the transfer of the pre-activated prodrug metabolite from the surrounding medium into the SOS-R4 recipients. This transfer was detected by the fold increase in GFP expression relative to an unchallenged control condition. Evidently, the small panel of prodrug metabolites tested were not highly unstable or completely neutralised by components of the culture and successfully penetrated the SOS-R4 recipient cells.

It is also possible that toxicity of GFP to *E. coli* may have negatively influenced the accuracy of the bacterial bystander effect assay. Previous studies have noted the toxic effects of wild-type GFP aggregate bodies in *E. coli* due to poor protein solubility (Cormack et al., 1996; Cramer et al., 1996). In our lab, Dr Rich showed that the background levels of GFP

were found to contribute to growth inhibition of *E. coli* when exposed to lethal concentrations of nitroaromatic compounds (Rich, 2017). Thus, background levels of GFP can confound the results of SOS-R4 selective screening assays – we have previously observed that once cell death is initiated, the level of detectable SOS signal diminishes. Dr Rich suggested alternative fluorescent reporter proteins that do not have a cytotoxic effect in *E. coli* for use in a screening strain like SOS-R4. Fluorescent proteins that are excited at longer wavelengths than those required for the detection of GFP, are of particular interest as this would limit background signal due to *E. coli* autofluorescence.

Ideally, the bacterial bystander effect assay would have been performed with an optimized reporter strain that expresses an alternative fluorescent protein that is not toxic to *E. coli*. This may have resulted in a more accurate assessment of the bystander effect or at least a more sensitive assay. Yet a pragmatic approach was taken, and the current bystander effect assay using a SOS-GFP reporter was proven to detect relative bystander effects between different prodrugs.

7.3.2 Investigating the effect of the bacterial bystander effect on FACS selection efficiency

Although this work was able to compare the effects of different prodrugs on the proportion of *nfsA*-expressing cells recovered, a concern was that no strong enrichment of *nfsA*-expressing cells was observed using any prodrug, contrasting with the previous observations of Copp et al. (2014) and Copp et al. (2017). A major reason for this appears to have been our selection of an empty plasmid control for the null nitroreductase strain, rather than a strain expressing an inactive nitroreductase at high levels, as was utilised by Copp et al. (2014).

Competition assays comparing our *nfsA*-expressing activator strain to the null nitroreductase strain revealed that the latter had a significant growth advantage in unamended medium that contained no prodrug. It is likely that this growth advantage would have been exaggerated under prodrug challenge conditions; wherein the *nfsA*-expressing activator strain would have suffered higher levels of prodrug-mediated damage that would only exacerbate a growth disadvantage.

In a genuine FACS procedure, for a directed evolution campaign, the collection gates are set based on the activation of the target prodrug with the wild-type enzyme progenitor of the variant library. However, setting very strict collection gates may exclude the recipient cells altogether and thereby limit the influence of the bystander effect on FACS.

Conversely, setting the collection gates too strictly may also result in poor recovery of cells post-FACS due to excessive DNA damage by prodrug activation. GFP is inherently toxic to the SOS-R4 screening strain and thus influences the recovery of cells post-FACS collection (Rich, 2017). SOS-R4 expressing the most efficient nitroreductase variants may experience a high level of GFP toxicity as well as prodrug induced genotoxicity and may not recover post FACS. I observed that less than 25% of the individual cells collected into a microplate by FACS were able to recover post-FACS under any prodrug condition.

With hindsight, this investigation would ideally be re-performed using a model library where all the cells express a catalytically active versus a catalytically inactive nitroreductase variant in conjunction with a non-toxic DNA damage reporter protein. The limited availability of the mustard prodrugs and nitro-CBI-DEI, as well as the high cost of FACS equipment hire from the Malaghan Institute of Medical Research, made this undesirable during the timeframe of my project.

To optimize FACS as a screening strategy a balance must be achieved between choosing high enough prodrug concentrations, which induce a stringent selection pressure to generate satisfactory library enrichment, versus low enough prodrug concentrations where the *E. coli* hosts expressing the most efficient nitroreductase variants can recover post-FACS. Perhaps challenging a nitroreductase library at a very low prodrug concentration and then using very restrictive fluorescence selection gates may aid the recovery of cells expressing highly efficient nitroreductases.

It would be also interesting to assess in a genuine nitroreductase variant library, whether the non-functional variants possess a significant growth advantage over cells expressing functional nitroreductases in the cultures prior to prodrug challenge in the FACS procedure. This may be a further confounding factor of using FACS as a screening strategy. Unfortunately there are not any obvious safeguards that one could take to ameliorate growth competition between different variants in a genuine nitroreductase library

without introducing further steps of preparation. Liquid culture with pre-screening supplements such as niclosamide or chloramphenicol could remove non-functional nitroreductase variants from the library prior to starting a FACS procedure. However, it must be considered that such an approach has potential to eliminate variants that are active with the desired prodrug substrate, but inactive with niclosamide or chloramphenicol.

7.3.3 Comparing directed evolution outcomes using two different screening strategies: FACS and pre-selection

This thesis has identified potential flaws in two different directed evolution strategies that are commonly used in the Ackerley lab: 1) that pre-selection with positive selection compounds may miss variants that are active with the desired substrate but not the positive selection molecule; and 2) that FACS selection may be confounded by prodrug bystander and toxicity issues. I aimed to directly compare the two approaches. Ultimately, no clear “winner” was identified, however it is possible that further rounds of evolution may have identified one strategy as being generally superior.

After a single cycle of directed evolution, there was no detectable trend within or between the top twenty variants recovered from either selection approach. Further sequencing of a greater number of variants captured from each strategy may have revealed an evolutionary pattern. It was my intention to perform further cycles of directed evolution to detect any evolutionary patterns but this was inhibited by research time constraints and the expense of performing FACS.

Future investigation with FACS, CB1954 and the 7SM library would benefit from secondary screening methods. These methods could include those employed by Copp et al. (2014) who, after performing two FACS selections, was able to achieve a 90,000-fold enrichment of a functional prodrug-activating nitroreductase from a model library. This was done by collecting a tube of cells from FACS, as opposed to single cells in a microtitre plate, culturing of those variants together and then subjecting the culture to a secondary prodrug challenge and FACS. Of note Copp et al. (2014) did not perform mutagenesis between these two sequential FACS procedures.

A secondary round of FACS on the tubes collected in this investigation would have introduced another variable that would have made it difficult to compare to the pre-selection strategy in a meaningful manner. Furthermore, it may be relevant to note that the top five performing variants with CB1954 from the FACS strategy were all derived from variants collected into individual wells in a microtitre plate and not from the culture collected into microcentrifuge tubes.

A further issue was the concentration of the chloramphenicol that I used in the selection. In retrospect I should have used a higher concentration of chloramphenicol, one that resulted in a significant difference between the growth inhibition of the variants collected under no selection pressure and those under chloramphenicol selection pressure (see Figure 5.4). An improved experimental design could normalize selection pressure experienced by the 7SM library under CB1954, niclosamide or chloramphenicol. This could have been achieved by using concentrations of CB1954 and the two pre-selection agents that resulted in similar levels of growth inhibition.

7.4 Future directions

7.4.1 BDEPT with CB1954

CB1954 is a first-generation prodrug that has undergone significant clinical development. Next-generation prodrugs such as PR-104A surpass CB1954 in VDEPT models, both in terms of bystander effect and therapeutic outcome (Singleton et al., 2007; Wilson et al., 2002). However, my research has indicated that the 2-nitro-reduced metabolites of CB1954 have a surprisingly high bacterial bystander effect from *E. coli* vectors compared to the reduction products of next generation prodrugs including PR-104A and analogues thereof. Future BDEPT clinical development should reconsider CB1954 in partnership with an NfsA-family nitroreductase and thereby leverage past clinical safety data already obtained from Phase I trials with CB1954 (Onion et al., 2009; Patel et al., 2009).

7.4.2 Bacterial bystander effect model with other BDEPT vectors

The bacterial bystander effect assay developed in this research can, in future, be used to assess potential pairings of prodrug activating enzymes and prodrugs for use in BDEPT.

To immediately further the use of the bacterial bystander effect assay, developing alternative bacterial activator strains, such as *Salmonella* or *Clostridium* that express

nitroreductases of clinical interest may prove useful. Confounding factors may arise by co-incubating *E. coli* reporters with other types of bacteria. Therefore it would be beneficial to, for example, have *Salmonella* activators and reporters. Optimization of the assay with different bacterial species would be necessary.

Salmonella has known SOS-DNA repair genes, from which promoters could be linked to GFP expression as in the *E. coli* SOS-GFP strains already developed by the Ackerley laboratory. It has been demonstrated that certain antioxidant molecules activate oxidative stress and DNA repair promoters in *S. typhimurium* (Karimov et al., 2019). These DNA repair promoters could be linked to GFP expression. Having access to a broader range of nitroreductase expressing and DNA-damage reporting bacterial strains would enable us to measure the bystander effect of an array of potential prodrugs and nitroreductase partnerships in the intended vector *in vitro*.

7.4.3 Developing a bystander effect model of CDEPT with carcinoma cells

An ideal model would co-incubate human cells with *C. sporogenes* vectors. At present this is fraught with difficulties due to natural oncolytic activity exhibited by *C. sporogenes* as discussed earlier. A potential approach to overcome this is to isolate the medium surrounding *C. sporogenes* activator cells after prodrug challenge and then incubating it with human cancer cells.

Another priority is to develop an assay to measure the bystander effect from bacterial cells to carcinoma cells *in vitro*. Such a method requires separating liquid medium containing active prodrug metabolites, released into the medium from bacterial activators, and then incubating said medium with carcinoma cells. The relative level of carcinoma cell death compared to a no prodrug control would be a measure of the receipt of the active prodrug.

The methodology presented in section 4.3.1 for null bystander condition could be used as a starting point wherein the *E. coli* activator strain is separately challenged with a particular prodrug (e.g., a prodrug challenge of 50 μ M CB1954 for a 3.5 hour incubation). The medium surrounding the cells could then be collected by centrifugation and subjected to microfiltration to remove any bacterial debris or contaminants. A small portion of this medium would then be introduced to a culture of human carcinoma cells grown to

confluence. Cell death would then be monitored across a dilution series either by visual inspection or the use of MTS reagent, a tetrazolium salt, for monitoring cell viability and proliferation.

To optimize this assay, consideration of the prodrug concentration used to challenge the bacterial cells should be considered and adjusted as necessary. This will be particularly relevant for prodrugs such as PR-104A that are inefficient at exiting *E. coli* bacterial activators. The length of the prodrug challenge time could also be increased to provide more time in which the prodrug can be activated. Treatment of the media post challenge could be considered, e.g. concentration by ultra-centrifugation or further filtration procedures. The relative volume of the medium containing the active-prodrug metabolite to the volume of and density of the human carcinoma cells should also be considered.

As a preliminary investigation into this avenue, medium containing active prodrug metabolites was separated from *E. coli* activators that had been incubated with PR-104A, in work performed by Dr Sharrock. As I had already demonstrated that PR-104A has a poor bacterial bystander effect, Dr Sharrock further enzymatically lysed the cells in an effort to release the active prodrug metabolites. The lysate was filtered and serially diluted in a 1:1 ratio before addition to HEK293 cultures in T25 flasks. MTS assays indicated that there was no significant difference between the HEK293 cells exposed to lysate from 7NT *nfsA*-expressing cells challenged with PR-104A compared to the nitroreductase-null 7NT control strain also challenged with PR-104A.

These initial experiments were confounded by the fact that the control medium collected from around *E. coli* cells not challenged with a prodrug was also toxic to human cells, even post-filtration. This suggests that some kind of toxin had been released by the bacteria, most likely the Gram-negative lipopolysaccharide, sometimes referred to as "endotoxin", shed by the Gram negative outer membrane. Unfortunately this established a high cell-killing background that made it difficult to discern additional BDEPT killing contributions. Therefore, methods to remove or neutralize the endotoxin by ultrafiltration, ion exchange chromatography or even enzymatic treatment of the supernatant could also be considered (Magalhães et al., 2011).

Another approach could be to use a semi-permeable membrane located between the bacterial activator cells and recipient cancer cells. The activated prodrug metabolites could pass across the membrane from the activators to the recipients. The recipient cells could be further isolated and lysed and their contents analysed by HPLC or LCMS. In this fashion we could measure unbound activated prodrug metabolites inside of the cancer cell. However using this approach would not reflect the whole pathway of the drug. It would not be able to determine quantity of the metabolites permanently bound to DNA.

In future, prodrugs such as CB1954 and nitro-CBI-DEI, which have demonstrated a high bacterial bystander effect in the micro-plate assay developed in this thesis, could be assessed in a manner similar to that tested by Dr Sharrock but with testing for (and possible neutralisation of) bacterial endotoxins. Once optimized, such a system could be developed for other bacterial vectors; to assess the bystander effect potential of a particular bacterial vector with a prodrug with a specific cancer cell type *in vitro*.

7.4.4 Further optimizing FACS for future nitroreductase directed evolution

The FACS screening approach is attractive in terms of scale, time and resource consumption including prodrug. These attributes may outweigh drawbacks of cost and accuracy of selection, with a high bacterial bystander effect prodrug such as CB1954. In future these drawbacks may be overcome by using a non-toxic reporter protein and further optimization of prodrug concentration and highly stringent fluorescence selection gates.

A further experimental design could include elements of pre-selection. As suggested above, use of liquid culture or solid media with pre-screening agents, niclosamide or chloramphenicol, could remove non-functional nitroreductase variants from the library, prior to FACS, thus limiting collection of clones with a non-functional nitroreductase. The efficiency of FACS may be also improved by using agents that block the bacterial bystander effect. During my research, I considered the use of purified DNA as a supplement to the medium used to culture the 7SM library prior to FACS. A bystander blocking agent should “mop-up” the active prodrug metabolite as it is released in the medium. We theorize that purified DNA in the medium would be cross-linked by the active genotoxin, thereby acting as a trap to prevent the genotoxin from accessing neighbouring cells. I performed some preliminary experiments using either purified plasmid or genomic DNA from bacteria.

However, the bystander effect was not consistently blocked to a significant degree in the bacterial bystander effect assay performed with either CB1954 or nitro-CBI-DEI. Although preliminary experiments were not successful, future investigation could explore bystander blocker agents for use in the culture medium prior to performing FACS.

7.4.5 Optimizing bacterial vectors for BDEPT

The results of this thesis highlight the importance of evaluating enzyme-prodrug combinations in models relevant to the intended GDEPT vector. Evidently there can be profound differences in efficacy between viral or bacterial vectors using the same prodrug. Accounting for the fundamental physiological differences associated with different gene-delivery systems will identify the optimal enzyme-prodrug combinations for each GDEPT system.

Gram-negative bacteria possess an inner membrane, a periplasmic space, a cell wall and an outer membrane. Gram-positive bacteria have an inner membrane and a thick cell wall. These membranes can interfere with the diffusion rate of prodrugs, particularly charged prodrugs, into the cytoplasm of the bacterial vectors (Lehouritis et al., 2013). At present, activation of the prodrug by bacterial vectors typically occurs inside the cytoplasm of the bacteria where the prodrug activating enzyme, once expressed, is located. Once activated, the genotoxic drug must traverse the membranes of the bacterial vector and cross the tumour cell plasma membrane in order to reach the target DNA in the nucleus of the cancer cells (Chan-Hyams et al., 2018; Lehouritis et al., 2013).

When designing a BDEPT vector, deciding to maintain or knock out multidrug efflux pump genes needs to be considered in tandem with the intended prodrug. If the prodrug takes a long time to be activated then prodrug may be effluxed from the bacteria before it is activated. Conversely, a bacterial vector with no means of active drug transport may be sterilized by the active genotoxic prodrug metabolites. These design factors will influence the bystander effect potential of the therapy.

Transporting the prodrug activating enzyme to the surface of the bacterial vector is one approach to overcome the physical barriers of the bacterial membranes. In this scenario, the prodrug would not have to cross the bacterial membranes as inactive prodrug or as an active genotoxin. Lehouritis et al. (2013), considered secretion of the therapeutic

proteins after tumour infiltration. Forays into this technology have used secretion tags to direct expressed therapeutic proteins to the surface of the bacteria or at least beyond the inner membrane. Secretion of recombinant proteins into the extracellular medium of either Gram-positive (Sandkvist & Bagdasarian, 1996) or Gram-negative (Jeong & Lee, 2002) bacteria is well known. Secretion of recombinant proteins to the surface of Clostridial vectors for CDEPT has been explored (Theys et al., 2001). A promoter and leader sequence was used to successfully secrete a functional therapeutic protein, *E. coli* cytosine deaminase, to the exterior of *Clostridium acetobutylicum* (Theys et al., 2001). However, nitroreductases are dependent on co-factors and NADPH found inside of the cellular environment. Therefore secreting nitroreductase enzymes to the surface of a bacterial vector is not a feasible strategy for improving nitroreductase-led BDEPT.

7.5 Concluding remarks and recommendations for immediate future work

This thesis demonstrated the development of a robust and sensitive method for measuring the bacterial bystander effect in a microplate based assay that was validated by flow cytometry. This fulfilled a previously unmet need in the field of GDEPT; for an *in vitro* method of quantifying the bystander effect to model cell-to-cell transfer of activated prodrug metabolites during BDEPT. This thesis also demonstrated the negative influence of the bystander effect on FACS of nitroreductase variant libraries during a directed evolution cycle. It also identified promising nitroreductase candidates to be partnered with next generation prodrugs for future CDEPT development. It considered the influence of multi-drug efflux pumps on the bacterial bystander effect and highlighted the importance of evaluating enzyme-prodrug combinations in models relevant to the intended GDEPT vector, as there can evidently be profound differences in efficacy in different settings. Finally, this investigation revealed that the prodrug CB1954 had a surprising high bacterial bystander effect and holds promise for future BDEPT development, in particular using Gram-negative vectors such as *E. coli*.

References cited

- Al-Dimassi, S., Abou-Antoun, T., & El-Sibai, M. (2014). Cancer cell resistance mechanisms: a mini review. *Clinical and Translational Oncology*, *16*(6), 511–516.
- American Cancer Society. (2020). Cancer facts & figures 2020. *American Cancer Society 2020*, No. 500820.
- Anderson, R. F., Smaill, J. B., Patterson, A. V., Ashoorzadeh, A., Ackerley, D. F., Copp, J. N., Mowday, A. M., Williams, E. M., Guise, C. P., Koch, C., Kachur, A., & Dolbier, J. W. R. (2014). Compounds and methods for selective imaging and/or ablation. *WO2014007650 A1*.
- Anlezark, G. M., Melton, R. G., Sherwood, R. F., Coles, B., Friedlos, F., & Knox, R. J. (1992). The bioactivation of 5-(aziridin-1-yl)-2,4-dinitrobenzamide (CB1954)-I. Purification and properties of a nitroreductase enzyme from *Escherichia coli*-A potential enzyme for antibody-directed enzyme prodrug therapy (ADEPT). *Biochemical Pharmacology*, *44*(12), 2289–2295.
- Baker, S. L. (2011). Use of a direct, positive selection strategy to generate improved prodrug-activating enzymes for cancer gene therapy. *University of Birmingham*.
- Bernstein, V., Ellard, S. L., Dent, S. F., Tu, D., Mates, M., Dhesy-Thind, S. K., & Panasci, L. (2018). A randomized phase II study of weekly paclitaxel with or without pelareorep in patients with metastatic breast cancer: final analysis of Canadian cancer trials group IND.213. *Breast Cancer Research and Treatment*, *167*(2), 485–493.
- Bewicke-Copley, F., Mulcahy, L. A., Jacobs, L. A., Samuel, P., Akbar, N., Pink, R. C., & Carter, D. R. F. (2017). Extracellular vesicles released following heat stress induce bystander effect in unstressed populations. *Journal of Extracellular Vesicles*, *6*(1340746), 1–6.
- Boland, M. P., Knox, R. J., & Roberts, J. J. (1991). The differences in kinetics of rat and human DT diaphorase result in a differential sensitivity of derived cell lines to CB 1954 (5-(aziridin-1-yl)-2,4-dinitrobenzamide). *Biochemical pharmacology*, *41*(6-7), 867–875.
- Bornscheuer, U. T., Huisman, G. W., Kazlauskas, R. J., Lutz, S., Moore, J. C., & Robins, K.

- (2012). Engineering the third wave of biocatalysis. *Nature*, *485*(7397), 185–194.
- Braybrooke, J. P., Slade, A., Deplanque, G., Harrop, R., Madhusudan, S., Forster, M. D., Gibson, R., Makris, A., Talbot, D. C., Steiner, J., White, L., Kan, O., Naylor, S., Carroll, M. W., Kingsman, S. M., & Harris, A. L. (2005). Phase I study of MetXia-P450 gene therapy and oral cyclophosphamide for patients with advanced breast cancer or melanoma. *Clinical Cancer Research*, *11*(4), 1512–1520.
- Breitbach, C. J., Reid, T., Burke, J., Bell, J. C., & Kirn, D. H. (2010). Navigating the clinical development landscape for oncolytic viruses and other cancer therapeutics: No shortcuts on the road to approval. *Cytokine and Growth Factor Reviews*, *21*(2–3), 85–89.
- Bridgewater, J. A., Knox, R. J., Pitts, J. D., Collins, M. K., & Springer, C. J. (1997). The Bystander effect of Nitroreductase/CB1954 enzyme/prodrug system is due to cell permeable metabolite. *Human Gene Therapy*, *8*(6), 709–717.
- Carmeliet, P., & Jain, R. K. (2000). Angiogenesis in cancer and other diseases. *Nature*, *407*(6801), 249–257.
- Cattaneo, R., Miest, T., Shashkova, E. V., & Barry, M. A. (2008). Reprogrammed viruses as cancer therapeutics: Targeted, armed and shielded. *Nature Reviews Microbiology*, *6*(7), 529–540.
- Chan-Hyams, J. V. E., & Ackerley, D. F. (2020). MethodsX Protocol for evaluating the abilities of diverse nitroaromatic prodrug metabolites to exit a model Gram negative bacterial vector. *MethodsX*, *7*, 100797.
- Chan-Hyams, J. V. E., Copp, J. N., Smaill, J. B., Patterson, A. V., & Ackerley, D. F. (2018). Evaluating the abilities of diverse nitroaromatic prodrug metabolites to exit a model Gram negative vector for bacterial-directed enzyme-prodrug therapy. *Biochemical Pharmacology*, *158*, 192–200.
- Chica, R. A., Doucet, N., & Pelletier, J. N. (2005). Semi-rational approaches to engineering enzyme activity: Combining the benefits of directed evolution and rational design. *Current Opinion in Biotechnology*, *16*(4), 378–384.

- Choi, J. W., Lee, J., Nishi, K., Kim, Y. S., Jung, C. H., & Kim, J. S. (2008). Crystal structure of a minimal nitroreductase, ydjA, from *Escherichia coli* K12 with and without FMN cofactor. *Journal of Molecular Biology*, *377*(1), 258–267.
- Chorobik, P., Czaplicki, D., Ossysek, K., & Bereta, J. (2013). Salmonella and cancer: From pathogens to therapeutics. *Acta Biochimica Polonica*, *60*(3), 285–297.
- Chung-Faye, G., Palmer, D., Anderson, D., Clark, J., Downes, M., Baddeley, J., Hussain, S., Murray, P. I., Searle, P., Seymour, L., Harris, P. A., Ferry, D., & Kerr, D. J. (2001). Virus-directed , enzyme prodrug therapy with nitroimidazole reductase : a Phase I and pharmacokinetic study of its virus-directed , enzyme prodrug therapy with nitroimidazole reductase : a Phase I and pharmacokinetic study of its prodrug, CB1954. *Clinical Cancer Research*, *7*(9), 2662–2668.
- Cobb, L. M., Connors, T. A., Elson, L. A., Khan, A. H., Mitchley, B. C. V., Ross, W. C. J., & Whisson, M. E. (1969). 2,4-Dinitro-5-ethyleneiminobenzamide (CB1954): a potent and selective inhibitor of the growth of the Walker carcinoma 256. *Biochemical pharmacology*, *18*(6), 1519–1527.
- Coffey, M. C., Strong, J. E., Forsyth, P. A., & Lee, P. W. K. (1998). Reovirus therapy of tumors with activated Ras pathway. *Science*, *282*(5392), 1332–1334.
- Copp, J. N., Mowday, A. M., Williams, E. M., Guise, C. P., Ashoorzadeh, A., Sharrock, A. V., Flanagan, J. U., Smail, J. B., Patterson, A. V., & Ackerley, D. F. (2017). Engineering a multifunctional nitroreductase for improved activation of prodrugs and PET probes for cancer gene therapy. *Cell Chemical Biology*, *24*(3), 391–403.
- Copp, J. N., Williams, E. M., Rich, M. H., Patterson, A. V., Smail, J. B., & Ackerley, D. F. (2014). Toward a high-throughput screening platform for directed evolution of enzymes that activate genotoxic prodrugs. *Protein Engineering, Design and Selection*, *27*(10), 399–403.
- Cormack, B. P., Valdivia, R. H., & Falkow, S. (1996). FACS-optimized mutants of the green fluorescent protein (GFP). *Gene*, *173*(1 Spec No), 33–38.
- Crofts, T. S., Sontha, P., King, A. O., Wang, B., Bidy, B. A., Zanolli, N., Gaumnitz, J., & Dantas, G. (2019). Discovery and characterization of a nitroreductase capable of

- conferring bacterial resistance to chloramphenicol. *Cell Chemical Biology*, 26(4), 559–570.
- Currin, A., Swainston, N., Day, P. J., & Kell, D. B. (2015). Synthetic biology for the directed evolution of protein biocatalysts: navigating sequence space intelligently. *Chemical Society Reviews*, 44(5), 1172–1239.
- Dachs, G. U., Hunt, M. A., Syddall, S., Singleton, D. C., & Patterson, A. V. (2009). Bystander or no bystander for gene directed enzyme prodrug therapy. *Molecules*, 14(11), 4517–4545.
- Dang, L. H., Bettegowda, C., Huso, D. L., Kinzler, K. W., & Vogelstein, B. (2001). Combination bacteriolytic therapy for the treatment of experimental tumors. *Proceedings of the National Academy of Sciences of the United States of America*, 98(26), 15155–15160.
- Denny, W. A. (2002). Nitroreductase-based GDEPT. *Current Pharmaceutical Design*, 8(15), 1349–1361.
- Duarte, S., Carle, G., Faneca, H., de Lima, M. C., & Pierrefite-Carle, V. (2012). Suicide gene therapy in cancer: Where do we stand now? *Cancer Letters*, 324(2), 160–170. <https://doi.org/10.1016/j.canlet.2012.05.023>
- Duong, M. T. Q., Qin, Y., You, S. H., & Min, J. J. (2019). Bacteria-cancer interactions: bacteria-based cancer therapy. *Experimental & Molecular Medicine*, 51(12), 152.
- Feder, H. M. J., Osier, C., & Maderazo, E. G. (1981). Chloramphenicol: a review of its use in clinical practice. *Reviews of Infectious Diseases*, 3(3), 479–491.
- Fernández-Martínez, L. T., Borsetto, C., Gomez-Escribano, J. P., Bibb, M. J., Al-Bassam, M. M., Chandra, G., & Bibb, M. J. (2014). New insights into chloramphenicol biosynthesis in *Streptomyces venezuelae* ATCC 10712. *Antimicrobial Agents and Chemotherapy*, 58(12), 7441–7450.
- Foehrenbacher, A., Patel, K., Abbattista, M. R., Guise, C. P., Secomb, T. W., Wilson, W. R., & Hicks, K. O. (2013). The role of bystander effects in the antitumor activity of the hypoxia-activated prodrug PR-104. *Frontiers in Oncology*, 3(263), 1–18.

- Forbes, N. S. (2010). Engineering the perfect (bacterial) cancer therapy. *Nature Reviews Cancer*, 10(11), 785–794.
- Forbes, N. S., Munn, L. L., Fukumura, D., & Jain, R. K. (2003). Sparse initial entrapment of systemically injected *Salmonella typhimurium* leads to heterogeneous accumulation within tumors. *Cancer Research*, 63(17), 5188–5193.
- Fountzilas, C., Patel, S., & Mahalingam, D. (2017). Review: oncolytic virotherapy, updates and future directions. *Oncotarget*, 8(60), 102617–102639.
- Freeman, S. ., Abboud, C. ., Whartenby, K. ., Packman, C. H., Koeplin, D. S., Moolten, F. L., & Abraham, G. N. (1993). The “Bystander Effect”: tumor regression when a fraction of the tumor mass is genetically modified. *Cancer Research*, 53(21), 5274–5283.
- French, C. S., & Milner, H. W. (1950). Disintegration of bacteria and small particles by high-pressure extrusion. *Methods in Enzymology*, 633(111), 64–67.
- Freytag, S. O., Khil, M., Stricker, H., Peabody, J., Menon, M., DePeralta-Venturina, M., Nafziger, D., Pegg, J., Paielli, D., Brown, S., Barton, K., Lu, M., Aguilar-Cordova, E., & Kim, J. H. (2002). Phase I study of replication-competent adenovirus-mediated double suicide gene therapy for the treatment of locally recurrent prostate cancer. *Cancer Research*, 62(17), 4968–4976.
- Gillam, E., Copp, J., & Ackerley, D. (2011). *Directed Evolution Library Creation Methods and Protocols*. Springer Protocols. <https://doi.org/10.1007/978-1-4419-7931-5>
- Goldman, P., Koch, R. L., Yeung, T. C., Chrystal, E. J., Beaulieu, B. B. J., McLafferty, M. A., & Sudlow, G. (1986). Comparing the reduction of nitroimidazoles in bacteria and mammalian tissues and relating it to biological activity. *Biochemical Pharmacology*, 35(1), 43–51.
- Green, L. K., La Flamme, A. C., & Ackerley, D. F. (2014). *Pseudomonas aeruginosa* MdaB and WrbA are water-soluble two-electron quinone oxidoreductases with the potential to defend against oxidative stress. *Journal of Microbiology*, 52(9), 771–777.
- Green, L. K., Storey, M. A., Williams, E. M., Patterson, A. V., Smaill, J. B., Copp, J. N., & Ackerley, D. F. (2013). The flavin reductase MsuE is a novel nitroreductase that can

- efficiently activate two promising next-generation prodrugs for gene-directed enzyme prodrug therapy. *Cancers*, 5(3), 985–997.
- Green, L. K., Syddall, S. P., Carlin, K. M., Bell, G. D., Guise, C. P., Mowday, A. M., Hay, M. P., Smaill, J. B., Patterson, A. V., & Ackerley, D. F. (2013). *Pseudomonas aeruginosa* NfsB and nitro-CBI-DEI - a promising enzyme/prodrug combination for gene directed enzyme prodrug therapy. *Molecular Cancer*, 12(1), 1.
- Grove, J. I., Lovering, A. L., Guise, C., Race, P. R., Wrighton, C. J., White, S. A., Hyde, E. I., & Searle, P. F. (2003). Generation of *Escherichia coli* nitroreductase mutants conferring improved cell sensitization to the prodrug CB1954. *Cancer Research*, 63(17), 5532–5537.
- Guise, C. P., Abbattista, M. R., Singleton, R. S., Holford, S. D., Connolly, J., Dachs, G. U., Fox, S. B., Pollock, R., Harvey, J., Guilford, P., Doñate, F., Wilson, W. R., & Patterson, A. V. (2010). The bioreductive prodrug PR-104A is activated under aerobic conditions by human aldo-keto reductase 1C3. *Cancer Research*, 70(4), 1573–1584.
- Guise, C. P., Grove, J. I., Hyde, E. I., & Searle, P. F. (2007). Direct positive selection for improved nitroreductase variants using SOS triggering of bacteriophage lambda lytic cycle. *Gene Therapy*, 14(8), 690–698.
- He, F. (2011). Laemmli-SDS-PAGE. *Bio-Protocol*, 1(11).
<https://doi.org/10.21769/BioProtoc.80>
- Heap, J. T., Pennington, O. J., Cartman, S. T., Carter, G. P., & Minton, N. P. (2007). The Clostron: a universal gene knock-out system for the genus *Clostridium*. *Journal of Microbiological Methods*, 70(3), 452–464.
- Heap, J. T., Theys, J., Ehsaan, M., Kubiak, A. M., Dubois, L., Paesmans, K., Van Mellaert, L., Knox, R., Kuehne, S. A., Lambin, P., & Minton, N. P. (2014). Spores of *Clostridium* engineered for clinical efficacy and safety cause regression and cure of tumors in vivo. *Oncotarget*, 5(7), 1761–1769.
- Helsby, N. A., Ferry, D. M., Patterson, A. V., Pullen, S. M., & Wilson, W. R. (2004). 2-Amino metabolites are key mediators of CB1954 and SN23862 bystander effects in nitroreductase GDEPT. *British Journal of Cancer*, 90(5), 1084–1092.

- Helsby, N. A., Wheeler, S. J., Pruijn, F. B., Palmer, B. D., Yang, S., Denny, W. A., & Wilson, W. R. (2003). Effect of nitroreduction on the alkylating reactivity and cytotoxicity of the 2,4-dinitrobenzamide-5-aziridine CB1954 and the corresponding nitrogen mustard SN23862: distinct mechanisms of bioreductive activation. *Chemical Research in Toxicology*, *16*(4), 469–478.
- Heo, J., Reid, T., Ruo, L., Breitbach, C. J., Rose, S., Bloomston, M., Cho, M., Lim, H. Y., Chung, H. C., Kim, C. W., Burke, J., Lencioni, R., Hickman, T., Moon, A., Lee, Y. S., Kim, M. K., Daneshmand, M., Dubois, K., Longpre, L., Kirn, D. H. (2013). Randomized dose-finding clinical trial of oncolytic immunotherapeutic vaccinia JX-594 in liver cancer. *Nature Medicine*, *19*(3), 329–336.
- Hoffman, R. M. (2011). Tumor-seeking Salmonella amino acid auxotrophs. *Current Opinion in Biotechnology*, *22*(6), 917–923.
- Holay, N., Kim, Y., Lee, P., & Gujar, S. (2017). Sharpening the edge for precision cancer immunotherapy: targeting tumor antigens through oncolytic vaccines. *Frontiers in Immunology*, *8*(800), 1–9.
- Hoption Cann, S. A., Van Netten, J. P., & Van Netten, C. (2003). Dr William Coley and tumour regression: a place in history or in the future. *Postgraduate Medical Journal*, *79*(938), 672–680.
- Hunt, M. A., Li, D., Hay, M. P., Currie, M. J., Robinson, B. A., Patterson, A. V., & Dachs, G. U. (2012). Characterisation of enzyme prodrug gene therapy combinations in coated spheroids and vascular networks *in vitro*. *The Journal of Gene Medicine*, *14*(1), 62–74. <https://doi.org/10.1002/jgm.1635>
- Huttunen, K. M., Mähönen, N., Raunio, H., & Rautio, J. (2008). Cytochrome P450-activated prodrugs : targeted drug delivery. *Current Medicinal Chemistry*, *15*(23), 2346–2365.
- Jaberipour, M., Vass, S. O., Guise, C. P., Grove, J. I., Knox, R. J., Hu, L., Hyde, E. I., & Searle, P. F. (2010). Testing double mutants of the enzyme nitroreductase for enhanced cell sensitisation to prodrugs: effects of combining beneficial single mutations. *Biochemical Pharmacology*, *79*(2), 102–111.
- Jameson, M. B., Rischin, D., Pegram, M., Gutheil, J., Patterson, A. V., Denny, W. A., &

- Wilson, W. R. (2010). A phase I trial of PR-104, a nitrogen mustard prodrug activated by both hypoxia and aldo-keto reductase 1C3, in patients with solid tumors. *Cancer Chemotherapy and Pharmacology*, *65*(4), 791–801.
- Jarrom, D., Jaberipour, M., Guise, C. P., Daff, S., White, S. A., Searle, P. F., & Hyde, E. I. (2009). Steady-state and stopped-flow kinetic studies of three *Escherichia coli* NfsB mutants with enhanced activity for the prodrug CB1954. *Biochemistry*, *48*(32), 7665–7672.
- Jeong, K. J., & Lee, S. Y. (2002). Excretion of human beta-endorphin into culture medium by using outer membrane protein F as a fusion partner in recombinant *Escherichia coli*. *Applied and Environmental Microbiology*, *68*(10), 4979–4985.
- Karbach, J., Neumann, A., Brand, K., Wahle, C., Siegel, E., Maeurer, M., Ritter, E., Tsuji, T., Gnjatic, S., Old, L. J., Ritter, G., & Jäger, E. (2012). Phase I clinical trial of mixed bacterial vaccine (Coley's toxins) in patients with NY-ESO-1 expressing cancers: immunological effects and clinical activity. *Clinical Cancer Research*, *18*(19), 5449–5459.
- Karimov, I. F., Kondrashova, K. S., Kulikova, N. A., & Manukhov, I. V. (2019). Effects of antioxidant molecules on sensor and reporter luminescent strains. *Applied Biochemistry and Microbiology*, *55*(3), 237–242.
- Kasinskas, R. W., & Forbes, N. S. (2006). *Salmonella typhimurium* specifically chemotax and proliferate in heterogeneous tumor tissue in vitro. *Biotechnology and Bioengineering*, *94*(4), 710–721.
- Kasinskas, R. W., & Forbes, N. S. (2007). *Salmonella typhimurium* lacking ribose chemoreceptors localize in tumor quiescence and induce apoptosis. *Cancer Research*, *67*(7), 3201–3209.
- Knox, R., Burke, P., Chen, S., & Kerr, D. (2005). CB1954: from the Walker tumor to NQO2 and VDEPT. *Current Pharmaceutical Design*, *9*(26), 2091–2104.
- Kobori, T., Sasaki, H., Lee, W. C., Zenno, S., Saigo, K., Murphy, M. E. P., & Tanokura, M. (2001). Structure and site-directed mutagenesis of a flavoprotein from *Escherichia coli* that reduces nitrocompounds: alteration of pyridine nucleotide binding by a

- single amino acid substitution. *Journal of Biological Chemistry*, 276(4), 2816–2823.
- Konopleva, M., Thall, P. F., Yi, C. A., Borthakur, G., Coveler, A., Bueso-Ramos, C., Benito, J., Konoplev, S., Gu, Y., Ravandi, F., Jabbour, E., Faderl, S., Thomas, D., Cortes, J., Kadia, T., Kornblau, S., Daver, N., Pemmaraju, N., Nguyen, H. Q., Kantarjian, H. (2015). Phase I/II study of the hypoxia-activated prodrug PR104 in refractory/relapsed acute myeloid leukemia and acute lymphoblastic leukemia. *Haematologica*, 100(7), 927–934.
- Kuehne, S. ., & Minton, N. P. (2012). Clostron-mediated engineering of *Clostridium*. *Bioengineered*, 3(4), 247–254.
- Lehouritis, P., Springer, C., & Tangney, M. (2013). Bacterial-directed enzyme prodrug therapy. *Journal of Controlled Release*, 170(1), 120–131.
- Leitsch, D. (2019). A review on metronidazole: an old warhorse in antimicrobial chemotherapy. *Parasitology*, 146(9), 1167–1178.
- Leschner, S., Westphal, K., Dietrich, N., Viegas, N., Jablonska, J., Lyszkiewicz, M., Lienenklaus, S., Falk, W., Gekara, N., Loessner, H., & Weiss, S. (2009). Tumor invasion of *Salmonella enterica serovar Typhimurium* is accompanied by strong hemorrhage promoted by TNF- α . *PLoS ONE*, 4(8), e6692.
- Liu, S. C., Ahn, G. O., Kioi, M., Dorie, M. J., Patterson, A. V., & Brown, J. M. (2008). Optimized *Clostridium*-directed enzyme prodrug therapy improves the antitumor activity of the novel DNA cross-linking agent PR-104. *Cancer Research*, 68(19), 7995–8003.
- Lomovskaya, O., Warren, M. S., Lee, A., Galazzo, J., Fronko, R., Lee, M., Blais, J., Cho, D., Chamberland, S., Renau, T., Leger, R., Hecker, S., Watkins, W., Hoshino, K., Ishida, H., & Lee, V. . J. (2001). Identification and characterization of inhibitors of multidrug resistance efflux pumps in *Pseudomonas aeruginosa*: novel agents for combination therapy. *Antimicrobial Agents and Chemotherapy*, 45(1), 105–116.
- Lovering, A. L., Hyde, E. I., Searle, P. F., & White, S. A. (2001). The structure of *Escherichia coli* nitroreductase complexed with nicotinic acid: three crystal forms at 1.7 Å, 1.8 Å and 2.4 Å resolution. *Journal of Molecular Biology*, 309(1), 203–213.

- Ludlum, D. B., Colinas, R. J., Kirk, M. C., & Mehta, J. R. (1988). Reaction of reduced metronidazole with guanosine to form an unstable adduct. *Carcinogenesis*, *9*(4), 593–596.
- Magalhães, P. O., Lopes, A. ., Mazzola, P. G., Rangel-yagui, C., & Penna, T. C. V. (2011). Methods of endotoxin removal from biological preparations : a review. *Journal of Pharmaceutical Sciences*, *10*(3), 1–15.
- McKeage, M. J., Gu, Y., Wilson, W. R., Hill, A., Amies, K., Melink, T. J., & Jameson, M. B. (2011). A phase I trial of PR-104, a pre-prodrug of the bio-reductive prodrug PR-104A, given weekly to solid tumour patients. *BMC Cancer*, *11*(432), 1–12.
- McKeage, M. J., Jameson, M. B., Ramanathan, R. K., Rajendran, J., Gu, Y., Wilson, W. R., Melink, T. J., & Tchekmedyian, N. S. (2012). PR-104 a bio-reductive pre-prodrug combined with gemcitabine or docetaxel in a phase Ib study of patients with advanced solid tumours. *BMC Cancer*, *12*(496), 1–10.
- Miller, A.-F., Park, J. T., Ferguson, K. L., Pitsawong, W., & Bommarius, A. S. (2018). Informing efforts to develop nitroreductase for amine production. *Molecules (Basel, Switzerland)*, *23*(2), 1–22.
- Minton, N. (2003). *Clostridia* in cancer therapy. *Nature Reviews. Microbiology*, *1*(3), 237–242.
- Mowday, A. M., Ashoorzadeh, A., Williams, E. M., Copp, J. N., Silva, S., Bull, M. R., Abbattista, M. R., Anderson, R. F., Flanagan, J. U., Guise, C. P., Ackerley, D. F., Smaill, J. B., & Patterson, A. V. (2016). Rational design of an AKR1C3-resistant analog of PR-104 for enzyme-prodrug therapy. *Biochemical Pharmacology*, *116*, 176–187.
- Mowday, A. M., Guise, C. P., Ackerley, D. F., Minton, N. P., Lambin, P., Dubois, L. J., Theys, J., Smaill, J. B., & Patterson, A. V. (2016). Advancing *clostridia* to clinical trial: past lessons and recent progress. *Cancers*, *8*(7), 1–14.
- Nasu, Y., Saika, T., Ebara, S., Kusaka, N., Kaku, H., Abarzua, F., Manabe, D., Thompson, T. C., & Kumon, H. (2007). Suicide gene therapy with adenoviral delivery of HSV-tK gene for patients with local recurrence of prostate cancer after hormonal therapy. *Molecular Therapy*, *15*(4), 834–840.

- Nemunaitis, J., Cunningham, C., Senzer, N., Kuhn, J., Cramm, J., Litz, C., Cavagnolo, R., Cahill, A., Clairmont, C., & Sznol, M. (2003). Pilot trial of genetically modified, attenuated *Salmonella* expressing the *E. coli* cytosine deaminase gene in refractory cancer patients. *Cancer Gene Therapy*, *10*(10), 737–744.
- Niemans, R., Yaromina, A., Theys, J., Ashoorzadeh, A., Anderson, R., Bull, M., Guise, C., Hsu, H. L., Abbattista, M., Mowday, A., Patterson, A. V., Smaill, J. B., Dubois, L., & Lambin, P. (2017). OC-0591: hypoxic cell killing by SN36506, a novel hypoxia-activated prodrug. *Radiotherapy and Oncology*, *123*(ESTRO 36), S311.
- NIH National Cancer Institute. (2015). *Chemotherapy to Treat Cancer*. <https://www.cancer.gov/about-cancer/treatment/types/chemotherapy>
- NIH National Cancer Institute. (2019). *Radiation Therapy to Treat Cancer*. January. <https://www.cancer.gov/about-cancer/treatment/types/radiation-therapy>
- NZ Ministry of Health, N. (2019). *Ministry of Health. 2019. New Zealand Cancer Action Plan 2019–2029 – Te Mahere mō te Mate Pukupuku o Aotearoa 2019–2029*. NZ Ministry of Health.
- Onion, D., Patel, P., Pineda, R. ., James, N., & Mautner, V. (2009). Antivector and tumor immune responses following adenovirus-directed enzyme prodrug therapy for the treatment of prostate cancer. *Human Gene Therapy*, *20*(11), 1249–1258.
- Patel, P., Young, J. G., Mautner, V., Ashdown, D., Bonney, S., Pineda, R. G., Collins, S. I., Searle, P. F., Hull, D., Peers, E., Chester, J., Wallace, D. M., Doherty, A., Leung, H., Young, L. S., & James, N. D. (2009). A phase I/II clinical trial in localized prostate cancer of an adenovirus expressing nitroreductase with CB1984. *Molecular Therapy*, *17*(7), 1292–1299.
- Patterson, A. V., Ferry, D. M., Edmunds, S. J., Gu, Y., Singleton, R. S., Patel, K., Pullen, S. M., Hicks, K. O., Syddall, S. P., Atwell, G. J., Yang, S., Denny, W. A., & Wilson, W. R. (2007). Mechanism of action and preclinical antitumor activity of the novel hypoxia-activated DNA cross-linking agent PR-104. *Clinical Cancer Research*, *13*(13), 3922–3932.
- Portsmouth, D., Hlavaty, J., & Renner, M. (2007). Suicide genes for cancer therapy.

Molecular Aspects of Medicine, 28(1), 4–41.

Prosser, G. A., Copp, J. N., Mowday, A. M., Guise, C. P., Syddall, S. P., Williams, E. M., Horvat, C. N., Swe, P. M., Ashoorzadeh, A., Denner, W. A., Smail, J. B., Patterson, A. V., & Ackerley, D. F. (2013). Creation and screening of a multi-family bacterial oxidoreductase library to discover novel nitroreductases that efficiently activate the bioreductive prodrugs CB1954 and PR-104A. *Biochemical Pharmacology*, 85(8), 1091–1103.

Prosser, G. A., Copp, J. N., Syddall, S., Williams, E. M., Smaill, J. B., Wilson, W. R., Patterson, A. V., & Ackerley, D. F. (2010). Discovery and evaluation of *Escherichia coli* nitroreductases that activate the anti-cancer prodrug CB1954. *Biochemical Pharmacology*, 79(5), 678–687.

Prosser, G. A., Patterson, A. V., & Ackerley, D. F. (2010). UvrB gene deletion enhances SOS chromotest sensitivity for nitroreductases that preferentially generate the 4-hydroxylamine metabolite of the anti-cancer prodrug CB1954. *Journal of Biotechnology*, 150(1), 190–194.

Race, P. R., Lovering, A. L., White, S. A., Grove, J. I., Searle, P. F., Wrighton, C. W., & Hyde, E. (2007). Kinetic and structural characterisation of *Escherichia coli* nitroreductase mutants showing improved efficacy for the prodrug substrate CB1954. *Journal of Molecular Biology*, 368(2), 481–492.

Rafii, F., & Cerniglia, C. E. (1995). Reduction of azo dyes and nitroaromatic compounds by bacterial enzymes from the human intestinal tract. *Environmental Health Perspectives*, 103(5), 17–19.

Rainov, N. G. (2000). A Phase III clinical evaluation of Herpes Simplex Virus Type 1 thymidine kinase and Ganciclovir gene therapy as an adjuvant to surgical resection and radiation in adults with previously untreated Glioblastoma Multiforme. *Human Gene Therapy*, 11(17), 2389–2401.

Reetz, M. T., Kahakeaw, D., & Lohmer, R. (2008). Addressing the numbers problem in directed evolution. *ChemBiochem : A European Journal of Chemical Biology*, 9(11), 1797–1804.

- Rich, M. H. (2017). Discovery and directed evolution of nitroreductase enzymes for activation of prodrugs and PET imaging compounds. *Victoria University of Wellington*, Wellington, New Zealand.
- Rickard, A. G., Palmer, G. M., & Dewhirst, M. W. (2019). Clinical and pre-clinical methods for quantifying tumor hypoxia. *Advances in Experimental Medicine and Biology*, 1136, 19–41.
- Roberts, N. ., Zhang, L., Janku, F., Collins, A., Bai, R., Staedtke, V., Rusk, A. W., Tung, D., Miller, M., Roix, J., Khanna, V., Murthy, R., Benjamin, R. S., Helgason, T., Szvalb, A. D., Bird, J. E., Roy-chowdhuri, S., Zhang, H. H., Qiao, Y., Zhou, S. (2014). Intratumoral injection of *Clostridium novyi-NT* spores induces antitumor responses. *Science Translational Medicine*, 6(249), 1–27.
- Roldán, M. D., Pérez-Reinado, E., Castillo, F., & Moreno-Vivián, C. (2008). Reduction of polynitroaromatic compounds: the bacterial nitroreductases. *FEMS Microbiology Reviews*, 32(3), 474–500.
- Ruff, A. ., Dennig, A., Wirtz, G., Blanusa, M., & Schwaneberg, U. (2012). Flow cytometer-based high-throughput screening system for accelerated directed evolution of P450 monooxygenases. *ACS Catalysis*, 2(12), 2724–2728.
- Sandkvist, M., & Bagdasarian, M. (1996). Secretion of recombinant proteins by Gram-negative bacteria. *Current Opinion in Biotechnology*, 7(5), 505–511.
- Sharrock, A. V. (2019). Engineering Nitroreductase Enzymes for Improved Cancer Gene Therapy and Targeted Cellular Ablation. *Victoria University of Wellington*, Wellington, New Zealand.
- Siim, B. G., Denny, W. A., & Wilson, W. R. (1997). Nitro reduction as an electronic switch for bioreductive drug activation. *Oncology Research*, 9(6–7) , 357–369.
- Singleton, D., Li, D., Bai, S. Y., Syddall, S. P., Smaill, J. B., Shen, Y., Denny, W. A., Wilson, W. R., & Patterson, A. V. (2007). The nitroreductase prodrug SN 28343 enhances the potency of systemically administered armed oncolytic adenovirus ONYX-411NTR. *Cancer Gene Therapy*, 14(12), 953–967.

- Staedtke, V., Roberts, N. J., Bai, R. Y., & Zhou, S. (2016). *Clostridium novyi-NT* in cancer therapy. *Genes and Diseases*, 3(2), 144–152.
- Stritzker, J., Weibel, S., Hill, P. J., Oelschlaeger, T. A., Goebel, W., & Szalay, A. A. (2007). Tumor-specific colonization, tissue distribution, and gene induction by probiotic *Escherichia coli* Nissle 1917 in live mice. *International Journal of Medical Microbiology*, 297(3), 151–162.
- Sulavik, M. C., Houseweart, C., Cramer, C., Jiwani, N., Murgolo, N., Greene, J., DiDomenico, B., Shaw, K. J., Miller, G. . H., Hare, R., & Shimer, G. (2001). Antibiotic susceptibility profiles of *Escherichia coli* strains lacking multidrug efflux pump genes. *Antimicrobial Agents and Chemotherapy*, 45(4), 1126–1136.
- Swe, P. M., Copp, J. N., Green, L. K., Guise, C. P., Mowday, A. M., Smaill, J. B., Patterson, A. V., & Ackerley, D. F. (2012). Targeted mutagenesis of the *Vibrio fischeri flavin* reductase FRase i to improve activation of the anticancer prodrug CB1954. *Biochemical Pharmacology*, 84(6), 775–783.
- Sznol, M., & Lin, S. (2000). The treatment of cancer. *British Medical Journal*, 1(2515), 693.
- Taguchi, S., Fukuhara, H., Homma, Y., & Todo, T. (2017). Current status of clinical trials assessing oncolytic virus therapy for urological cancers. *International Journal of Urology*, 24(5), 342–351.
- Takeda, K., Sato, J., Goto, K., Fujita, T., Watanabe, T., Abo, M., Yoshimura, E., Nakagawa, J., Abe, A., Kawasaki, S., & Niimura, Y. (2010). *Escherichia coli* ferredoxin-NADP+ reductase and oxygeninsensitive nitroreductase are capable of functioning as ferric reductase and of driving the Fenton reaction. *BioMetals*, 23(4), 727–737.
- Tang, M. H. Y., Helsby, N. A., Goldthorpe, M. A., Thompson, K. M., Al-Ali, S., & Tingle, M. D. (2007). Hepatic nitroreduction, toxicity and toxicokinetics of the anti-tumour prodrug CB1954 in mouse and rat. *Toxicology*, 240(1–2), 70–85.
- Theys, J., Landuyt, W., Nuyts, S., Van Mellaert, L., van Oosterom, A., Lambin, P., & Anne, J. (2001). Specific targeting of cytosine deaminase to solid tumors by engineered *Clostridium acetobutylicum*. *Cancer Gene Therapy*, 8(4), 294–297.

- Tracewell, C., & Arnold, F. H. (2009). Directed enzyme evolution: climbing fitness peaks one amino acid at a time. *Biochemistry*, *13*(1), 3–9.
- Tu, R., Martinez, R., Prodanovic, R., Klein, M., & Schwaneberg, U. (2011). A flow cytometry-based screening system for directed evolution of proteases. *Journal of Biomolecular Screening*, *16*(3), 285–294.
- Valiauga, B., Williams, E. M., Ackerley, D. F., & Čėnas, N. (2017). Reduction of quinones and nitroaromatic compounds by *Escherichia coli* nitroreductase A (NfsA): characterization of kinetics and substrate specificity. *Archives of Biochemistry and Biophysics*, *614*, 14–22.
- Vass, S. O., Jarrom, D., Wilson, W. R., Hyde, E. I., & Searle, P. F. (2009). *E. coli* NfsA: an alternative nitroreductase for prodrug activation gene therapy in combination with CB1954. *British Journal of Cancer*, *100*(12), 1903–1911.
- Vaupel, P., & Mayer, A. (2016). Tumor hypoxia: causative mechanisms, microregional heterogeneities, and the role of tissue-based hypoxia markers. *Advances in Experimental Medicine and Biology*, *923*, 77–86.
- Wang, G., & Maier, R. J. (2004). An NADPH quinone reductase of *Helicobacter pylori* plays an important role in oxidative stress resistance and host colonization. *Infection and Immunity*, *72*(3), 1391–1396.
- WHO IARC. (2014). *World Cancer Report 2014: Press Release N° 224. February*, 1–2.
- Williams, E. M. (2013). Development of bacterial nitroreductase enzymes for noninvasive imaging in cancer gene therapy. *Victoria University of Wellington*, Wellington, New Zealand.
- Williams, E. M., Little, R. F., Mowday, A. M., Rich, M. H., Chan-Hyams, J. V. E., Copp, J. N., Smail, J. B., Patterson, A. V., & Ackerley, D. F. (2015). Nitroreductase gene-directed enzyme prodrug therapy: insights and advances toward clinical utility. *Biochemical Journal*, *471*(2), 131–153.
- Wilson, W. R., Hicks, K. O., Pullen, S. M., Ferry, D. M., Helsby, N. A., & Patterson, A. V. (2007). Bystander effects of bioreductive drugs: potential for exploiting pathological

- tumor hypoxia with dinitrobenzamide mustards. *Radiat Res*, 167(6), 625–636.
- Wilson, W. R., Pullen, S. M., Hogg, A., Helsby, N. A., Hicks, K. O., & Denny, W. A. (2002). Quantitation of bystander effects in nitroreductase suicide gene therapy using three-dimensional cell cultures. *Cancer Research*, 62(5), 1425–1432.
- Wilson, W. R., Stribbling, S. M., Pruijn, F. B., Syddall, S. P., Patterson, A. V., Liyanage, H. D. S., Smith, E., Botting, K. J., & Tercel, M. (2009). Nitro-chloromethylbenzindolines: hypoxia-activated prodrugs of potent adenine N3 DNA minor groove alkylators. *Molecular Cancer Therapeutics*, 8(10), 2903–2913.
- Yu, X., Lin, C., Yu, J., Qi, Q., & Wang, Q. (2019). Bioengineered *Escherichia coli* Nissle 1917 for tumour-targeting therapy. *Microbial Biotechnology - Minireview*, 1–8.
- Zenno, S., Koike, H., Kumar, A. N., Jayaraman, R., Tanokura, M., & Saigo, K. (1996). Biochemical characterization of NfsA, the *Escherichia coli* major nitroreductase exhibiting a high amino acid sequence homology to Frp, a *Vibrio harveyi* flavin oxidoreductase. *Journal of Bacteriology*, 178(15), 4508–4514.
- Zenno, S., Saigo, K., Kanoh, H., & Inouye, S. (1994). Identification of the gene encoding the major NAD(P)H-flavin oxidoreductase of the bioluminescent bacterium *Vibrio fischeri* ATCC 7744. *Journal of Bacteriology*, 176(12), 3536–3543.
- Zhang, J., Kale, V., & Chen, M. (2015). Gene-Directed Enzyme Prodrug Therapy. *The AAPS Journal*, 17(1), 102–110.
- Zhao, M., Yang, M., Li, X. M., Jiang, P., Baranov, E., Li, S., Xu, M., Penman, S., & Hoffman, R. M. (2005). Tumor-targeting bacterial therapy with amino acid auxotrophs of GFP-expressing *Salmonella typhimurium*. *Proceedings of the National Academy of Sciences of the United States of America*, 102(3), 755–760.
- Zhou, S., Gravekamp, C., Bermudes, D., & Liu, K. (2017). Tumor-targeting bacteria engineered to fight cancer. *Physiology & Behavior*, 176(1), 139–148.

Appendices

Appendix A: Supplementary material Chapter 4 - Number of recovered activator and recipient cells for bystander and null bystander conditions from as model library subjected to FACS

No Prodrug	Bystander Effect					% Yield recipients	Null Bystander Effect				
	NfsA	Empty	Total	%	% Yield recipients		NfsA	Empty	Total	%	% Yield recipients
	pUCX	pUCX	cells	Yield NfsA			pUCX	pUCX	cells	Yield NfsA	
Rep 1	7	89	96	7	93	7	88	95	7	93	
	2	88	90	2	98						
Rep 2	8	87	95	8	92	11	84	95	12	88	
Rep 3	4	91	95	4	96	6	89	95	6	94	
Rep 4	3	92	95	3	97	4	90	94	4	96	
Ave	5	89	94	5	95	7	88	95	7	93	
Stdev	3	2	2	3	3	3	3	1	3	3	

2 μ M Metronidazole	Bystander Effect					% Yield recipients	Null Bystander Effect				
	NfsA	Empty	Total	%	% Yield recipients		NfsA	Empty	Total	%	% Yield recipients
	pUCX	pUCX	cells	Yield NfsA			pUCX	pUCX	cells	Yield NfsA	
Rep 1	14	81	95	15	85	9	86	95	9	91	
Rep 2	6	65	71	8	92	6	89	95	6	94	
Rep 3	6	88	94	6	94	9	86	95	9	91	
Ave	9	78	87	10	90	8	87	95	8	92	
Stdev	5	12	14	4	4	2	2	0	2	2	

10 μ M CB1954	Bystander Effect					% Yield recipients	Null Bystander Effect				
	NfsA pUCX	Empty pUCX	Total cells	% Yield NfsA	NfsA pUCX		Empty pUCX	Total cells	% Yield NfsA	% Yield recipients	
	Rep 1	4	91	95	4		96	17	78	95	18
Rep 2	6	88	94	6	94	11	84	95	12	88	
Rep 3	10	82	92	11	89	21	64	85	25	75	
Ave	7	87	94	7	93	16	75	92	18	82	
Stdev	3	5	2	3	3	5	10	6	7	7	

10 μ M PR- 104A	Bystander Effect					% Yield recipients	Null Bystander Effect				
	NfsA pUCX	Empty pUCX	Total cells	% Yield NfsA	NfsA pUCX		Empty pUCX	Total cells	% Yield NfsA	% Yield recipients	
	Rep 1	6	89	95	6		94	12	70	82	15
Rep 2	4	82	86	5	95	11	84	95	12	88	
Rep 3	2	88	90	2	98	6	89	95	6	94	
Ave	4	86	90	4	96	10	81	91	11	89	
Stdev	2	4	5	2	2	3	10	8	4	4	

10 μ M SN27686	Bystander Effect					% Yield recipients	Null Bystander Effect				% Yield recipients
	NfsA pUCX	Empty pUCX	Total cells	% Yield NfsA	NfsA pUCX		Empty pUCX	Total cells	% Yield NfsA		
	Rep 1	13	82	95	14		86	11	84	95	
	10	85	95	11	89	15	75	90	17	83	
Rep 2	4	89	93	4	96	11	75	86	13	87	
Rep 3	5	90	95	5	95	10	84	94	11	89	
Ave	8	87	95	8	92	12	80	91	13	87	
Stdev	4	4	1	4	4	2	5	4	3	3	

1 μ M nitro CBI-DEI	Bystander Effect					% Yield recipients	Null Bystander Effect				% Yield recipients
	NfsA pUCX	Empty pUCX	Total cells	% Yield NfsA	NfsA pUCX		Empty pUCX	Total cells	% Yield NfsA		
	Rep 1	11	83	94	12		88	30	48	78	
	9	72	81	11	89	27	67	94	29	71	
Rep 2	9	86	95	9	91	18	77	95	19	81	
Ave	10	80	90	11	89	25	64	89	29	71	
Stdev	1	7	8	1	1	6	15	10	10	10	

50 μ M CB1954	Bystander Effect					% Yield recipients	Null Bystander Effect				
	NfsA pUCX	Empty pUCX	Total cells	% Yield NfsA	NfsA pUCX		Empty pUCX	Total cells	% Yield NfsA	% Yield recipients	
	Rep 1	13	82	95	14		86	24	71	95	25
	10	85	95	11	89	23	69	92	25	75	
Rep 2	13	82	95	14	86	34	61	95	36	64	
	13	82	95	14	86	25	70	87	29	80	
Ave	12	83	95	13	87	27	68	92	29	74	
Stdev	2	2	0	2	2	5	5	4	5	7	

40 μ M PR-104A	Bystander Effect					% Yield recipients	Null Bystander Effect				
	NfsA pUCX	Empty pUCX	Total cells	% Yield NfsA	NfsA pUCX		Empty pUCX	Total cells	% Yield NfsA	% Yield recipients	
	Rep 1	21	73	94	22		78	22	49	71	31
	16	74	90	18	82	16	44	60	27	73	
Rep 2	8	52	60	13	87	16	79	95	17	83	
	8	86	94	9	91	30	65	95	32	68	
Rep 3	14	80	94	15	85	25	68	93	27	73	
	11	75	86	13	87	28	64	92	30	70	
Ave	13	73	86	15	85	23	62	84	27	73	
Stdev	5	12	13	5	5	6	13	15	6	6	

50 μ M SN27686	Bystander Effect					Null Bystander Effect				
	NfsA	Empty	Total	%	% Yield	NfsA	Empty	Total	%	% Yield
	pUCX	pUCX	cells	Yield		pUCX	pUCX	cells	Yield	
	NfsA					NfsA				
Rep 1	13	80	93	14	86	25	64	89	28	72
	18	77	95	19	81	32	56	88	36	64
Rep 2	7	88	95	7	93	45	50	95	47	53
	22	73	95	23	77	48	47	95	51	49
Rep 3	18	77	95	19	81	51	44	95	54	46
	19	74	93	20	80	40	55	95	42	58
Ave	18	76	94	19	81	39	53	92	42	58
Stdev	3	3	1	3	3	11	8	4	10	10

Table A 1 Number of recovered activator and recipient cells for bystander and null bystander conditions (number of *nfsA*-expressing activator cells as diagnosed by niclosamide for all prodrug conditions). The number of activator cells (*NfsA* pUCX) and recipient (*Empty* pUCX) was calculated from a minimum of three biological replicates for each prodrug treatment and bystander effect condition. The results of niclosamide diagnosis of *NfsA* expression for each biological replicate is recorded in the table.

Appendix B: Supplementary material Chapter 5 – SDS-PAGE gel of purified His6-tagged CB1954 improved nitroreductase variants

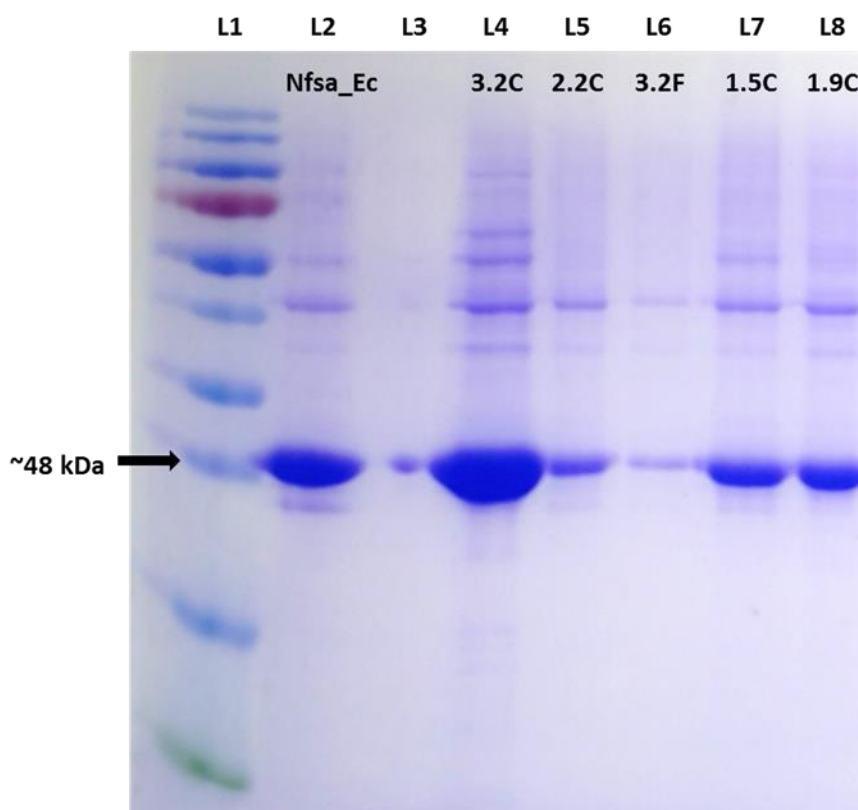


Figure B 2 SDS-PAGE gel of purified His6-tagged CB1954 improved nitroreductase variants(L1). Ladder (L2). NfsA_Ec, (L3). No protein sample (L4). 3.2C (L5). 2.2C (L6) 3.2F (L7) 1.5C (L8) 1.9C. Samples of 30 μ L of the His6-tagged purified protein were boiled at 100 $^{\circ}$ C for 10 minutes prior to electrophoresis. Gel was run in 1 \times SDS-Run buffer, at constant voltage (175 Volts) for 45-60 minutes. Protein bands stained by gentle shaking in Coomassie blue stain solution overnight on an orbital shaker and destained the following day. A lane was deliberately left empty of a sample between the wild-type nitroreductase and the first variant to avoid any overlap of the nitroreductase protein band. NfsA *E. coli* is approximately 47 kDa. A protein product band was observed across all samples at just above the 48 kDa ladder marker.

Appendix C: Supplementary material Chapter 6 - Michaelis-Menten curves derived from reduction of PR-104A and SN36506 by purified His6-tagged nitroreductases

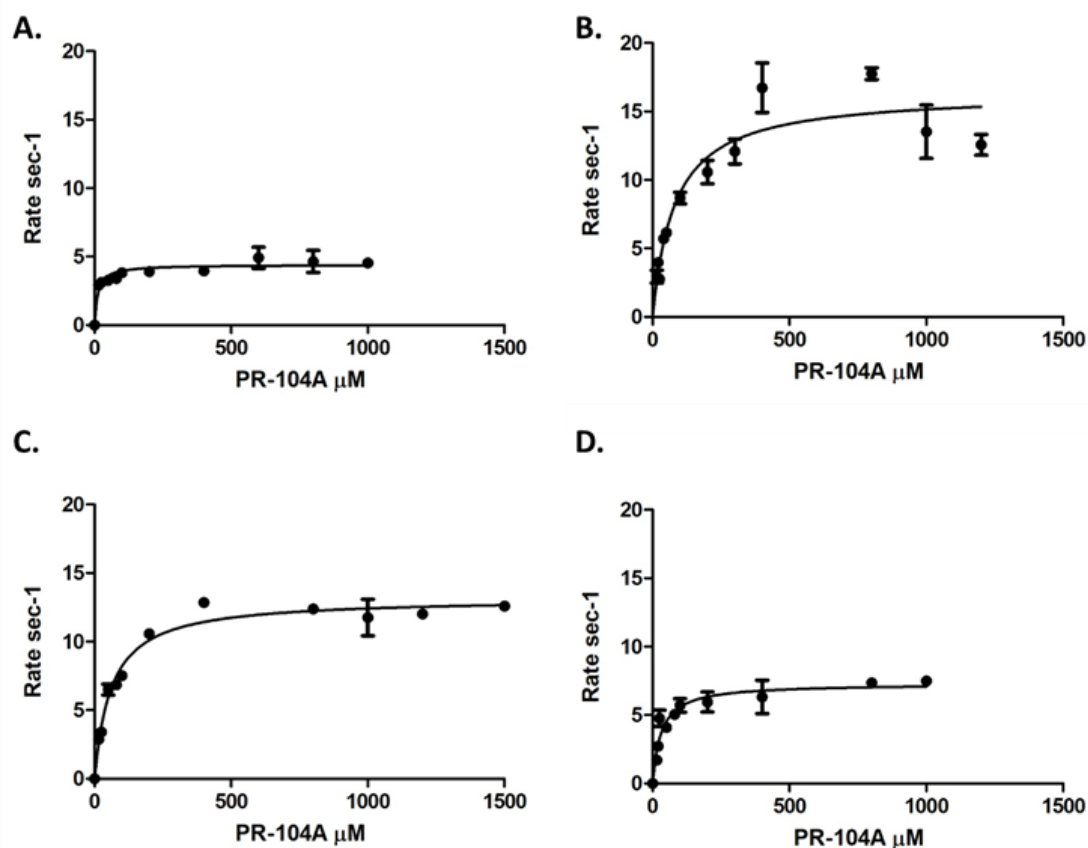


Figure C 1 Michaelis-Menten curves derived from reduction of PR-104A by purified His6-tagged NfsA nitroreductase candidates. (A). NfrA_Bs, (B). NfsA_E, (C). NfsA_Es, (D). YcnD_Bs Rate of reduction at varying concentrations of PR-104A and a fixed concentration of excess NADPH (0.25 mM) were monitored by decrease in absorbance at 400 nm, rates measured in quadruplicate reactions. Apparent K_m and k_{cat} derived using GraphPad Prism 7.0 (GraphPad Software Inc.; La Jolla, CA, USA). The extinction coefficient used was $6000 \text{ M}^{-1} \text{ cm}^{-1}$. The data has been normalized according the total concentration of the enzyme (μM) used in the reactions thus the y-axis displays rate in sec^{-1} .

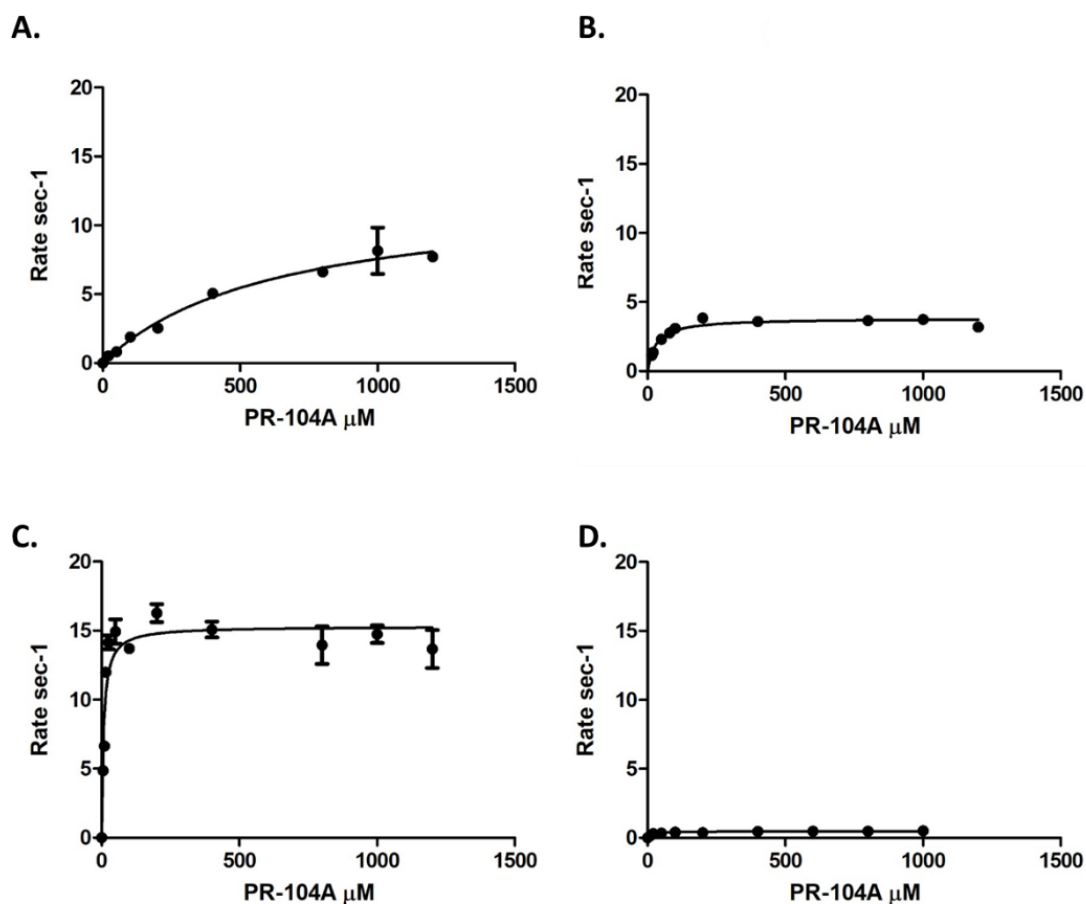


Figure C 2 Michaelis-Menten curves derived from reduction of PR-104A by purified His6-tagged NfsB nitroreductase candidates. (A). NfsB_Ec, (B). NfsB_Vv, (C). NfsB_Vv F70A/F108Y mutant (D). Ydgl_Bs. Rate of reduction at varying concentrations of PR-104A and a fixed concentration of excess NADPH (0.25 mM) were monitored by decrease in absorbance at 400 nm, rates measured in quadruplicate reactions. Apparent K_m and k_{cat} derived using GraphPad Prism 7.0 (GraphPad Software Inc.; La Jolla, CA, USA). The extinction coefficient used was $6000 \text{ M}^{-1} \text{ cm}^{-1}$. The data has been normalized according the total concentration of the enzyme (μM) used in the reactions thus the y-axis displays rate in sec^{-1} .

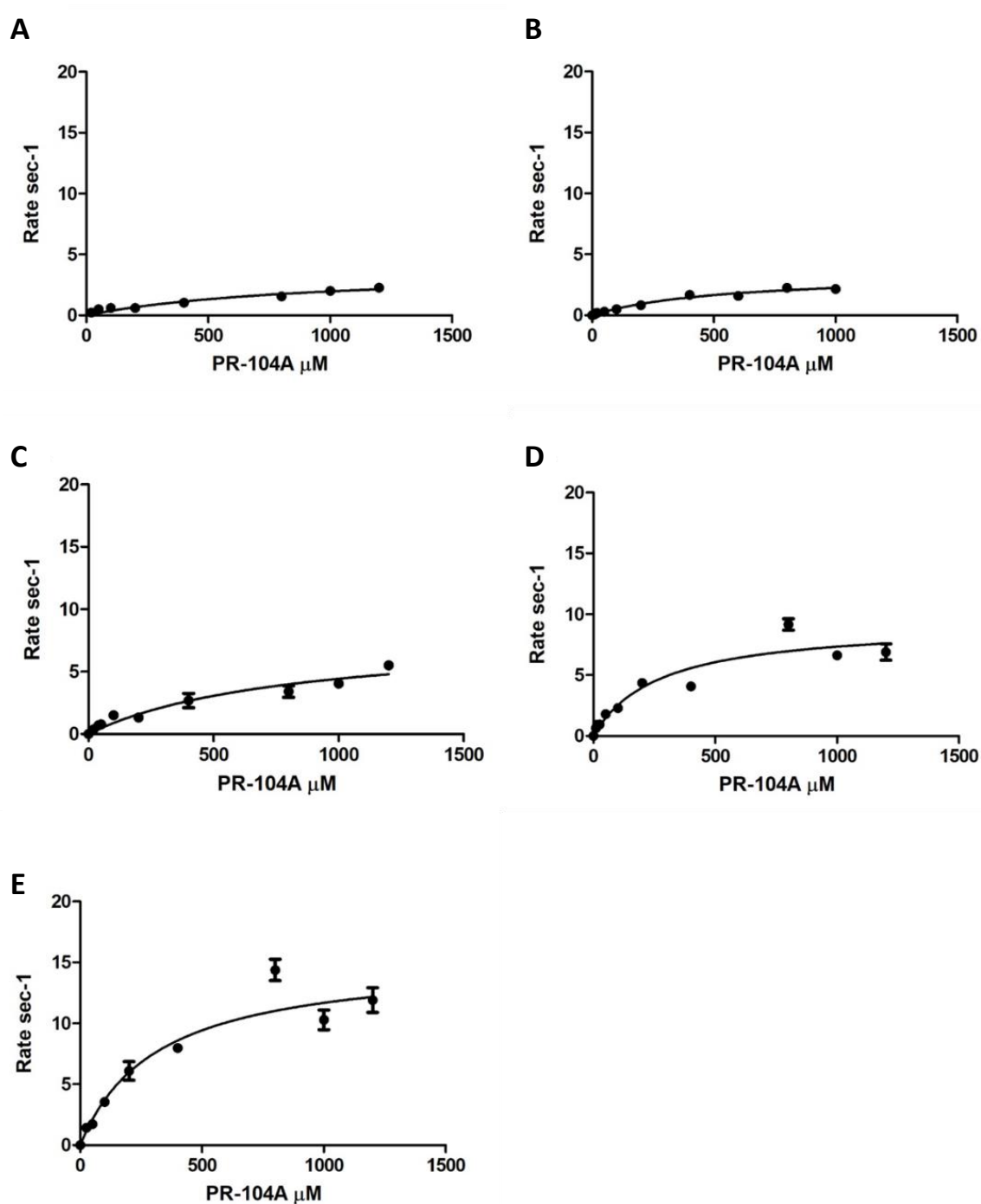


Figure C 3 Michaelis-Menten curves derived from reduction of PR-104A by purified His6-tagged NfsB nitroreductase candidates (A). *NfsB_Nme*, (B). *YfkO_Bli*, (C). *YfkO_Bs*, (D). *YfkO_Bs* mutant 1-88, (E). *YfkO_Bs* mutant 3-62. Rate of reduction at varying concentrations of PR-104A and a fixed concentration of excess NADPH (0.25 mM) were monitored by decrease in absorbance at 400 nm, rates measured in quadruplicate reactions. Apparent K_m and k_{cat} derived using GraphPad Prism 7.0 (GraphPad Software Inc.; La Jolla, CA, USA). The extinction coefficient used was $6000 \text{ M}^{-1} \text{ cm}^{-1}$. The data has been normalized according the total concentration of the enzyme (μM) used in the reactions thus the y-axis displays rate in sec^{-1} .

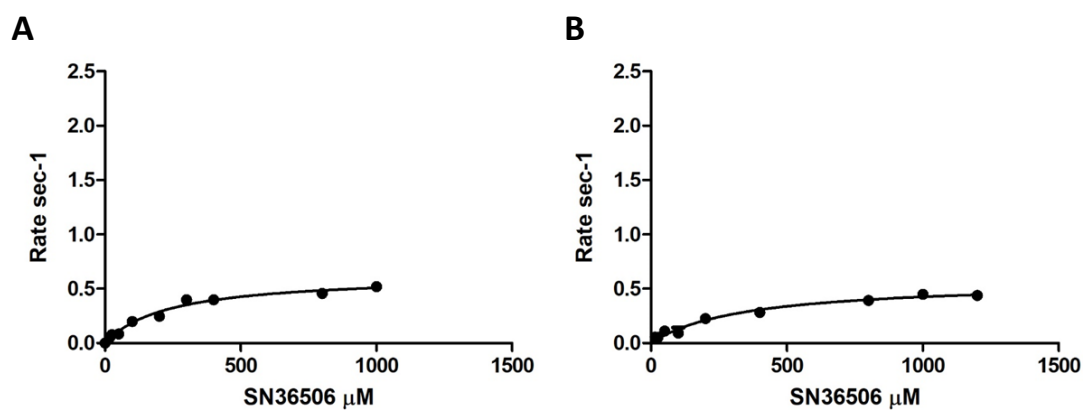


Figure C 4 Michaelis-Menten curves derived from reduction of SN36506 by purified His6-tagged NfsA nitroreductase candidates. (A). NfsA_Es, (B). YcnD_Bs. Rate of reduction at varying concentrations of SN36506 and a fixed concentration of excess NADPH (0.25 mM) were monitored by decrease in absorbance at 400 nm, rates measured in quadruplicate reactions. Apparent K_m and k_{cat} derived using GraphPad Prism 7.0 (GraphPad Software Inc.; La Jolla, CA, USA). The extinction coefficient used was $6000 \text{ M}^{-1} \text{ cm}^{-1}$. The data has been normalized according the total concentration of the enzyme (μM) used in the reactions thus the y-axis displays rate in sec^{-1} .

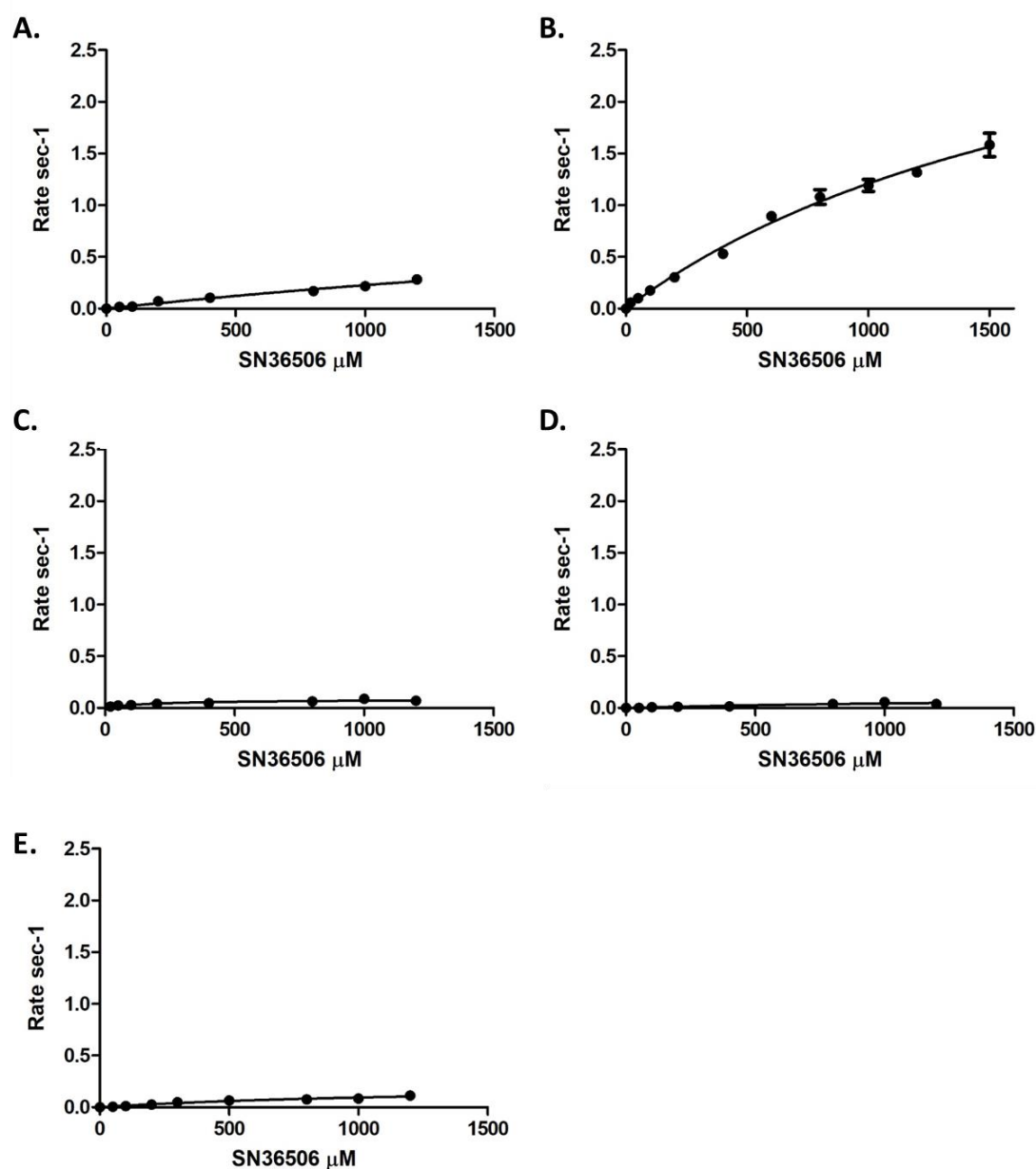


Figure C 5 Michaelis-Menten curves derived from reduction of SN36506 by purified His6-tagged NfsB nitroreductase candidates. (A). NfsB_Vv, B. NfsB_Vv F70A/F108Y mutant (C). Ydgl_Bs, (D). YfkO_Bs mutant 1-88, (E). YfkO_Bs mutant 3-62. Rate of reduction at varying concentrations of SN36506 and a fixed concentration of excess NADPH (0.25 mM) were monitored by decrease in absorbance at 400 nm, rates measured in quadruplicate reactions. Apparent K_m and k_{cat} derived using GraphPad Prism 7.0 (GraphPad Software Inc.; La Jolla, CA, USA). The extinction coefficient used was $17,400 \text{ M}^{-1} \text{ cm}^{-1}$. The extinction coefficient used was $6000 \text{ M}^{-1} \text{ cm}^{-1}$. The data has been normalized according the total concentration of the enzyme (μM) used in the reactions thus the y-axis displays rate in sec^{-1} .